Nonperturbative vacuum pair creation in strong fields and analogies in graphene

Dissertation

zur Erlangung des Doktorgrades

an der Fakultät für Mathematik, Informatik und Naturwissenschaften

Fachbereich Physik

der

Universität Hamburg

vorgelegt von

Ibrahim Akal

Hamburg

2018

Details

Dissertation

submitted

in partial fulfillment of the requirements
for the degree of *Doctor rerum naturalium*

in Physics

to the Department of Physics of
Hamburg University

by

Ibrahim Akal

affiliated with

Theory Group, DESY Hamburg

Abstract

In this thesis, nonperturbative pair creation from the quantum field theoretic ground state in the presence of strong macroscopic gauge fields is studied. Employing different approaches such as the string inspired worldline formalism, the worldline instanton method, semiclassical WKB techniques as well as quantum kinetic theory, we investigate various aspects of this so-called Schwinger effect. More specifically, we study the explicit dependence of the pair production rate on the underlying background structure. Here, we mainly focus on purely time dependent as well as spatiotemporal inhomogeneous and oscillatory electric backgrounds which give rise to substantial enhancement effects. Employing an effective reflection approach, we analyze many properties and characteristic features of the corresponding mechanisms. We also study the impact of microscopic details of the background on nonperturbative and perturbative aspects. Imposing explicit symmetry constraints, we generalize the methods for multidimensional backgrounds which facilitate the nonlocal nature of vacuum pair production. In addition, we investigate analogous effects in condensed matter systems such as bandgapped graphene. Constructing appropriate descriptions in lower dimensional spacetimes via Kaluza-Klein compactifications, we find that creating quasiparticle-hole pairs in this Dirac material resembles pair creation from the quantum vacuum by the dynamical Schwinger mechanism.

Zusammenfassung

In der vorliegenden Arbeit befassen wir uns mit der nichtperturbativen Paarerzeugung aus dem quantenfeldtheoretischen Grundzustand in makroskopisch starken Hintergrundfeldern. Mit Hilfe unterschiedlicher Beschreibungen wie dem String-inspirierten Weltlinienformalismus, der Weltlinieninstantonmethode, semiklassischer WKB-Näherungen sowie der quantenkinetischen Theorie untersuchen wir verschiedene Aspekte dieses sogenannten Schwingereffekts. Insbesondere, untersuchen wir die explizite Abhängigkeit der Paarproduktionsrate von der zugrunde liegenden Hintergrundstruktur. Hierbei konzentrieren wir uns hauptsächlich auf rein zeitabhängige sowie raumzeitliche inhomogene und oszillatorische elektrische Felder, welche zu erheblichen Verstärkungseffekten verhelfen. Durch das Entwickeln eines effektiven Ansatzes analysieren wir verschiedene Eigenschaften und charakteristische Merkmale der entsprechenden Mechanismen. Ebenso untersuchen wir die Auswirkungen von mikroskopischen Details des Hintergrundfeldes auf die nichtperturbativen und perturbativen Aspekte. Indem wir die zugrunde liegenden Symmetrien explizit auferlegen, verallgemeinern wir die Methoden für mehrdimensionale Hintergründe, welche unter anderem die nichtlokale Natur der Vakuumpaarproduktion hervorheben. Darüber hinaus untersuchen wir analoge Effekte in Systemen aus der kondensierten Materie wie im Beispiel von Graphen in Gegenwart einer Bandlücke. Mit Hilfe von geeigneten Beschreibungen in niederdimensionalen Raumzeiten mittels Kaluza-Klein-Kompaktifizierungen zeigen wir, dass die Erzeugung von Quasiteilchen-Loch-Paaren in diesem Diracmaterial der Paarbildung aus dem Quantenvakuum mittels des dynamischen Schwingermechanismus entspricht.

Papers

The main body of this thesis is based on the following publications:

[1] **Super Gaussian enhancers in the Schwinger mechanism**
<u>*Ibrahim Akal*</u>
e-print: arXiv:1712.05368 [quant-ph] (2017),

[2] **Quantum tunnelling from vacuum in multidimensions**
<u>*Ibrahim Akal*</u> *and Gudrid Moortgat-Pick*
journal: Phys. Rev. **D96** (2017) no. 9, 096027
e-print: arXiv:1710.04646 [hep-th] (2017),

[3] **Euclidean mirrors: enhanced vacuum decay from reflected instantons**
<u>*Ibrahim Akal*</u> *and Gudrid Moortgat-Pick*
journal: J. Phys. **G45** (2018) no. 5, 055007
e-print: arXiv:1706.06447 [hep-th] (2017),

[4] **Low-dimensional approach to pair production in an oscillating electric field: Application to bandgap graphene layers**
<u>*Ibrahim Akal*</u>*, Reinhold Egger, Carsten Müller and Selym Villalba-Chávez*
journal: Phys. Rev. **D93** (2016) no. 11, 116006
e-print: arXiv:1602.08310 [hep-ph] (2016).

Parts of the publications above are used either directly or indirectly in this thesis.

Acronyms

Acronyms introduced in this thesis are listed below.

1PI   one-particle irreducible

AAM   Affleck-Alvarez-Manton

AdS   anti-de Sitter

BCS   Bardeen-Cooper-Schrieffer

BK   Bern-Kosower

BSM   Beyond the Standard Model

CEF   constant electric field

CFT   conformal field theory

CP   charge conjugation parity

CM   center of mass

EFT   effective field theory

EH   Euler-Heisenberg

ELE   Euler-Lagrange equation

ELI   Extreme Light Infrastructure

FT   Fourier transform

GUT   Grand Unified Theory

HJE   Hamilton-Jacobi equation

IP	interaction point
LC	linear collider
LHC	Large Hadron Collider
ODE	ordinary differential equation
OEF	oscillating electric field
PDF	parton distribution function
QBVE	quantum Boltzmann-Vlasov equation
QCD	Quantum Chromodynamics
QED	Quantum Electrodynamics
QFT	quantum field theory
QGP	Quark Gluon Plasma
RHIC	Relativistic Heavy Ion Collider
SM	Standard Model
SPDF	single particle distribution function
sQED	scalar Quantum Electrodynamics
VEV	vacuum expectation value
VPP	vacuum pair production
WKB	Wentzel-Kramers-Brillouin
WQFT	worldline quantum field theory
XFEL	X-Ray Free-Electron Laser

Conventions

Unless explicitly stated otherwise we will use natural units $\hbar = 1$ and $c = 1$ throughout this thesis. The most commonly appearing notations are listed below.

x_μ, x^μ	covariant, contravariant four vector
A^μ	gauge (background) field
$F^{\mu\nu}$	field tensor associated with gauge (background) field
$\mathcal{A}^\mu$	external background field
$\mathcal{F}^{\mu\nu}$	field tensor associated with external background field
∂_t, $\frac{\partial}{\partial t}$	partial derivative with respect to variable t
$\dot{x}$, $\ddot{x}$	first, second time derivative
$\times$	scalar multiplication
∇	Nabla operator
Δ	Laplace operator
$\square$	d'Alembert operator
$\Re$	real part
$\Im$	imaginary part
$\mathrm{Res}_a f$	residue of f at a
$\mathbf{x}, \mathbf{E}, \boldsymbol{\delta}, \boldsymbol{K}, ...$	vectors
$\hat{a}, \hat{G}, \hat{H}, ...$	operators
$\mathbb{S}$	S-matrix
$\mathbb{T}$	transfer matrix
Det	functional determinant
det	matrix determinant
Tr	functional trace
tr	matrix trace
$x \cdot y \equiv \sum x_\mu y^\mu$	Einstein summation convention
γ^μ	Dirac gamma matrices
$\mathbf{1}$	identity matrix
$i = \sqrt{-1}$	imaginary unit

$[a, b] \equiv ab - ba$	commutator
$\{a, b\} \equiv ab + ba$	anticommutator
δ_{xy}	Kronecker delta
$\delta^{(n)}$	n-dimensional Dirac delta
ln	natural logarithm
exp, e	exponential function

$E_{\mathrm{S}} = 1.32 \times 10^{18}$ V/m	critical electric field in QED
$B_{\mathrm{cr}} = 4.41 \times 10^{22}$ T	critical magnetic field in QED
c	speed of light in vacuum
$\hbar$	reduced Planck constant
e	electric charge
m	particle mass
$v_f \approx \frac{c}{300}$	Fermi velocity in graphene
m	effective mass in graphene
$E_{\mathit{g}} = \frac{\mathit{m}^2 v_f^3}{e}$	critical electric field strength in graphene
$a_0 = 1.42$ Å	carbon-carbon distance in graphene, 1 Å = 0.1 nm

$\mathbb{R}$	set of real numbers
$\mathbb{C}$	set of complex numbers
$\mathbb{N}$	set of natural numbers
$\mathbb{Z}$	set of integer numbers

Structure of thesis

In the following, we outline the structure of this thesis.

Part I serves as a broad overview about the topic. In chapter 1, we begin with a short summary of general aspects in elementary particle physics, motivate and review the different frontiers and connect to the strong field regime. Then, we discuss the phenomenon of vacuum decay in strong fields against matter-antimatter pair creation. We introduce the basic notions and sketch the different mechanisms. Following this, we describe the main properties of graphene and the analogies to pair production from the quantum vacuum. In chapter 2, we comment on the general assumptions and theoretical ideas in dealing with strong fields in quantum field theory. After a brief motivation, we sketch the emergence of classical backgrounds in field theory by formulating the problem in terms of quantum coherent states. We close with an overview about possible sources of strong fields. In chapter 3, we present the theoretical description of vacuum pair production in more detail and portray some of the early approaches for the case of static backgrounds. Introducing the relevant quantities, we discuss characteristic attributes inherent to this nonperturbative phenomenon.

Part II encompassing chapters 4 - 7 introduces the different approaches which constitute the basis for the methods developed and applied in this thesis. After a brief motivation, we first introduce the worldline formalism in quantum field theory. We discuss the basics and sketch the derivation of certain scattering amplitudes which are of particular relevance for the present studies. Then, in the subsequent two chapters, we describe semiclassical methods including instanton and WKB techniques. The last chapter introduces a completely different approach building on ideas in nonequilibrium quantum field theory.

Part III is based on the original papers [1–3]. In chapter 8, an effective reflection approach is developed. The techniques are applied to study enhancement effects in the presence of various types of time dependent backgrounds. In chapter 9, these methods, in combination with further approaches, are employed to study nonperturbative and perturbative aspects of vacuum pair production. In chapter 10, an advanced approach combining recent ideas is developed. The techniques are applied in order to study vacuum pair production in multidimensional backgrounds with genuine space and time dependence.

Part IV is based on the original paper [4]. Here, we investigate analogies of the Schwinger effect in graphene. We first develop corresponding descriptions for vacuum pair production in lower dimensional spacetimes. The resulting equations we then apply in order to study the production of quasiparticle-hole pairs in bandgapped graphene layers.

Horror vacui

Contents

Part I

Introduction

Chapter 1

Review

1.1 Elementary gauge interactions

QUANTUM forces are described by gauge theories which are invariant under certain transformations with spacetime dependent parameters. The Standard Model (SM) of elementary particle physics is the gauge theory which describes the fundamental strong, weak and electromagnetic interaction [5–8]. Recently, its missing piece has been confirmed at the Large Hadron Collider (LHC) through the discovery of the Higgs boson [9, 10]. This scalar particle is central for explaining the origin of masses through spontaneous symmetry breaking [11, 12] in the electroweak sector via the BEGHHK[1] mechanism [13–15]. This nowadays called Higgs mechanism also guarantees unitarity that is crucial for the SM to be a consistent quantum field theory (QFT) of gauge interactions. It has another extremely important consequence — it leads to a renormalizable theory with massive vector bosons so that infinities due to higher order quantum corrections can be reabsorbed into the parameters of the Lagrangian.

The group structure of the SM is

$$SU(3)_{\mathrm{C}} \times SU(2)_{\mathrm{W}} \times U(1)_{\mathrm{Y}}. \tag{1.1}$$

The model includes 6 leptons and 6 quarks described by fermionic fields, 12 vector fields and a complex doublet scalar field H, the Higgs field [16]. The strong and weak interactions are governed by the $SU(3)_{\mathrm{C}}$ and $SU(2)_{\mathrm{W}}$ factors. The $SU(3)_{\mathrm{C}}$ factor mixes 3 different colors of quarks and antiquarks where $SU(2)_{\mathrm{W}}$ is the weak

_____

[1] R. Brout, F. Englert, G. Guralnik, C. R. Hagen, P. Higgs and T. Kibble

isospin. The remaining $U(1)_{\mathrm{Y}}$ factor is of the weak hypercharge Y. All gauge fields and fermions transform under the fundamental group representations. As usual, we speak about spontaneous symmetry breaking if the vacuum state of the theory does not respect the initial symmetry anymore. In the SM, the electroweak sector is governed by the $SU(2)_{\mathrm{W}} \times U(1)_{\mathrm{Y}}$ gauge symmetry. The Higgs field has nonvanishing vacuum expectation value (VEV), $\langle H \rangle \neq 0$. Due to this, the latter symmetry is spontaneously broken via the Higgs mechanism to the electromagnetic $U(1)_{\mathrm{EM}} \equiv U(1)$. As a consequence, the $W^{\pm}$ and Z^{0} bosons being responsible for the weak interaction become massive whereas the corresponding gauge boson that accounts for the electromagnetic interaction, the photon γ, remains massless. This difference explains why the electromagnetic force is long ranged and the weak force is short ranged. The gauge bosons that carry the strong interaction are called gluons. They *glue* the quarks and antiquarks together in form of baryons and mesons. At large distances, the strong interaction becomes very strong such that the glued particles cannot be separated. This phenomenon is known as confinement.

Despite the huge success of the SM in predicting experimental data of particle collisions at high energies with an enormous precision, many fundamental questions are still unanswered. Since the Higgs mechanism is rather an ad hoc attempt in order to realize the breakdown in the electroweak sector, a deeper explanation for the structure of the Higgs sector is for sure indispensable. Furthermore, the mass of the Higgs boson is extremely sensitive to higher order quantum corrections. It may probably be stabilized at the visible mass at $m_H \sim 125$ GeV by some so far unknown mechanism or by an extremely precise fine-tuning. This open question is often referred to as the hierarchy problem.

The SM also lacks a prediction of neutrino masses which contradicts the experimental confirmation of neutrino oscillations indicating that neutrinos must have some mass [17], albeit a tiny one. There are also cosmological observations which remain unexplained within the SM. For instance, many investigations show a huge asymmetry between matter and antimatter in the universe. This Baryon asymmetry can only be explained if sufficient charge conjugation parity (CP) violation appears in addition to the one in the quark sector which clearly necessitates the extension of the SM.

These shortcomings, among others, have triggered many extensions of the SM which go under the name of Beyond the Standard Model (BSM). Moreover, it is believed that the SM is a low energy effective description of some Grand Unified Theory (GUT). Similar as for the unification of the electromagnetic and weak forces above the electroweak scale $\Lambda_{\mathrm{EW}} \sim 2 \times 10^2$ GeV, the strong and the electroweak forces may be unified above some hypothetical GUT scale $\Lambda_{\mathrm{GUT}} \sim 10^{16}$ GeV in form of a single force governed by some preferably Lie group representation. Many of the proposed GUT candidates predict the existence of topological defects such as magnetic monopoles [18]. However, none of the predictions has been observed so far.

Unfortunately, all the mentioned theories do not describe gravitation whose inclusion, however, is mandatory to understand the very early universe at the Planck scale $\Lambda_{\mathrm{Planck}} \sim 10^{19}$ GeV. Although, we still have many question marks in understanding the nature of quantum gravity, there has recently been made tremendous progress in string theory which may enlighten some fascinating connections and unveil deep insights into the structure of space, time and matter.

1.2 Frontiers of fundamental physics

The SM predicts most of the data from collision experiments with an enormous precision. To specify which of the suggested generalizing models points towards the right direction is therefore an enormous challenge. High energy particle colliders are extremely important for exploring signatures of new physics or to preclude some of the possible directions. On the other hand, many of the embeddings of the SM into a more general unified framework predict some new physics at the sub-eV scale. These may be probed for instance by utilizing strong electromagnetic fields or microwave cavities which are, complementary to particle colliders, examples of alternative approaches at the low energy frontier [19, 20].

Furthermore, one may also look for completely different parameter regions of the SM in order to seek for mismatches which can help to extend and deepen our understanding of nature. Possibilities are nonlinear and nonperturbative phenomena in the low energy and intensity regime. A well known example is the confining

phase of Quantum Chromodynamics (QCD) which is still not well understood. Another direction is related to vacuum phenomena in strong macroscopic gauge fields. In Quantum Electrodynamics (QED), which has been tested experimentally to a very high precision at high energies [21], the vacuum has crucial imprints in the strong field regime. QFTs intrinsically allow quantum fluctuations of virtual particles having the consequence that their vacua cannot be seen as totally empty. Instead, the quantum vacuum behaves like a polarizable medium that can be described by some refractive and absorptive index. Such effects are less relevant in particle collisions where all observables are measured with reference to the unaffected ground state. The situation changes in the strong field regime where the vacuum structure gives rise to significant quantum phenomena. The gauge bosons in QED cannot interact with each other. This restriction is dictated by the Abelian $U(1)$ gauge symmetry. However, in virtue of vacuum fluctuations, their mutual interaction becomes possible. This can polarize the vacuum resulting in nonlinear and even nonperturbative effects such as vacuum birefringence and vacuum pair production (VPP).

1.3 Vacuum pair production

Destabilizing the quantum vacuum against the production of matter-antimatter pairs in the presence of a strong macroscopic gauge field is an important nonperturbative prediction in QFT. The first complete derivation in QED in the presence of a strong static electric field was established by Schwinger in his seminal paper [22]. It is one of the very few nonperturbative analytic results in quantum gauge theories that has a clear physical prediction. Nowadays, the phenomenon of VPP has also become known as the so-called Schwinger effect or Schwinger pair creation.[2] The leading order vacuum decay rate per unit volume and unit time in the weak field and weak coupling limit has a much celebrated closed series representation,

$$\mathcal{R} \simeq \frac{e^2 E^2}{8\pi^3} \sum_{n=1}^{\infty} \frac{1}{n^2} \exp\left(-\frac{\pi n E_\mathrm{S}}{E}\right). \tag{1.2}$$

This infinite sum is sometimes referred to as the Schwinger formula. The first term in the latter expression is the corresponding VPP rate [23, 24]. Here, e is

---

[2] The mechanism behind nonperturbative VPP in a static Abelian gauge field, as initially studied in [22], is called the Schwinger mechanism. Other possibilities beyond the simple static limit are described in section 1.4.

the electron charge and E denotes the electric field strength. The prefactor takes into account effects from quantum fluctuations. The characteristic exponential possesses a nonanalytic dependence on the field strength which already signals the nonperturbative quantum mechanical tunneling behavior of this absorptive process. The damping factor in the exponent scales linearly with the critical field strength

$$E_{\mathrm{S}} = \frac{m^2}{e} \approx 1.32 \times 10^{18} \text{ V/m} \tag{1.3}$$

where m stands for the particle mass. As can be seen from the tunneling exponential, for field strengths close to E_{S} spontaneous pair production from the vacuum is expected to be significant.

Despite its elegant and relatively simple derivation in nonlinear QED, the process of VPP still could not yet be realized in the laboratory. The technical challenge goes back to the extremely large value of E_{S} being many orders of magnitude larger than field strengths feasible in most experiments. For instance, the intensity which corresponds to the critical value E_{S} is almost 7 orders of magnitude larger than the highest intensity ever reached with a laser, see section 2.6. Unfortunately, intensities corresponding to the critical field E_{S} cannot be made attainable in the near future. However, during the last couple of years significant efforts, both on experimental as well as on theoretical side, have been progressed. Such promising advances may bring the Schwinger effect to experimentally accessible terrain [25–30]. Namely, strong field laser facilities with field strengths approaching $E \sim 10^{-3} E_{\mathrm{S}}$ or even higher will be available soon. In addition, there have been predicted highly promising catalyzing mechanisms to achieve a tremendous enhancement of the decay rate in the presence of time dependent, inhomogeneous electric fields. One of the most prominent approaches is the so-called dynamically assisted mechanism [31–37]. Overlapping multiple pulsed fields [38] and optimizing the field shape correspondingly [39–43] can drive the rate higher as well. Besides, remarkable effects appear if magnetic field components are taken into account [44–47]. Substantial contributions to the VPP rate also apply due to finite temperature effects [48–56]. It has also been discussed that VPP can show universal features that are independent of the details of the background configuration [57–59].

The Schwinger effect is not necessarily restricted to QED. More general, it applies to QFTs with a $U(1)$ gauge field. There may be also generalizations to non-Abelian gauge fields as in QCD [60–63]. The latter, in particular, may give rise to a mechanism for confinement/deconfinement phase transition which is regarded as highly relevant for the Relativistic Heavy Ion Collider (RHIC) and LHC experiments with both strong electromagnetic as well as color fields involved. These considerations essentially motivate studies of the Schwinger effect in confining gauge theories which, however, proves as a very challenging task if described by ordinary methods in QFT.

Recently, in order to access the Schwinger effect also in strongly coupled theories, there has been made interesting progress by studying the problem within certain holographic gauge theories. In this way, various remarkable effects have been worked out such as catastrophic vacuum instability [64–68] and the appearance of an additional lower critical field strength due to the presence of confinement. Below the lower one the vacuum remains nonperturbatively stable against pair production [69–75]. Even more surprising, the direct connection between the Schwinger effect and the recently proposed ER = EPR conjecture [76] has been unveiled [77, 78] providing further insight into the intriguing connection between spacetime geometry and quantum entanglement [79–81].

It should be noted that studying VPP can be also relevant in several other contexts, cf. e.g. [82, 83]. For instance, it may be enlightening in understanding the strong electromagnetic environment of astrophysical objects [84–88]. Recently, some evidence for strong field effects such as vacuum birefringence has been observed [89]. A more comprehensive investigation of the Schwinger effect in QFTs may also lead to more general insights. These could be valuable for studies of false vacuum decay [90–97], cosmological pair creation [97–102], Hawking radiation [103–109], black hole creation [110] as well as the spontaneous production of topological defects in expanding universes [111]. In recent years, much progress has also been made in scrutinizing the Schwinger effect in Dirac materials like graphene [4, 112–117], semiconductors [116, 118] and ultracold atoms trapped in optical lattices [119–122] as well as semimetals [123]. Such findings reveal interesting similarities between nonlinear QFT and nonequilibrium condensed matter systems.

On the other hand, the study of strong field effects like VPP requires theoretical ideas which urgently need to be capable to describe the underlying nonperturbative physics. This is in general challenging and necessitates formalisms that go beyond the standard perturbative approach via Feynman diagrams. Depending on the specific focus and, more importantly, on the nature and explicit shape of the acting field, various techniques have been developed.[3] After the very early approach in the static field limit via the direct computation of the nonperturbative imaginary part of the one-loop Euler-Heisenberg (EH) effective action, a variety of semiclassical methods for beyond the static field limit have been introduced. Main concepts are based on Wentzel-Kramers-Brillouin (WKB) approximations and Bogoliubov transformations. A completely different, but more modern and powerful technique is the worldline instanton method which is based on the string inspired worldline formulation of the underlying effective field theory (EFT) [124, 125]. Apart from EFT descriptions, there are ideas which build on nonequilibrium quantum kinetic formulations. These methods are in particular very advantageous for studying the phase space of the produced pairs via numerical computation techniques, principally, also in the case of higher dimensional inhomogeneous fields. Other numerical techniques have been discussed in [121, 126, 127]. Due to its intrinsically nonperturbative character, the Schwinger effect can be also considered as a toy problem for testing recent theoretical nonperturbative methods in QFT such as resurgent transseries [128–130] and Lefschetz thimbles [129, 131, 132].

In the Abelian case, it has been found that the VPP rate beyond the static field limit highly depends on the field shape. Namely, large inhomogeneities in spacetime are capable to trigger a drastic enhancement even far below E_S [3, 31, 32, 34, 36–39, 41, 43]. It is worth mentioning that in a static magnetic field VPP cannot occur [133–135], since the underlying divergent, but alternating expansion of the relevant one-loop EH effective Lagrangian is Borel summable and therefore has no imaginary part [135]. In plane wave or null electromagnetic fields, respectively, the imaginary part of the effective action vanishes simply due to symmetry reasons [22].

---

[3] We will introduce many of the methods in detail, see chapters 4 – 7. These methods are utilized directly or indirectly to study various aspects of VPP in inhomogeneous external backgrounds.

In most cases, preferably for purely electric fields, investigations rely on numerical solving techniques, see e.g. [136–140]. Analytical results have been so far obtained only for certain special cases, see e.g. [111, 141–156]. However, due to the extremely high sensitivity to the field shape, a deeper understanding of the impact of more complex field constellations is highly desirable to better understand the formation process of matter.

From a slightly different perspective, such strong field effects may particularly be interesting in the notion of Liouville integrability [157]. There, the underlying constants of motion would directly be related to the field shape. However, it should be noted that inhomogeneous fields may not obey the Maxwell equations in vacuum and can lead to complicated symmetries rendering the exact identification of symmetries even more exhausting.

Beyond one-dimensional fields, already purely electric, the identification of the particles is in general highly demanding and hence diagonalizing techniques, such as Bogoliubov transformations as well as WKB techniques, are difficult to enforce. As will be shown, the mentioned semiclassical treatment via the worldline instanton approach proves highly efficient for that purpose. The latter approach permits in general a direct multidimensional treatment, since the imaginary part of the one-loop EH effective action is simply evaluated on classical periodic paths in Euclidean spacetime [2, 3, 37, 55, 144, 146, 152, 154, 158–163]. Thus, the basic challenge is to find the associated worldline instantons which have also various other applications in completely different contexts [73, 164, 165].

Similarly, such closed trajectories also arise in trace formulas [166, 167] relating the state density to certain properties of periodic orbits in phase space, namely, for systems with integrable as well as chaotic, nonintegrable classical limit [168–170]. Indeed, such orbits serve as topological equivalences in QFT [171, 172]. Reformulating the problem of VPP with the help of the Gutzwiller trace formula [173] leads to a weighted topological sum [174] evaluated on grouped periodic orbits. The different contributions to the quantum fluctuation prefactor can be collected in a single determinant specified by the associated monodromy matrix for a six-dimensional phase space surface transverse to the invariant, classical

orbit [175]. Interestingly, these orbits may become multiple periodic in the case of spatiotemporal fields [45]. Assuming that the Hamiltonian of the system defines an integrable dynamical system, the described multiperiodicity may indicate the existence of an additional constant of motion reflected by continuous, smooth trajectories in the Poincaré sections [174, 176] which may provide, together with the Maslov index, valuable information about system [45]. Those aspects clearly reinforce the complications regarding the identification of symmetries governed by such multidimensional systems.

1.4   Beyond the Schwinger mechanism

VPP in an electric field can in principle be realized via different mechanisms. The basic concepts can be illustrated by drawing on a simple single particle picture describing a negative Dirac sea and a positive excitation continuum. As we will see in a moment, this is an efficient way to highlight important aspects of VPP such as the characteristic nonperturbative tunneling behavior. We should notice that such a picture is of course not adequate from various points of view. However, despite the conceptual inconsistencies, we can already gain many useful insights.

We may think of the vacuum as a perfect gap insulator consisting of a valence band (negative Dirac sea) and a conduction band (positive continuum). The bandgap has the width of two times the rest mass of the excited particles, say an electron and a positron. The picture is the following: in the perfectly insulating initial phase there exist no excitations in the positive continuum and the whole valence band is filled up with virtual particles of negative energy. This situation is sketched in figure 1.1 (a).

In figure 1.1 (b), the situation is shown where the pair is produced via the absorption of multiple high energy photons approaching energies of the order m. This process is known as multiphoton pair production. It is a purely perturbative phenomenon and hence substantially different from the standard Schwinger mechanism. Pictorially, the absorption of multiple photons lifts a particle from the negative valence band (dark gray) to the positive conduction band (light gray) and leaves behind a hole (red circle) in the Dirac sea. The presence of that hole can be interpreted as a produced positron, whereas the particle (red dot) in the

positive continuum corresponds to the other pair constituent, the electron.
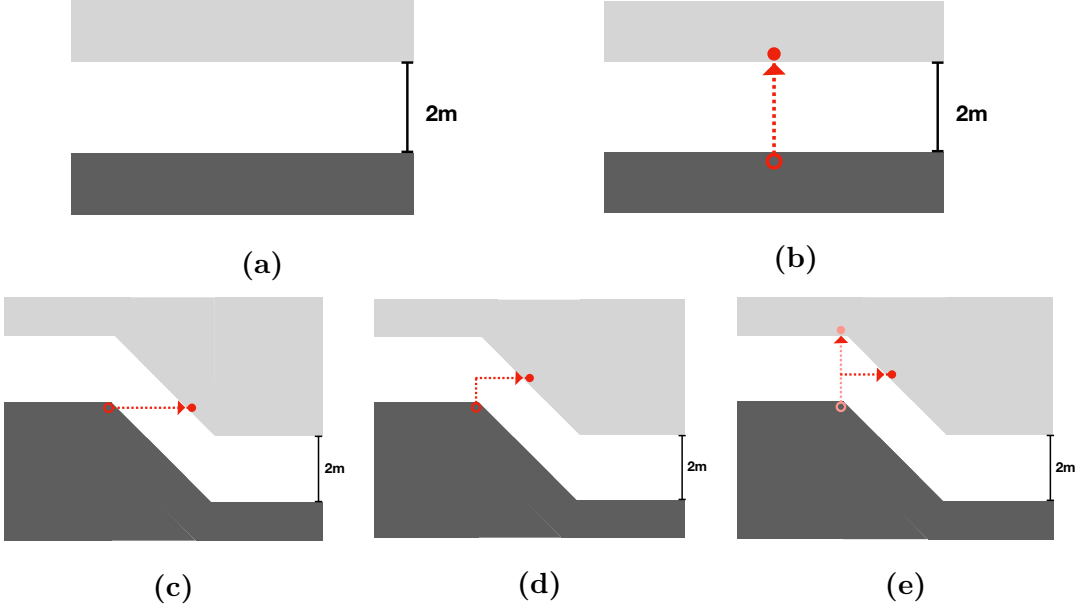
Figure 1.1: Mechanisms for VPP: **(a)** vacuum in insulating phase, electric field is absent **(b)** multi photon process, **perturbative (c)** standard Schwinger mechanism, **nonperturbative (d)** assisted mechanism, **nonperturbative (e)** dynamical mechanism, **nonperturbative** → **perturbative**. For explanations see discussion in the text.

The Schwinger mechanism, i.e. nonperturbative VPP in a static electric field, is sketched in figure 1.1 (c). The presence of the electric field tilts the bandgap such that the production process becomes possible via tunneling from the negative valence band to the positive continuum band. How much the gap is tilted, depends on the applied field strength E.

In figure 1.1 (d) the so-called dynamically assisted mechanism is illustrated. It applies in a superimposed electric field consisting of a (locally) static strong mode and a weak, but rapidly varying mode. The mechanism can be understood as follows: the weak mode photons, being still insufficient to push the particle to the positive continuum, lift the particle out of the valence band into the gap. The strong static mode takes over the remaining work and drives the tunneling of the lifted particle to the conduction band. As a consequence, the pair production process becomes enhanced due to the effective bandgap reduced by the additional weak mode. In the deeply weak regime, the dynamically assisted mechanism requires the full coupling to both modes and therefore operates in the nonperturbative regime.

Figure 1.1 (e) depicts the purely dynamical Schwinger mechanism where a single-mode electric field varies in time. For sufficiently large frequencies VPP gets enhanced due to the presence of energetic photons. For moderate frequencies, means much smaller than m, the process resembles nonperturbative VPP (Schwinger mechanism). With larger frequencies it will be shifted toward the perturbative regime (multiphoton process).

1.5 Analogies in Dirac materials

Electric fields of upcoming modern high intense lasers with micrometer extensions and femtosecond duration may come close to the critical field strength E_S. Together with an appropriate design of the field shape, these facilities turn out to be very promising in order to circumvent the huge suppression in the nonperturbative regime. However, these strategies do not constitute the only way to observe the destabilization of the vacuum against nonperturbative VPP. As briefly mentioned in the introduction, alternatively, one may follow a complementary route by resorting to appropriate low energy condensed matter systems where analogies of the Schwinger effect can be mimicked and detected with much less efforts.
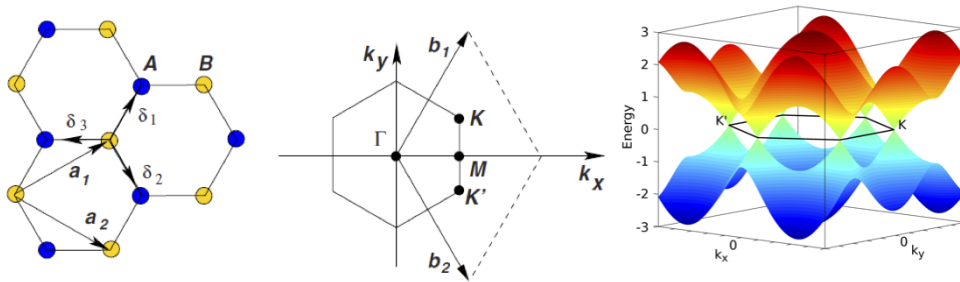
Figure 1.2: Left: lattice structure of graphene including sublattices A (blue) and B (yellow). The lattice vectors $\mathbf{a}_1$ and $\mathbf{a}_2$ as well as the vectors $\boldsymbol{\delta}_{1,2,3}$ connect nearest neighbor atoms. Center: Brillouin zone with the reciprocal lattice vectors $\mathbf{b}_1$ and $\mathbf{b}_2$. Right: dispersion relation of the π-bonds in the nearest neighbor tight binding model. The plots are taken from [177, 178].

For that purpose, graphene [177, 179–183] has become a very promising material since its recent discovery. It consists of a layer of carbon atoms arranged in a honeycomb lattice as shown in figure 1.2 (left). Each of the unit cells of the hexagonal Bravais lattice has two carbon atoms which build up two independent

sublattices A and B. The atoms in the sublattice A (B) are surrounded by the nearest neighbors that are part of the sublattice B (A). Obviously, the lattice can be seen as a bipartite system if only the nearest neighbor coupling is taken into account. Close to the Fermi level, the electronic states consist of p_z orbitals lying outside of the carbon plane. Thus, they form bond states with neighboring atoms and give rise to so-called π-bonds[4] as depicted in figure 1.2 (right). To understand the basic properties one can write down the Hamiltonian for the tight binding model consisting of an hopping term

$$\hat{H} = -\sum_{\langle i,j \rangle} \hat{a}_i^\dagger \hat{b}_j + \hat{a}_j^\dagger b_i \tag{1.4}$$

between the nearest neighbor atoms. Here, $\hat{a}_i$ and $\hat{b}_i$ denote the annihilators for the electrons in the p_z orbitals of the two carbon atoms associated with the sublattices A and B in a unit cell i [184] in form of the diamond-like shaped Brillouin zone[5] spanned by the vectors $\mathbf{b}_1$ and $\mathbf{b}_2$ in figure 1.2 (center). We have set the hopping parameter in front of the sum in (1.4) [177] to unity. Since each unit cell has two atoms, the Hamiltonian can be represented in momentum space by a 2×2 matrix,

$$H(\mathbf{k}) = \begin{pmatrix} 0 & \Omega(\mathbf{k}) \\ \Omega^*(\mathbf{k}) & 0 \end{pmatrix} \tag{1.5}$$

where

$$\Omega(\mathbf{k}) = -\left[e^{i\delta_1 \cdot \mathbf{k}} + e^{i\delta_2 \cdot \mathbf{k}} + e^{i\delta_3 \cdot \mathbf{k}} \right]. \tag{1.6}$$

The latter expression includes the three partial hopping amplitudes connecting each of the atoms in the sublattice A (B) with the three nearest neighbor atoms in sublattice B (A) through the vectors $\boldsymbol{\delta}_{1,2,3}$. The energy band is described by

$$E(\mathbf{k}) = \pm|\Omega(\mathbf{k})|. \tag{1.7}$$

---

[4] Each of the carbon atoms contribute one p_z orbital that participates in the bonds.

[5] The first Brillouin zone is a primitive cell uniquely defined in reciprocal space. The reciprocal lattice is divided into such Brillouin zones with boundaries given by planes related to the reciprocal points. This is analogous to dividing the Bravais lattice in real space into Wigner-Seitz cells. The importance of the Brillouin zone stems from the Bloch wave description in a periodic medium. There the solutions can entirely be characterized by their behavior in a single Brillouin zone. In the first Brillouin zone all reciprocal points are closer to the origin than to any other reciprocal lattice point.

The right-hand side only vanishes at the two inequivalent $\boldsymbol{K}_\pm$ points. There, the bands are degenerate and the hopping amplitudes destructively interfere to zero,

$$\Omega(\mathbf{k}) \propto e^0 + e^{i\frac{2\pi}{3}} + e^{-i\frac{2\pi}{3}} = 0. \tag{1.8}$$

The Fermi level lies at $E(\boldsymbol{K}_\pm) = 0$. In the small vicinity of these so-called Dirac points the Hamiltonian reads, up to a constant phase,

$$H(\boldsymbol{K}_\pm + \mathbf{p}) = \hbar v_f \begin{pmatrix} 0 & p_x \pm i p_y \\ p_x \mp i p_y & 0 \end{pmatrix} \tag{1.9}$$

which is just the Dirac Hamiltonian

$$H_D = c\boldsymbol{\sigma} \cdot \mathbf{p} + mc^2 \sigma_z \tag{1.10}$$

with $m \to 0$ and $c \to v_f$ [178]. Here, $\boldsymbol{\sigma} = (\sigma_x, \sigma_y)$ where σ_x, σ_y are the standard Pauli matrices.

The previous expression shows that the particles close to one of the two Dirac points in the two-dimensional monolayer exhibit a dispersion relation like massless Dirac fermions, where the speed of light c in vacuum is just replaced by the characteristic Fermi velocity $v_f \approx \frac{c}{300}$. Moreover, the eigenstates have a Dirac spinor structure in sublattice space [184]. Thus, graphene induces four distinguishable flavors of Dirac fermions giving rise to two real electron spin degenerate cones in the vicinity of the Dirac points. The associated pseudospin goes back to the degrees of freedom of the sublattice and is therefore fundamentally different from the fermionic spin. The graphene Dirac particles are derived from the electronic band structure so that they basically are charged electron/hole quasiparticles.

In the limit $m \to 0$, there is no gap in the spectrum of the Dirac Hamiltonian H_D and the quasiparticle dispersion relation turns out to be linear. This is very different from the parabolic dispersion relation of metals or semiconductors. In figure 1.3 the Fermi sea of massless Dirac materials as in two-dimensional graphene monolayers is compared with the corresponding one for conventional metals and insulators. Even in the case with $m \neq 0$, positive and negative energy eigenstates of H_D are based on the same space of spinor functions. This has the interesting consequence that particles and holes possess the same effective mass m which gives rise to a well defined spectral gap $2mc^2$ [185]. Differently, in metals and semiconductors electrons and holes obey separate Schrödinger equations with different

effective masses. So in these cases there does not exist any unique relation between gap and mass. Therefore, massive Dirac fermions are still substantially different from usual Schrödinger fermions.

Graphene, probably the most known Dirac material — here we should note that systems such as cuprate superconductors [186], silicene and germanene [187], topological insulators having a gapped spectrum in the bulk but Dirac fermions on the surface [188–193] as well as ultracold atoms in optical lattices [194, 195] also provide realizations of Dirac fermions — serves as an ideal low energy environment for fundamental relativistic quantum phenomena as, for instance, Klein tunneling [196], Coulomb supercriticality [182], many body renormalization effects [183] and also universal scaling phenomena [197].
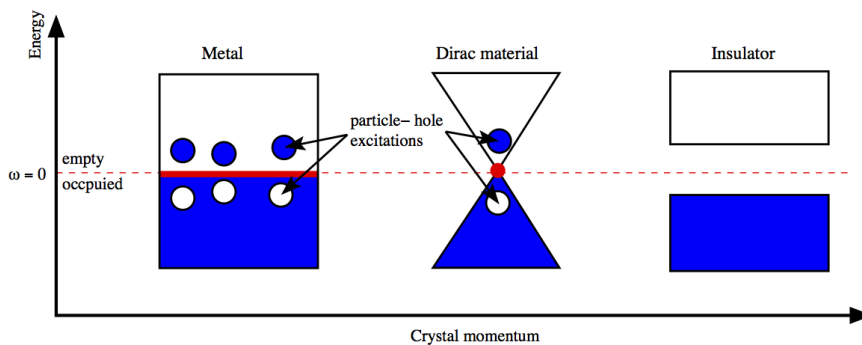
Figure 1.3: The Fermi sea of massless Dirac materials (center) compared to metals (left) and insulators (right). In d dimensional metals, the Fermi surface has dimension $d_{FS} = d - 1$. If the Fermi level coincides with the Dirac point, the Fermi surface for Dirac materials with $d \geq 2$ has dimensionality of one order less, i.e. $d_{FS} \leq d - 2$. For the case of graphene layers, i.e. $d = 2$, the Fermi surface reduces to a point placed between the two cones. Note that Dirac materials still exhibit quasiparticles with arbitrarily low energies both above and below the Fermi energy. The plot is taken from [178].

More importantly, even the Schwinger effect, means particle-hole pair production in an external field, has been theoretically investigated in graphene. Such studies were examined by applying techniques in $2 + 1$ dimensional QED in the presence of a static electric field [112],[6] a Sauter-like pulse [203] and a time dependent oscillating field [115, 204]. However, as discussed above, due to the lack of an energy gap at the Dirac points, the charge carriers behave as massless Dirac fermions. So

---

[6] Various effects which might provide experimental signatures of electron-hole pair production have been explored in a static electric field [198–202].

this does not allow the existence of an analogous critical field strength in graphene. Accordingly, the tunneling exponential in the production rate is missing which on the other side is a main characteristic feature in the standard Schwinger effect that may not be undermined.

There are various techniques on the market which allow to induce a bandgap $\Delta\varepsilon$ in graphene, for instance, the method of epitaxial growth on suitable substrates [205, 206], elastic strain [183] as well as Rashba spin splittings on magnetic substrates [207]. A nonvanishing mass $m = \frac{\Delta\varepsilon}{2v_f^2}$ of the charge carriers still allows the mobility of relativistic particles as long as their momenta are smaller than ~ 3 eV$/v_f$ [177]. In this case, the field induced particle-hole production may be expected to possess very similar characteristics as VPP in QED. Such an analogy for sure allows the opportunity to gain valuable insights about nonperturbative pair production mimicked in an experimentally accessible low energy condensed matter environment.

Chapter 2

Coherence, strong fields and quantum fields

2.1 An hybrid approach

WE consider an electromagnetic field composed of an immense amount of individual photons. In conventional QFT describing this situation by relying on the standard procedure in Fock space is extremely exhausting and basically out of reach. The standard treatment in perturbation theory would require a huge number of diagrams taking into account each of the photons participating in the underlying subprocesses [208–212]. Usually, it is argued that strong coherent electromagnetic fields as, for instance, generated with intense lasers can be assumed as being free of any depletion and enhancement effects. This mainly is assumed due to a large total number of photons compared to those which participate in the interactions [83]. As a consequence, these coherently accumulated photons can be treated macroscopically by introducing an external background field which does not change during the interactions.

Quantum mechanics in the presence of a classical potential is described in the Furry picture [213, 214]. It can be seen as an hybrid between the Heisenberg picture and the Dirac picture. The external potential is added to the free Hamiltonian which leads to modified eigenstates embedded in the classical potential.

Transferring the idea to QED, the latter procedure would require the exact solutions of the Dirac equation in the presence of the electromagnetic background.

However, a solution for a general background does not exist. Differently, for null[1]
backgrounds such as plane waves the equation has known solutions called Volkov
states [215–218]. This is possible due to the intrinsic symmetry properties of
a plane wave which in fact renders the problem under consideration superinte-
grable [219].

In the usual S-matrix language, the corresponding states would then be repre-
sented by Volkov states. In order to employ the usual picture of asymptotically
free states merging and dispersing in the interaction point, it is necessary that
such states preserve the single particle picture for the Dirac equation including the
background. This is only possible for certain cases such as plane waves. For those
the quantization of the Dirac field can be realized analogous to standard vacuum
QED [51, 220–222]. In this fashion, it is possible to construct some background
field theory, usually referred to as strong field QED, obeying the usual Feynman
rules in vacuum but with the modification that every free propagator of a charged
particle is replaced by the corresponding modified Volkov propagator nonpertur-
batively coupled to the external background field.

In the presence of various other backgrounds including the purely electric one,
as we particularly consider in this thesis, we need to take into account that the
Schwinger effect can be possible. Therefore, studying the Schwinger effect in strong
electric fields requires to go beyond the formalism described above [222]. As we
will discuss, in QFT this is usually carried out by resorting to the EFT description
which gives rise to the famous one-loop EH vacuum diagram.

However, the a priori introduction of any classical background, a *c*-number, is un-
satisfactory for a consistent quantum field theoretic description. In the following,
we will demonstrate that representing an electromagnetic field in terms of appro-
priate quantum states will render very advantageous. Indeed, assuming the field
to be fully coherent and not subjected to any depletion during the interaction, the
rigorous quantum description based on canonical photon coherent states [223–227]
will show that the former property is equivalent to shifting the photon field oper-
ator by a *c*-number. In other words, coherent states allow the smooth transition
from rigorously quantum states to an emergent classical entity described by macro-

---

[1] Fields for which the Lorentz invariants of the field tensors vanish are so-called null fields.

scopic properties like intensity and shape.

2.2   From quantum to classics

Coherent states have immediately been proposed after the invention of quantum mechanics by Schrödinger [228]. The basic concern was to study quantum states which can imitate their classical counterparts through the time evolution of the position operator

$$\hat{x}(t) = e^{i\hat{H}t}\hat{x}e^{-i\hat{H}t} \tag{2.1}$$

where a typical Hamilton operator is of the form

$$\hat{H} = \frac{\hat{p}^2}{2m} + V(\hat{x}). \tag{2.2}$$

The meaning of a classical behavior was understood by Schrödinger through the property that the expectation value of the position operator in (2.1), i.e.

$$x(t) = \langle z|\hat{x}(t)|z \rangle, \tag{2.3}$$

with respect to some state $|z\rangle$ obeys the classical equations of motion

$$m\ddot{x}(t) + \frac{\partial V(x)}{\partial x} = 0. \tag{2.4}$$

States which fulfill such properties became known as coherent states.

Let us consider an explicit example: in case of the quantum harmonic oscillator, as first considered by Schrödinger, we have the potential term

$$V(\hat{x}) = \frac{1}{2}m\omega^2\hat{x}^2 \tag{2.5}$$

where the standard commutator relation $[\hat{x}, \hat{p}] = i$ is satisfied. The ladder operators are given by the following expressions [229]

$$\begin{aligned}
\hat{a} &= \sqrt{\frac{m\omega}{2}}\left(\hat{x} + \frac{i}{m\omega}\hat{p}\right), \\
\hat{a}^\dagger &= \sqrt{\frac{m\omega}{2}}\left(\hat{x} - \frac{i}{m\omega}\hat{p}\right).
\end{aligned} \tag{2.6}$$

The latter satisfy canonical bosonic commutation relations, i.e.

$$[\hat{a}, \hat{a}^\dagger] = 1, \qquad [\hat{a}^\dagger, \hat{a}^\dagger] = 0 = [\hat{a}, \hat{a}]. \tag{2.7}$$

With the help of the ladder operators, the Hamilton operator in (2.2) can be rewritten in the following way

$$\hat{H} = \omega \left(\hat{a}\hat{a}^\dagger + \frac{1}{2} \right). \tag{2.8}$$

The corresponding eigenstates of the Schrödinger equation $\hat{H}|n\rangle = E_n|n\rangle$ are

$$|n\rangle = \frac{(\hat{a}^\dagger)^n}{\sqrt{n!}}|0\rangle \tag{2.9}$$

with eigenvalues

$$E_n = \hbar\omega \left(n + \frac{1}{2} \right). \tag{2.10}$$

Computing the momentum and space uncertainties by applying the standard definitions,

$$(\Delta x)^2 \equiv \langle n|\hat{x}^2|n\rangle - \langle n|\hat{x}|n\rangle^2,$$
$$(\Delta p)^2 \equiv \langle n|\hat{p}^2|n\rangle - \langle n|\hat{p}|n\rangle^2, \tag{2.11}$$

we find accordingly

$$\Delta x \Delta p = \hbar(n + \frac{1}{2}) \geq \frac{\hbar}{2} \tag{2.12}$$

where $n = 0$ corresponds to the ground state.

For the present discussion, let us introduce the following normalized[2] coherent state, i.e. $\langle z|z\rangle = 1$,

$$|z\rangle = e^{z\hat{a}^\dagger - z^*\hat{a}}|0\rangle = e^{-\frac{1}{2}|z|^2}e^{z\hat{a}^\dagger}|0\rangle \tag{2.13}$$

---

[2] In case of the unnormalized coherent state given by

$$|z\rangle = e^{z\hat{a}^\dagger}|0\rangle, \qquad \langle z| = \langle 0|e^{z^*\hat{a}}$$

we get

$$\langle z|z\rangle = \langle 0|e^{z^*\hat{a}}e^{z\hat{a}^\dagger}|0\rangle = e^{z^*z}\langle 0|e^{z\hat{a}^\dagger}e^{z^*\hat{a}}|0\rangle = e^{|z|^2}$$

by using $[\hat{a}, \hat{a}^\dagger] = 1$, the Baker-Hausdorff formula

$$e^{\hat{A}}e^{\hat{B}} = e^{[\hat{A},\hat{B}]}e^{\hat{B}}e^{\hat{A}}$$

and the following relations $e^{z^*\hat{a}}|0\rangle = |0\rangle$ and $\langle 0|e^{z'\hat{a}^\dagger} = \langle 0|$.

The matrix element for two different states reads

$$\langle z|z'\rangle = e^{z^*z'}\langle 0|e^{z'\hat{a}^\dagger}e^{z^*\hat{a}}|0\rangle = e^{z^*z'}.$$

parameterized by some number $z = |z|e^{i\varphi} \in \mathbb{C}$. The coherent state is constructed via acting with the displacement operator

$$\hat{D}(z) = e^{z\hat{a}^\dagger - z^*\hat{a}} \tag{2.14}$$

on the ground state of the quantum system defined in the usual way by $\hat{a}|0\rangle = 0$. This explains why coherent states are also called displaced ground states. The normalized coherent state in (2.13) is an eigenstate of the annihilation operator,

$$\hat{a}|z\rangle = z|z\rangle. \tag{2.15}$$

It can also be written in terms of an exact expansion in Fock space

$$|z\rangle = e^{-\frac{|z|^2}{2}} \sum_{n=0}^{\infty} \frac{z^n}{\sqrt{n!}}|n\rangle. \tag{2.16}$$

The dynamics of the eigenstates of the harmonic oscillator, $|n\rangle$, reads

$$e^{-i\hat{H}t}|n\rangle = e^{-i\omega t\left(n+\frac{1}{2}\right)}|n\rangle. \tag{2.17}$$

From this, the time evolution of the coherent state is obtained as

$$\begin{aligned} e^{-i\hat{H}t}|z\rangle &= e^{-\frac{|z|^2}{2}} \sum_{n=0}^{\infty} \frac{(z\hat{a}^\dagger)^n}{n!} e^{-i\hat{H}t}|0\rangle \\ &= e^{-\frac{|z|^2}{2}} \sum_{n=0}^{\infty} \frac{z^n}{\sqrt{n!}} e^{-i\hat{H}t}|n\rangle = e^{-i\frac{\omega}{2}t}|ze^{-i\omega t}\rangle. \end{aligned} \tag{2.18}$$

It can be seen that, except the constant phase in the rightmost expression, the dynamics of the coherent state is obtained by making the replacement

$$z \to z(t) = ze^{-i\omega t}. \tag{2.19}$$

Indeed, it can be shown that the coherent state recovers the familiar sinusoidal solutions for the quantum averages [230],

$$\begin{aligned} \langle\hat{x}\rangle(t) &= \langle z|\hat{x}(t)|z\rangle \simeq x_0|z|\cos(\omega t - \varphi), \\ \langle\hat{p}\rangle(t) &= \langle z|\hat{p}(t)|z\rangle \simeq p_0|z|\sin(\omega t - \varphi) \end{aligned} \tag{2.20}$$

which simply solve the classical harmonic oscillator equation where $p_0 = m\omega x_0$. Here, $x_0 = \sqrt{\frac{2\hbar}{m\omega}}$ denotes a fundamental quantum length depending on the universal Planck constant $\hbar$ and the constants m and ω which characterize the quantum counterpart of the harmonic oscillator. So in this way, the coherent state $|z\rangle$, even though it is rigorously quantum, allows a smooth transition from quantum to

classical mechanics and hence generally allows a classical understanding in various quantum mechanical situations. This unique attribute results from a set of properties satisfied by such so-called canonical or standard coherent states, respectively.

In addition to their classicality, coherent states have the property that they can be expanded in terms of a complete set of states even though they are not orthogonal.[3] The completeness relation reads

$$\int \frac{dz dz^*}{\pi} |z\rangle\langle z| = \mathbf{1}, \tag{2.21}$$

see appendix A for the complete proof. More precisely, coherent states are over-complete, in other words, one can expand any coherent state in terms of all the other coherent states due to their nonorthogonality which means that they cannot be taken as linearly independent.

Another property is that coherent states are minimally uncertain. Namely, starting on basis of the normalized coherent state introduced in (2.13), we can find that

$$\langle z|\hat{x}|z\rangle = \sqrt{\frac{2}{m\omega}}\Re(z), \qquad \langle z|\hat{x}^2|z\rangle = \frac{1}{2m\omega}\left[4(\Re(z))^2 + 1\right], \tag{2.22}$$
$$\langle z|\hat{p}|z\rangle = \sqrt{2m\omega}\Im(z), \qquad \langle z|\hat{p}^2|z\rangle = \frac{m\omega}{2}\left[4(\Im(z))^2 + 1\right].$$

We use the standard definitions in (2.11) where we replace the eigenstate $|n\rangle$ by the coherent state $|z\rangle$. Putting again $\hbar$ into the relevant expressions and using the relations in (2.22), we get

$$(\Delta x)^2 = \frac{\hbar}{2m\omega}, \qquad (\Delta p)^2 = \frac{m\omega\hbar}{2}. \tag{2.23}$$

From the latter we find that the coherent state $|z\rangle$ saturates the Heisenberg inequality,

$$\Delta x \Delta p = \frac{\hbar}{2}, \tag{2.24}$$

---

[3] For the matrix element $\langle z'|z\rangle$ we get by using the unnormalized expansion in (2.18)

$$\langle z'|z\rangle \simeq \sum_{n'=0}^{\infty}\sum_{n=0}^{\infty}\langle n'|\frac{(z'^*)^n}{\sqrt{n'!}}\frac{(z)^n}{\sqrt{n!}}|n\rangle = \sum_{n=0}^{\infty}\frac{\left(z'^* z\right)^n}{n!} = e^{z'^* z}$$

which obviously does not vanish even if $z' \neq z$. This is due to the reason that a coherent state is an eigenstate of the annihilation operator which is not Hermitian, see equation (2.15). Basically, eigenstates of some operator with different eigenvalues are orthogonal to each other when the corresponding operator is Hermitian.

being minimally uncertain in position and momentum as the ground state of the quantum harmonic oscillator, cf. equation (2.12).

The amplitude $|z| \equiv |z(0)|$ from above is related to the mean value of the occupation number operator $\hat{N} = \hat{a}^\dagger \hat{a}$,

$$\langle \hat{N} \rangle = \langle z(t)|\hat{a}^\dagger \hat{a}|z(t) \rangle = |z(t)|^2 = |z|^2. \tag{2.25}$$

The time evolution of $\langle \hat{N} \rangle$ follows from $[\hat{H}, \hat{N}] = 0$. If $\langle \hat{N} \rangle \gg 1$, then for most times t this leads to

$$|\langle \hat{x} \rangle(t)|^2 \gg \Delta x, \qquad |\langle \hat{p} \rangle(t)|^2 \gg \Delta p. \tag{2.26}$$

Hence a coherent state with large occupation number $\langle \hat{N} \rangle$ results in a quasiclassically behaving harmonic oscillator. Such type of coherent states are also called quasiclassical states.

2.3 Boson coherent states

Except some earlier applications in condensed matter [231–233] and quantum field theory [234–237], coherent states were actually not intensively studied until their first promising application to field theory [223, 224, 238–240] almost four decades after their first construction by Schrödinger.

Since then, coherent states and their many generalizations have been applied in different areas such as nuclear, atomic, and condensed matter physics, quantum field theory, path integral formulations and quantum information [227, 230, 241, 242]. We should note that different to the simple formulations proposed for light beams, many of the generalizations are generated by more involved composite operators [242].

The most celebrated application of coherent states is to the quantum electromagnetic field in field theory. These states constitute the basis of modern quantum optics [243, 244]. Due to their unique properties such as coherence, overcompleteness and intrinsic geometrization [230] coherent states are very powerful descriptions with many applications in particle physics [245].

Here, we particularly discuss the special photon coherent states in order to describe the electromagnetic field. Let us consider the n-th order correlation function of the electromagnetic field

$$G^n(x_1, \ldots, x_n, x_{n+1}, \ldots, x_{2n}) = \text{tr}\left(\hat{\rho}\hat{\mathbf{E}}^-(x_1)\cdots\hat{\mathbf{E}}^-(x_n)\hat{\mathbf{E}}^+(x_{n+1})\cdots\hat{\mathbf{E}}^+(x_{2n})\right).$$
$$(2.27)$$

According to Glauber [223, 224], optical coherence of the radiation field is given if all correlations satisfy the factorization condition

$$G^n(x_1, \ldots, x_n, x_{n+1}, \ldots, x_{2n}) = \mathbf{E}^*(x_1)\cdots\mathbf{E}^*(x_n)\mathbf{E}(x_{n+1})\cdots\mathbf{E}(x_{2n}). \qquad (2.28)$$

This means that all electric field operators must behave classically having eigenstates $|\Xi\rangle$ with the classical field variables as their eigenvalues,

$$\hat{\mathbf{E}}^+(x_i)|\Xi\rangle = \mathbf{E}(x_i)|\Xi\rangle,$$
$$\langle\Xi|\hat{\mathbf{E}}^-(x_j) = \langle\Xi|\mathbf{E}^*(x_j). \qquad (2.29)$$

Actually, this is a highly nontrivial property to fulfill on a pure quantum level. For the quantum harmonic oscillator these properties are satisfied by standard coherent states as introduced above reflected by the resulting minimal uncertainty relation (2.24). So the corresponding wave packets (2.13) governed by the Hamilton function of the harmonic oscillator follow classical trajectories without any spread in time.

Quantum fields by construction consist of an infinite number of harmonic oscillators. The Hamilton function of the classical electromagnetic field reads

$$H = \int d^3x \left[\mathbf{E}^2 + \mathbf{B}^2\right] \qquad (2.30)$$

where

$$\mathbf{E} = -\partial_t\mathbf{A},$$
$$\mathbf{B} = \nabla \times \mathbf{A} \qquad (2.31)$$

denote the electric and magnetic field, respectively. As usual, the corresponding photon field operator, $\hat{A}^\mu$, can be decomposed in terms of plane waves [246, 247]

$$\hat{A}^\mu(x) = \int \frac{d^3k}{\sqrt{(2\pi)^3}} \frac{1}{\sqrt{2|\mathbf{k}|}} \sum_{\lambda=1,2} \left(\hat{a}_k\epsilon_k^\mu e^{-ikx} + \hat{a}_k^\dagger\epsilon_k^{\mu*}e^{ikx}\right) \qquad (2.32)$$

with $\epsilon_k^* \cdot \epsilon_{k'} = -\delta_{kk'}$ [248–250]. The operator $\hat{a}_k$ ($\hat{a}_k^\dagger$) is the photon annihilator (creator) where k numbers the mode $(\mathbf{k}, \lambda)$ with wave vector $\mathbf{k}$ and polarization λ. In close analogy to the Hamilton operator for the single quantum harmonic oscillator in (2.8), here we have the following Hamilton operator

$$\hat{H} = \sum_k \omega_k \left(\hat{a}_k^\dagger \hat{a}_k + \frac{1}{2} \right). \tag{2.33}$$

Each of these individual modes correspond to the field photons. As a generalization of the coherent state in (2.13), the so-called photon or more general boson coherent state, respectively, describing the coherent electromagnetic field can be written as

$$
\begin{aligned}
|\{z_k\}\rangle &= \exp \left(\int d^3k \sum_\lambda z_k \hat{a}_k^\dagger - z_k^* \hat{a}_k \right) |\text{vac}\rangle \\
&= \exp \left(-\frac{1}{2} \int d^3k \sum_\lambda |z_k|^2 \right) \exp \left(\int d^3k \sum_\lambda z_k \hat{a}_k^\dagger \right) |\text{vac}\rangle
\end{aligned}
\tag{2.34}
$$

where $|\text{vac}\rangle$ stands for the vacuum state defined in the usual way by $\hat{a}_k|\text{vac}\rangle = 0$. The photon coherent state (2.34) is an eigenstate of the positive electric field operator [227],

$$\hat{\mathbf{E}}^+ |\{z_k\}\rangle = \mathbf{E}|\{z_k\}\rangle, \tag{2.35}$$

where

$$\mathbf{E}(x) = i \int \frac{d^3k}{\sqrt{(2\pi)^3}} \sqrt{\frac{\omega_k}{2}} \sum_\lambda z_k \vec{\epsilon}_k e^{-i(\omega_k t - \mathbf{k} \cdot \mathbf{x})}. \tag{2.36}$$

As for the standard coherent states, the photon coherent states are overcomplete and satisfy the following relation

$$\int \prod_k \frac{dz_k dz_k^*}{\pi} \, |\{z_k\}\rangle\langle\{z_k\}| = \mathbf{1}. \tag{2.37}$$

This is of course different from the usual completeness relation of states in Fock space $\mathcal{F} = \otimes_n \mathcal{H}_n$ as a direct sum of Hilbert spaces associated with each excitation. Together with the analyticity, the property of overcompleteness allows to expand the density operator $\hat{\rho}$ in diagonal form in terms of the photon coherent state,

$$\hat{\rho} = \int \prod_k dz_k dz_k^* \, P(\{z_k\}) |\{z_k\}\rangle\langle\{z_k\}|, \tag{2.38}$$

known as the so-called P-representation [223, 224]. Here, $P(z)$ is some weight function and the density operator trace reads

$$\text{tr}(\hat{\rho}) = \int \prod_k dz_k dz_k^* \, P(\{z_k\}) = \mathbf{1}. \tag{2.39}$$

According to the equations in (2.35), (2.38) and (2.39), the defining factorization condition for optical coherence in (2.28) is satisfied by the photon coherent states which have a well defined phase for each mode.

2.4   Vacuum expectation value and S-matrix

As we have discussed above, a coherent photon field can be described in terms of a photon coherent state $|\{z_k\}\rangle$ [223, 224]. The photon coherent state is generated by acting with the displacement operator

$$\hat{D}(z_k) = \int d^3k \sum_\lambda z_k \hat{a}_k^\dagger - z_k^* \hat{a}_k \tag{2.40}$$

on the vacuum state in Fock space, see equation (2.34), so that

$$|\{z_k\}\rangle = \hat{D}(z_k)|\text{vac}\rangle. \tag{2.41}$$

We note that $|\text{vac}\rangle$ is defined in the usual way

$$\hat{a}_k|\text{vac}\rangle = 0 \,\forall\, k \tag{2.42}$$

with $\langle\text{vac}|\text{vac}\rangle = 1$. The operator $\hat{a}_k$ is the photon annihilator where k numbers the corresponding mode. The photon field operator is given in equation (2.32) where the creation and annihilation operators obey the commutation relation

$$[\hat{a}_k, \hat{a}_{k'}^\dagger] = (2\pi)^3 \delta^3(\mathbf{k} - \mathbf{k}')\delta_{\lambda\lambda'}. \tag{2.43}$$

Let $\mathcal{A}^\mu(x)$ be some classical electromagnetic field associated with the photon coherent state denoted in the following as $|C\rangle$. As in the case of the photon field in (2.32), the electromagnetic field can be decomposed as [250, 251]

$$\mathcal{A}^\mu(x) = \int \frac{d^3k}{\sqrt{(2\pi)^3}} \frac{1}{\sqrt{2|\mathbf{k}|}} \sum_{\lambda=1,2} \left(\alpha_k \epsilon_k^\mu e^{-ikx} + \alpha_k^* \epsilon_k^{\mu*} e^{ikx} \right) \tag{2.44}$$

with $\alpha_k \equiv \alpha_\mu(k)$. The unitary displacement operator for constructing the corresponding photon coherent state becomes

$$\hat{D} = \exp\left(\sum_\lambda \int \frac{d^3k}{\sqrt{(2\pi)^3}} \frac{1}{\sqrt{2|\mathbf{k}|}} \left[\alpha_k a_k^\dagger - \alpha_k^* a_k \right] \right) \tag{2.45}$$

obtained after setting $(z_k, z_k^*) = \frac{(\alpha_k, \alpha_k^*)}{\sqrt{2(2\pi)^3|\mathbf{k}|}}$ in equation (2.40) which then leads to

$$\begin{aligned} \hat{D}^{-1}\hat{a}_k\hat{D} &= \hat{a}_k + \alpha_k, \\ \hat{D}^{-1}\hat{a}_k^\dagger\hat{D} &= \hat{a}_k^\dagger + \alpha_k^*. \end{aligned} \tag{2.46}$$

From the unitarity of $\hat{D}$ it follows that $\langle C|C \rangle = 1$, similar as for the standard vacuum state $|\text{vac}\rangle$. The commutation relations of the photon creation and annihilation operators introduced in (2.32) with $\hat{D}$ read

$$[\hat{a}_k, \hat{D}] = \alpha_k \hat{D},$$
$$[\hat{a}_k^\dagger, \hat{D}] = \alpha_k^* \hat{D}. \tag{2.47}$$

Computing the matrix element of the photon field operator in the presence of the photon coherent state, we find that $\hat{D}$ results in a shift of the photon field operator $\hat{A}^\mu$ such that the latter obtains a VEV,

$$\langle C|A^\mu(x)|C \rangle = \alpha^\mu(x) + \alpha^{\mu*}(x) \equiv \mathcal{A}^\mu(x), \tag{2.48}$$

giving rise to the classical electromagnetic field $\mathcal{A}^\mu$. Hence, the photon coherent state serves as the most classical state of the photon field which yields a simple correspondence between optical coherence and classical fields in QFT, see e.g. [225]. Assuming that the coherence is preserved during the interactions, we end up with the same coherent state on both sides of the S-matrix elements for any scattering process, so

$$\langle C|\dots|C \rangle = \langle \text{vac}|\hat{D}^{-1} \dots \hat{D}|\text{vac}\rangle. \tag{2.49}$$

Taking into account that $\hat{D}^{-1} A^\mu \hat{D} = A^\mu + \mathcal{A}^\mu$, we find that instead of considering interactions between photon coherent states we can shift the photon field operator by a *c*-number and consider S-matrix elements between vacuum states as in ordinary QFT [222].

Consider for instance the photon field interacting with a classical source described by the Lagrangian

$$\mathcal{L} = -\frac{1}{4}F_{\mu\nu}F^{\mu\nu} - A_\mu j^\mu. \tag{2.50}$$

The classical current shall be conserved, $\partial^\mu j_\mu = 0$. Using Lorenz gauge, $\partial_\mu A_\mu = 0$, the equation of motion for the photon field is [229]

$$\partial_\mu F^{\mu\nu} = \Box A^\nu = j^\nu \tag{2.51}$$

which has formal solution $A^\nu = \frac{1}{\Box} j^\nu$ where the inverse $\frac{1}{\Box}$ is called Green's function. The general solution is [252]

$$A^\mu(x) = A_0^\mu(x) + \int d^4y \; G(x-y) j^\mu(y). \tag{2.52}$$

$A_0^\mu(x)$ is the free field solution and [229, 250]

$$G(x, y) = G(x - y) = \frac{1}{(2\pi)^4} \int d^4y \, \frac{e^{-ip \cdot (x-y)}}{p^2 \pm i\epsilon} \tag{2.53}$$

is the Green's function obtained after Fourier expanding the initial equation

$$\Box_x G(x - y) = -\delta^{(4)}(x - y) \tag{2.54}$$

to in order to find $p^2 G(p) = 1$. Here, $\Box_x$ is the d'Alembert operator acting on x. Switching on the interaction adiabatically in a finite time duration, the general solution (2.52) can be written as

$$\begin{aligned} A^\mu(x) &= A_{\text{in}}^\mu(x) + \int d^4y \, G_{\text{ret}}(x - y) j^\mu(y) \\ &= A_{\text{out}}^\mu(x) + \int d^4y \, G_{\text{adv}}(x - y) j^\mu(y) \end{aligned} \tag{2.55}$$

where

$$G_{\substack{\text{ret} \\ \text{adv}}}(x - y) = \lim_{\epsilon \to 0} \frac{1}{(2\pi)^4} \int d^4p \, \frac{e^{-ip \cdot (x-y)}}{(p_0 \pm i\epsilon)^2 - \mathbf{p}^2} \tag{2.56}$$

denotes the $\substack{\text{retarded} \\ \text{advanced}}$ Green's function and $A_{\substack{\text{in} \\ \text{out}}}^\mu$ is the photon field $\substack{\text{before} \\ \text{after}}$ the interaction with the classical current. The corresponding in- and out-states, $|\text{in}\rangle$ and $|\text{out}\rangle$, respectively, form two complete sets of free states. So there has to exist a unitary[4] transformation $\mathbb{S}$ such that

$$A_{\text{out}}^\mu = \mathbb{S}^\dagger A_{\text{in}}^\mu \mathbb{S}, \qquad |\text{out}\rangle = \mathbb{S}^\dagger |\text{in}\rangle. \tag{2.57}$$

As usual, $\mathbb{S}$ is called the S-matrix. From the solutions in (2.55) we get

$$A_{\text{out}}^\mu(x) = A_{\text{in}}^\mu(x) + \mathcal{A}^\mu(x) \tag{2.58}$$

where, noting that $G_{\text{ret}} - G_{\text{adv}} = G$,

$$\mathcal{A}^\mu(x) = \int d^4y \, [G_{\text{ret}}(x - y) - G_{\text{adv}}(x - y)] \, j^\mu(y) \tag{2.59}$$

corresponds to the classical field generated by the classical current j^μ. The S-matrix can be written as

$$\mathbb{S} = \exp\left(-i \int d^4x \, A_{\text{out}} \cdot j(x)\right) = \exp\left(-i \int d^4x \, A_{\text{in}} \cdot j(x)\right) \tag{2.60}$$

---

[4] See section 3.1 for more on unitarity.

such that the final state after the interaction of the photon field A^μ with the classical current $j^\mu(x)$ becomes, see equation (2.57),

$$|\text{out}\rangle = \exp\left(i\int d^4x \; A_{\text{in}}(x)\cdot j(x)\right)|\text{in}\rangle. \tag{2.61}$$

Fourier expanding the photon field operator as in (2.32) and setting

$$z_k = \epsilon_k \cdot \widetilde{j}(k), \tag{2.62}$$

where $\widetilde{j}(k)$ denotes the Fourier transform of $j(x)$, the final state can be expressed as

$$|\text{out}\rangle = \exp\left(-\frac{1}{2}\int d^3k \sum_\lambda |z_k|^2\right)\exp\left(\int d^3k \sum_\lambda z_k \hat{a}_k^\dagger\right)|\text{in}\rangle. \tag{2.63}$$

As we can easily see, this equals to the introduced photon coherent state from (2.34) after setting $|\text{in}\rangle = |\text{vac}\rangle$. Hence, as discussed above, the final state after the interaction of the photon field with a classical current, here associated with the classical background field $\mathcal{A}^\mu$, becomes a photon coherent state.

2.5 Path integral and coherent states

When quantum fields interact with each other the situation changes and one generally does not end up with a coherent state as a final state. In the following, we will see that in such cases coherent states can be used to derive the path integral. As we have discussed, standard coherent states are special states which, in addition to their minimal position and momentum uncertainty, are overcomplete fulfilling the condition (2.21). The analogous relation for the overcomplete photon coherent states is (2.37). Here, we discuss how the quantum mechanical path integral directly arises from the coherent state. Consider the standard evolution operator in quantum mechanics

$$\hat{U}(t_f, t_i) = e^{-i\hat{H}(t_f - t_i)}. \tag{2.64}$$

Formally, the matrix element of the evolution operator is

$$\langle x_f(t_f)|x_i(t_i)\rangle = \langle x_f|\hat{U}(t_f, t_i)|x_i\rangle. \tag{2.65}$$

The set of position states, $\{|x\rangle\}$, build up a complete set. Hence, the states obey the completeness condition

$$\int dx \; |x\rangle\langle x| = \mathbf{1}. \tag{2.66}$$

These form in contrast to the coherent state $|z\rangle$ an orthonormal basis, i.e. $\langle x'|x\rangle = \delta(x' - x)$. Inserting the resolution of the identity in (2.66), many times between each of the factors in the matrix element from above, we may write the formal integral

$$
\langle x_f(t_f)|x_i(t_i)\rangle = \int dx_1 \ldots dx_N \, \langle x_f, t_f|x_N, t_N\rangle
$$
$$
\times \ldots \times \langle x_N, t_N|x_{N-1}, t_{N-1}\rangle \ldots \langle x_1, t_1|x_i, t_i\rangle.
$$
(2.67)

Taking the finite time interval $|t_f - t_i|$ to be fixed, in the limit $N \to \infty$ the discretized time interval $\tau \equiv t_j - t_{j-1}$ becomes infinitesimally small. Hence, we can write approximately

$$
\langle x_j, t_j|x_{j-1}, t_{j-1}\rangle \approx \delta(x_j - x_{j-1}) - i\tau \langle x_j|\hat{H}|x_{j-1}\rangle + \mathcal{O}(\tau^2)
$$
(2.68)

which is exact for $N \to \infty$. Next, we additionally introduce the complete set of momentum states $\{|p\rangle\}$ and analogously the associated condition

$$
\int \frac{dp}{2\pi} \, |p\rangle\langle p| = \mathbf{1}
$$
(2.69)

where $\langle x|p\rangle = e^{ipx}$ holds as usual. For instance, using the Hamilton function introduced in section 2.2, the matrix elements on the right-hand side of equation (2.68) read

$$
\langle x_j|\hat{H}|x_{j-1}\rangle = \int \frac{dp}{2\pi} e^{ip(x_j - x_{j-1})} \left[\frac{p^2}{2m} + V(x_j) \right].
$$
(2.70)

Approximating up to the order $\mathcal{O}(\tau^2)$, we can also write (2.68) as

$$
\langle x_j, t_j|x_{j-1}, t_{j-1}\rangle \approx \int \frac{dp}{2\pi} e^{ip(x_j - x_{j-1}) - \tau H\left(p, \frac{x_j + x_{j-1}}{2}\right)},
$$
(2.71)

where we have used $x_j \to \frac{x_j + x_{j-1}}{2}$ in $H(p, x)$. Inserting the expressions in (2.68) and (2.71) into the integral (2.67), we find for the original matrix element

$$
\langle x_f(t_f)|x_i(t_i)\rangle = \lim_{N \to \infty} \int \prod_{j=1}^{N} dx_j \int \prod_{j=1}^{N+1} \frac{dp_j}{2\pi}
$$
$$
\times \exp\left(i \sum_{j=1}^{N+1} p_j(x_j - x_{j-1}) - \tau H\left(p_j, \frac{x_j + x_{j-1}}{2}\right) \right).
$$
(2.72)

In the limit $N \to \infty$, we can formally write the latter as

$$
\langle x_f(t_f)|x_i(t_i)\rangle = \int \mathcal{D}p \mathcal{D}x \, \exp\left(i \int_{t_i}^{t_f} dt \, L(p, x) \right)
$$
(2.73)

with the Lagrange function

$$L(p,x) = p\dot{x} - H(p,x) \tag{2.74}$$

and the integration measure

$$\mathcal{D}p\mathcal{D}x \equiv \lim_{N\to\infty} \prod_{j=1}^{N} \frac{dp_j dx_j}{2\pi}. \tag{2.75}$$

The configuration $(x(t), p(t))$ has to satisfy the conditions $x(t_i) = x_i$ and $x(t_f) = x_f$. There are no initial and final conditions for the momenta, since the states have well defined positions. Hence, the matrix element is expressed as a sum over different histories in phase space weighted by an exponential factor $\exp(\int dt\ L)$. For the matrix element, we may write in compact form

$$\langle x_f(t_f)|x_i(t_i)\rangle = \int \mathcal{D}p\mathcal{D}x\ e^{i\mathcal{S}(,x,p)} \tag{2.76}$$

where $\mathcal{S}$ is the action of each history $(x(t), p(t))$ which do not need to satisfy any condition such as the equations of motion. The only exceptions are the mentioned initial and final conditions. The expression in (2.76) is the standard path integral. The latter can be brought into a simpler form. Namely, assuming that the kinetic energy is quadratic in the momenta, we can explicitly integrate out the momenta in the path integral, simply, due to its Gaussian form.[5] Then, the result depends only on histories of the space coordinate. This is known as the Feynman path integral written as

$$\langle x_f(t_f)|x_i(t_i)\rangle = \int \mathcal{D}x\ \exp\left(i \int_{t_i}^{t_f} dt\ L(x,\dot{x})\right) \tag{2.77}$$

where

$$L(x,\dot{x}) = \frac{m\dot{x}^2}{2} - V(x). \tag{2.78}$$

Accordingly, in the classical limit there is only one contributing path, $x_c(t)$, on which the action is stationary, $\delta\mathcal{S} = 0$. This is known as the least action principle. The stationary path x_c solves the classical Euler-Lagrange equation (ELE),

$$\frac{\partial L}{\partial x} - \frac{d}{dt}\frac{\partial L}{\partial \dot{x}} = 0. \tag{2.79}$$

---

[5] Here, we use the following result

$$\int \frac{dp}{2\pi} \exp\left(i\left(p\dot{x} - \frac{p^2}{2m}\right)\tau\right) = \sqrt{\frac{m}{2\pi i\tau}} \exp\left(\frac{i\tau\dot{x}^2}{2}\right).$$

Now the path integral in (2.73) can be derived in an alternative way. Namely, instead of using the complete basis of position states satisfying the condition (2.66), we can resolve the identity using the coherent states. For these, we insert the corresponding completeness relation (2.21) between the factors in the following matrix element

$$\langle z_f(t_f)|z_i(t_i)\rangle = \langle z_f|\hat{U}(t_f, t_i)|z_i\rangle. \tag{2.80}$$

Taking into account that

$$\frac{dz\,dz^*}{\pi} = \frac{2d\Re(z)\,d\Im(z)}{\pi} \tag{2.81}$$

and setting

$$z = \frac{x + ip}{\sqrt{2}} \equiv \hat{a}, \qquad z^* = \frac{x - ip}{\sqrt{2}} \equiv \hat{a}^\dagger \tag{2.82}$$

where $\omega m = 1$, see operators in (2.6), it can be shown that [253]

$$\langle z_f(t_f)|z_i(t_i)\rangle = \int \mathcal{D}p\mathcal{D}x \,\exp\left(i\int_{t_i}^{t_f} dt\, L(x(t), p(t))\right) \tag{2.83}$$

where

$$L(p, x) = \langle z|id/dt|z\rangle - \langle z|H|z\rangle = \frac{1}{2}\left(p\dot{x} - x\dot{p}\right) - H(p, x). \tag{2.84}$$

Thus, using the coherent state one automatically arrives at the quantum mechanical path integral introduced above.

Similarly, one can derive the path integral in field theory by defining the corresponding boson coherent state. For including fermion fields as well, it is necessary to introduce a fermion coherent state which has to be the eigenstate for the fermionic annihilation operator

$$\hat{a}_i|\theta\rangle = \theta_i|\theta\rangle. \tag{2.85}$$

Here θ_i represents a Grassmann variable, see section 4.2.3. For instance, satisfying the underlying properties, the associated coherent state can explicitly be written as

$$|\theta\rangle = \exp\left(\sum_i \theta_i\hat{a}_i^\dagger - \theta_i^*\hat{a}_i\right) = \exp\left(-\frac{1}{2}\sum_i \theta_i^*\theta_i\right)\exp\left(\theta_i\hat{a}_i^\dagger\right)|0\rangle. \tag{2.86}$$

2.6 Strong field sources

2.6.1 Lasers

Modern optical lasers can be used to generate strong electromagnetic fields. For instance, intensities of the order $I = 2 \times 10^{22}$ W/cm^2 have already been achieved with the HERCULES laser [254]. More intense petawatt (10^{15} W) or even exawatt (10^{18} W) lasers such as the Extreme Light Infrastructure (ELI) will be ready within the next couple of years [255]. These would exceed intensities of the order $I \sim 10^{25}$ W/cm^2 corresponding to field strengths $E \simeq 10^{-3} E_{\mathrm{S}}$ which may shed light on the nonlinear regime in QED.[6] Such high intense lasers operate in form of pulsed beams with very short duration in the range of a few up to tens femtoseconds.

Another promising source for strong electromagnetic fields are free electron lasers with coherent light sources having wavelengths in the X-ray regime. For these high frequent lasers, the output power is several orders of magnitude smaller than for the mentioned lasers with optical frequencies. However, their short wavelength allows a smaller diffraction limited focus which makes it possible to generate higher peak fields. For the European X-Ray Free-Electron Laser (XFEL) the field strength is of the order $E \simeq 10^{17}$ V/m [25, 26, 256].

A typical optical petawatt laser has an energy of the order 100 J which corresponds to a total number of $\sim 10^{20}$ photons. This is sufficient for fundamental QED processes. At intensities $I \simeq 10^{22}$ W/cm^2, it is expected that roughly 10^{15} photons will be absorbed from the strong field [83]. This is just a tiny portion of the value from above which justifies the expectation of an unaffected field that can be considered as a fixed background.

2.6.2 Astrophysical objects

On astrophysical scales there exist objects which naturally have extremely super strong field environments. The most known one are pulsars [257]. These are rotating neutron stars which periodically emit electromagnetic radiation. They

---

[6] The critical value $B_{\mathrm{cr}} = 4.41 \times 10^{22}$ T corresponds to the magnetic field strength at which the electron Landau levels have an energy gap equal to the electron's rest mass. The associated intensity with E_{S} and B_{cr} is $I = 2.32 \times 10^{29}$ W/cm^2.

can have surface magnetic fields of the order of $B \simeq 10^8$ T which almost reach the critical limit. Much larger field strengths, namely exceeding the critical value at orders $B \simeq 10^{11}$ T, are possible for so-called magnetars [258, 259]. There are many other sources like black holes, active galactic nuclei and gamma ray bursts [260] that may generate super strong electromagnetic fields as well.

2.6.3   Linear colliders

An electron-positron linear collider (LC) may be very important in electroweak precision physics and Higgs phenomenology. In particular, these facilities are very important for BSM physics. In contrast to the LHC, a LC is able to produce a clean environment in the lepton beam interaction point (IP) [261]. The LHC strikingly suffers from QCD background processes, since the colliding particles are protons which are composite objects build up by gluons and quarks; so-called partons. Using an appropriate parton distribution function (PDF) allows to model the internal structure of protons which is not known exactly. At the LC a main background process is beamstrahlung caused due to the radiating electrons and positrons in the electromagnetic field of the oncoming particle bunch. Indeed, the colliding particles at the IP will see a strong external electromagnetic field generated by the superposition of the collective fields originating from the two beams. In particular, each colliding, boosted, particle will see the field originated by the opposing bunch. This macroscopically extended field can be approximated as a static strong background [262].

In order to probe the high precision frontier at a future LC, particularly needed for BSM physics, a very high luminosity is required. The achievable values are expected to be very high compared to the LHC, namely of orders of 10^{-34} up to 10^{-35} cm^{-2}s^{-1}. In order to reach these intense values, the denseness of the colliding bunches have to be very high. This leads to the presence of very strong background fields in the rest frame of the oncoming bunch particles which may approach the critical field strength $E_{\rm S}$. Thus, several fundamental processes such as Breit-Wheeler ($\gamma + \gamma \rightarrow e^- + e^+$), Bethe-Heitler ($\gamma + e^{\mp} \rightarrow e^{\mp} + e^- + e^+$) as well as pair creation à la Schwinger mechanism may take place in such strong environments. This can result in significant depletion effects of the initial beams at their collision time [263].

2.6.4 Relativistic heavy ion collisions

Heavy nuclei with a large charge number generate very strong Coulomb fields in their vicinity. For instance, based on the corresponding assumptions, the point at which the $1s$ electron wave function joins the negative energy continuum has been approximated as $Z_\mathrm{c} \approx 173$ [264]. A single stable nucleus with such a high charge number is not known. The critical number Z_c is believed to be realizable in relativistic heavy ion collision experiments. There, the electron dynamics can be considered as much faster than the dynamics of the colliding nuclei. This may lead to the formation of some kind of quasimolecules with charge numbers $Z > Z_\mathrm{c}$ leading to pair production [265, 266].

A QCD analog to the original Schwinger effect in QED may be realizable at the RHIC or at the LHC during the formation of the so-called Quark Gluon Plasma (QGP). Namely, one possible way to describe the formation of this nonequilibrium process is to consider the colliding heavy ion nuclei as traversing through each other such that a chromoelectric flux tube is created that can be broken up against the production of quark-antiquark pairs [60]. Despite the shortcomings for this phenomenological model, one may expect that a non-Abelian chromoelectric field can have similar effects as its Abelian counterpart [267].

Chapter 3

Vacuum decay

3.1 Unitarity

U NITARITY is fundamental for any physical local QFT. The assumption that nothing can be produced or just disappear without external influences requires unitarity. It can be understood as the conservation of probabilities in the underlying quantum system and dictates how states in the Hilbert space transform in unitary representations of the Poincaré group. Since the S-matrix has to be unitary, the latter also constraints how and which interactions take place in a physical QFT. Single and multi particle states being eigenstates of the momentum operator transform in the usual four vector representation of the Lorentz group. The former type of states transform under the irreducible unitary representations of this group as well. For the multi particle state the relevant transformations are the one for the particles in that state. The ground state in QFT is assumed to be Lorentz invariant.

The Hilbert space, $\mathcal{H}$, has the property of completeness. For the sum over single and multi particle states $|X\rangle$ this simply means that [229]

$$\sum_X d\Pi_X \, |X\rangle\langle X| = \mathbf{1} \tag{3.1}$$

where

$$d\Pi_X = \prod_{s \in X} \frac{d^3 p_s}{(2\pi)^3} \frac{1}{2E_s}. \tag{3.2}$$

The latter integration measure is related to the Lorentz invariant phase space

(LIPS) measure

$$d\Pi_{\text{LIPS}} = (2\pi)^4 \delta^4 \left(\sum p \right) d\Pi_X. \tag{3.3}$$

Hence, for the completeness relation in equation (3.1) all states need to be included. This is a direct consequence of demanding unitarity in QFT.

3.2 Optical theorem

In the following, we discuss the optical theorem which is powerful in relating cross sections and the imaginary part of the scattering amplitudes in a nonperturbative fashion.

3.2.1 Generalized version

In perturbation theory, the optical theorem can relate loops to tree level diagrams [229, 247]. Since loop diagrams are higher order quantum corrections, the optical theorem elucidates in an elegant way that higher order quantum corrections must be determined by more classical tree level cross sections. This is a direct consequence of unitarity.

Let $|\Psi; t\rangle$ be a state in the Schrödinger picture. As we have discussed in section 3.1, the norm of such a state has to be the same at any time t, so we write

$$\langle \Psi; t | \Psi; t \rangle = \langle \Psi; 0 | \Psi; 0 \rangle \tag{3.4}$$

where [250]

$$|\Psi; t\rangle = e^{-iHt} |\Psi; 0\rangle. \tag{3.5}$$

Since the Hamilton function H has to be unitary, i.e. $H^\dagger = H$, this implies for the S-matrix

$$\mathbb{S} = e^{-iHt} \tag{3.6}$$

unitarity as well, that is

$$\mathbb{S}^\dagger \mathbb{S} = \mathbf{1}. \tag{3.7}$$

The general definition for the S-matrix elements can be obtained from

$$\langle f|\mathbb{T}|i\rangle = (2\pi)^4\delta^4(p_i - p_f)\mathcal{M}_{i\to f} \tag{3.8}$$

where $|f\rangle$ and $|i\rangle$ denote some final and initial state, respectively. The transfer matrix $\mathbb{T}$ is related to the S-matrix according to

$$\mathbb{S} = \mathbf{1} + i\mathbb{T}. \tag{3.9}$$

Due to the condition (3.7), we get

$$i(\mathbb{T}^\dagger - \mathbb{T}) = \mathbb{T}^\dagger\mathbb{T} \tag{3.10}$$

which results in

$$\langle f|i(\mathbb{T}^\dagger - \mathbb{T})|i\rangle = i(2\pi)^4\delta^4(p_i - p_f)\left[\mathcal{M}^*_{f\to i} - \mathcal{M}_{i\to f}\right]. \tag{3.11}$$

On the other hand, using the completeness relation in equation (3.1) we can write

$$\langle f|\mathbb{T}^\dagger\mathbb{T}|i\rangle = \sum_X \int d\Pi_X \ \langle f|\mathbb{T}^\dagger|X\rangle\langle X|\mathbb{T}|i\rangle. \tag{3.12}$$

Using the unitarity condition from equation (3.10) brings us to the generalized optical theorem

$$\mathcal{M}_{i\to f} - \mathcal{M}^*_{f\to i} = \sum_X \int d\Pi_X \ i(2\pi)^4\delta^4(p_i - p_X)\mathcal{M}_{i\to X}\mathcal{M}^*_{f\to X}. \tag{3.13}$$

3.2.2 Special version

The left-hand side of the generalized optical theorem (3.13) has linear dependence on matrix elements whereas the right-hand side has quadratic dependence. Noticing that the optical theorem holds for all orders in perturbation theory, shows that the imaginary parts of loops are actually determined by tree level diagrams. For instance, assuming $|i\rangle = |f\rangle = |A\rangle$ where $|A\rangle$ shall be some particle state, one obtains from the general theorem in equation (3.13)

$$2i\Im(\mathcal{M}_{A\to A}) = i\sum_X \int d\Pi_X \ (2\pi)^4\delta^4(p_A - p_X)|\mathcal{M}_{A\to X}|^2. \tag{3.14}$$

Let $|A\rangle$ be a single particle state. Then the decay rate is [229]

$$\mathcal{R}_{A\to X} = \frac{1}{2m_A}\int d\Pi_X \ (2\pi)^4\delta^4(p_A - p_X)|\mathcal{M}_{A\to X}|^2. \tag{3.15}$$

So what follows is the relation

$$\Im\left(\mathcal{M}_{A\to A}\right) = m_A \sum_X \mathcal{R}_{A\to X} = m_A \mathcal{R}_{\mathrm{tot}} \tag{3.16}$$

where $\mathcal{R}_{\mathrm{tot}}$ is the decay rate of $|A\rangle$ being equal to the inverse of the lifetime of the initial state.

Instead, if $|A\rangle$ is assumed to be a two particle state, the cross section in the center of mass (CM) frame is

$$\sigma_{A\to X} = \frac{1}{4 E_{\mathrm{CM}} |\mathbf{p}_i|} \int d\Pi_X \ (2\pi)^4 \delta^4(p_A - p_X) |\mathcal{M}_{A\to X}|^2 \tag{3.17}$$

where E_{CM} is the energy in the CM frame. From this, one arrives at the following relation

$$\Im\left(\mathcal{M}_{A\to A}\right) = 2 E_{\mathrm{CM}} |\mathbf{p}_i| \sum_X \sigma_{A\to X} \tag{3.18}$$

which is known as the special optical theorem.

3.3   Vacuum decay rate

In the presence of a strong static electric background the quantum vacuum decays against matter-antimatter pairs [268–270]; this is the standard Schwinger mechanism. It is a nonperturbative absorptive process which requires the full coupling to the electric background, see section 3.4.2 for more regarding the nonperturbative character. At leading order, the Schwinger effect is determined by the one-loop EH effective action[1] which is valid for energy scales much below the high energy degrees of freedom of the underlying theory and hence manifests itself as a low energy EFT [135, 271]. In QED, the high energy degrees of freedom are the massive electron and positron fields.

On the other hand, we may ask why pair production is determined by some effective action for which the particle field is integrated out and therefore not present?

---

[1] In general, as we will see later in chapter 5, the leading order instanton contribution is referred to as the VPP rate which involves just a tiny portion of the whole information which is basically included in the total vacuum decay rate from equation (3.22). The latter is not necessarily restricted to the one-loop EH effective action. Actually, it involves an infinite number of vacuum diagrams accounting for all permitted combinations of particle loops and gauge boson lines.

The reason lies in the unitary construction of any physical QFT as described above.

Let us recall the optical theorem in equation (3.14) written in the form

$$\text{Im}\mathcal{M}_{A \to A} = \sum_X d\Pi^X_{\text{LIPS}} |\mathcal{M}_{A \to X}|^2. \tag{3.19}$$

Assuming that the initial state corresponds to a strong external background consisting of a huge number of coherently accumulated low energy photons described by some photon coherent state, $|A\rangle \equiv |C\rangle$, see section 2.4, the left-hand side is in both full QED and EFT the same. However, the right-hand side would differ if the mentioned degrees of freedom are integrated out. Hence, the EFT approach turns out to be nonunitary, a sign for the instability against pair production. However, this basically makes the direct application of the optical theorem unsuitable, since one strictly would need to sum over an infinite number of multi particle states [229] which clearly reveals the immense amount of related subprocesses.

An alternative approach works as follows: if $|A\rangle$ remains unchanged, this corresponds to the situation where no pairs are produced and the initial state corresponds to the final state. This can simply be written as

$$\langle A|\mathbb{S}|A\rangle = \langle 0|\mathbb{S}_{\mathcal{A}}|0\rangle = 1 \tag{3.20}$$

where the dressed S-matrix reads $\mathbb{S}_{\mathcal{A}} = e^{i\Gamma[\mathcal{A}]}$. The EH effective action Γ is obtained after integrating out the high energy degrees of freedom. Since it is just a number for some given external background, the probability that no pair production occurs follows from the modulo squared vacuum to vacuum transition amplitude

$$|\langle 0|0\rangle|^2 := |\langle A|\mathbb{S}|A\rangle|^2 = |e^{i\Gamma[\mathcal{A}]}|^2 = \exp\left(-2VT\Im(\mathcal{L}_{\text{eff}})\right) \tag{3.21}$$

with $\Im(\mathcal{L}_{\text{eff}})$ denoting the imaginary part of the effective Lagrangian [270, 272]. Here, it has been assumed that $|0\rangle \equiv |0_{\text{out}}\rangle = |0_{\text{in}}\rangle$. Taking into account that the effective action Γ is generally small for backgrounds in the nonperturbative regime, the probability for vacuum decay against the production of any number of pairs is

$$\mathcal{P} = 1 - |\langle 0|0\rangle|^2 = 1 - e^{-2\mathcal{R}} \approx 2\mathcal{R} \tag{3.22}$$

with the corresponding vacuum decay rate

$$\mathcal{R} = \Im(\Gamma). \tag{3.23}$$

This basically corresponds to the continuum field version of the optical theorem introduced in equation (3.16). We should note that in most cases we will restrict ourselves to the one-loop EH effective action which we call Γ_{EH}.

As demanded, the EH effective action only depends on the electromagnetic background. Formally, the general (not necessarily one-loop) EH effective action $\Gamma[\mathcal{A}]$ can be defined according to

$$\int \mathcal{DA} \, \exp\left(i\Gamma\right) = \int \mathcal{DADADF} \, \exp\left(i \int d^4x \, \mathcal{L}\right), \qquad (3.24)$$

writing $\mathcal{DF} := \mathcal{D}\bar{\psi}\mathcal{D}\psi$ in QED and $\mathcal{DF} := \mathcal{D}\bar{\phi}\mathcal{D}\phi$ in the scalar case. Here, $\mathcal{L}$ denotes the full Lagrangian of the theory under consideration.

We keep all diagrams with a single particle loop and drop off all higher loop contributions, see figure 3.1. In other words, we ignore the dynamical gauge field contribution and therefore all correlations between particle loops connected by photon lines, see equations (3.40) and (3.44). As will be used later, this approach is sufficient in the weak field limit due to strong exponential suppression of higher order vacuum diagrams.

Notably, including additional photon exchanges within the single particle loop results in the all-loop quenched vacuum diagram, see e.g. [158, 273, 274]. We will be mostly focusing on the leading single particle loop contribution without internal photon lines determined by the one-loop EH effective action Γ_{EH}.

Performing the standard Gaussian integrations, Γ_{EH} can most compactly be written as

$$\Gamma_{\text{EH}} = \ln \text{Det}(i\slashed{D} - m) \qquad (3.25)$$

in the spinor case

$$\Gamma_{\text{EH}} = \ln \text{Det}(D^2 - m^2) \qquad (3.26)$$

in the scalar case. $D^\mu = \partial^\mu - ie\mathcal{A}^\mu$ denotes the covariant derivative and $\slashed{D} = \gamma_\mu D^\mu$, where γ^μ are the Dirac gamma matrices in relativistic quantum mechanics [270–272].

The formal representations for one-loop EH effective actions in (3.25) and (3.26) can be developed in a perturbative expansion in powers of the external background field $\mathcal{A}^\mu$. As shown first by Euler and Heisenberg for QED [275] and by Weisskopf for scalar Quantum Electrodynamics (sQED) [276], in case of an external background where $\mathcal{F}_{\mu\nu}$ is assumed to be constant, it is possible to derive closed form expressions which generate all perturbative orders.

Before we continue with the sketch of Schwinger's original proper time approach to the problem, it should be noted that in addition to the decay of the quantum vacuum in a strong background field, the EH effective action has many other interesting applications as for instance: derivation of the QED β-function, chiral anomaly, and the low energy limit for n photon scattering including the light by light scattering cross section [135, 277, 278].

3.4   One-loop EH effective Lagrangian in static background

In this section, we sketch the original derivation of the one-loop EH effective action in a static external background based on the proper time formulation.

3.4.1   Proper time approach

3.4.1.1   Notion of time

Before we start with the actual calculation, let us first discuss the notion of proper time. The key ingredient we need is the identity

$$\frac{i}{A + i\epsilon} = \int_0^\infty ds \; e^{is(A+i\epsilon)} \tag{3.27}$$

where $A \in \mathbb{R}$ and $\epsilon > 0$. Using (3.27), the Feynman propagator for a scalar field with mass m can be written as

$$D_F(x, y) = \int \frac{d^4 p}{(2\pi)^4} \frac{i e^{ip(x-y)}}{p^2 - m^2 + i\epsilon} = \int \frac{d^4 p}{(2\pi)^4} e^{ip(x-y)} \int_0^\infty ds \; e^{is(p^2 - m^2 + i\epsilon)}. \tag{3.28}$$

The Gaussian momentum integral can be done exactly

$$D_F(x, y) = \frac{-i}{16\pi} \int_0^\infty \frac{ds}{s^2} \; \exp\left(-i\left[\frac{(x-y)^2}{4s} + sm^2 - i\epsilon s\right]\right). \tag{3.29}$$

For the massless case the result reads

$$D_F(x, y) = -\frac{1}{4\pi^2} \frac{1}{(x-y)^2 - i\epsilon}. \tag{3.30}$$

An alternative way to integrate over p can be followed by resorting to standard quantum mechanics. Consider a one particle Hilbert space spanned by the state $|x\rangle$ such that $\langle p|x\rangle = e^{ipx}$ [251]. Inserting the latter into (3.28), we get

$$D_F(x, y) = \int \frac{d^4p}{(2\pi)^4} \langle y|p\rangle\langle p|x\rangle \int_0^\infty ds\ e^{is(p^2 - m^2 + i\epsilon)}. \tag{3.31}$$

Now, introducing $\hat{p}^\mu|p\rangle = p^\mu|p\rangle$ and taking $\hat{H} = -\hat{p}^2$ as an Hamilton operator, we end up with

$$e^{isp^2}\langle p|x\rangle = \langle p|e^{-is\hat{H}}|x\rangle. \tag{3.32}$$

Hence, inserting the latter into equation (3.31),

$$\langle y|p\rangle e^{isp^2}\langle p|x\rangle = \langle y|p\rangle\langle p|e^{-is\hat{H}}|x\rangle, \tag{3.33}$$

we get

$$D_F(x, y) = \langle y|\hat{G}|x\rangle = \int_0^\infty ds\ e^{-s\epsilon} e^{-ism^2}\langle y; 0|x; s\rangle \tag{3.34}$$

after using the completeness relation for $|p\rangle$. Here, we have introduced the notation

$$\langle y; 0|x; s\rangle \equiv \langle y|e^{-is\hat{H}}|x\rangle. \tag{3.35}$$

The operator $\hat{G}$ in equation (3.34) denotes the Green's function operator in terms of $\hat{p}^\mu$ and $\hat{x}^\mu$. Hence, interpreting s as some time variable, the obtained propagator can be understood as the amplitude for a propagating particle from x to y in proper time s integrated over s.

3.4.1.2 Background dependent expectation value

Let us first elaborate the expectation value in the presence of the external background $\mathcal{A}^\mu$. In the following, we particularly focus on the fermionic case. The QED Lagrangian reads

$$\mathcal{L} = -\frac{1}{4}\mathcal{F}_{\mu\nu}^2 + \bar{\psi}(i\slashed{\partial} - m)\psi - e\mathcal{A}_\mu\bar{\psi}\gamma^\mu\psi. \tag{3.36}$$

The dynamical gauge field A^μ can be simply inserted by adding an additional term $-\frac{1}{4}F_{\mu\nu}^2$ and coupling A^μ to the current $J^\mu \equiv \bar{\psi}\gamma^\mu\psi$. For the one-loop EH

effective Lagrangian these contributions will be neglected. Now, to integrate out the irrelevant degrees of freedom, we replace the corresponding fields by their expectation value. To this end, we will replace the current J^μ coupled to $\mathcal{A}^\mu$ by its expectation value in the presence of the background. This leads to an effective Lagrangian of the form

$$\mathcal{L}_{\text{eff}} = -\frac{1}{4}\mathcal{F}_{\mu\nu}^2 - e\mathcal{A}_\mu J^\mu_{|C\rangle} \tag{3.37}$$

with $J^\mu_{|C\rangle} := \langle C|J^\mu|C\rangle$ being the VEV of the current in the presence of the photon coherent state $|C\rangle$, see again section 2.4. Using the proper time approach and the dressed spinor Green's function operator [229], i.e.

$$\hat{G}_\mathcal{A} = \frac{i}{\not{\hat{p}} - e\not{\mathcal{A}}(\hat{x}) - m + i\epsilon}, \tag{3.38}$$

we obtain the corresponding propagator,[2]

$$G_\mathcal{A}(x,y) = \langle y|\hat{G}_\mathcal{A}|x\rangle = \int ds \; e^{-s\epsilon}e^{-ism^2}\langle y|(\not{\hat{p}} - e\not{\mathcal{A}}(\hat{x}) + m)e^{-i\hat{H}s}|x\rangle. \tag{3.39}$$

The EH effective Lagrangian, as we demand, only depends on the background $\mathcal{A}^\mu$,

$$\mathcal{L}_{\text{eff}} = -\frac{1}{4}\mathcal{F}_{\mu\nu}^2 + \frac{i}{2}\int_0^\infty \frac{ds}{s}\; e^{-s\epsilon}e^{-ism^2}\text{Tr}\langle x|e^{-i\hat{H}s}|x\rangle \tag{3.40}$$

where $\text{Tr}(\cdots)$ denotes the Dirac trace and

$$\hat{H} = -(\hat{p}^\mu - e\mathcal{A}^\mu(\hat{x}))^2 + \frac{e}{2}\mathcal{F}_{\mu\nu}(\hat{x})\sigma^{\mu\nu} \tag{3.41}$$

is the associated Hamilton function operator.

For the scalar case the Green's function operator is [229]

$$\hat{G}_\mathcal{A} = \frac{i}{(\hat{p} - e\mathcal{A}(\hat{x}))^2 - m^2 + i\epsilon} \tag{3.42}$$

leading to the corresponding propagator

$$G_\mathcal{A}(x,y) = \langle y|\hat{G}_\mathcal{A}|x\rangle = \int ds \; e^{-s\epsilon}e^{-ism^2}\langle y|e^{-i\hat{H}s}|x\rangle. \tag{3.43}$$

---

[2] Note that the prefactor $(\not{\hat{p}} - e\not{\mathcal{A}}(\hat{x}) + m)$ in front of the exponential occurs due to rewriting the Green's function operator as

$$\hat{G}_\mathcal{A} = \frac{i}{\not{\hat{p}} - e\not{\mathcal{A}}(\hat{x}) - m + i\epsilon} = (\not{\hat{p}} - e\not{\mathcal{A}}(\hat{x}) + m)\frac{i}{(\hat{p}^\mu - e\mathcal{A}^\mu(\hat{x}))^2 - \frac{e}{2}F_{\mu\nu}(\hat{x})\sigma^{\mu\nu} - m^2 + i\epsilon}.$$

Thus, the analogous expression for the one-loop EH effective Lagrangian in sQED is

$$\mathcal{L}_{\text{eff}} = -\frac{1}{4}\mathcal{F}_{\mu\nu}^2 - i \int_0^\infty \frac{ds}{s} \; e^{-s\epsilon} e^{-ism^2} \langle x|e^{-i\hat{H}s}|x\rangle \tag{3.44}$$

where

$$\hat{H} = -(\hat{p}^\mu - e\mathcal{A}^\mu(\hat{x}))^2. \tag{3.45}$$

Note the sign change in front of the integrals in equations (3.40) and (3.44). This applies due to the difference between fermion and boson statistics in addition to a factor $\frac{1}{2}$ for the spin effect.[3]

3.4.1.3 Diagrammatic representation

The one-loop EH effective Lagrangians in equations (3.40) and (3.44) already indicate the types of associated diagrams. Let us illustrate this for the scalar case. Considering the integral in (3.44), we notice that the integrand, except the factor $\frac{1}{is}$, is just the expression for the scalar propagator (3.43) embedded in the background for the case $y \to x$. Hence, a natural interpretation would be to understand the included diagrams as some expansion with a single closed loop coupled perturbatively to the background in which the particle evolves in proper time s. In terms of diagrams, we may therefore represent the imaginary[4] part of the one-loop EH effective Lagrangian as in figure 3.1 [279–284].

Due to charge conjugation symmetry in QED these diagrams appear with even numbers of external photon lines. This expansion rule is known as Furry's theorem [285]. Interestingly, the first loop in figure 3.1 is not coupled to any background photon, so it corresponds to the limit $\mathcal{A} \to 0$ and should therefore account for the vacuum energy. Indeed, treating the resulting integral appropriately, the computation of this contribution leads to the finite Casimir force [229, 250].

---

[3] The polarization properties in matter are described in terms of the electric induction and the magnetic field. Similarly, writing the effective Lagrangian as $\mathcal{L}_{\text{eff}} = \mathcal{L}_0 + \delta\mathcal{L}$ where $\mathcal{L}_0 = -\frac{1}{4}\mathcal{F}_{\mu\nu}^2$, the contribution $\delta\mathcal{L}$ takes into account the effect of vacuum polarization; the *interaction* of the background with the vacuum fluctuations of the particle and antiparticle fields.

[4] The real part of the effective Lagrangian describes dispersive effects such as vacuum birefringence and the imaginary part is responsible for absorptive effects such as VPP. It is important to note that only dispersive effects may be computed in perturbation theory. The process of VPP, as we will discuss later, is a purely nonperturbative effect. It can be understood as a tunneling process from the vacuum, see discussion in section 3.4.2.2.
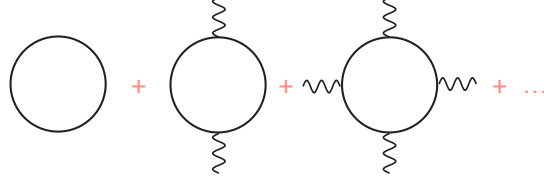
Figure 3.1: Diagrammatic representation of the one-loop EH effective Lagrangian as a perturbative expansion with respect to the number of external gauge bosons indicated by the wavy lines. The single loop corresponds to the particle loop described in the text.

3.4.1.4   Time propagation

We focus on the fermionic one-loop EH effective Lagrangian from (3.40) with a constant $\mathcal{F}_{\mu\nu}$. The space operator in the quantum mechanical Heisenberg picture is written in terms of the related operator in Schrödinger picture,

$$\hat{x}^\mu(s) = e^{i\hat{H}s}\hat{x}e^{-i\hat{H}s}. \tag{3.46}$$

The first step is the computation of $\langle x|e^{-i\hat{H}s}|x\rangle$ in (3.40). We again use the notation $\langle y|e^{-i\hat{H}s}|x\rangle = \langle y;0|x;s\rangle$. Once, an appropriate expression is found, the coincidence limit, $y \to x$, will be taken.

First, we obtain the following relation

$$i\partial_s\langle y;0|x;s\rangle = \langle y|e^{-i\hat{H}s}\hat{H}|x\rangle. \tag{3.47}$$

The next step is to rewrite $\hat{H}$ in terms $\hat{x}(0)$ and $\hat{x}(s)$ in order to obtain a differential equation whose solution is exactly given by $\langle y;0|x;s\rangle$ [229]. Let us introduce $\hat{\Pi}^\mu = \hat{p}^\mu - e\mathcal{A}^\mu(\hat{x})$ which leads to the following relations [270]

$$\begin{aligned}
[\hat{x}^\mu(s), \hat{\Pi}^\nu(s)] &= -ig^{\mu\nu}, \\
[\hat{\Pi}^\mu(s), \hat{\Pi}^\nu(s)] &= -ie\mathcal{F}^{\mu\nu}
\end{aligned} \tag{3.48}$$

where $[\hat{x}^\mu, \hat{p}^\mu] = -ig^{\mu\nu}$. From this, we can deduce

$$\hat{H}(s) = -\hat{\Pi}(s)\cdot\hat{\Pi}(s) + \frac{e}{2}\mathcal{F}_{\mu\nu}\sigma^{\mu\nu}. \tag{3.49}$$

noticing that we have written $x\cdot y \equiv x_\mu y^\mu$. Solving the corresponding equations of motion for $\hat{\Pi}$ and $\hat{x}$ in the Heisenberg picture generated by the Hamilton operator $\hat{H}(s)$, means

$$\begin{aligned}
\frac{d\hat{\Pi}^\mu}{ds} &= i[\hat{H}, \hat{\Pi}] = 2e\mathcal{F}_{\mu\nu}\Pi^\mu, \\
\frac{d\hat{x}^\mu}{ds} &= i[\hat{H}, \hat{x}] = 2\Pi^\mu,
\end{aligned} \tag{3.50}$$

leads to the solution of the mentioned differential equation which becomes after taking the limit $y \to x$

$$\langle x; 0|x; s\rangle = \frac{-i}{16\pi^2 s^2} \exp\left(-i\frac{es\sigma_{\mu\nu}\mathcal{F}^{\mu\nu}}{2} + \frac{1}{2}\text{tr}\ln\left(\frac{\sinh(es\mathcal{F}_{\mu\nu})}{e\mathcal{F}_{\mu\nu}}\right)\right). \quad (3.51)$$

Inserting the latter into equation (3.40) and performing the Dirac trace $\text{Tr}\langle x; 0|x; s\rangle$ yields the following unrenormalized one-loop effective Lagrangian [270]

$$\mathcal{L}_{\text{EH}} = -\frac{1}{4}\mathcal{F}_{\mu\nu}^2 - \frac{e^2}{32\pi^2}\int_0^\infty \frac{ds}{s}e^{-s\epsilon}e^{-ism^2}\frac{\Re(\cos(esX))}{\Im(\cos(esX))}\mathcal{F}_{\mu\nu}\tilde{\mathcal{F}}_{\mu\nu} \quad (3.52)$$

with $X \equiv \sqrt{2(\mathcal{F} + i\mathcal{G})}$ depending on the Lorentz invariants

$$\mathcal{F} = \frac{1}{4}\mathcal{F}_{\mu\nu}^2, \qquad \mathcal{G} = -\frac{1}{4}\mathcal{F}_{\mu\nu}\tilde{\mathcal{F}}_{\mu\nu} \quad (3.53)$$

where the tilde indicates the dual field tensor.

3.4.1.5 Normalization

What remains to be done is the normalization of the effective EH Lagrangian in (3.52). For this the integrand can perturbatively be expanded in the coupling e. In that way, one notes that the first two leading terms are divergent in the small time asymptotics. These UV divergences can be removed by minimal subtraction. The final QED result for the one-loop EH effective Lagrangian in a static electromagnetic background is then given by

$$\begin{aligned}
\mathcal{L}_{\text{EH}} = &-\frac{1}{4}\mathcal{F}_{\mu\nu}^2 - \frac{e^2}{32\pi^2}\int_0^\infty \frac{ds}{s}\ \exp(is\epsilon)\exp(-sm^2) \\
&\times \left[\frac{\Re(\cosh(esX))}{\Im(\cosh(esX))}\mathcal{F}_{\mu\nu}\tilde{\mathcal{F}}_{\mu\nu} - \frac{4}{e^2s^2} - \frac{2}{3}\mathcal{F}_{\mu\nu}^2\right].
\end{aligned} \quad (3.54)$$

This result was first obtained by Euler and Heisenberg [269] by finding exact solutions to the Dirac equation in the static background and later rederived by Schwinger [270] by utilizing the proper time approach discussed above.

3.4.2 Schwinger effect: a nonperturbative phenomenon

In this part, we explicitly discuss the nonperturbative character of the Schwinger mechanism. We show that it is a purely electric effect which can be examined by considering the asymptotic behavior of the perturbative expansion in the weak

field limit, $E \ll E_{\mathrm{S}}$. The one-loop EH effective Lagrangian in the spinor case previously introduced in equation (3.54) can be rewritten as

$$\mathcal{L}_{\mathrm{EH}} \overset{\mathrm{QED}}{=} -\frac{1}{8\pi^2} \int_0^\infty \frac{ds}{s^3} e^{-seE_S} \left[\frac{e^2 abs^2}{\tanh(ebs)\tan(eas)} - 1 - \frac{e^2 s^2}{3}(b^2 - a^2) \right]. \quad (3.55)$$

Note that the prefactor is chosen as in [135]. The exponent depends on the critical field strength E_{S} from (1.3) and the invariants above are defined as

$$
\begin{aligned}
a &:= \sqrt{\sqrt{\mathcal{F}^2 + \mathcal{G}^2} - \mathcal{F}}, \\
b &:= \sqrt{\sqrt{\mathcal{F}^2 + \mathcal{G}^2} + \mathcal{F}},
\end{aligned}
\quad (3.56)
$$

where $\mathcal{F}$ and $\mathcal{G}$ have been introduced in (3.53). Note that the definitions a and b fulfill[5]

$$
\begin{aligned}
a^2 - b^2 &= \mathbf{E}^2 - \mathbf{B}^2, \\
ab &= \mathbf{E} \cdot \mathbf{B}
\end{aligned}
\quad (3.57)
$$

where $\mathbf{E}$ denotes the electric field and $\mathbf{B}$ the magnetic field, respectively. The analogous expression for the scalar case reads

$$\mathcal{L}_{\mathrm{EH}} \overset{\mathrm{sQED}}{=} \frac{1}{16\pi^2} \int_0^\infty \frac{ds}{s^3} e^{-seE_S} \left[\frac{e^2 abs^2}{\sinh(ebs)\sin(eas)} - 1 - \frac{e^2 s^2}{6}(b^2 - a^2) \right]. \quad (3.58)$$

The effective Lagrangians in equations (3.55) and (3.58) are nonlinear in the background dependent invariants a and b. The quartic and higher terms correspond to additional nonlinear interactions which are not present in the tree level Maxwell action [275, 276]. The nonlinearities can be seen as dielectric fields in a vacuum showing the behavior of a polarizable medium [266]. The expressions above already indicate that for plane wave backgrounds obeying the null property, $\mathcal{F}, \mathcal{G} = 0$ and therefore $a, b = 0$, nonlinear vacuum phenomena cannot exist [270]. According to the relations in (3.57), it is clear that VPP is not possible due to symmetry reasons. Namely, during the delocalization of the virtual particles the magnetic field with equal strength, $a^2 - b^2 = 0$, always counteracts against the orthogonal electric field, $ab = 0$.

In the following, we briefly comment on the weak field expansion for the effective Lagrangians (3.55) and (3.58). These are of special interest, since they directly

---

[5] For differences regarding the convention that appear in the literature we would like to refer to the remark in [135].

lead to the famous Schwinger formula determining the decay rate according to

$$\mathcal{R} \simeq \Im(\Gamma_{\text{EH}}) = 2VT\Im(\mathcal{L}_{\text{EH}}), \tag{3.59}$$

see equation (3.23). For the second equality, we already have assumed a static background as in the derivation of the formulas (3.55) and (3.58).

3.4.2.1 Critical field and weak field expansion

In the static limit, the only parameter which is relevant for the VPP rate is the field strength of the background. For very small values the rate is exponentially suppressed with the critical field strength (1.3).

Let us first demonstrate how this extremely large value follows from simple energy conservation. Namely, the energy xeE that is needed during the delocalization process of the virtual particles to make the pair real along the distance x has to be equal to the energy gap $2m$ between the Dirac see and the excitation level, the positive continuum. Taking into account the Compton wavelength $\lambda_c \sim \frac{1}{m}$, we have to set $x = \frac{2}{m}$ which leads to the critical field strength E_{S}.

Generating field strengths of that order in the laboratory is still extremely challenging [26, 27, 256, 286, 287]. Here, we will focus on the weak field regime for purely electric backgrounds, i.e.

$$E \ll E_{\text{S}}. \tag{3.60}$$

We may ask how the tunneling exponential will be modified in the presence of backgrounds beyond the simple static case. Before addressing these aspects, we first discuss the weak field expansion for the results (3.55) and (3.58) in a static electric and magnetic background in order to highlight the substantial differences.

For the one-loop EH effective Lagrangian (3.55) the weak field expansion in terms of the invariants a and b from (3.56) is [135]

$$\mathcal{L}_{\text{EH}} \simeq -m^4 \sum_{n=2}^{\infty} (2n-3)! \sum_{k=0}^{n} \frac{\mathcal{B}_{2k}\mathcal{B}_{2n-k}}{(2k)!(2n-2k)!} \left(\frac{2eb}{m^2}\right)^{2n-2k} \left(\frac{2iea}{m^2}\right)^{2k}. \tag{3.61}$$

For the scalar case in (3.58), the result is slightly modified as

$$\mathcal{L}_{\text{EH}} \simeq \frac{m^4}{2} \sum_{n=2}^{\infty} (2n-3)! \sum_{k=0}^{n} \frac{\bar{\mathcal{B}}_{2k}\bar{\mathcal{B}}_{2n-2k}}{(2k)!(2n-2k)!} \left(\frac{2eb}{m^2}\right)^{2n-2k} \left(\frac{2iea}{m^2}\right)^{2k}. \tag{3.62}$$

Here, the expressions

$$\mathcal{B}_{2n} = (-1)^{n+1} \frac{2(2n)!}{(2\pi)^{2n}} \zeta_R(2n) \tag{3.63}$$

denote Bernoulli numbers with ζ_R being the Riemann zeta function and $\bar{\mathcal{B}}$ defined as [135]

$$\bar{\mathcal{B}}_{2n} := \frac{(1 - 2^{2k-1})}{2^{2k-1}} \mathcal{B}_{2n}. \tag{3.64}$$

The expansion formula (3.61) and (3.62) already reveal that the background type crucially affects the asymptotic behavior of the series expansions and hence their exact summability.

3.4.2.2 Electric background

For a purely electric background the resulting integral representations for (3.61) and (3.62), respectively, have an asymptotic expansion which are divergent and nonaltering. In other words, they are not Borel summable, means there exists an imaginary nonperturbative contribution [135, 288] giving rise to VPP. The imaginary part in QED has the form

$$\Im(\mathcal{L}_{\mathrm{EH}}) \simeq \frac{e^2 E^2}{8\pi^3} \sum_{n=1}^{\infty} \frac{1}{n^2} \exp\left(-\frac{\pi n E_{\mathrm{S}}}{E}\right) \tag{3.65}$$

and in sQED the analogous expression reads

$$\Im(\mathcal{L}_{\mathrm{EH}}) \simeq \frac{e^2 E^2}{16\pi^3} \sum_{n=1}^{\infty} \frac{(-1)^{n-1}}{n^2} \exp\left(-\frac{\pi n E_{\mathrm{S}}}{E}\right). \tag{3.66}$$

These expressions are sometimes called Schwinger formulas.

As we will discuss later, the prefactor is the result of quantum fluctuations over the stationary instanton solution. The higher order terms included in the characteristic tunneling exponential depend on the so-called winding number of the instanton.

Interestingly, the exponential is identical for both cases. Differences occur only in the prefactors which go back to different spin statistics between fermions and bosons. Since the exponential plays a substantial role in the weak field regime where nonperturbative VPP is strongly suppressed, we will be mostly focusing on this factor. In light of this, the Schwinger mechanism may be understood as a tunneling process through a potential barrier with an extremely small tunneling rate
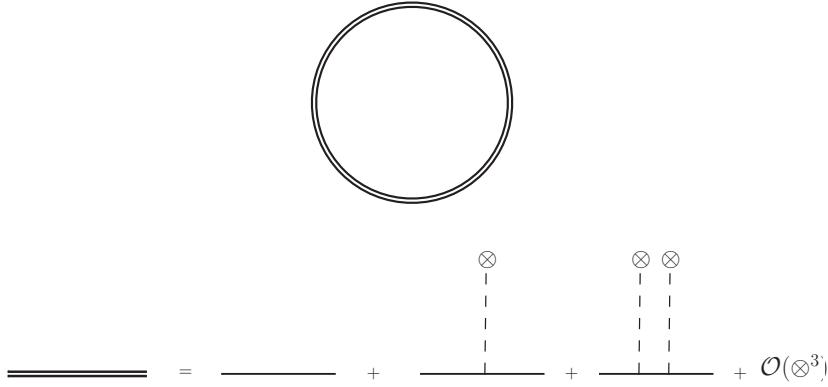
Figure 3.2: Top: all-order vacuum diagram for the one-loop EH effective Lagrangian corresponding to the sum of all diagrams appearing in figure 3.1. Bottom: the double line indicates the arbitrary many couplings to the background.

for field strengths far below E_{S}. To some extend, the exponential dependence in the Schwinger formula indicates a close similarity to ionization in atomic physics[6] which can be also interpreted as a tunneling phenomenon through a potential well.

3.4.2.3 Magnetic background

For a purely magnetic background the weak field expansions in equations (3.61) and (3.62) are divergent but alternating. In this case, the expansions are Borel summable leading exactly to the original integral representations in (3.55) and (3.58), respectively [135]. Hence, there will be no imaginary part for the effective Lagrangian which means that VPP is simply not possible in a static magnetic background [133, 270, 289, 290].

3.4.3 Schwinger effect: perturbative aspects

The VPP rate determined by the fermionic (3.65) and bosonic (3.66) Schwinger formula, respectively, has an exponential dependence on the inverse of the electric field strength. This already indicates the nonperturbative character of this process which therefore invites to interpret VPP by the Schwinger mechanism as a

---

[6] For an electron bound in an atom with binding energy $-V_0 \equiv -V(0)$ the ionization probability in the presence of a static electric field with strength E is proportional to [250]

$$\mathcal{P}_{\mathrm{ion}} \propto \exp\left(-\frac{4V_0}{3eE}\sqrt{2mV_0}\right)$$

which for a potential well with $V_0 = 2m$ is quite similar to the exponential factor in the Schwinger formula.

tunneling process. Consequently, for subcritical electric fields with $E \ll E_S$ and extremely small frequencies $\omega \ll m$ there will be no chance to see VPP at lower orders in perturbation theory.[7]

The breakdown of perturbation theory in the mentioned tunneling regime shall be illustrated in the following. As discussed in chapter 2, if we want to compute the corresponding S-matrix element we just need to shift the photon field by some c-number which we have associated with the classical background $\mathcal{A}^\mu$. The dressed S-matrix in terms of the interaction Hamiltonian $\mathcal{H}_I(x) = e\bar{\psi}(x)\gamma^\mu\psi(x)\mathcal{A}_\mu(x)$ is written as

$$\mathbb{S}_\mathcal{A} = \mathcal{T}\exp\left(-i\int d^4x\ \mathcal{H}_I(x)\right) \tag{3.67}$$

where $\mathcal{T}$ denotes the standard time ordering operator. Then, the formal expression for vacuum persistence in an arbitrary electromagnetic background becomes

$$\langle C|\mathbb{S}|C\rangle = \langle 0|\mathbb{S}_\mathcal{A}|0\rangle = \sum_{n=0}^{\infty} \frac{(-ie)^n}{n!}\int dx_1\dots dx_n$$
$$\times \langle 0|\mathcal{T}[\bar{\psi}(x_1)\mathcal{A}(x_1)\psi(x_1)\dots]|0\rangle. \tag{3.68}$$

Applying the whole machinery of the Wick theorem, one can rewrite the modulus squared of the persistence amplitude as [250]

$$|\langle 0|\mathbb{S}_\mathcal{A}|0\rangle|^2 = \exp\left(-W\right). \tag{3.69}$$

Accordingly, pairs will be not produced if $W = 0$. One can expand W perturbatively in the coupling constant $\alpha \propto e^2$. At lowest order, the final expression in the fermionic case for an electromagnetic background with constant $\mathcal{F}$ reads [250]

$$W^{(1)} = \frac{\alpha}{3}\int d^4q\ \theta(q^2 - 4m^2)\left(a^2 - b^2\right)\sqrt{1 - \frac{4m^2}{q^2}}\left[1 + \frac{2m^2}{q^2}\right]. \tag{3.70}$$

In the bosonic case, the corresponding result is

$$W^{(1)} = \frac{\alpha}{12}\int d^4q\ \theta(q^2 - 4m^2)\left(a^2 - b^2\right)\sqrt{1 - \frac{4m^2}{q^2}}\left[1 - \frac{4m^2}{q^2}\right]. \tag{3.71}$$

So one can check that in the presence of a static electric background the exponent in (3.69) already vanishes at the lowest perturbative order which can be regarded

---

[7] In the static case, i.e. standard Schwinger mechanism, there is no way to see the effect at any finite order in perturbation theory.

as a clear indicator for the nonperturbative behavior, see also [229]. This tunneling regime which has never been directly observed in the experiment is of course the interesting case. Due to the fact that the VPP rate is one of the very few nonperturbative analytic results in QFT with clear physical predictions, the realization of the Schwinger effect may also help to understand further nonperturbative aspects in QFTs [26].

The one-loop EH effective Lagrangians in (3.40) and (3.44) are exact in the background. We have seen that an arbitrary number of contributing background photons, as shown in figure 3.1, are encoded in a single vacuum diagram sketched in figure 3.2. Interestingly, including the dynamical gauge field in addition, these expressions are even fully exact. However, the full effective action including also higher orders in the coupling constant is not known.

As discussed in section 1.4, with increasing frequencies approaching energies comparable to or even larger than the particle mass, VPP is possible perturbatively[8] via multi photon absorptions [141–143, 291].

---

[8] The probability that an electron-positron pair is produced per unit time and unit volume in an alternating external field is proportional to [141, 142]

$$\sim \exp\left(-\pi g(\gamma)\frac{E_{\mathrm{S}}}{E}\right).$$

The function in the exponent satisfies

$$g(\gamma) = \begin{cases} 1 - \frac{\gamma^2}{8} + \mathcal{O}(\gamma^4) & \gamma \ll 1 \\ \frac{4}{\pi\gamma}\ln\left(\frac{4\gamma}{e}\right) + \mathcal{O}\left(\frac{1}{\gamma^3}\right) & \gamma \gg 1 \end{cases}$$

where γ is a dimensionless inhomogeneity parameter, see discussion below. As can be seen, for increasing frequencies, $\gamma \gg 1$, the probability is described by perturbation theory where the terms correspond to the number of quanta required to produce the pair.

Part II

Worldlines, semiclassics and nonequilibrium QFT

Chapter 4

Worldline quantum field theory

4.1 Scattering amplitudes: from strings to particles

P ATH integrals over the space of closed loops represent one-loop scattering amplitudes in relativistic QFT and are relatable to the Feynman path integral in nonrelativistic quantum mechanics [292, 293]. Integrals of that kind can be treated via string inspired methods.[1] Namely, it has been shown that techniques used in string perturbation theory can be directly applied to improve the computation efficiency in QFT. These achievements are based on the fact that string theory in certain limits reduces to ordinary QFT. For instance, this is the case when the string tension of the string becomes infinite such that all massive string modes become suppressed [294].[2] Then, what only remains are the massless string modes which can be identified with standard massless point particles such as gauge bosons.

---

[1] The methods are called string inspired, since they have analogies to computations in string perturbation theory and their development was historically triggered by efforts in using a systematic organization of string amplitudes with respect to both gauge invariance and exchange symmetry. However, as will be demonstrated later, the knowledge of string theory is basically not necessary for the practical application of these techniques.

[2] The fact that string theory should lead to local QFT in the infinite string tension limit of field theory limit, respectively, was clear after the string interpretation of the Veneziano model which was taken as an attempt to explain the physical properties of strongly interacting mesons, see e.g. [295].

Especially, the systematic organization[3] of appropriately chosen (super) string amplitudes, which involve a much smaller number of scattering diagrams, allows a significant reduction of the number of terms which otherwise have to be taken into account in ordinary gauge theory computations. This property substantially simplifies the derivation of powerful closed parameter integral representations for certain one-loop amplitudes in ordinary QFT by resorting to the infinite tension limit for the corresponding string amplitude. As an example, consider, for instance, the following two-point diagram depicted in figure 4.1 for the closed string. In the infinite tension limit, the underlying Riemann surface basically reduces to ordinary Feynman graphs with two different topologies as sketched in figure 4.2 [296]. Since scattering amplitudes in string theory are usually calculated in first and not
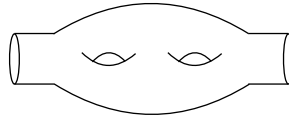
Figure 4.1: Closed string diagram at two-loop level.

second quantization, the corresponding gauge theory amplitudes are written down as first quantized integral representations. The first computations of this type have led to the correct one-loop β function coefficient for pure Yang-Mills theory starting from the partition function of an open string propagating in a Yang-Mills background [296].[4] More investigations of the infinite string tension limit were un-
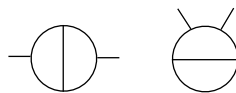
Figure 4.2: Feynman graphs with two different topologies resulting from figure 4.1 in the infinite string tension limit.

dertaken after the pioneering contributions by Bern and Kosower [294] where the corresponding techniques have been applied to complete on-shell QCD scattering amplitudes. There, the basic idea was to calculate, in some sense, gauge boson scattering amplitudes by choosing an appropriate string description containing

---

[3] In fact, string amplitudes contain the complicated rearrangement of different Feynman diagrams contributing to the scattering amplitude which would emerge in the standard way by calculating the S-matrix elements in field theory [294].

[4] We should note that this computation also leads to the critical dimension $D = 26$ of the open string which corresponds to the case where the β-function vanishes, see e.g. [297].

$SU(N)$ gauge theory up to the level where a closed parameter integral representation could be written down. The corresponding field theory amplitude then followed by performing the infinite tension limit through eliminating all propagating massive string modes. The detailed analysis of the Bern-Kosower (BK) approach has led to the so-called BK master formula [294] and to the BK rules [298–300] allowing the construction of final integral representations without explicitly starting from string diagrams. The BK rules look very different from Feynman rules but it can be shown that they are indeed equivalent [301]. Applying the BK rules, the N point gluon amplitude [298, 299] and the four point graviton amplitude [302] have been successfully computed.

Let us briefly recap some of the basic observations to illuminate the similarities we want to emphasize. The string scattering amplitude can be computed by using the Polyakov path integral. For the simplest case, the closed bosonic string propagating in flat spacetime, it is of the form

$$\langle V_1 \cdots V_N \rangle \simeq \sum_{\text{topology}} \int \mathcal{D}h \int \mathcal{D}x(\sigma, \tau) \ V_1 \cdots V_N \ e^{-S[x,h]}. \tag{4.1}$$

The integral $\int \mathcal{D}x$ is over the string worldsheets with a fixed topology where $\int \mathcal{D}h$ is the integral over all worldsheet metrics. The analogy for the higher order loop expansions in usual field theory is the sum over all corresponding topologies as illustrated in figure 4.3. The Gaussian action in (4.1) has the form

$$S[x,h] \simeq T \int d\sigma d\tau \ \sqrt{h} h^{\alpha\beta} g_{\mu\nu} \partial_\alpha x^\mu \partial_\beta x^\nu \tag{4.2}$$

with $g_{\mu\nu}$ being the metric on the target space. The factor in front, $T \equiv \frac{1}{2\pi\alpha'}$, denotes the string tension and V_j with $j = 1, \ldots, N$ are the vertex operators for different scattering states. Differently, in case of the open string being the more
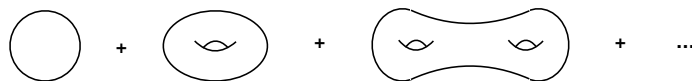
Figure 4.3: Higher order expansion in closed string perturbation theory.

interesting situation for the present discussion, the worldsheet is bounded and the vertex operators are attached to the boundary. At one-loop level the worldsheet has the form of an annulus where a vertex operator may be integrated along one of the two boundary segments parameterized by τ which form the annulus as shown

in figure 4.4 (left). For the closed string, the corresponding one-loop amplitude is represented by a punctured torus in the right panel of figure 4.4. The vertex operators can, for instance, represent a scalar and a gauge boson, respectively,

$$V = \int d\tau \; \exp\left(ik \cdot x(\tau)\right), \qquad V = \int d\tau \; T^{\alpha}\epsilon_{\mu}\dot{x}^{\mu}\exp\left(ik \cdot x(\tau)\right), \qquad (4.3)$$

with definite polarization and momentum where T^{α} denotes the gauge group generator in some representation. Then, performing the Gaussian $\int \mathcal{D}x$ integral by Wick contractions

$$\langle x^{\mu}(\tau_1)x^{\nu}(\tau_2)\rangle = G_{\mathrm{B}}(\tau_1, \tau_2)g^{\mu\nu}, \qquad (4.4)$$

with G_{B} being the bosonic Green's function for the Laplacian on the annulus with respect to its boundary, leads to the mentioned BK master formula for the one-loop N point gluon amplitude serving as a generating functional that has no analogue in ordinary QFT. The BK formalism in its original form was established for tree-

Figure 4.4: Left: vertex operators on the boundary of the annulus for the open string at one-loop level. Right: punctured torus as the analog for the closed string.

level and one-loop amplitudes. In the original version, going beyond the one-loop case corresponds to finding the particle limits of higher genus string amplitudes as demonstrated in figure 4.3, which is actually a striking task due to the complex structure of moduli space. There are some partial attempts for the generalization to the multi-loop case, see e.g. [303, 304].

After the invention of the BK approach, a more efficient method entirely based on known representations of purely field theoretic amplitudes in terms of (super) particle path integrals was proposed by Strassler, again for the one-loop case [124]. There, the path integrals are treated as one-dimensional analogs of the Fradkin-Tseytlin path integral [305] using worldline correlation functions on the circle. This approach has also become suitable for multi-loop amplitudes as well [306, 307] and even for generalizations involving external background fields [308, 309]. In the following section, we introduce this alternative first-quantized approach in detail which also goes under the name of worldline quantum field theory (WQFT). Before

proceeding in that direction, we briefly introduce the one-loop effective action in a Maxwell background involving a scalar loop represented in terms of the following worldline path integral

$$\Gamma[A] = \int_0^\infty \frac{ds}{s} \, \exp\left(-sm^2\right) \int \mathcal{D}x(s) \exp\left(-\int_0^s d\tau \, \frac{1}{4}\dot{x}^2 + ieA \cdot \dot{x}\right), \qquad (4.5)$$

see section 4.2.2. Here, without going into details, we note that expanding the interaction term in the exponent results in terms which correspond to standard Feynman diagrams describing a scalar loop perturbatively interacting with the background field. For instance, the N photon amplitude follows after setting the background to be the sum of plane waves with definite polarizations. This results in the same photon vertex operator as in string perturbation theory, with the exception that it is attached to a circle and not to the mentioned annulus. However, we recall that the annulus in the open string case gets squeezed to a circle in the infinite tension limit, $x(\sigma, \tau) \to x(\tau)$.[5] Consequently, the corresponding vertex operators are inserted on a circle so that the path integral in (4.5) can be considered as the infinite string tension limit of the previous path integral (4.1) based on the Polyakov action. The resulting integral for the N photon scattering amplitude then reduces to the Wick contractions

$$\langle \dot{x}_1^{\mu_1} e^{ik_1 \cdot x_1} \cdots \dot{x}_N^{\mu_N} e^{ik_N \cdot x_N} \rangle. \qquad (4.6)$$

A detailed discussion regarding the latter is included in the following sections, see in particular section 4.3.2.

4.2 One-loop effective actions

In this section, we first discuss the basic quantities which are relevant for most of the computations in WQFT. Afterwards, we introduce certain one-loop effective actions using the language of this first-quantized approach. One-loop effective actions are generally expressed as a determinant of the kinetic differential operator in the underlying field theory. As we will see, in WQFT the formal expression can

---

[5] In string perturbation theory, we sum over different metrics and topologies of the string worldsheet. Considering string theory as a σ-model, the loops become suppressed for $T \to \infty$ which results in a reduction to quantum mechanical point excitations. Consequently, the string loops reduce to certain sets of Feynman graphs. The UV divergences in local QFT, which do not plague string theory, reappear in the one-dimensional worldline limit due to the absence of physical analogs of counterterms in QFT, the worldsheet σ-model divergences.

be transformed into an integral over the space of all closed paths in spacetime of a moving quantum mechanical particle.

An open ended path integral represents the corresponding propagator in the field theory. It is performed over the space of paths which connect two fixed spacetime points with appropriate boundaries [125].

Here, we do not consider propagator path integrals since our main goal is to discuss the rate for VPP that is to leading order determined by the one-loop EH effective action, see section 3.3.

4.2.1 Scalar field theory

Let ϕ be a real massive scalar field in D dimensional Euclidean space which self-interacts according to some potential $U(\phi)$. The normalized one-loop effective action can formally be written[6] as [229]

$$\Gamma[\phi] = -\frac{1}{2}\mathrm{Tr}\ln\left(\frac{-\Box + m^2 + U''}{-\Box + m^2}\right) \tag{4.7}$$

where $\Box$ denotes the associated Euclidean d'Alembert operator. Such a logarithmic expression can be rewritten by using an appropriate integral form.[7]

Neglecting the potential independent contribution and performing a functional trace over position eigenstates $|x\rangle$ in Hilbert space leads to the following integral representation for the effective action

$$\Gamma[\phi] = \frac{1}{2}\int_0^\infty \frac{ds}{s}\int d^D x\ \langle x|e^{-s\left(-\Box + m^2 + U''(\phi)\right)}|x\rangle. \tag{4.8}$$

Having this in mind, we now consider a quantum mechanical particle with mass $\tilde{m}$. The evolution in a time dependent potential $\tilde{V}(x)$ in nonrelativistic quantum mechanics can be written with the help of Feynman's path integral formulation [229, 310]

$$\langle x_2|e^{-i(t_2-t_1)H}|x_1\rangle = \int_{x(t_1)}^{x(t_2)} \mathcal{D}x(t)\ \exp\left(i\int_{t_1}^{t_2} dt\ \left(\frac{\tilde{m}\dot{x}^2}{2} - \tilde{V}(x)\right)\right). \tag{4.9}$$

---

[6] Here, we use the relation $\ln\mathrm{Det}\,\mathcal{O} = \mathrm{Tr}\ln\mathcal{O}$.

[7] We use

$$-\mathrm{Tr}\ln\left(\frac{A}{B}\right) = \int_0^\infty \frac{ds}{s}\ \mathrm{Tr}\left(e^{-As} - e^{-Bs}\right)$$

where A and B are some positive definite operators.

Here, $L(x, \dot{x}) = \frac{1}{2}\tilde{m}\dot{x}^2 - \tilde{V}(x)$ is just the classical Lagrange function [311]. The connection to the kinetic operator from above can be made by interpreting

$$H(x) = \frac{p^2}{2\tilde{m}} + \tilde{V}(x) \tag{4.10}$$

as the Hamilton function operator for a moving particle in spacetime if we identify

$$\tilde{V}(x) = m^2 + U''(\phi(x)), \quad \tilde{m} = 1/2, \quad i(t_2 - t_1) = s, \tag{4.11}$$

such that

$$i(t_2 - t_1)H \rightarrow s\left(-\Box + m^2 + U''\right). \tag{4.12}$$

Thus, without performing the standard path integral discretization [310] we can immediately write by taking $t \rightarrow -is$ the following correspondence

$$\langle x|e^{-s\left(-\Box + m^2 + U''(\phi)\right)}|x\rangle = \int_{x(0)}^{x(s)} \mathcal{D}x(s) \, \exp\left(\frac{\dot{x}^2}{4} + m^2 + U''(\phi(x))\right) \tag{4.13}$$

where $x(0) = x(s) = x$ follows due to the trace performed over position eigenstates. The final path integral representation for the effective action then reads

$$\Gamma[\phi] = \frac{1}{2}\int_0^\infty \frac{ds}{s} \, \exp\left(-sm^2\right) \oint \mathcal{D}x(s) \, \exp\left(-\int_0^s d\tau \, \left[\frac{\dot{x}^2}{4} + U''(\phi(x))\right]\right) \tag{4.14}$$

for which the following relation

$$\int d^4x \int_{x(s)=x(0)=x} \mathcal{D}x(s) = \oint \mathcal{D}x(s) \tag{4.15}$$

has been used.

4.2.2 Bosons

Using equation (4.13), we can analogously obtain the path integral representation for the Euclidean effective action in sQED, namely in the presence of an arbitrary background[8] minimally[9] coupled to the massive scalar field. The corresponding kinetic operator is

$$D^2 - m^2 \tag{4.16}$$

---

[8] In the present first quantized WQFT formalism, the photon background field A^μ is not a classical background as introduced before denoted by $\mathcal{A}^\mu$. The generalization with an additional classical background $\mathcal{A}^\mu$ will be discussed later.

[9] By minimally coupled it is meant that the derivative ∂^μ acting on the charged field is replaced by the covariant derivative $D^\mu = \partial^\mu + ieA^\mu$ to ensure (local) gauge invariance [250].

where $D^\mu = \partial^\mu + ieA^\mu$ denotes the standard covariant derivative. The formal expression for the one-loop effective action is

$$\Gamma[A] = -\frac{1}{2}\text{Tr}\ln\left(\frac{-D^2 + m^2}{-\partial^2 + m^2}\right). \tag{4.17}$$

Constructing the following artificial Hamilton function[10]

$$H = \frac{(p + eA)^2}{2\tilde{m}} + m^2, \tag{4.18}$$

the effective action can be transformed[11] to

$$\Gamma[A] = \int_0^\infty \frac{ds}{s} \, \exp\left(-sm^2\right) \oint \mathcal{D}x(s) \, \exp\left(-\int_0^s d\tau \, \mathcal{W}_{\text{boson}}\right) \tag{4.19}$$

where

$$\mathcal{W}_{\text{boson}} := \frac{1}{4}\dot{x}^2 + ie\dot{x} \cdot A(x). \tag{4.20}$$

This is the worldline path integral representation introduced before in (4.5). For later purpose, we will focus on the scalar case, since it is particularly suitable for saddle point approximations as we will extensively study, see chapter 5. However, for reasons of completeness, but also due to the connection to worldline supersymmetry, the generalization to fermions will be briefly discussed in the following.

4.2.3 Fermions

The worldline path integral representation for Dirac fermions can be achieved in different ways where one needs to take the spin degrees of freedom into account. Possible techniques, for instance, are based on the explicit incorporation of γ matrices [312, 313], or resorting to the formulation over Grassmann variables having the same algebraic properties. The latter will be used in the following. As we will see, a direct connection to the fermionic coherent states brought up in section 2.5 will appear.

The formal expression for the fermionic Euclidean one-loop effective action is formally written as

$$\Gamma[A] = \ln\text{Det}\left(\slashed{p} + e\slashed{A} - im\right). \tag{4.21}$$

---

[10] Note that $i(t_2 - t_1)H \to s(-D^2 + m^2)$ since $(p + eA)^2 \to -(\partial + ieA)^2$ with $p = -i\partial$.

[11] The factor $\frac{1}{2}$ in front of the original integral is canceled due to the trace operation for which a double number of degrees of freedom for the scalar field has to be taken into account [125].

For the fermionic case the direct application of known results from quantum mechanics as we have seen for sQED is not possible. In the following, we will go through the relevant steps reviewed in [125]. Resorting to the same conventions,[12] let us first introduce the following useful expressions

$$
\left(\not{p} + e\not{A}\right)^2 = -(\partial_\mu + ieA_\mu)^2 - \frac{ie}{2}\sigma^{\mu\nu}F_{\mu\nu},
$$
$$
\text{Det}\left(\not{p} + e\not{A} - im\right) = \text{Det}\left(\not{p} + e\not{A} + im\right) = \sqrt{\text{Det}\left((\not{p} + e\not{A})^2 - m^2\right)}.
$$
(4.22)

Then, using the relations in footnote 7, we may first write

$$
\ln\sqrt{\text{Det}\,\mathcal{O}} = -\frac{1}{2}\text{Tr}\int_0^\infty \frac{ds}{s}\, e^{-s\mathcal{O}}
$$
(4.23)

in order to find the following integral expression for the effective action

$$
\Gamma[\mathcal{A}] = -\frac{1}{2}\text{Tr}\int_0^\infty \frac{ds}{s}\,\exp\left(-sm^2\right)\exp\left(-s\left[-(\partial + ieA)^2 - \frac{ie}{2}\sigma^{\mu\nu}F_{\mu\nu}\right]\right).
$$
(4.24)

This expression is very similar to the previous one in the scalar case, except the sign change including a factor $\frac{1}{2}$ in front and the appearance of an additional potential term defined as

$$
V(x) := -\frac{ie}{2}\sigma_{\mu\nu}F^{\mu\nu}.
$$
(4.25)

Here, the field tensor $F_{\mu\nu}$ only depends on the photon background field A^μ. Having achieved this, what remains to be done is the calculation of the following functional trace

$$
\text{Tr}\,e^{-s\Sigma}
$$
(4.26)

where $\Sigma := -(\partial + ieA(x))^2 + V(x)$. The transformation of (4.26) into a quantum mechanical path integral can be done via fermionic coherent states [314–317] leading to the Grassmann representation of the path integral [318–321]. Originally, applied in supersymmetric formulations, Grassmann variables are suitable tools for describing spin and internal degrees of freedom of elementary particles, particularly in the path integral quantization scheme. In addition, there are many other applications in statistical physics which have tremendously been simplified in terms of path integrals over Grassmann variables.

---

[12] Note: $\sigma^{\mu\nu} = \frac{1}{2}[\gamma^\mu, \gamma^\nu]$ and $\{\gamma_\mu, \gamma_\nu\} = 2g_{\mu\nu}\mathbf{1}_4$ where $\mathbf{1}_4$ denotes the 4×4 identity matrix.

For the present purpose, the first step is the definition of certain matrices

$$a_1^\pm := \frac{1}{2}(\gamma_1 \pm i\gamma_3),$$
$$a_2^\pm := \frac{1}{2}(\gamma_2 \pm i\gamma_4) \tag{4.27}$$

which satisfy the Fermi-Dirac anticommutation relations

$$\{a_u^+, a_v^-\} = \delta_{uv},$$
$$\{a_u^+, a_v^+\} = 0 = \{a_u^-, a_v^-\} \tag{4.28}$$

where $u, v = \{1, 2\}$. Interpreting these as creation $(+)$ and annihilation $(-)$ operators, one may construct the Hilbert space with its corresponding ground state defined by

$$a_u^- |0\rangle = 0 = \langle 0| a_u^+. \tag{4.29}$$

Now, let θ_u and $\bar{\theta}_u$ with $u = \{1, 2\}$ be Grassmann variables that commute with the vacuum state $|0\rangle$ but anticommute mutually and with the operators $a_u^\pm$. Related to these, one can introduce the corresponding Grassmann integrals defined as

$$\int \theta_u \, d\theta_u = i = \int \bar{\theta}_u \, d\bar{\theta}_u. \tag{4.30}$$

Here, $d\theta_u$ and $d\bar{\theta}_u$ commute mutually and with the vacuum state, but anticommute with $\theta_u, \bar{\theta}_u$ and $a_u^\pm$. Constructing the following coherent states

$$\langle \bar{\theta}| := \langle 0| e^{-a_1^- \bar{\theta}_1 - a_2^- \bar{\theta}_2}, \quad |\bar{\theta}\rangle := i(\bar{\theta}_1 - a_1^+)(\bar{\theta}_2 - a_2^+)|0\rangle,$$
$$\langle \theta| := i\langle 0|(\theta_1 - a_1^-)(\theta_2 - a_2^-), \quad |\theta\rangle := e^{-\theta_1 a_1^+ - \theta_2 a_2^+}|0\rangle, \tag{4.31}$$

which resemble the version discussed in section 2.5, leads to the following completeness relations

$$\int |\theta\rangle\langle\theta| \, d\theta_2 d\theta_1 = -i\mathbf{1} = \int d\bar{\theta}_1 d\bar{\theta}_2 \, |\bar{\theta}\rangle\langle\bar{\theta}|. \tag{4.32}$$

Then the trace in Fock space spanned by the generators $a_u^\pm$ can be written as [315, 316]

$$\text{Tr } \mathcal{O} = i \int d\theta_2 d\theta_1 \, \langle -\theta| \mathcal{O} |\theta\rangle. \tag{4.33}$$

Inserting a complete set of coordinate states and fermionic coherent states from (4.31), the trace in (4.26) can be written as

$$\text{Tr } e^{-s\Sigma} = i^N \int \prod_{j=1}^{N} \left[d^4 x^j d\theta_2^j d\theta_1^j \, \left\langle x^j, \theta^j \left| \exp\left(-\frac{s}{N}\Sigma\right) \right| x^{j+1}, \theta^{j+1} \right\rangle \right] \tag{4.34}$$

with boundary conditions $\left(x^{N+1}, \theta^{N+1}\right) = (x^1, -\theta^1)$ for the x and θ integrations. The exponential function involves certain combinations of gamma matrices. Therefore, it is useful to consider the matrix element for the product of two gamma matrices $\gamma_A \gamma_B$ with $A \neq B$ and $A, B = \{1, \ldots, 4\}$,

$$\langle \theta^j | \gamma_A \gamma_B | \theta^{j+1} \rangle = -i \int d\bar{\theta}_2^{j,j+1} d\bar{\theta}_1^{j,j+1} \ \langle \theta^j | \bar{\theta}^{j,j+1} \rangle \langle \bar{\theta}^{j,j+1} | \theta^{j+1} \rangle \ 2 \ ^j\psi_A \psi_B^{j+1} \quad (4.35)$$

where

$$\begin{aligned}
^j\psi_{1,2} &:= \frac{1}{\sqrt{2}} \left(\theta_{1,2}^j + \bar{\theta}_{1,2}^{j,j+1} \right), & \psi_{1,2}^{j+1} &:= \frac{1}{\sqrt{2}} \left(\theta_{1,2}^{j+1} + \bar{\theta}_{1,2}^{j,j+1} \right), \\
^j\psi_{3,4} &:= \frac{i}{\sqrt{2}} \left(\theta_{1,2}^j - \bar{\theta}_{1,2}^{j,j+1} \right), & \psi_{3,4}^{j+1} &:= \frac{i}{\sqrt{2}} \left(\theta_{1,2}^{j+1} - \bar{\theta}_{1,2}^{j,j+1} \right).
\end{aligned} \quad (4.36)$$

The former equation (4.35) can be verified by writing the gamma matrices in terms of the Fermi operators $a_u^\pm$ and inserting a complete set of the coherent states $|\bar{\theta}^{j,j+1}\rangle$ in between.

Noting that the superscript $\phi^{j,j+1}$ denotes the average of ϕ with respect to the discrete points j and $j+1$, one finds after expanding the exponential $e^{-\frac{s}{N}\Sigma}$ in $\frac{s}{N}$ and reordering the positions of the Grassmann variables

$$\begin{aligned}
\mathrm{Tr}\, e^{-s\Sigma} = \int \prod_{j+1}^{N} & \left(\frac{dx^j \ d^4 p^{j,j+1} \ d\theta_2^j d\theta_1^j \ d\bar{\theta}_1^{j,j+1} d\bar{\theta}_2^{j,j+1}}{(2\pi)^{4N}} \right) \\
\times \prod_{j+1}^{N} & \left[1 - (\tau^j - \tau^{j+1}) \Sigma_j + \mathcal{O}\left(\frac{s^2}{N^2} \right) \right] \\
\times \exp & \left(\sum_{j=1}^{N} \left[i(x^j - x^{j+1}) p^{j,j+1} + \frac{1}{2} \left(\theta_u^j - \theta_u^{j+1} \right) \bar{\theta}_u^{j,j+1} - \frac{1}{2} \theta_u^j \left(\bar{\theta}_u^{j-1,j} - \bar{\theta}_u^{j,j+1} \right) \right] \right).
\end{aligned} \quad (4.37)$$

Since the Hamilton operator depends on the momentum operator, background A^μ and gamma matrices, we use the notation $\Sigma_j := \Sigma \left(p^{j,j+1}, A^{j,j+1}, 2\ ^j\psi_A \psi_B^{j+1} \right)$. Here, the boundary conditions for the integrals on x, θ and $\bar{\theta}$ are

$$\left(x^{N+1}, \theta^{N+1}, -\bar{\theta}^{N,N+1} \right) = \left(x^1, -\theta^1, \bar{\theta}^{0,1} \right). \quad (4.38)$$

Note that in the expression above the interpolating proper time with

$$\begin{aligned}
\tau^1 &= s, \\
\tau^{N+1} &= 0, \\
\tau^j - \tau^{j+1} &= \frac{s}{N}
\end{aligned} \quad (4.39)$$

has been used.

Now, taking the limit $N \to \infty$, the second product in the integrand in (4.37) becomes the standard path ordered exponential which leads to the following worldline path integral

$$\text{Tr } e^{-s\Sigma} = \int \mathcal{D}p \int \mathcal{D}x \int_{\text{AP}} \mathcal{D}\theta\mathcal{D}\bar{\theta} \; e^{\int_0^s d\tau \, \left[i\dot{x}\cdot p + \frac{1}{2}\dot{\theta}_u\bar{\theta}_u - \frac{1}{2}\theta_u\dot{\bar{\theta}}_u - \Sigma(p,A,2\psi_A\psi_B) \right]}. \quad (4.40)$$

Taking the continuum limit of the equations (4.36), one can make a variable change by rewriting

$$\frac{1}{2}\dot{\theta}_u\bar{\theta}_u - \frac{1}{2}\theta_u\dot{\bar{\theta}}_u = -\frac{1}{2}\psi^A\dot{\psi}_A \quad (4.41)$$

which changes the boundary conditions to $(x(s), \psi(s)) = (x(0), -\psi(0))$. Afterwards, rearranging the terms which involve the momentum in equation (4.40), the resulting Gaussian momentum path integral can be done.

The final result after inserting the solution of (4.40) into equation (4.24) reads

$$\Gamma[A] = -\frac{1}{2} \int_0^\infty \frac{ds}{s} e^{-sm^2} \int_{\text{P}} \mathcal{D}x \int_{\text{AP}} \mathcal{D}\psi \; \exp\left(-\int_0^s d\tau \, \mathcal{W}_{\text{fermion}} \right). \quad (4.42)$$

The fermionic worldline Lagrangian is given by

$$\mathcal{W}_{\text{fermion}} = \mathcal{W}_{\text{boson}} + \frac{1}{2}\psi_A\dot{\psi}^A - ie\psi^A F_{AB}\psi^B. \quad (4.43)$$

Here, $\mathcal{W}_{\text{boson}}$ is the bosonic version in (4.20).

As can be seen, the bosonic coordinate path integral $\mathcal{D}x$ with periodic boundary (P) is identical with the version for sQED. In addition to this, we have the $\mathcal{D}\psi$ integration over anticommuting Grassmann functions with antiperiodic (AP) boundary conditions, $\psi(s) = -\psi(0)$. Thus, the resulting path integral for a Dirac spinor breaks down into a convective part and a spin part [277]. Moreover, there appears a photon vertex operator in the exponential which acquires an additional Grassmann dependence. The global prefactor is the result of different statistics and degrees of freedom between fermions and bosons.

4.2.4   Worldline correlators

An important part of computations in WQFT is related to internal bosonic worldline and Grassmann contractions. Generally, the idea is that one expands the

background A^μ in some appropriate CM coordinate and performs the corresponding Wick contractions in some relative coordinate on a circle[13] [124, 293].

Consider the one-loop effective action (4.19) which describes a massive scalar particle circulating in a loop. For a fixed proper time s, this first quantized particle path integral is set over the space of periodic worldlines $x^\mu(\tau)$ with period s. Let us assume the Euclidean space to be D-dimensional which is generally advantageous for dimensional regularization. In this case, the path integral (4.19) can be evaluated by following a one-dimensional perturbative expansion of the interaction potential,

$$\exp\left(-ie\int_0^s d\tau \ \dot{x} \cdot A\right) = \sum_{N=0}^\infty \frac{(-ie)^N}{N!} \prod_{j=1}^N \int_0^s d\tau_j \ \dot{x}(\tau_j) \cdot A(\tau_j). \tag{4.44}$$

The diagrammatic representation for each term of this series is depicted in figure 3.1 describing a fixed number of interactions of the scalar loop with the background photons.

As a first example, we consider the amplitude for two photon scattering, $N = 2$, which can be achieved by making a specific choice for the background, namely decomposing it in form of a sum of two plane waves with definite polarization,

$$A_\mu(x) = \epsilon_\mu^{(1)} e^{ik_1 \cdot x} + \epsilon_\mu^{(2)} e^{ik_2 \cdot x}. \tag{4.45}$$

Here, only terms that contain every polarization vector just once will be taken into account.[14] This leads to vertex operators[15] of the following form

$$V_A = \int d\tau_j \ \epsilon_\mu^{(j)} \dot{x}^\mu(\tau_j) e^{ik_j \cdot x(\tau_j)}. \tag{4.46}$$

So the evaluation of the path integral reduces to the Wick contraction

$$\left\langle \dot{x}_1^{\mu_1} e^{ik_1 \cdot x_1} \dot{x}_2^{\mu_N} e^{ik_2 \cdot x_2} \right\rangle. \tag{4.47}$$

---

[13] As mentioned in section 4.1, this procedure is usually used in string perturbation theory and thus explains why the worldline approach is called the string inspired approach.

[14] This also removes the $\frac{1}{N!}$ factor in the integral.

[15] Note that this is the vertex operator introduced before in the context of string perturbation theory. Again, since the vertex operator is inserted on a circle, it can be understood as the path integral in the infinite string tension limit for the Polyakov path integral for which the annulus for the open string gets squeezed to a circle.

As mentioned, the integrations can be carried out via splitting the path integral coordinate x^μ into some CM coordinate x_0^μ and a relative coordinate y^μ,

$$x^\mu(\tau) = x_0^\mu + y^\mu(\tau),$$
$$\int_0^s d\tau \; y^\mu(\tau) = 0 \tag{4.48}$$

such that

$$\int \mathcal{D}x = \int dx_0 \int \mathcal{D}y. \tag{4.49}$$

According to the latter convention, the resulting normalization[16] for free path integrals then reads [277, 306, 308, 322]

$$\int \mathcal{D}y \; \exp\left(-\int_0^s d\tau \; \frac{1}{4}\dot{y}^2 \right) = (4\pi s)^{-D/2}. \tag{4.50}$$

In general, other free path integrals are normalized to unity [306, 308].[17] Applying the coordinate splitting in (4.48) leads to the expression

$$\epsilon_1^{\mu_1} \epsilon_2^{\mu_2} (ie)^2 \int_0^\infty \frac{ds}{s} \int dx_0 \int \mathcal{D}y(\tau) \int_0^s d\tau_1 d\tau_2$$
$$\times \dot{y}_1^{\mu_1} e^{ik_1 \cdot (x_0 + y_1)} \dot{y}_2^{\mu_N} e^{ik_2 \cdot (x_0 + y_2)} \exp\left(-\int_0^s d\tau \; \frac{1}{4}\dot{y}^2 \right). \tag{4.51}$$

A basic quantity, as we will discuss in section 4.3.1, is the bosonic Green's function for the Laplacian on the circle,

$$G_{\mathrm{B}}(\tau_1, \tau_2) = |\tau_1 - \tau_2| - \frac{(\tau_1 - \tau_2)^2}{s} =: G_{\mathrm{B}12}, \tag{4.52}$$

that solves the equation

$$\frac{d^2}{d\tau_1^2}\left[\frac{1}{2} G_{\mathrm{B}12} \right] = \delta(\tau_1 - \tau_2) - \frac{1}{s} \tag{4.53}$$

with periodic[18] behavior [322]; the constant $\frac{1}{s}$ can be neglected, see footnote 23.

---

[16] The s dependence can be obtained by an appropriate regularization scheme, e.g. zeta function regularization [317].

[17] For instance,

$$\int \mathcal{D}\psi \; \exp\left(-\int_0^s d\tau \; \frac{1}{2}\psi\dot{\psi} \right) = 1.$$

[18] The kinetic operator is invertible in the reduced Hilbert space without any zero mode. Using the eigenfunctions of the Laplacian on the circle with circumference s, the inverse can be obtained.

The fermionic Green's function is given by

$$G_{\mathrm{F}}(\tau_1, \tau_2) = \mathrm{sign}(\tau_1 - \tau_2) =: G_{\mathrm{F}12} \tag{4.54}$$

which is the solution of

$$\frac{d}{d\tau_1} \left[\frac{1}{2} G_{\mathrm{F}12} \right] = \delta(\tau_1 - \tau_2) \tag{4.55}$$

with anti-periodic[19] behavior. The Green's function for the bosonic field y^μ with periodic behavior then reads[20]

$$\langle y_1^\mu y_2^\nu \rangle = -g^{\mu\nu} G_{\mathrm{B}12} \tag{4.56}$$

and the fermionic one is

$$\langle \psi_1^\mu \psi_2^\nu \rangle = \frac{1}{2} g^{\mu\nu} G_{\mathrm{F}12}. \tag{4.57}$$

For contractions involving exponentials depending on y^μ, the formulas are known from string perturbation theory [124]. Using the usual conventions,[21] those are given by [306, 323]

$$\begin{aligned}
\langle \dot{y}_1^\mu \dot{y}_2^\nu \rangle &= -g^{\mu\nu} \dot{G}'_{\mathrm{B}12}, \\
\langle e^{y_1 \partial_1} e^{y_2 \partial_2} \rangle &= e^{-G_{\mathrm{B}12} \partial_1 \partial_2}, \\
\langle \dot{y}_1 e^{y_1 \partial_1} e^{y_2 \partial_2} \rangle &= -\dot{G}_{\mathrm{B}12} \partial_2 e^{-G_{\mathrm{B}12} \partial_1 \partial_2}.
\end{aligned} \tag{4.58}$$

Taking the normalization (4.50) and the identity

$$\int dx_0 \, e^{ix_0 \cdot (k_1 + k_2)} = (2\pi)^D \delta(k_1 + k_2) \tag{4.59}$$

into account leads to the final expression

$$\begin{aligned}
&\epsilon_1^{\mu_1} \epsilon_2^{\mu_2} (ie)^2 \int_0^\infty \frac{ds}{s} \, (4\pi s)^{-D/2} \int_0^s d\tau_1 \int_0^s d\tau_2 \\
&\times \left(-g^{\mu\nu} \dot{G}'_{\mathrm{B}12} + \dot{G}^2_{\mathrm{B}12} k_1^\mu k_2^\nu \right) e^{G_{\mathrm{B}12} k_1 \cdot k_2} (2\pi)^D \delta(k_1 + k_2).
\end{aligned} \tag{4.60}$$

---

[19] Due to the anti-periodicity of ψ there is no zero mode. The Green's function follows from inverting the first derivative in the Hilbert space of anti-periodic functions.

[20] Note that we use the notation $y_j \equiv y(\tau_j)$.

[21] The dot in $\dot{G}_{\mathrm{B}12} = G_{\mathrm{B}}(\tau_1, \tau_2)$ denotes a derivative with respect to the first variable. The derivative with respect to the second variable is denoted by a prime, see (4.58).

4.2.5   Propagators

In sQED, the position space propagator in D dimensions can be written in integral form by using the Schwinger proper-time representation [277], see identity (3.27), resulting in

$$\langle \phi(x_1)\phi(x_2) \rangle = \int_0^\infty ds \ e^{-sm^2}(4\pi s)^{-D/2}\exp\left(-\frac{(x_1 - x_2)^2}{4s}\right) \qquad (4.61)$$

where $x_j \equiv x(\tau_j)$. For the massless case one can derive the closed form

$$\langle \phi(x_1)\phi(x_2) \rangle|_{m=0} = \frac{\Gamma(D/2 - 1)}{4\pi^{D/2}(x_1 - x_2)^{D-2}} \qquad (4.62)$$

where Γ is the standard Gamma function. The extension of the path integral representation to the fermionic propagator in a background is far more complicated [222, 320, 321, 324], since this goes beyond the even subspace of the Clifford algebra as applied in section 4.2.3 [308].

4.2.6   Non-Abelian gauge theory

Motivated by the BK approach, the worldline formalism in QFT can be also generalized to non-Abelian gauge theories. The simplest example is the scalar one-loop contribution to the gluon scattering amplitude originally considered by Bern and Kosower. We can start on basis of the previous single scalar path integral from equation (4.19) for an Abelian background field. Then the corresponding modifications for a non-Abelian background field will be the introduction of a global color trace, tr. Second, the exponential in the integrand has to be path ordered, since the quantum mechanical Hamilton operators do not necessarily commute at different times. So the generalization of the scalar expression in equation (4.19) to the non-Abelian case can be written as

$$\Gamma_{\text{nA}}[A] \stackrel{\text{scalar}}{=} \text{tr} \int_0^\infty \frac{ds}{s} \ \exp\left(-sm^2\right) \oint \mathcal{D}x(s) \ \mathcal{P}\exp\left(-\int_0^s d\tau \ \mathcal{W}_{\text{nA}}\right) \qquad (4.63)$$

where

$$\mathcal{W}_{\text{nA}} := \frac{1}{4}\dot{x}^2 + ig\dot{x} \cdot A^a T^a. \qquad (4.64)$$

Here, g is the associated coupling constant, T^a denotes the corresponding gauge group generator in some representation and $\mathcal{P}$ is the mentioned path ordering operator.

4.2.7 Worldline supersymmetry

A remarkable property of the fermionic worldline Lagrangian in equation (4.43) is its supersymmetric formulation which formally resembles the scalar case. Let us briefly recap the main aspects. Namely, the Lagrangian is invariant under the transformations [222, 318, 320]

$$
\begin{aligned}
\delta x^\mu &= -2\eta\psi^\mu, \\
\delta\psi^\mu &= \theta\dot{x}^\mu
\end{aligned}
\tag{4.65}
$$

where θ denotes some Grassmann constant. This globally supersymmetric form of the Lagrangian can be seen as remnant of local SUSY after gauge fixing [322, 325–327]. The different boundary conditions for x^μ and ψ^μ, which are not respected by the transformations in (4.65) for some constant θ, break the supersymmetry [125]. For computational reasons, it is still convenient and advantageous to reformulate the path integral in the super field formalism introducing some superfield $X^\mu(\tilde{\tau})$ on a super worldline $\tilde{\tau} = (\tau, \theta)$ with the constant Grassmann θ according to

$$
\begin{aligned}
X^\mu(\tilde{\tau}) &= x_0^\mu + Y^\mu(\tau), \\
Y^\mu(\tau) &= y^\mu(\tau) + \sqrt{2}\theta\psi^\mu(\tau).
\end{aligned}
\tag{4.66}
$$

Defining in addition

$$
D = \frac{\partial}{\partial\theta} - \theta\frac{\partial}{\partial\tau}
\tag{4.67}
$$

with $\int d\theta\,\theta = 1$, the path integral representation (4.42) for the effective action can be rewritten in form of the following super path integral

$$
\begin{aligned}
\Gamma[A] = -\frac{1}{2}\int_0^\infty \frac{ds}{s}\exp\left(-sm^2\right) \\
\times \int \mathcal{D}X \exp\left(-\int_0^s d\tau \int d\theta\left[-\frac{1}{4}X\cdot D^3 X - ieDX\cdot A(X)\right]\right).
\end{aligned}
\tag{4.68}
$$

Just formally, this expression is quite similar to the scalar case described by the worldline action in equation (4.20).

4.3 One-loop amplitudes in vacuum

4.3.1 N point amplitude in scalar field theory

We begin with the simplest example for an one-loop amplitude which is the N point amplitude in massive ϕ^3 theory with potential

$$
U(\phi) = \frac{\lambda}{3!}\phi^3.
\tag{4.69}
$$
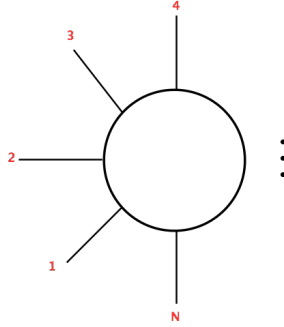
Figure 4.5: N point diagram in vacuum for massive ϕ^3 theory with potential U from (4.69). The dots indicate the remaining legs, $5, \ldots, N-1$, connected to the single particle loop.

The diagrammatic representation is depicted in figure 4.5. The corresponding effective action in the path integral representation can directly be obtained from (4.14) by inserting the derivative

$$U'' = \lambda \phi(x). \tag{4.70}$$

In standard QFT the one-particle irreducible (1PI)[22] N point function can be deduced from the N-fold derivative of the one-loop effective action $\Gamma[\phi]$ with respect to ϕ. In coordinate space, this can be done by expanding the interaction exponential [125]

$$e^{-\lambda \int_0^\infty d\tau \; \phi(x(\tau))} \tag{4.71}$$

in the coupling constant λ to N-th order and inserting δ functions in the appropriate places in the path integral such that

$$
\begin{aligned}
\Gamma[x_1, \ldots, x_N] &= \frac{(-\lambda)^N}{2} \int_0^\infty \frac{ds}{s} \, e^{-sm^2} \int \mathcal{D}x \prod_{j=1}^N \int_0^s d\tau_j \; \delta(x(\tau_j) - x_j) e^{-\int_0^s \frac{1}{4}\dot{x}^2} \\
&= \frac{(-\lambda)^N}{2} \left\langle \prod_{j=1}^N \int_0^s d\tau_j \; \delta(x(\tau_j) - x_j) \right\rangle.
\end{aligned}
\tag{4.72}
$$

A more efficient way operates as follows.

Namely, in momentum space, we can decompose the background ϕ into the sum of plane waves like

$$\phi(x) = \sum_{j=1}^N e^{ip_j \cdot x}. \tag{4.73}$$

---

[22] A diagram is called 1PI if it is still connected after any single line is cut [251].

Taking the contribution into account that contains every p_j only once leads to

$$\Gamma[p_1, \ldots, p_N] = \frac{(-\lambda)^N}{2} \int_0^\infty \frac{ds}{s} \, e^{-sm^2} \prod_{j=1}^N \int_0^s d\tau_j \int dx_0$$
$$\times \int \mathcal{D}y \, e^{i \sum_{j=1}^N p_j \cdot x(\tau_j)} e^{-\int_0^s \frac{1}{4}\dot{x}^2} \tag{4.74}$$

such that every external line is now represented by a scalar vertex operator of the form

$$V^\phi[p_j] = \int d\tau_j \, e^{ip_j \cdot x(\tau_j)}. \tag{4.75}$$

It is convenient to use the string-motivated variable splitting in (4.48). Then, the integral over the CM coordinate x_0 results in the generalized momentum conservation

$$\int dx_0 \, e^{ix_0 \cdot \sum_{j=1}^N p_j} = (2\pi)^D \delta \left(\sum_{j=1}^N p_j \right), \tag{4.76}$$

cf. equation (4.59). The remaining $\mathcal{D}y$ integration is Gaussian. After performing the relevant operations[23] in order to rewrite the second exponential and using the

---

[23] Choosing the momentum representation and splitting the bosonic *coordinate field* x^μ as in (4.48) leads to an integral of the form

$$\int \mathcal{D}y \, e^{-\int_0^s \frac{1}{4}\dot{y}^2 d\tau} \int_0^s \prod_{j=1}^N d\tau_j \, e^{i \sum_{j=1}^N p_j \cdot y(\tau_j)},$$

cf. (4.74). For the Gaussian integration the corresponding worldline *action* needs to be brought into an appropriate form. In general, this can be done by solving the equations of motion, obtained from the variation of the classical action, $\frac{\delta S}{\delta y(\tau)} = 0$, resulting in

$$-\frac{1}{4} 2\ddot{y}(\tau) - i \sum_{i=1}^N p_i^\mu \delta(\tau - \tau_i) = 0.$$

The solution can formally be written as

$$y(\tau) = -i \sum_{i=1}^N p_i^\mu \frac{1}{2} G_{\rm B}(\tau, \tau_i)$$

where $\frac{1}{2}G_{\rm B}$ denotes the Green's function for the Laplacian on the circle with circumference s. Using this, the second exponent becomes $\frac{1}{2} \sum_{j,i} G_{\rm B}(\tau_j, \tau_i) \, p_j \cdot p_i$. The bosonic function is given by [293]

$$G_{\rm B}(\tau_1, \tau_2) = |\tau_1 - \tau_2| - \frac{(\tau_1 - \tau_2)^2}{s} + C$$

where C is a constant usually set to $1/s$ which occurs due to some zero mode contribution. Note that if the momentum is preserved, which basically follows from the integral over the CM

elementary formula[24] leads to the following parameter integral

$$
\Gamma[p_1; \ldots; p_N] = \frac{(-\lambda)^N}{2} (2\pi)^D \delta\left(\sum p_j\right) \int_0^\infty \frac{ds}{s} \; (4\pi s)^{-D/2} e^{-sm^2}
$$
$$
\times \prod_{j=1}^N \int_0^s d\tau_j \; e^{\sum_{j,i=1}^N \frac{1}{2} G_{\mathrm{B}ji} \; p_j \cdot p_i} \tag{4.77}
$$

where the normalization constant in equation (4.50) has been applied. This can be taken as the simplest BK type master formula.

4.3.2 N photon amplitude in sQED
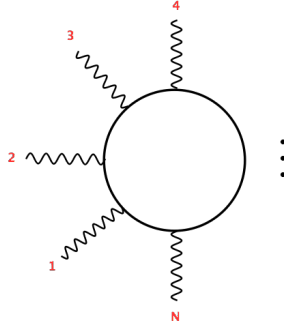
Figure 4.6: N photon diagram in vacuum for sQED, see equation (4.82). The dots indicate the remaining photon lines, $5, \ldots, N-1$, connected to the single scalar loop.

Gaining from the two photon example in section 4.2.4 and using the results for the N point amplitude in ϕ^3 theory in section 4.3.1, we can conduct the extension to the N photon amplitude in vacuum which is shown in figure 4.6. Starting on basis

---

coordinate x_0, any constant added to G_{B} drops out. Thus C can be usually deleted at the beginning, see (4.52).

Alternatively, we can interpret the momenta p_j^μ as sources of $y^\mu(\tau)$ [124],

$$
J^\mu(\tau) = i \sum_{i=1}^N p_i^\mu \delta(\tau - \tau_i),
$$

simply due to $i \sum p_i \cdot y_i = \int d\tau J \cdot y$, to write the exponential as

$$
e^{\int d\tau \int d\tau' \; \left[-\frac{1}{2} J^\mu(\tau) G_{\mathrm{B}}(\tau,\tau') J_\mu(\tau') \right]} = e^{\sum_{j,i=1}^N \frac{1}{2} G_{\mathrm{B}ji} \; p_j \cdot p_i}.
$$

---

[24] The Gaussian integral has the general solution

$$
\int dx \; e^{-x \cdot A \cdot x + 2b \cdot x} \simeq \frac{1}{\sqrt{\mathrm{Det}(A)}} e^{b \cdot A^{-1} \cdot b}.
$$

of the interaction potential (4.44) for the scalar case, the background will now be decomposed as a sum of N plane waves with definite polarization

$$A_\mu(x) = \sum_{j=1}^{N} \epsilon_\mu^{(j)} e^{ik_j \cdot x}. \tag{4.78}$$

Hence, one has to compute the following Wick contraction

$$\left\langle \dot{x}_1^{\mu_1} e^{ik_1 \cdot x_1} \cdots \dot{x}_N^{\mu_N} e^{ik_N \cdot x_N} \right\rangle \tag{4.79}$$

already commented on in (4.6). Accordingly, we end up with the expression

$$\epsilon_1^{\mu_1} \cdots \epsilon_N^{\mu_N} (ie)^N \int_0^\infty \frac{ds}{s} \int dx_0 \int \mathcal{D}y(\tau) \int_0^s d\tau_1 \cdots d\tau_N \tag{4.80}$$
$$\times \dot{y}_1^{\mu_1} \exp\left(ik_1 \cdot (x_0 + y_1)\right) \cdots \dot{y}_N^{\mu_N} \exp\left(ik_N \cdot (x_0 + y_N)\right) \exp\left(-\int_0^s d\tau \, \frac{1}{4} \dot{y}^2\right).$$

Note that the polarization vectors can be taken into account if one exponentiates the relevant expressions. The final result after the computation then has to be linearized[25] again in the polarization vectors such that the only terms to be used will be those which contain one ϵ_j. By doing so, the corresponding vertex operator can be written as

$$V^A[k_j] = \int d\tau_j \; e^{\epsilon_j \cdot \dot{x}(\tau) + ik_j \cdot x(\tau_j)} \Big|_{\text{linear in } \epsilon_j}. \tag{4.81}$$

The final result is the following parameter integral

$$\Gamma[k_1, \epsilon_1; \ldots; k_N, \epsilon_N] = (-ie)^N (2\pi)^D \delta\left(\sum k_j\right) \int_0^\infty \frac{ds}{s} \, (4\pi s)^{-D/2} \, e^{-sm^2}$$
$$\times \prod_{j=1}^{N} \int_0^s d\tau_j \; e^{\sum_{j,i=1}^N \left[\frac{1}{2} G_{\text{B}ji} \, k_j \cdot k_i - i \dot{G}_{\text{B}ji} \, \epsilon_j \cdot k_i + \frac{1}{2} \ddot{G}_{\text{B}ji} \, \epsilon_j \cdot \epsilon_i\right]} \Big|_{\text{linear in each } \epsilon}. \tag{4.82}$$

As before, D denotes the spacetime dimensionality. Notably, the Green's function now appears also in its first and second derivative.[26] Resorting to the superfield formalism discussed in section 4.2.7, it is possible to obtain an analogous formula for the fermionic case by computing Grassmann integrals [308].

---

[25] In other words, we rewrite the expression for any polarization vector as

$$\epsilon_j \cdot \dot{x}_j e^{ik_j \cdot x_j} = e^{\epsilon_j \cdot \dot{x}_j + ik_j \cdot x_j}\Big|_{\text{linear in } \epsilon_j}.$$

[26] The derivatives are given by

$$\dot{G}_{\text{B}}(\tau_1, \tau_2) = \text{sign}(\tau_1 - \tau_2) - 2\frac{(\tau_1 - \tau_2)}{s},$$
$$\ddot{G}_{\text{B}}(\tau_1, \tau_2) = 2\delta(\tau_1 - \tau_2) - \frac{2}{s}$$

where the derivative indicated by dots is with respect to the first variable.

4.4 One-loop amplitudes in static external background

In this section, we derive the N photon amplitude (4.82) for sQED in the presence of an external background.

4.4.1 Modified worldline correlators

Let $\mathcal{A}^{\mu}(x)$ be the external background satisfying $\mathcal{F}_{\mu\nu} = $ constant. It can be included similar to the procedure in dressed field theory where free propagators become simply embedded in the external background, see section 2.

In the present case, the external background will be absorbed into the free worldline correlators introduced in section 4.2.4 which are still quadratic in the worldline fields. Resorting to Fock-Schwinger gauge[27] centered at the CM coordinate x_0, we write

$$\mathcal{A}_{\mu}(x) = \frac{1}{2}y_{\nu}\mathcal{F}_{\mu\nu}. \tag{4.83}$$

This results in additional contributions[28] in the fermionic worldline Lagrangian,

$$\mathcal{W}_{\text{fermion}} \supset \frac{1}{2}iey^{\mu}\mathcal{F}_{\mu\nu}\dot{y}^{\nu} - ie\psi^{\mu}\mathcal{F}_{\mu\nu}\psi^{\nu} \tag{4.84}$$

in comparison to the pure vacuum amplitude (4.43). Hence, the equations determining the associated Green's functions generalize to

$$\langle\tau_1|\left(\frac{d^2}{d\tau^2} - 2ie\mathcal{F}\frac{d}{d\tau}\right)^{-1}|\tau_2\rangle = \frac{1}{2}\mathcal{G}_{\text{B}12},$$

$$\langle\tau_1|\left(\frac{d}{d\tau} - 2ie\mathcal{F}\right)^{-1}|\tau_2\rangle = \frac{1}{2}\mathcal{G}_{\text{F}12} \tag{4.85}$$

---

[27] In the background field approach, the Fock-Schwinger gauge with the condition $y_{\mu}\mathcal{A}_{\mu}(y) = 0$ is an efficient choice. It allows a representation of the gauge four-potential expanded only in terms of gauge covariant quantities such as field strength tensor and covariant derivatives [328]. For the static case, $\mathcal{F}_{\mu\nu} = $ constant, this results in the given relation (4.83).

[28] With the definitions in the superfield formalism introduced in section 4.2.7, these contributions can be written in a more compact form,

$$\mathcal{W}_{\text{fermion}} \supset -\frac{1}{2}ieY^{\mu}\mathcal{F}_{\mu\nu}DY^{\nu}.$$

having the solutions [125]

$$\mathcal{G}_{\text{B}12} = \frac{s}{2(e\mathcal{F}s)^2} \left[\frac{(e\mathcal{F}s)e^{-i(e\mathcal{F}s)\dot{G}_{\text{B}12}}}{\sin(e\mathcal{F}s)} + i(e\mathcal{F}s)\dot{G}_{\text{B}12} - 1 \right],$$
$$\mathcal{G}_{\text{F}12} = G_{\text{F}12} \frac{e^{-i(e\mathcal{F}s)\dot{G}_{\text{B}12}}}{\cos(e\mathcal{F}s)}. \tag{4.86}$$

These solutions can be seen as a power series in the Lorentz matrix $e\mathcal{F}s$. The modified Green's functions are still translation invariant in τ, so it means that they again depend only on $\tau_1 - \tau_2$ as in the vacuum case, see equations (4.52) and (4.54). Due to the complicated matrix structure, the contractions have the following tensorial form

$$\langle y_1^\mu y_2^\nu \rangle = -\mathcal{G}_{\text{B}12}^{\mu\nu},$$
$$\langle \psi_1^\mu \psi_2^\nu \rangle = \frac{1}{2}\mathcal{G}_{\text{F}12}^{\mu\nu}. \tag{4.87}$$

Similar to the vacuum case, the first and second derivatives of the bosonic Green's function will be relevant. Reducing the derivative order in the kinetic operator, the corresponding equations read

$$\langle \tau_1 | \left(\frac{d}{d\tau} - 2ie\mathcal{F} \right)^{-1} | \tau_2 \rangle = \frac{1}{2}\dot{\mathcal{G}}_{\text{B}12},$$
$$\langle \tau_1 | \left(\mathbb{I} - 2ie\mathcal{F} \left(\frac{d}{d\tau} \right)^{-1} \right)^{-1} | \tau_2 \rangle = \frac{1}{2}\ddot{\mathcal{G}}_{\text{B}12}, \tag{4.88}$$

which have solutions of the form

$$\dot{\mathcal{G}}_{\text{B}12} = \frac{i}{(e\mathcal{F}s)} \left[\frac{(e\mathcal{F}s)e^{-i(e\mathcal{F}s)\dot{G}_{\text{B}12}}}{\sin(e\mathcal{F}s)} - 1 \right],$$
$$\ddot{\mathcal{G}}_{\text{B}12} = 2\delta_{12} - \frac{2(e\mathcal{F}s)e^{-i(e\mathcal{F}s)\dot{G}_{\text{B}12}}}{s\sin(e\mathcal{F}s)}. \tag{4.89}$$

As we expect, expanding the functions $\mathcal{G}_{\text{B}12}, \dot{\mathcal{G}}_{\text{B}12}, \ddot{\mathcal{G}}_{\text{B}12}, \mathcal{G}_{\text{F}12}$ in the background field tensor, $\mathcal{F}_{\mu\nu}$, all higher order terms vanish in the limit $\mathcal{F}_{\mu\nu} \to 0$ and one obtains the free counterparts $G_{\text{B}12}, \dot{G}_{\text{B}12}, \ddot{G}_{\text{B}12}, G_{\text{F}12}$ [308].

In contrast to the vacuum functions $\dot{G}_{\text{B}}$ and G_{F}, the background dressed counterparts have nonvanishing coincidence limits,

$$\dot{\mathcal{G}}_{\text{B}}(\tau, \tau) = i\cot(e\mathcal{F}s) - \frac{i}{e\mathcal{F}s},$$
$$\mathcal{G}_{\text{F}}(\tau, \tau) = -i\tan(e\mathcal{F}s), \tag{4.90}$$

leading to the following substitution relation

$$\dot{\mathcal{G}}_{\mathrm{B}}(\tau, \tau) - \mathcal{G}_{\mathrm{F}}(\tau, \tau) = \frac{i}{\sin(e\mathcal{F}s)\cos(e\mathcal{F}s)} - \frac{i}{e\mathcal{F}s}. \tag{4.91}$$

4.4.2   EH effective Lagrangian

The goal is to derive the one-loop results from section 4.3 generalized to the case with a static external background. So we have to find out how the free path integral normalization determinants, see (4.50), change in the presence of the external background. It can be shown that these are given as [308, 329]

$$
\begin{aligned}
(4\pi s)^{-D/2} &\longrightarrow (4\pi s)^{-D/2}\det{}^{-\frac{1}{2}}\left(\frac{\sin(e\mathcal{F}s)}{e\mathcal{F}s}\right) &\text{(scalar)}, \\
(4\pi s)^{-D/2} &\longrightarrow (4\pi s)^{-D/2}\det{}^{-\frac{1}{2}}\left(\frac{\tan(e\mathcal{F}s)}{e\mathcal{F}s}\right) &\text{(spinor)}.
\end{aligned}
\tag{4.92}
$$

Here, we distinguish between the standard matrix determinant and the functional determinant.
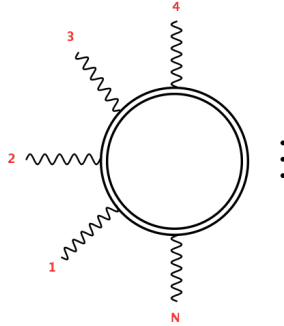
Figure 4.7: N photon diagram in static external background $\mathcal{A}^{\mu}$, see equation (4.4.3). The dots indicate the remaining photon lines, $5, \ldots, N-1$, connected to the single double lined scalar loop dressed by $\mathcal{A}^{\mu}$.

In the following, we demonstrate this modification for the scalar case. It is the following free path integral[29]

$$\int \mathcal{D}y \; e^{-\int_0^s d\tau \frac{1}{4}\dot{y}^2} = \frac{1}{\sqrt{\check{\mathrm{Det}}\left(-d^2/d\tau^2\right)}} \equiv (4\pi s)^{-D/2} \tag{4.93}$$

---

[29] Note that the second equality follows from $\int d\tau \; \dot{y}^2 = \int d\tau \; y\frac{-\partial^2}{\partial\tau^2}y$ plus the integral solution in footnote 24.

that has to be replaced by

$$\check{\mathrm{Det}}^{-\frac{1}{2}}\left(-\frac{d^2}{d\tau^2}+ie2\mathcal{F}\frac{d}{d\tau}\right) = (4\pi s)^{-D/2}\check{\mathrm{Det}}^{-\frac{1}{2}}\left(\mathbf{1}-ie2\mathcal{F}\left(\frac{d}{d\tau}\right)^{-1}\right). \tag{4.94}$$

We first transform $1/\sqrt{\check{\mathrm{Det}}(\cdots)}$, where $\check{\mathrm{Det}}$ is meant to be the determinant in the absence of the zero mode. Rewriting the expression in logarithmic form[30] and using the Mercator series,[31] we can find the following transform

$$\check{\mathrm{Det}}^{-\frac{1}{2}}\left(\mathbf{1}-ie2\mathcal{F}\left(\frac{d}{d\tau}\right)^{-1}\right) = \exp\left(\frac{1}{2}\sum_{n=1}^{\infty}\frac{(ie2)^n}{n}\mathrm{tr}(\mathcal{F}^n)\mathrm{Tr}\left(\left(\frac{d}{d\tau}\right)^{-n}\right)\right). \tag{4.95}$$

Using the relation [308]

$$\mathrm{Tr}\left(\left(\frac{d}{d\tau}\right)^{-n}\right) = -\frac{\mathcal{B}_n}{n!}s^n \tag{4.96}$$

for periodic functions, where $\mathcal{B}_n$ denotes the Bernoulli numbers[32] with even order n, the right-hand side of equation (4.95) can be written as

$$\exp\left(\frac{1}{2}\sum_{n=1}^{\infty}\frac{(ie2)^n}{n}\mathrm{tr}(\mathcal{F}^n)\mathrm{Tr}\left(\left(\frac{d}{d\tau}\right)^{-n}\right)\right) = \exp\left(\frac{1}{2}\sum_{n=1}^{\infty}\frac{\mathcal{B}_{2n}2^{2n}(-1)^n x^{2n}}{(2n)!(2n)}\right). \tag{4.97}$$

Applying the expansion formula afterwards,[33] we find by interchanging the map

---

[30] For this we use the relation

$$\mathrm{Det}^{-\frac{1}{2}}\hat{\mathcal{O}} = \exp\left(-\frac{1}{2}\ln\,\mathrm{Det}\hat{\mathcal{O}}\right).$$

[31] The Taylor series for the natural logarithm of the form $\ln(1+x)$ is known as the Mercator series

$$\ln(1+x) = \sum_{n=1}^{\infty}\frac{(-1)^{n+1}}{n}x^n.$$

[32] One should distinguish between the Bernoulli polynomials $\mathcal{B}_n(x)$ and the Bernoulli numbers $\mathcal{B}_n(0)$ being special values of the former. Here, the Bernoulli numbers are denoted as $\mathcal{B}_n$. Note that for all odd $n > 1$ one has $\mathcal{B}_n = 0$. Furthermore, we can write

$$\mathcal{B}_{2n} = \frac{-2(-1)^n(2n)!\zeta_{\mathrm{R}}(2n)}{(2\pi)^{2n}}$$

$\forall\,n \geq 1$ where ζ_{R} denotes the Riemann zeta function.

[33] Note that

$$\ln\left(\frac{\sin(x)}{x}\right) = -\sum_{n=1}^{\infty}\frac{\zeta_{\mathrm{R}}(2n)x^{2n}}{n\pi^{2n}}.$$

order for the logarithm of the trace the following exact resummation

$$\exp\left(\frac{1}{2}\sum_{n=1}^{\infty}\frac{\mathcal{B}_{2n}2^{2n}(-1)^n x^{2n}}{(2n)!(2n)}\right) = \exp\left(-\frac{1}{2}\ln\left(\operatorname{tr}\left(\frac{\sin(e\mathcal{F}s)}{e\mathcal{F}s}\right)\right)\right). \qquad (4.98)$$

The right-hand side leads to the given sQED result in (4.92).

Using the normalization determinant from (4.92), we can directly write the Euclidean one-loop EH effective action for sQED

$$\Gamma_{\mathrm{EH}} = VT\int_0^{\infty}\frac{ds}{s}\,(4\pi s)^{-D/2}e^{-sm^2}\det^{-\frac{1}{2}}\left(\frac{\sin(e\mathcal{F}s)}{e\mathcal{F}s}\right) \qquad (4.99)$$

where V and T denote the unit volume and unit time, respectively. Inserting the trace result [329]

$$\operatorname{tr}^{1/2}\left(\frac{\sin(e\mathcal{F}s)}{e\mathcal{F}s}\right) = \frac{\sin(eas)\sinh(ebs)}{(eas)(ebs)}, \qquad (4.100)$$

where

$$\operatorname{tr}(\mathcal{F}^{2n}) = 2\left[(a^2)^n + (-b^2)^n\right] \qquad (4.101)$$

applies for the static background with a and b as defined in (3.56), we arrive at the one-loop EH effective Lagrangian in (3.58).

4.4.3 N photon amplitude in sQED

Now, we have all relevant quantities in order to write down the effective action for the scalar N photon amplitude in the presence of a static electromagnetic background. The corresponding diagram is shown in figure 4.7. The single scalar loop dressed by the background (double line) is coupled to N background photon lines. Using the previous vacuum result (4.82) and inserting the modified normalization determinant from (4.92) as well as the modified worldline correlators (4.86) and (4.89), we finally arrive at the generalized BK type master formula

$$\begin{aligned}
\Gamma[k_1,\epsilon_1;\ldots;k_N,\epsilon_N] &= (-ie)^N\,(2\pi)^D\,\delta\left(\sum k_j\right) \\
&\times \int_0^{\infty}\frac{ds}{s}\,(4\pi s)^{-D/2}\,\det^{-\frac{1}{2}}\left(\frac{\sin(e\mathcal{F}s)}{e\mathcal{F}s}\right)\exp\left(-sm^2\right) \qquad (4.102) \\
&\times \prod_{j=1}^{N}\int_0^s d\tau_j\,\exp\left(\sum_{j,i=1}^{N}\left[\frac{1}{2}k_j\cdot\mathcal{G}_{\mathrm{B}ji}\cdot k_i - ie_j\cdot\dot{\mathcal{G}}_{\mathrm{B}ji}\cdot k_i + \frac{1}{2}\epsilon_j\cdot\ddot{\mathcal{G}}_{\mathrm{B}ji}\cdot\epsilon_i\right]\right)\Bigg|_{\substack{\text{linear in}\\\text{each }\epsilon}}.
\end{aligned}$$

Despite the additional determinant in front, the last exponent looks as in the pure vacuum case, with the exception that the worldline correlators now appear in tensorial form. This powerful formula we will use later for studying certain aspects in the assisted Schwinger mechanism.

Chapter 5

Worldline instantons

5.1 Weak coupling

WE consider sQED in the presence of an external background. As motivated in chapter 2 and carried out in the previous computations, we split the vector field again into the dynamical part A^μ and the external part $\mathcal{A}^\mu$. As before, we work in Euclidean space.[1] The corresponding action is

$$\int d^4x \ \left(\frac{1}{4} F^{\mu\nu} + |D^\mu \phi|^2 + m^2 |\phi^2| \right) \tag{5.1}$$

with the decomposed covariant derivative

$$D^\mu = \partial^\mu + ieA^\mu + ie\mathcal{A}^\mu. \tag{5.2}$$

In order to arrive at the one-loop EH effective action, we again neglect all contributions from the dynamical part of the vector field. This is referred to as the weak coupling regime. As will be discussed further below, using the present approach, it is also possible to make the generalization to the arbitrary coupling regime which gives rise to the quenched all-loop diagram.[2]

Proceeding as described above, the worldline Lagrangian $\mathcal{W}_{\text{boson}}$ in (4.20) with an external background $\mathcal{A}^\mu$ will include an additional contribution of the form

$$\mathcal{W}_{\text{boson}} \supset ie\dot{x} \cdot \mathcal{A}(x). \tag{5.3}$$

---

[1] See section 5.2 for details.

[2] For the quenched all-loop diagram see figure 5.4.

This yields the following worldline path integral representation

$$
\Gamma[\mathcal{A}] = \int_0^\infty \frac{ds}{s} \, \exp\left(-sm^2\right) \int d^4x_0 \int_{x(0)=x(s)=x_0} \mathcal{D}x(s)
$$
$$
\times \exp\left(-\int_0^s d\tau \, \frac{1}{4}\dot{x}^2 + ie\dot{x} \cdot \mathcal{A}(x)\right). \tag{5.4}
$$

For simplification we perform a variable rescaling [146, 158, 273]

$$
\tau \to us, \qquad sm^2 \to s \tag{5.5}
$$

which results in the following expression for the Euclidean effective action

$$
\Gamma[\mathcal{A}] = \int_0^\infty \frac{ds}{s} \, e^{-s} \oint \mathcal{D}x \, \exp\left(-\left(\frac{m^2}{4s}\int_0^1 du \, \dot{x}^2 + ie\int_0^1 du \, \dot{x} \cdot \mathcal{A}\right)\right). \tag{5.6}
$$

The previous periodicity condition in (5.4) now reads

$$
x^\mu(1) = x^\mu(0). \tag{5.7}
$$

Due to the integration over x_0, the worldline $x^\mu(u)$ becomes a closed periodic path in spacetime.

We begin with the proper time integral. For this, we introduce the following representation for the modified Bessel function of the second kind,

$$
K_0(x) = \frac{1}{2}\int_0^\infty \frac{ds}{s} \, e^{-\left(\frac{x^2}{4s}+s\right)}. \tag{5.8}
$$

Assuming x to be large, the latter has the following asymptotic behavior

$$
K_0(x) \approx \sqrt{\frac{\pi}{2x}} e^{-x}. \tag{5.9}
$$

Furthermore, we make the assumption

$$
m\sqrt{\int_0^1 du \, \dot{x}^2} \gg 1 \tag{5.10}
$$

which is often called the large mass approximation. As we will see below, this corresponds to the subcritical regime.

Now imposing the condition (5.10), we may use the asymptotic formula (5.9) to find

$$
\Gamma[\mathcal{A}] \simeq \oint \mathcal{D}x(u) \, \sqrt{\frac{2\pi}{m^2 s_0}} e^{-\mathcal{W}} \tag{5.11}
$$

with the worldline action

$$\mathcal{W} = \mathcal{W}_{\text{kin}} + \mathcal{W}_{\text{ext}} = m^2 s_0 + ie \int_0^1 du \; \dot{x} \cdot \mathcal{A} \tag{5.12}$$

that consists of a kinetic part $\mathcal{W}_{\text{kin}}$, which is the free scalar loop contribution, and an external part $\mathcal{W}_{\text{ext}}$ generating the arbitrary many couplings to the external background photons [273], cf. figure 3.1. The proper time stationary point is

$$s_0 = \frac{1}{m} \sqrt{\int_0^1 du \; \dot{x}^2(u)}. \tag{5.13}$$

This approximation is equivalent to the Laplace method or, in general, to the method of steepest descent. It is notable that performing the integrations in the opposite order, means first the path integral and then the proper time integral, will lead to the one-loop EH effective action.

5.2   Nonperturbative imaginary part

In the previous steps, we have focused on the real part of the Euclidean worldline path integral. In Minkowski spacetime the decay rate in (3.22) is determined by the imaginary part of the effective action. After continuing to the complex plane, the relevant quantity for pair production from vacuum will be the real part of the Euclidean effective action,

$$\Im(\Gamma_{\text{Mink}}) = \Re(\Gamma_{\text{Eucl}}). \tag{5.14}$$

In other words, we resign the Lorentzian time direction via a rotation in the complex plane in order to get a real valued action describing the decay of the vacuum state.

However, in order to guarantee this, one has to be careful with the choice for the external background. For the many examples we consider in this thesis, the Euclidean gauge potential $\mathcal{A}^\mu(x)$ is always a symmetric, complex valued function. This implies that the corresponding stationary path in spacetime is a closed real path. Accordingly, the stationary worldline action will be real as well which is in agreement with the correspondence from above.

5.3 Instanton equations

For the remaining path integral (5.11) we may use again the Laplace method.[3] For this, we need the stationary solution for the nonlocal worldline action

$$\mathcal{W} = m\sqrt{\int_0^1 du \ \dot{x}^2} + ie \int_0^1 du \ \dot{x} \cdot \mathcal{A} \tag{5.15}$$

which corresponds the extremum of the exponential. The condition is a vanishing first order functional derivative of the worldline action,

$$\delta \mathcal{W}_{:\mu} \equiv \frac{\delta \mathcal{W}_{:\mu}}{\delta x^\nu} \delta x^\nu + \frac{\delta \mathcal{W}_{:\mu}}{\delta \dot{x}^\nu} \delta \dot{x}^\nu \overset{!}{=} 0 \tag{5.16}$$

where $\mathcal{W}_{:\mu} \equiv \mathcal{W}[x^\mu(u), \dot{x}^\mu(u)]$. Using the standard functional operations[4] the latter computation gives first

$$\delta \mathcal{W}_{:\mu} = \int_0^1 du \ \left[\left(\frac{m\dot{x}^\nu(u)}{\sqrt{\int dk \ \dot{x}^2}} + ie\mathcal{A}^\nu \right) \delta \dot{x}^\nu + ie(\partial_\nu \mathcal{A}^\rho)\dot{x}^\rho \delta x^\nu \right] \tag{5.17}$$

---

[3] The underlying idea can be demonstrated for the following real integral

$$\int dx \ e^{-Mf(x)}$$

with a real function $f(x)$ of class $\mathcal{C}^2$. Assuming $M \gg 1$, this integral can be approximated with the Laplace method or, more generally in the complex case, with the method of steepest descent.

Namely, suppose the function $f(x)$ has some global minimum at x_0. Then, a small perturbation around x_0 will already be strongly suppressed exponentially. Hence, one may take only the value in x_0 as the dominating contribution for the integral. Taking this, the original function can be expanded around the minimum up to second order where the linear term will of course vanish by construction. Inserting the expansion into the initial integral and performing the integral, which can be done exactly due to its Gaussian character, finally gives

$$\int dx \ e^{-Mf(x)} \simeq e^{-Mf(x_0)} \int dx \ e^{\frac{M}{2}f''(x_0)(x-x_0)^2} = \sqrt{\frac{2\pi}{Mf''(x_0)}} e^{-Mf(x_0)}.$$

[4] Applying the functional operations

$$\frac{\delta S[F[x]]}{\delta x(u)} = \frac{\partial S[F[x]]}{\partial F[x]} \frac{\delta F[x]}{\delta x(u)}, \qquad \frac{\delta F[x(k)]}{\delta x(u)} = \frac{\delta \int dk \ F'[x(k)]}{\delta x(u)} = \frac{\partial F'}{\partial x}[x(u)]$$

consecutively, we derive first

$$\frac{\delta \sqrt{\int_0^1 dk \ \dot{x}^2}}{\delta \dot{x}^\nu(u)} = \frac{1}{2} \left(\int_0^1 dk \ \dot{x}^2 \right)^{-\frac{1}{2}} \frac{\delta \int_0^1 dk \ \dot{x}^2(k)}{\delta \dot{x}^\nu(u)} = \frac{1}{2} \left(\int_0^1 dk \ \dot{x}^2 \right)^{-\frac{1}{2}} 2 \ \dot{x}^\nu(u) = \frac{\dot{x}^\nu(u)}{\sqrt{\int dk \ \dot{x}^2(k)}}.$$

followed by

$$\delta\mathcal{W}_{;\mu} = -\int_0^1 du \left[\frac{m\ddot{x}^\nu(u)}{\sqrt{\int dk \ \dot{x}^2}} + ie(\partial_\rho\mathcal{A}^\nu)\dot{x}^\rho - ie(\partial_\nu\mathcal{A}^\rho)\dot{x}^\rho \right] \delta x^\nu \tag{5.18}$$

after partially integrating the first two terms multiplied with the variation $\delta\dot{x}^\nu$. In order to obey the condition (5.16), the following equation

$$\frac{m\ddot{x}^\nu}{\sqrt{\int_0^1 dk \ \dot{x}^2}} = ie\mathcal{F}_{\nu\rho}\dot{x}^\rho \tag{5.19}$$

has to be satisfied, where $\mathcal{F}_{\nu\rho}$ denotes the antisymmetric field tensor. It is easy to see that the left-hand side transforms to

$$\frac{m}{\sqrt{\int_0^1 dk \ \dot{x}^2}} \frac{d}{du} x^2 \tag{5.20}$$

after contracting with $\dot{x}^\nu$. Due to the fact that

$$\mathcal{F}_{\nu\rho}\dot{x}^\rho\dot{x}^\nu = 0, \tag{5.21}$$

we obtain an internal kinematic invariant denoted as

$$\dot{x}^2 =: a^2 = \text{constant.} \tag{5.22}$$

Finally, rewriting the proper time stationary point in (5.19) as $s_0 = \frac{a}{m}$, we end up with the following set of coupled second order differential equations

$$m\ddot{x}^\mu = iae\mathcal{F}_{\mu\nu}\dot{x}^\nu. \tag{5.23}$$

The solutions of the latter, so-called worldline instantons which we denote for a while as w^μ, are the mentioned closed periodic paths in spacetime. The leading order contribution to the tunneling rate is then determined by

$$\mathcal{R} \simeq e^{-\mathcal{W}_0}. \tag{5.24}$$

Using the second operation yields

$$\frac{\delta \int dk \ \mathcal{A}^\rho(x^\mu)\dot{x}^\rho}{\delta\dot{x}^\nu(u)} = \mathcal{A}^\nu(x^\mu(u)),$$

$$\frac{\delta \int dk \ \mathcal{A}^\rho(x^\mu)\dot{x}^\rho}{\delta x^\nu(u)} = (\partial_\nu\mathcal{A}^\rho)\dot{x}^\rho(u).$$

with $\partial_\nu \equiv \frac{\partial}{\partial_{x^\nu}}$.

The exponent

$$\mathcal{W}_0 \equiv \mathcal{W}[\text{instanton}] = ma + ie \int_0^1 du \, \dot{w} \cdot \mathcal{A}(w) \tag{5.25}$$

is the stationary worldline action from (5.12) evaluated on the instanton path. The complete solution including the fluctuation prefactor which will be discussed below is exact [151, 158, 161] for an action quadratic in $x^\mu(u)$ and approximate for actions with higher order dependence.

5.4   Stationary action: integral representation

For certain type of backgrounds one can follow an alternative way to compute the stationary worldline action $\mathcal{W}_0$ without deriving the instanton paths explicitly.

Let us assume a purely temporal electric background field oriented in the $\hat{x}_3$ direction. Furthermore, we restrict our discussion to the large mass limit (5.10), means, we only consider the leading $n = 1$ contribution. We write the Euclidean vector potential in the general form

$$\mathcal{A}_3(x_4) = -i\frac{E}{\omega}\mathfrak{F}(\omega x_4) \tag{5.26}$$

where $\mathfrak{F}$ is assumed to be an odd analytic function. The corresponding instanton equations in (5.23) then become

$$\begin{aligned}
\ddot{x}_3 &= -\frac{aeE}{m}\mathfrak{F}'(\omega x_4)\dot{x}_4, \\
\ddot{x}_4 &= +\frac{aeE}{m}\mathfrak{F}'(\omega x_4)\dot{x}_3
\end{aligned} \tag{5.27}$$

where $\dot{x}_1 = \dot{x}_2 = 0$. In order to find closed paths one can neglect all integration constants. Thus, the above equations can be integrated as

$$\begin{aligned}
\dot{x}_3 &= -a\frac{\mathfrak{F}(\omega x_4)}{\gamma}, \\
\dot{x}_4 &= \pm a\sqrt{1 - \frac{\mathfrak{F}^2(\omega x_4)}{\gamma^2}}.
\end{aligned} \tag{5.28}$$

The so-called adiabatic Keldysh parameter $\gamma = \frac{m\omega}{eE}$ serves as a useful measure to characterize the inhomogeneity of the background, see discussion in section 8.3. Due to the assumed symmetry property for $\mathfrak{F}$, the instanton path will be symmetric for each quarter in the (x_3, x_4) plane as illustrated in figure 5.1, see section 8.3
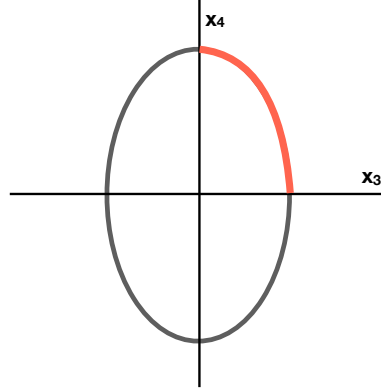
Figure 5.1: Sketch of a symmetric worldline instanton in the (x_3, x_4) plane. The path segment in first quarter is colored.

and [37]. Thus, one can evaluate the action over the first quarter and multiply the result by four afterwards. Proceeding in this way and expressing x_3, x_4 in units of $\frac{m}{eE}$, we obtain the stationary worldline action given in the following simplified integral form

$$\mathcal{W}_0 = \frac{4m^2}{eE} \int_0^{\mathfrak{z}} dz \ \sqrt{1 - \frac{\mathfrak{F}^2(\gamma z)}{\gamma^2}}. \tag{5.29}$$

The upper integration limit, $\mathfrak{z}$, which is taken as the turning point at the intersection with the neighbored quarter in the instanton plane, is determined by the relation

$$\gamma = \mathfrak{F}(\gamma \mathfrak{z}). \tag{5.30}$$

Hence, even without the explicit derivation of the instanton path it is possible to compute the stationary worldline action numerically, in certain cases, analytically as well.

In the following, we generalize the steps from above for an external background as a superposition of two time dependent fields varying at different time scales. We first write

$$\mathcal{A}_3(x_4) = -i\frac{E}{\omega} \left[\mathfrak{F}(\omega x_4) + \frac{\epsilon}{\widetilde{\omega}} \mathfrak{G}(\widetilde{\omega} x_4) \right] \tag{5.31}$$

where $\epsilon := \widetilde{E}/E$. The resulting instanton equations then read

$$\begin{aligned}
\ddot{x}_3 &= -\frac{aeE}{m}\left[\mathfrak{F}'(\omega x_4) + \epsilon\mathfrak{G}'(\widetilde{\omega} x_4)\right]\dot{x}_4, \\
\ddot{x}_4 &= +\frac{aeE}{m}\left[\mathfrak{F}'(\omega x_4) + \epsilon\mathfrak{G}'(\widetilde{\omega} x_4)\right]\dot{x}_3.
\end{aligned} \tag{5.32}$$

We can integrate the equations as

$$\begin{aligned}
\dot{x}_3 &= -a\frac{\mathfrak{F}(\omega x_4) + \epsilon(\gamma/\widetilde{\gamma})\mathfrak{G}(\widetilde{\omega} x_4)}{\gamma}, \\
\dot{x}_4 &= \pm a\sqrt{1 - \frac{\left[\mathfrak{F}(\omega x_4) + \epsilon(\gamma/\widetilde{\gamma})\mathfrak{G}(\widetilde{\omega} x_4)\right]^2}{\gamma^2}}
\end{aligned} \tag{5.33}$$

with $\widetilde{\gamma} := \frac{m\widetilde{\omega}}{eE}$. Expressing again x_3, x_4 in units of $\frac{m}{eE}$, we write the following integral for the worldline action evaluated on the instanton

$$\mathcal{W}_0 = \frac{4m^2}{eE}\int_0^{\mathfrak{z}} dz\,\sqrt{1 - \frac{\left[\mathfrak{F}(\gamma z) + \epsilon(\gamma/\widetilde{\gamma})\mathfrak{G}(\widetilde{\gamma} z)\right]^2}{\gamma^2}}. \tag{5.34}$$

The corresponding turning point $\mathfrak{z}$ at the intersection with the neighbored quarter in the instanton plane is determined by

$$\gamma = \mathfrak{F}(\gamma\mathfrak{z}) + \epsilon(\gamma/\widetilde{\gamma})\mathfrak{G}(\widetilde{\gamma}\mathfrak{z}). \tag{5.35}$$

This form will be useful for later purpose when we discuss the assisted mechanism delineated in section 1.4.

Without any complications, for a static electric background, means $\mathfrak{F}(\gamma z) = \gamma z$ and $\mathfrak{G} = 0$, we find the stationary action

$$\mathcal{W}_0 = \frac{4m^2}{eE}\int_0^1 dz\,\sqrt{1 - z^2} = \frac{\pi E_\mathrm{S}}{E} \tag{5.36}$$

which is precisely the leading order exponent in the Schwinger formula.

5.5   Fluctuation prefactor

So far we have discussed the leading order tunneling exponential determined by the stationary worldline action. In the following, we sketch the computing strategy for the remaining quantum fluctuation prefactor omitted in equation (5.24).

5.5.1   Semiclassical approximation

The exponential can be computed by evaluating the worldline action on the instanton. To derive the instanton equations we first have computed the proper time integral using the Laplace method. Afterwards, the remaining path integral has been evaluated by performing the method of steepest descends.

The tunneling exponential is the relevant part in studying enhancement effects via the assisted mechanism. However, the fluctuation prefactor can have significant impact for single mode backgrounds. For completeness its derivation will be discussed in the following.

The basic idea is to perform the integrations in the opposite order, namely, first approximating the path integral semiclassically and then performing the proper time integration by the method of steepest descents. Notably, even though the order is interchanged, the introduced instantons will remain as the stationary solutions so that these again constitute the basis for the relevant computations [330].

We start with the original path integral without rescaling the worldline time τ,

$$\oint \mathcal{D}x(s) \ e^{-S[x]}. \tag{5.37}$$

The action

$$S[x] = \int_0^s d\tau \ L \tag{5.38}$$

is determined by the Lagrange function

$$L[x, \dot{x}] = \frac{1}{4}\dot{x}^2 + ie\dot{x} \cdot \mathcal{A}(x). \tag{5.39}$$

The solutions for the classical Euclidean ELE

$$\ddot{x}^\mu = 2ie\mathcal{F}^{\mu\nu}\dot{x}^\nu \tag{5.40}$$

are given by the worldline instantons satisfying

$$\dot{x}^2 = (2m)^2. \tag{5.41}$$

To obtain the fluctuation prefactor, we need compute the fluctuations over the instanton paths. Hence, all paths in the functional integral can be expanded like

$$x^\mu(\tau) = w^\mu(\tau) + \eta^\mu(\tau) \tag{5.42}$$

where $\eta^\mu(0) = \eta^\mu(s) = 0$. Performing a semiclassical approximation for the path integral results in [331]

$$\oint \mathcal{D}x \ (\dots) \simeq \frac{e^{-S[w]}}{\sqrt{\text{Det}(\Lambda)}} \tag{5.43}$$

where $\Lambda^{\mu\nu}$ denotes the fluctuation operator

$$\Lambda^{\mu\nu} = -\frac{\delta_{\mu\nu}}{2}\frac{d^2}{d\tau^2} - \frac{d}{d\tau}\frac{\partial^2 L}{\partial x^\nu \partial \dot{x}^\mu} + \frac{\partial^2 L}{\partial x^\mu \partial \dot{x}^\nu}\frac{d}{d\tau} + \frac{\partial^2 L}{\partial x^\mu \partial x^\nu} \tag{5.44}$$

that determines the second order variation of the action [331, 332]

$$\delta^2 S[\eta] = \int_0^s d\tau \ \eta^\mu \Lambda^{\mu\nu} \eta^\nu. \tag{5.45}$$

5.5.2 Gel'fand–Yaglom method

The previous fluctuation operator Λ is just an ordinary differential operator. So it is possible to follow the Gel'fand–Yaglom approach to compute the determinant [310, 333–335]. Namely, according to the latter, this computation can be done without computing the eigenvalues of Λ. This is very advantageous for the underlying problem, since such an operation is strictly necessary for any proper time s in order to be able to perform the final integration over s.

The idea is to solve instead the equations of motion for the fluctuations η^μ over the stationary instanton path,

$$\Lambda^{\mu\nu}\eta^\nu(\tau) = 0. \tag{5.46}$$

These equations are known as the Jacobi equations [332]. Accordingly, the infinite dimensional functional determinant $\text{Det}(\Lambda)$ can be expressed in terms of a finite dimensional matrix determinant constructed from the values of the (four) independent solutions evaluated at $\tau = s$,

$$\text{Det}(\Lambda) = \det\left(\eta_\mu^{(\nu)}(s)\right). \tag{5.47}$$

The semiclassical approximation from (5.43) becomes

$$\oint \mathcal{D}x(s) \ e^{-S[x]} \simeq \frac{e^{i\theta}e^{-S[w](s)}}{(4\pi s)^2}\sqrt{\frac{\left|\det \eta_{\mu,\text{free}}^{(\nu)}(s)\right|}{\left|\det \eta_\mu^{(\nu)}(s)\right|}}. \tag{5.48}$$

The finite dimensional determinant $\det\left(\eta_\mu^{(\nu)}(s)\right)$ is determined by a 4×4 matrix formed by solutions for the Jacobi equations, i.e. $\eta_\mu^{(\nu)}(\tau)$, with initial conditions

$$\begin{aligned}
\eta_\mu^{(\nu)}(0) &= 0, \\
\dot{\eta}_\mu^{(\nu)}(0) &= \delta_{\mu\nu}
\end{aligned} \tag{5.49}$$

for $\mu, \nu = \{1, \ldots, 4\}$ [331, 332]. Analogously, $\det\left(\eta_{\mu,\text{free}}^{(\nu)}(s)\right)$ is determined by solutions of the free Jacobi equations

$$\Lambda_{\text{free}}^{\mu\nu} \eta_{\text{free}}^{\nu} = 0 \tag{5.50}$$

where

$$\Lambda_{\text{free}}^{\mu\nu} = -\frac{\delta_{\mu\nu}}{2} \frac{d^2}{d\tau^2}. \tag{5.51}$$

The phase θ in the constant factor $e^{i\theta}$ is related to the Morse index of the fluctuation operator Λ [332]. The Morse index accounts for the number of times the determinant $\det\left(\eta_\mu^{(\nu)}(\tau)\right)$ becomes zero for values $\tau \in [0, s]$ [336].

5.5.3 Analytical solutions

The closed instanton path $w^\mu(\tau)$ only depends on the (rescaled) worldline time. This renders the fluctuation operator (5.44) as a simple one-dimensional operator. For general backgrounds the computation of the determinant (5.47) can at least be treated numerically following the previous Gel'fand-Yaglom method. However, for certain one-dimensional backgrounds for which the instanton solution can be derived in closed form, a much more simple expression for the determinant of the fluctuation operator has been found.

For such backgrounds, the fluctuation operator is a reduced 2×2 matrix which depends, for instance, on the Euclidean worldline coordinates $x_3(\tau)$ and $x_4(\tau)$. In such a case, the solutions to the Jacobi equations (5.46) can be derived analytically where the boundary conditions can be easily imposed. Taking then the exact fluctuations satisfying all required properties, the determinant of the fluctuation operator can be written as [336]

$$\text{Det}(\Lambda) = \left(2m\dot{w}_4(s) \int_0^s \frac{d\tau}{[\dot{w}_4(\tau)]^2}\right)^2. \tag{5.52}$$

Inserting this closed form of the determinant into the corresponding integral, we find the Euclidean effective action

$$\int_0^\infty \frac{ds}{s} \frac{e^{-\left(sm^2+S[w](s)\right)}}{\sqrt{\mathrm{Det}(\Lambda)}}. \tag{5.53}$$

Performing the integral over τ in equation (5.52) and evaluating the proper time integral in expression (5.53) afterwards, leads to the complete VPP rate including the prefactor. In the weak field limit the latter integration can be done directly by applying the Laplace method.

5.6 Connection to Gutzwiller formula

In the following, we briefly sketch the derivation of the Gutzwiller trace formula. Afterwards, its application to the present problem is discussed.

5.6.1 Trace of Green's function

In the original worldline path integral representation (5.4), there are in total three integrals. Each of them contribute with its own prefactor to the final semiclassical result. As we will see in a moment, this resembles basically the derivation of the Gutzwiller trace formula [166, 175, 337]. The Gutzwiller formula expresses the trace of the Green's function in nonrelativistic quantum mechanics in terms of a weighted sum over classical, closed periodic orbits,

$$\mathrm{tr}(G(E)) = \int d^3x \; G(x,x;E)$$
$$= \int d^3x \int_0^\infty dt \; e^{iEt} \langle x|e^{iHt}|x\rangle = \sum_{\mathrm{orbit \; p}} T_\mathrm{p} \frac{e^{iS_\mathrm{p}(E)-i\pi\mathbf{m}_\mathrm{p}(E)/2}}{\sqrt{\det(\mathbf{1}-\mathbf{J}_\mathrm{p})}}. \tag{5.54}$$

Here, T_p stands for the period of the p-th orbit with energy E and $S_\mathrm{p}(E)$ for its action. The matrix $\mathbf{J}_\mathrm{p}$ denotes the so-called monodromy matrix and $\mathbf{m}_\mathrm{p}$ the Maslov index for the p-th orbit.

Starting with the sum on the right-hand side, the derivation works as follows: the first step is to approximate the split kernel semiclassically by making a WKB ansatz which leads to

$$K(x,x';t) := \langle x|e^{iHt}|x'\rangle$$
$$\simeq \sum_\mathrm{p} \sqrt{\left|\det\left(\frac{\partial W_\mathrm{p}(x,x';t)}{\partial x \partial x'}\right)\right|} e^{iW_\mathrm{p}(x,x';t)} e^{-i\pi\mathbf{m}_\mathrm{p}(x,x',t)/2}. \tag{5.55}$$

Here,

$$W_{\mathrm{p}}(x, x'; t) \equiv \int^{(x,x',t)} L(x''(t'), \dot{x}''(t')) \, dt' \tag{5.56}$$

denotes Hamilton's principal function defined as the function in the upper limit of the action integral with respect to the minimal trajectories of the system. These are in the present case all possible paths that connect the points x and x' in time t. We only focus on one contribution and therefore drop the subscript p representing the summation over all possible trajectory contributions. The Van Vleck determinant in front takes into account the variations with respect to x and x'. The Maslov index counts how often the sign of the determinant changes on the trajectory between x and x' [175].

As the second step, one performs the t integration in (5.54) by means of a stationary phase approximation.[5] From the expression in the exponent,

$$Et + W(x, x'; t), \tag{5.57}$$

obtained after plugging (5.55) into the integral in (5.54), we get the important condition

$$\partial_t W = -E. \tag{5.58}$$

Comparing the latter relation with the Hamilton-Jacobi equation (HJE)

$$\partial_t W = -H, \tag{5.59}$$

where H denotes the system's Hamilton function, the saddle point for t is just fixed as the time $T(x, x'; E)$ which the particle takes from x to x' at fixed energy E. Hence, introducing the Legendre transform

$$S(x, x'; E) = ET + W(x, x'; T), \tag{5.60}$$

we get from $W(x, x'; T)$ to the action $S(x, x'; E)$ for a closed trajectory with energy E. So, according to (5.60) we have

$$\frac{\partial S}{\partial E} = T, \qquad \frac{\partial W}{\partial T} = -E. \tag{5.61}$$

---

[5] This method is exact for time integrations from $-\infty$ to ∞. In case of integrating from 0 to ∞ it also leads to a good approximation when the saddle point is reached for a sufficiently large time.

From (5.56), we can write for the action

$$S(x, x'; E) = \int_0^T dt \ [L(x''(t), \dot{x}''(t)) + E]$$
$$= \int_0^T dt \ p(t)\dot{x}(t) = \int_x^{x'} p \ dx. \tag{5.62}$$

Noticing the previous transform, we have

$$\partial_x W = \partial_x S. \tag{5.63}$$

On the other hand, from the stationary point approximation for the t integral, we collect a second prefactor

$$\frac{1}{i\sqrt{\left.\frac{\partial^2 W}{\partial t^2}\right|_{t=T}}} = \frac{1}{\sqrt{-\left.\frac{\partial^2 W}{\partial t^2}\right|_{t=T}}} = \sqrt{\left.\frac{\partial^2 S}{\partial E^2}\right|_{t=T}} \tag{5.64}$$

where for the last equality the relation $\left.\frac{\partial S}{\partial E}\right|_{t=T} = T$ in (5.61) has been used. Inserting the obtained results into the trace expression (5.54), we find that

$$\int_0^\infty dt \ e^{iEt} \langle x|e^{iHt}|x'\rangle \approx \frac{\sqrt{\left|\det\left(\frac{\partial^2 W(x,x';t)}{\partial x \partial x'}\right)\right|_{t=T}}}{i\sqrt{\left.\frac{\partial^2 W}{\partial t^2}\right|_{t=T}}} e^{iS(x,x';E)} e^{-i\pi \mathbf{m}(x,x',T)/2}$$
$$= \sqrt{\left|\det\left(\frac{\partial^2 W(x,x';t)}{\partial x \partial x'}\right)\right|_{t=T}} \sqrt{\left.\frac{\partial^2 S}{\partial E^2}\right|_{t=T}} e^{iS(x,x';E)} e^{-i\pi \mathbf{m}(x,x',T)/2} \tag{5.65}$$

where we consider only one of the possible trajectories.

The third step is to take the limit $x' \to x$ due to the trace operation and integrate over x which forces the closed orbit to be periodic. It is advantageous to split the integration into the integral along the closed periodic orbit, $x_\parallel$, and transverse to it, $x_\perp$. Before taking the coincidence limit and integrating in configuration space, we first rewrite the prefactors in front of the exponentials by splitting up the coordinates. The determinant in (5.65) can be rewritten as

$$\det\left(-\frac{\partial^2 W(x,x';t)}{\partial x \partial x'}\right)\bigg|_{t=T} = \frac{\frac{\partial^2 W}{\partial t^2}}{\dot{x}_\parallel \dot{x}'_\parallel} \det\left(-\frac{\partial^2 S(x,x';E)}{\partial x_\perp \partial x'_\perp}\right). \tag{5.66}$$

Using the expression in (5.66), we arrive at the following approximation

$$G(x, x'; E) \approx \frac{\sqrt{\left|\det\left(-\frac{\partial S(x,x';E)}{\partial x_\perp \partial x'_\perp}\right)\right|}}{\sqrt{\dot{x}_\parallel \dot{x}'_\parallel}} e^{iS(x,x';E)} e^{-i\pi \mathbf{m}(x,x',T)/2} \tag{5.67}$$

which brings us to the trace

$$\text{tr}\left(G(E)\right) = \int d^d x \, G(x, x'; E)\Big|_{x=x'} = \int dx_\parallel d^{d-1} x_\perp \, G(x, x'; E)\Big|_{x=x'}. \qquad (5.68)$$

In the coincidence limit, the integral along the closed trajectory, the periodic orbit, gives

$$\oint \oint \sqrt{\frac{dx_\parallel}{\dot{x}_\parallel}} \sqrt{\frac{dx'_\parallel}{\dot{x}'_\parallel}} \Bigg|_{x=x'} = \oint \frac{dx_\parallel}{\dot{x}_\parallel} = \oint dt = T \qquad (5.69)$$

where T is the orbit period. The transverse integral produces a third prefactor

$$\frac{1}{\sqrt{\left|\det\left(\frac{\partial S}{\partial x_\perp \partial x_\perp} + \frac{\partial S}{\partial x_\perp \partial x'_\perp} + \frac{\partial S}{\partial x'_\perp \partial x_\perp} + \frac{\partial S}{\partial x'_\perp \partial x'_\perp}\right)\right|}}. \qquad (5.70)$$

where we should note that S only depends on the transversal coordinates due to the last integral along the closed orbit.

These prefactors, three in total, resulting from semiclassical approximations can be combined in form of a single determinant [166, 173]. The results finally lead to the compact expression

$$\int dx \left[\frac{\sqrt{\left|\det\left(\frac{\partial^2 W}{\partial x \partial x'}\right)\right|}\sqrt{\frac{\partial^2 S}{\partial E^2}}}{\sqrt{\left|\det\left(\frac{\partial^2 S}{\partial x_\perp \partial x_\perp}\right) + \cdots + \left(\frac{\partial^2 S}{\partial x'_\perp \partial x'_\perp}\right)\right|}}\right]_{x=x'} (\dots) \rightarrow \sum_{\text{orbit p}} T_{\text{p}} \frac{e^{iS_{\text{p}}(E)} e^{-i\pi \mathbf{m}_{\text{p}}(E)/2}}{\sqrt{|\det(\mathbf{1} - \mathbf{J}_{\text{p}})|}}. $$
$$(5.71)$$

The Maslov index and the sum over all possible orbit contributions have been restored. This single determinant is an invariant of the classical periodic orbit. In phase space, it characterizes the small deviations from the stable orbit described by the corresponding monodromy matrix $\mathbf{J}_{\text{p}}$.

5.6.2   Imaginary part of the effective action

Motivated by the previous discussion, we look for an analogous representation for the imaginary part of the one-loop EH effective action. We try to find an expression, again after resorting to Euclidean space, of the following form

$$\Gamma[\mathcal{A}] = \int d^4 x \int_0^\infty \frac{ds}{s} \, \langle x| e^{-s(-D_{\mathcal{A}}^2 + m^2)} |x\rangle = \sum_{\text{orbit p}} \frac{e^{-S_{\text{p}}(E)}}{\sqrt{|\det(\mathbf{1} - \mathbf{J}_{\text{p}})|}} \qquad (5.72)$$

where $D_{\mathcal{A}}^\mu = \partial^\mu + ie\mathcal{A}^\mu$ denotes the corresponding covariant derivative. Of course, we should be aware of that the Gutzwiller formula has been derived in Minkowski spacetime. In the present case, we also have an extra factor $\frac{1}{s}$. However, these changes still allow to proceed as in the previous case. It is advantageous to start with the second integral on the left-hand side in equation (5.72).

The first step is to make a WKB approximation for the underlying split kernel which results in

$$\langle x|e^{-s(-D_{\mathcal{A}}^2)}|x'\rangle \simeq \sqrt{\left|\det\left(\frac{\partial^2 W}{\partial x \partial x'}\right)\right|} e^{-W(x,x';s)}. \tag{5.73}$$

For simplifying reasons, we have dropped the exponent depending on the Maslov index $\mathbf{m}_\mathrm{p}$. The minus sign in the exponent appears due to the continuation to the complex domain. The Hamilton's principal function has to be understood with respect to the classical trajectory spanned between x and x' in Euclidean space for a single proper time interval s. Inserting the latter approximation into the integral, we get the exponent

$$sE + W(x, x'; s) \tag{5.74}$$

where

$$E = m^2 \tag{5.75}$$

can be understood as the conserved energy along the trajectory. Due to the irrelevance of the integration order, the trajectory is again determined by the classical ELE satisfying

$$\dot{x}^2 = (2m)^2. \tag{5.76}$$

So the critical point for the exponential is reached when

$$\partial_s W = -E. \tag{5.77}$$

Analogous to the derivation of the trace formula, it is appropriate to introduce a Legendre transform of the form

$$S(x, x'; E) = Es + W(x, x'; s). \tag{5.78}$$

The critical value for the proper time, $s_{\rm c}$, is approached when we set $E = m^2$. Hence, the original path integral can be approximated as

$$\int_0^\infty \frac{ds}{s} \; e^{-sE} \; \langle x|e^{-s(-D_A^2)}|x'\rangle \approx \frac{1}{s_{\rm c}} \sqrt{\left|\left.\det\left(\frac{\partial^2 W}{\partial x \partial x'}\right)\right|_{s=s_{\rm c}}\right|} \frac{1}{\sqrt{\left|\frac{\partial^2 W}{\partial s^2}\right|_{s=s_{\rm c}}}} e^{-S(x,x';E=m^2)}.$$

(5.79)

Then, splitting again the path along the classical trajectory into a transversal $x_\perp$ and a parallel coordinate $x_\parallel$, we find

$$\left.\frac{\det\left(\frac{\partial^2 W}{\partial x \partial x'}\right)}{\frac{\partial^2 W}{\partial s^2}}\right|_{s=s_{\rm c}} = \frac{1}{\dot{x}_\parallel \dot{x}'_\parallel} \det\left(\frac{\partial^2 S(x, x'; E = m^2)}{\partial x_\perp \partial x'_\perp}\right).$$

(5.80)

What remains to be done is to take the coincidence limit for the trace over position eigenstates. Due to translation invariance along the trajectory, the integration over the parallel coordinates gives

$$\int \frac{dx_\parallel}{\dot{x}_\parallel} = s_{\rm c}$$

(5.81)

which cancels the prefactor $\frac{1}{s_{\rm c}}$ in (5.79). Having included the third prefactor from the integration over $x_\perp$, i.e. (5.70) with $E = m^2$, we end up with the semiclassical approximation for the one-loop EH effective action

$$\Gamma \approx \frac{e^{-S(E=m^2)}}{\sqrt{|\det(\mathbf{1} - \mathbf{J})|}}$$

(5.82)

where the separate prefactors have been combined in form of a single prefactor determined by the monodromy matrix $\mathbf{J}$.

5.7 Tunneling exponential

In the following, we demonstrate the worldline instanton method for the static electric background. Using this method, the first derivation of the Schwinger formula, equation (3.66), has been derived in [158]. This is the simplest case where one can find a closed instanton path which has maximal symmetry in the two dimensional plane. As already pointed out in [158], this symmetry property leads to tremendous simplifications regarding the computation of higher loop diagrams, see section 5.9.2.

For a static background pointing in $\hat{x}_3$ direction we obtain the following relations from (5.23)

$$\dot{x}_4^2 + \dot{x}_3^2 = a^2, \qquad \frac{\ddot{x}_4}{\dot{x}_3} = \frac{a}{R}, \qquad \frac{\ddot{x}_3}{\dot{x}_4} = -\frac{a}{R}. \tag{5.83}$$

Here, a is the kinematic invariant from (5.22) and R represents some constant. Since $\frac{a}{R}$ is constant as well, we can integrate the second and third equation in (5.83) to obtain the system

$$\dot{x}_4 = \frac{a}{R} x_3, \qquad \dot{x}_3 = -\frac{a}{R} x_4 \tag{5.84}$$

where the integration constants vanish due to the periodicity condition (5.7) and the invariant (5.22). Squaring the latter equations and applying the first relation in (5.83) afterwards, we obtain the circle equation

$$x_4^2 + x_3^2 = R^2. \tag{5.85}$$

Hence, the instanton for a static field must be a circle. This observation one may also guess just by looking on the equations in (5.83). In particular the right-hand side of the last two equations is a fixed constant $\frac{a}{R}$. In other words, the ratio between the acceleration $\ddot{x}_4$ ($\ddot{x}_3$) in one direction and the velocity $\dot{x}_3$ ($\dot{x}_4$) in the remaining direction is constant. Kinematically, this situation is realized along a circle path. Hence, the electric field in Euclidean spacetime acts like a magnetic field leading to a circular instanton path.

Explicitly, with

$$\mathcal{A}_3(x_4) = -iEx_4, \tag{5.86}$$

the mentioned circular path in the (x_3, x_4) plane is described by [158]

$$\begin{aligned} x_3(u) &= R\cos\left(2\pi nu\right), \\ x_4(u) &= R\sin\left(2\pi nu\right), \end{aligned} \tag{5.87}$$

where $a = 2\pi nR$ and $R = \frac{m}{eE}$ follow due to (5.7), see figure 5.2.

Applying the instanton solution (5.87), we immediately see that the large mass approximation in (5.10) corresponds to the weak field limit

$$E \ll E_{\mathrm{S}}. \tag{5.88}$$
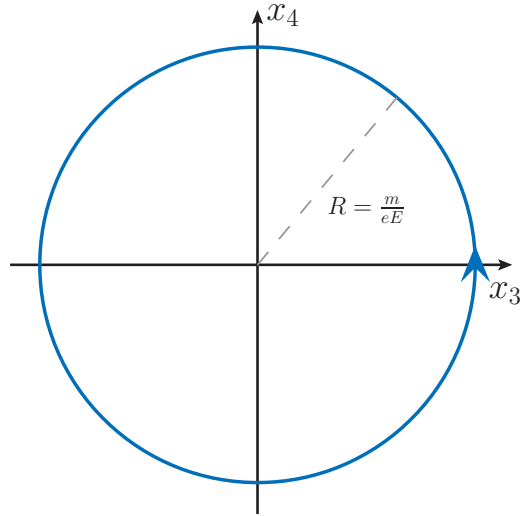
Figure 5.2: Worldline instanton for static electric background pointing in $\hat{x}_3$ direction.

Note that the distance along the spatial axis at time $x_4 = 0$ is

$$x = 2R = \frac{2m}{eE}. \tag{5.89}$$

As discussed in section 3.4.2.1, the latter relation can already be obtained from simple energy conservation. Therefore, the width of the effective energy gap between the excited particle states and the Dirac sea is naturally encoded in the spatial width[6] of the instanton at zero time.

Coming back to the circle solution from (5.87), we find the integer n included in a as the instanton's winding number that counts for the number of times the Euclidean path is traversed. The higher order instanton contributions with $n > 1$ correspond to the production of n pairs [338, 339]. It is not clear whether this argument is justified for the case of strongly coupled non-Abelian gauge theories. The term with $n = 1$ is the dominating contribution in the weak field limit (5.88) [158]. As mentioned in the introduction, this leading term is usually referred to as the VPP rate [339]. The fluctuation prefactor can be computed by inserting (5.87) into (5.52) and performing the s integral in (5.53) afterwards. The leading order result for the vacuum decay rate including all higher order instanton contributions then

---

[6] Note that backgrounds with temporal inhomogeneities in spacetime lead in general to a substantial reduction of the tunneling barrier, i.e. $m^* < m$, which corresponds then to a smaller spatial width $x^* < x$ of the instanton trajectory at $x_4 = 0$.

becomes

$$\mathcal{R} = \frac{(eE)^2}{(2\pi)^3} \sum_{n=1}^{\infty} \frac{(-1)^{n+1}}{n^2} e^{-\pi n \frac{E_{\mathrm{S}}}{E}}, \tag{5.90}$$

which is precisely the Schwinger formula introduced in (3.66).

5.8 Effect of inhomogeneities

As we have discussed in chapter 1, the effect of inhomogeneities on the VPP rate (3.23) can be enormous. Resorting to the worldline instanton approach these can be very elegantly illustrated in form of modified stationary paths in spacetime. It has been shown that temporal inhomogeneities of latter type tend to shrink the worldline instanton which leads to a larger VPP rate [146]. The reason for such an enhancement can therefore be obtained directly from the instanton equations in (5.23).

One should note that for arbitrary inhomogeneous backgrounds, particularly for spatiotemporal type, the situation can be very complicated due to the increasing nonlinear structure of the underlying differential equations (5.23). Hence, it can be quite difficult to get some approximate information directly from the instanton equations. Effects of spatiotemporal backgrounds have been recently studied [137–139, 152, 154, 162]. In the present case, we mainly focus on time dependent electric backgrounds.

In section 5.7, we have seen that the worldline instanton in a static electric background is a circle [158], see left panel in figure 5.3. Together with the quantum fluctuation prefactor these solutions including the higher order instanton contributions lead to the Schwinger formula (3.66). The situation with a nonstatic electric background is far more complicated. The system, one has to solve in this case, is given by

$$\dot{x}_4^2 + \dot{x}_3^2 = a^2, \qquad \frac{\ddot{x}_4}{\dot{x}_3} = f(x_4), \qquad \frac{\ddot{x}_3}{\dot{x}_4} = -f(x_4). \tag{5.91}$$

The constant right-hand side of the last two equations is now described by $\pm f(x_4)$. The function $f(x_4)$ is nothing but the analytic continuation — except the imaginary prefactor $-i$ — of the physical electric field. Therefore, inhomogeneous electric backgrounds may become unbounded positive monotonic functions in the

instanton equations, cf. lower right panel in figure 5.3.

Let us make this a bit more concrete. For instance, the sinusoidal cosine becomes after the rotation in the complex plane the hyperbolic cosine function. This in addition brings the imaginary prefactor[7] in front. In other words, the complex exponential of cosine becomes the unbounded real exponential.
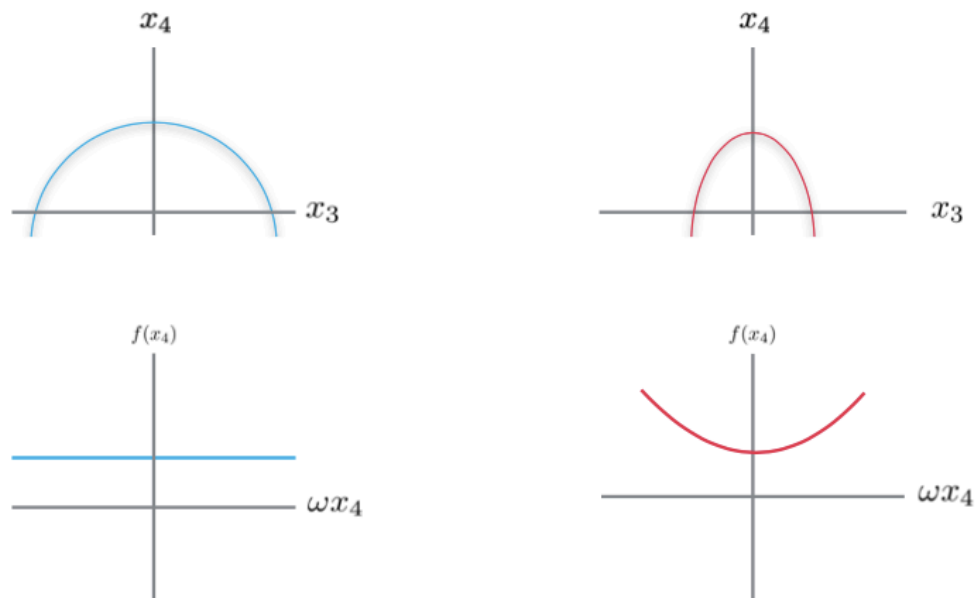
Figure 5.3: Effect of temporal field inhomogeneities: as an example, the comparison between a static and sinusoidal electric field is sketched. For the latter the bounded cosine function becomes after the rotation in the complex plane the (from above) unbounded hyperbolic cosine function (right). The static field remains static (left). Sketched instanton paths around the closing point are depicted on top.

In this case, one will find points where the acceleration in one direction may become much larger than the velocity in the other. The Euclidean equations of motion of such a system may have ellipse-like solutions which can curve much stronger than the usual circle path. As a consequence, the size of the worldline instanton can drastically be reduced for appropriate field parameters, e.g. sufficiently large temporal inhomogeneities [146]. From the previous discussion, this reduction would

---

[7] Note that it is this complex prefactor which forces the instanton solution to be real for the presently considered electric backgrounds.

correspond to a smaller instanton extension x^* at $x_4 = 0$ or smaller effective mass m^*, respectively. This can be understood as a reduction of the tunneling barrier. Consequently, the rate for VPP in such backgrounds will be increased. Note that the latter remains static even after continuation to the complex domain, cf. lower left panel in figure 5.3.

However, the huge impact of temporally inhomogeneous electric backgrounds on VPP is not only initiated by their unbounded shape in the instanton equations. Another effect results due to the appearance of pole structures in the instanton plane. It is this reason why despite the differences regarding interference effects,[8] a weak Sauter field leads to a stronger enhancement than a weak poleless sinusoidal field. Related studies are discussed in chapter 8.

5.9   Arbitrary coupling

5.9.1   Potential analysis

The nonanalytic dependence on the field strength E in the Schwinger formula (5.90) already indicates the nonperturbative behavior discussed in section 3.4.2. For VPP the virtual pair has to become real. This can only be achieved if the energy is larger then the static energy provided by the external source. Following an heuristic potential analysis, we may expect that the total potential barrier will basically consist of three parts,

$$V_{\text{tot}}(x) = 2m - eEx - \frac{\alpha}{x}, \tag{5.92}$$

where $\alpha = \frac{e^2}{4\pi} \approx \frac{1}{137}$ is the low-energy QED coupling constant. The first two terms are the static electron energy and the energy coming from the background, respectively. The third term arises due the Coulomb interaction between the pair constituents. This contribution has been completely neglected in the weak coupling approximation in section 5.1. In order to take this term into account, we

---

[8] With the standard worldline instanton approach one cannot directly access interference effects, see e.g. [34, 340–344]. A modification of the path integral via a Legendre transform proves helpful [160]. In this case, the saddle points have to be necessarily complexified which differ from the standard stationary worldline paths. The pole structure of the field can be essential for interference, cf. [37]. For further sensitivity and optimization studies such effects should be taken into account. In chapter 6, we introduce an alternative quantum mechanical scattering approach where different pairs of complex turning points give rise to quantum interference.

need to include the dynamical part of the vector field as well. This is nothing else than the introduction of arbitrary many virtual photon exchanges within the single scalar loop present in the one-loop EH diagram from figure 3.2. This situation is sketched in figure 5.4.
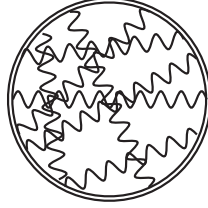
Figure 5.4: Quenched all-loop diagram with arbitrary many photon lines within the background dressed particle loop indicated by the double lined circle.

According to the potential analysis from above the tunneling exponential may be expected to be

$$\mathcal{R} \simeq \exp\left(-\frac{\pi E_{\mathrm{S}}}{E} + \alpha\pi\right). \tag{5.93}$$

Interestingly, using the electric-magnetic duality such an exponential behavior coincides with the production rate for a monopole and antimonopole pair in the Georgi-Glashow model [158, 345]. This coincidence can be considered as an evidence that the expression (5.93) is valid for arbitrary coupling in the weak field approximation.

Due to the potential barrier (5.92), we may expect the vacuum decay as soon as E surpasses the corresponding critical limit E_{c} which is easily computed as

$$E_{\mathrm{c}} = \frac{1}{\alpha}\frac{m^2}{e} \approx 137 E_{\mathrm{S}}. \tag{5.94}$$

This, obviously, exceeds the weak field condition $E \ll E_{\mathrm{S}}$ which brings the question in mind whether the catastrophic instability[9] can really happen or not. There has recently been made interesting progress on clarifying this open question in strongly coupled gauge theories using techniques based on the anti-de Sitter (AdS)/conformal field theory (CFT) correspondence [64, 66, 70, 71].

---

[9] The system is catastrophically unstable if the tunneling barrier vanishes for some critical value and pair production is driven without any exponential suppression.

5.9.2 Quenched amplitude

In the present instanton approach, the insertion of an arbitrary number of photon lines into the scalar loop leads to the following modified worldline path integral

$$
\mathcal{R} \simeq \int_0^\infty \frac{ds}{s} \exp\left(-m^2 s\right) \int d^4 x^{(0)} \int_{x(0)=x(s)} \mathcal{D}x(\tau)
$$
$$
\times \exp\left(-\int_0^s d\tau \left(\frac{\dot{x}^2}{4} + ie\mathcal{A}\cdot\dot{x}\right)\right) \left\langle \exp\left(ie \oint d\tau A\cdot\dot{x}\right)\right\rangle
\tag{5.95}
$$

where the average $\langle\cdots\rangle$ is defined as [158]

$$
\langle g(A)\rangle = \frac{\int \mathcal{D}A \exp\left(-\frac{1}{4}\int d^4 x\ F^2\right) g(A)}{\int \mathcal{D}A \exp\left(-\frac{1}{4}\int d^4 x\ F^2\right)}.
\tag{5.96}
$$

Here, we keep only diagrams with a single scalar loop and drop off all higher order scalar loop contributions. In other words, we ignore all correlations between different $\mathrm{Tr}\ln\left(-D^2 + m^2\right)$ [345] , see appendix B. It has been argued that higher order scalar loop correlations, as depicted in figure 5.5, are strongly suppressed in the weak field limit (5.88) or large mass approximation (5.10), respectively [158]. So the additional virtual photon lines within the scalar loop are included in form
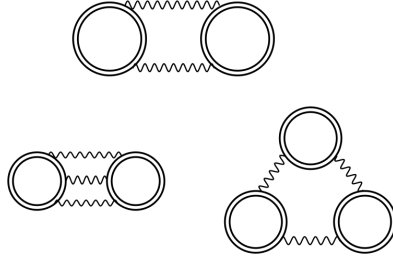
Figure 5.5: Diagrams at 3-loop (top) and 4-loop level (bottom) including multiple background dressed scalar loops (double lined loops) connected to each other via additional photon lines.

of an averaged $U(1)$ Wilson loop.

Now, assuming again (5.10) and using the asymptotic formula for the modified Bessel function (5.9), we perform the proper time integral in (5.95) and arrive at

$$
\mathcal{R} \sim \oint \mathcal{D}x(u) \sqrt{\frac{2\pi}{m^2 s_0}} \exp\left(-\mathcal{W}\right) \left\langle \exp\left(ie \oint d\tau A\cdot\dot{x}\right)\right\rangle,
\tag{5.97}
$$

where $\mathcal{W} \simeq \mathcal{W}_{\mathrm{kin}} + \mathcal{W}_{\mathrm{ext}}$ corresponds to the previous worldline action in the weak coupling regime, see (5.12). The additional averaged $U(1)$ Wilson loop in (5.97)

can be transformed to [158]

$$\left\langle \exp\left(ie \oint d\tau A \cdot \dot{x}\right)\right\rangle = \exp\left(\mathcal{W}_{\text{int}}\right) \tag{5.98}$$

with an internal Coulomb interaction exponent

$$\mathcal{W}_{\text{int}} = -\frac{\alpha}{2\pi} \oint \oint \frac{dx_1 \cdot dx_2}{(x_1 - x_2)^2} \tag{5.99}$$

where $x_j \equiv x(u_j)$. Accordingly, we find an extended worldline action of the form

$$\mathcal{W} = \mathcal{W}_{\text{kin}} + \mathcal{W}_{\text{ext}} + \mathcal{W}_{\text{int}}. \tag{5.100}$$

The remaining path integral (5.97) can be computed semiclassically by applying the circular instanton from (5.87). Basically, the stationary point should change due to the additional Coulomb interaction. However, the exponent $\mathcal{W}_{\text{int}}$ is invariant under scale transformations and rotations in the rotating plane of the instanton. Therefore, the worldline instanton in (5.87) does not change if one adds the additional Wilson loop as a perturbation. Evaluating the worldline action (5.100) on the circle instanton using dimensional regularization yields

$$\mathcal{R} \sim \exp\left(-\frac{\pi n E_{\text{S}}}{E} + \alpha \pi n\right). \tag{5.101}$$

This coincides with the heuristic prediction in (5.93) for $n = 1$ which is the dominant term in the weak field limit (5.88). The regularization is necessary due to an nonphysical divergence. Since the contributions of the Coulomb interaction are small, the previously introduced fluctuation prefactor does not change [158]. The final result for the rate is then given by

$$\mathcal{R} = \frac{(eE)^2}{(2\pi)^3} \sum_{n=1}^{\infty} \frac{(-1)^{n+1}}{n^2} \exp\left(-\frac{\pi n E_{\text{S}}}{E} + \alpha \pi n\right). \tag{5.102}$$

The latter expression is known as the Affleck-Alvarez-Manton (AAM) formula [158] which generalizes the standard Schwinger formula from (5.90).

5.9.3 All-loop conjecture

The AAM formula (5.102) is very interesting. Namely, according to [158] it includes an arbitrary number of loop diagrams in the quenched limit. Independent from the semiclassical derivation of the AAM formula in sQED, the imaginary part

of the EH effective Lagrangian at two-loop level for spinors was studied in [338]. The authors have found that

$$\Im\left(\mathcal{L}_{\mathrm{EH}}^{(2)}\right) = \frac{(eE)^2}{(2\pi)^3} \sum_{n=1}^{\infty} \alpha\pi K_n\left(\frac{E}{E_{\mathrm{S}}}\right) \exp\left(-\frac{\pi n E_{\mathrm{S}}}{E}\right) \tag{5.103}$$

which is similar to the standard Schwinger formula from (3.65) (corresponding to the one-loop effective Lagrangian) with the exception that each term in the sum is multiplied with a prefactor K_n depending on the summation index. These prefactors are not known exactly. However, in the weak field limit which has been assumed for the derivation of (5.100) their form is known [338]. Taking the dominant contributions in (3.65) and (5.103), it can be shown that

$$\Im\left(\mathcal{L}_{\mathrm{EH}}^{(1)}\right) + \Im\left(\mathcal{L}_{\mathrm{EH}}^{(2)}\right) \sim \frac{(eE)^2}{(2\pi)^3}\left(1 + \alpha\pi\right) e^{-\pi\frac{E}{E_{\mathrm{S}}}}. \tag{5.104}$$

According to [338] the additional $\alpha\pi$ can be seen as the truncation of an expansion series resulting due to an effective mass $m_*(E)$. Namely, a virtual pair that has to become real at a separation $x = \frac{2m}{eE}$, would experience a negative binding energy $-\frac{\alpha}{x}$ if the Coulomb attraction is taken into account leading to the mentioned effective mass

$$m_* \simeq m\left(1 - \frac{\alpha}{2}\frac{E}{E_{\mathrm{S}}}\right) \tag{5.105}$$

with higher order corrections in E/E_{S} [346, 347]. Then replacing the on-shell renormalized vacuum mass m in the tunneling exponential by the effective mass from above leads to

$$\begin{aligned}
\exp\left(-\pi\frac{m_*^2}{eE}\right) &= \exp\left(-\pi\frac{E}{E_{\mathrm{S}}} + \pi\alpha\right)\exp\left(-\pi\left(\frac{m\alpha}{2}\frac{E}{E_{\mathrm{S}}}\right)^2\right) \\
&= \left[1 + \alpha\pi + \mathcal{O}(\alpha^2)\right]\exp\left(-\pi\frac{E}{E_{\mathrm{S}}}\right).
\end{aligned} \tag{5.106}$$

In the weak field limit this result agrees with the $n = 1$ exponential in the generalized AAM formula[10] from (5.102). Motivated by this insight, one may think of (5.102) as an all-loop conjecture in the weak field limit.

Notably, for the self dual background in $3 + 1$ dimensions, defined by

$$\mathcal{F}_{\mu\nu} = \frac{1}{2}\epsilon_{\mu\nu\alpha\beta}\mathcal{F}^{\alpha\beta}, \tag{5.107}$$

---

[10] Note that in the weak field limit the expression is spin independent and varies just by a factor $1/2$ compared to the QED result.

the analogous functions to the prefactors in (5.103) are explicitly known. In the weak field limit the relation between the one-loop and the two-loop contributions for this case are the same as in (5.104) [281]. This case has not been extended to the three-loop level either. However, it has been shown that there is a similar behavior for the dual two-loop result in $1 + 1$ dimensional sQED [348]. For the spinor case the one- and two-loop contributions are surprisingly simpler [279]. Based on this, recently the three-loop extension has been studied for this lower dimensional case [280, 349]. The findings indicate some deviations from the conjectured scalar all-loop behavior described by the AAM formula given in (5.102). However, this is so far only obtained for QED in two dimensions. This will of course not cover the exact situation in the higher dimensional cases, but may at least provide some hints regarding the situation beyond the two-loop level.

Chapter 6

Wentzel-Kramers-Brillouin approximation

6.1 Scattering problem

F OR one-dimensional temporal electric backgrounds, it is possible to reformulate the problem of VPP as a quantum mechanical scattering problem where the antiparticle can be seen as a particle traveling backward in time [350]. The main task is to compute the reflection probability which determines the number of produced pairs in some momentum mode. This task is possible via numerical or WKB techniques [37, 133, 134, 141–143, 341, 351–356] where the latter can be seen as a relativistic version of the seminal Keldysh approach [357, 358] used for investigating ionization in time dependent electric fields. There is also an alternative way via the quantum kinetic approach [359–367] which we introduce in chapter 7.

We assume a background pointing in $\hat{x}_3$ direction where $E(t) = -\dot{\mathcal{A}}(t)$. For the purely electric case the quantum field operators can be decomposed in terms of spatial momenta which are appropriate quantum numbers. In the following, we discuss both sQED and QED. The number of pairs for a specific momentum mode is determined by the reflection coefficient for the corresponding quantum mechanical scattering problem.

6.1.1   Bosons

The bosonic field operator can be decomposed as

$$\Phi(\mathbf{x}, t) = \int d^3k \exp(i\mathbf{k} \cdot \mathbf{x}) \left[\phi_{\mathbf{k}}(t)\hat{a}_{\mathbf{k}} + \phi_{\mathbf{k}}^*(t)\hat{b}_{-\mathbf{k}}^\dagger \right]. \tag{6.1}$$

Here, $\hat{a}_{\mathbf{k}}$ ($\hat{a}_{\mathbf{k}}^\dagger$) is the particle creation (annihilation) operator for each mode $\mathbf{k}$ and $\hat{b}_{-\mathbf{k}}$ ($\hat{b}_{-\mathbf{k}}^\dagger$) denotes the antiparticle creation (annihilation) operator, respectively. As required, these operators obey the bosonic commutations relations.[1] Inserting the decomposed field operator Φ into the Klein-Gordon equation,

$$\left(\Box + m^2 \right) \Phi = 0, \tag{6.2}$$

with the standard d'Alembert operator $\Box$, the latter transforms into the following decoupled equation for each of the mode functions,

$$\ddot{\phi}_{\mathbf{k}}(t) + \Omega_{\mathbf{k}}^2(t)\phi_{\mathbf{k}}(t) = 0 \tag{6.3}$$

where

$$\Omega_{\mathbf{k}}^2(t) := m^2 + \mathbf{k}_\perp^2 + (k_\parallel - e\mathcal{A}(t))^2. \tag{6.4}$$

The quantity $\mathbf{k}_\perp$ denotes the momentum transversal to the background field orientation and $k_\parallel$ is the momentum component pointing in the same direction. We can define an effective potential

$$V(t) := -(k_\parallel - e\mathcal{A}(t))^2 \tag{6.5}$$

and energy

$$\varepsilon := m^2 + \mathbf{k}_\perp^2, \tag{6.6}$$

so that

$$\Omega_{\mathbf{k}}(t) = \varepsilon - V(t). \tag{6.7}$$

---

[1] The bosonic commutation relations are

$$[\hat{a}_{\mathbf{k}}, \hat{a}_{\mathbf{k}'}] = 0, \qquad \left[\hat{a}_{\mathbf{k}}^\dagger, \hat{a}_{\mathbf{k}'}^\dagger\right] = 0, \qquad \left[\hat{a}_{\mathbf{k}}, \hat{a}_{\mathbf{k}'}^\dagger\right] = \delta_{\mathbf{k},\mathbf{k}'}.$$

The operators $\hat{a}_{\mathbf{k}}$ and $\hat{a}_{\mathbf{k}}^\dagger$ are the creation and annihilation operators for the mode $\mathbf{k}$. Note that the present convention is different from the one introduced in chapter 7.

Then, the equation from above transforms into the time dependent Schrödinger equation,

$$-\ddot{\phi}_{\mathbf{k}}(t) + V(t) = \varepsilon\phi_{\mathbf{k}}(t). \tag{6.8}$$

Next, as the mentioned WKB ansatz, we rewrite the solution for each mode as

$$\phi_{\mathbf{k}}(t) = \frac{\alpha_{\mathbf{k}}(t)}{\sqrt{2\Omega_{\mathbf{k}}(t)}}e^{-i\int^t \Omega_{\mathbf{k}}} + \frac{\beta_{\mathbf{k}}(t)}{\sqrt{2\Omega_{\mathbf{k}}(t)}}e^{i\int^t \Omega_{\mathbf{k}}}, \tag{6.9}$$

$$\dot{\phi}_{\mathbf{k}}(t) = -i\Omega_{\mathbf{k}}(t)\left[\frac{\alpha_{\mathbf{k}}(t)}{\sqrt{2\Omega_{\mathbf{k}}(t)}}e^{-i\int^t \Omega_{\mathbf{k}}} + \frac{\beta_{\mathbf{k}}(t)}{\sqrt{2\Omega_{\mathbf{k}}(t)}}e^{i\int^t \Omega_{\mathbf{k}}}\right]. \tag{6.10}$$

Here, $\alpha_{\mathbf{k}}(t)$ and $\beta_{\mathbf{k}}(t)$ denote Bogoliubov coefficients which obey the following coupled first order differential equations

$$\dot{\alpha}_{\mathbf{k}}(t) = \frac{\dot{\Omega}_{\mathbf{k}}(t)}{\Omega_{\mathbf{k}}(t)}\frac{\beta_{\mathbf{k}}(t)}{2}e^{2i\int^t \Omega_{\mathbf{k}}}, \qquad \dot{\beta}_{\mathbf{k}}(t) = \frac{\dot{\Omega}_{\mathbf{k}}(t)}{\Omega_{\mathbf{k}}(t)}\frac{\alpha_{\mathbf{k}}(t)}{2}e^{-2i\int^t \Omega_{\mathbf{k}}}. \tag{6.11}$$

Introducing these coefficients leads to a change from the standard time independent creation and annihilation operators $\hat{a}_{\mathbf{k}}$ and $\hat{b}^{\dagger}_{-\mathbf{k}}$ to instantaneous, i.e. time dependent, operators $\hat{A}_{\mathbf{k}}(t)$ and $\hat{B}^{\dagger}_{-\mathbf{k}}(t)$. The relation between these operators is given by the linear transformation

$$\begin{pmatrix} \hat{A}_{\mathbf{k}}(t) \\ \hat{B}^{\dagger}_{-\mathbf{k}}(t) \end{pmatrix} = \begin{pmatrix} \alpha_{\mathbf{k}}(t) & \beta^*_{\mathbf{k}}(t) \\ \beta_{\mathbf{k}}(t) & \alpha^*_{\mathbf{k}}(t) \end{pmatrix} \begin{pmatrix} \hat{a}_{\mathbf{k}} \\ \hat{b}_{-\mathbf{k}} \end{pmatrix}. \tag{6.12}$$

The associated unitarity condition

$$|\alpha_{\mathbf{k}}(t)|^2 - |\beta_{\mathbf{k}}(t)|^2 = 1 \tag{6.13}$$

preserves the bosonic commutation relations for the instantaneous operators $\hat{A}_{\mathbf{k}}(t)$ and $\hat{B}_{-\mathbf{k}}(t)$. According to this convention, the number of pairs with momentum $\mathbf{k}$ produced from the vacuum is given by the modulus of the coefficient $\beta_{\mathbf{k}}(\infty)$,

$$N_{\mathbf{k}} = |\beta(t = +\infty)|^2. \tag{6.14}$$

The factor β describes the electron with momentum $\mathbf{k}$ excited in the positive continuum and, after leaving behind a hole in the negative Dirac sea, a positron with $-\mathbf{k}$, see also chapter 7. For the effective Schrödinger problem from above, the

number of produced pairs can be expressed in terms of the reflection probability[2]

$$|R_{\mathbf{k}}|^2 = \left|\frac{\beta_{\mathbf{k}}(t)}{\alpha_{\mathbf{k}}(t)}\right|^2_{t=\infty}, \tag{6.15}$$

namely as

$$N_{\mathbf{k}} = \frac{|R_{\mathbf{k}}|^2}{1 - |R_{\mathbf{k}}|^2}. \tag{6.16}$$

Since the potential V is defined to be negative and the energy E is positive, the present problem corresponds to an over-the-barrier scattering. Due to this, the reflection coefficient is exponentially small in the semiclassical regime, $E \ll m^2$, and one may use the approximation

$$N_{\mathbf{k}} \approx |R_{\mathbf{k}}|^2. \tag{6.17}$$

6.1.2   Fermions

In the fermionic case, the field operator can be decomposed in an analogous way with the exception that there appears an additional sum over helicity $s = \pm 1$,

$$\Psi(\mathbf{x}, t) = \sum_s \int d^3k \exp(i\mathbf{k} \cdot \mathbf{x}) \left[u_{\mathbf{k},s}(t)\hat{a}_{\mathbf{k},s} + v_{-\mathbf{k},s}\hat{b}^\dagger_{-\mathbf{k},s} \right]. \tag{6.18}$$

Here, the creation and annihilation operators have to satisfy the fermionic anti-commutation relations.[3] In some appropriate basis for the Dirac matrices γ^μ the underlying equation

$$\left(i\slashed{\partial} - m \right) \Psi = 0 \tag{6.19}$$

with $\slashed{\partial} \equiv \gamma^\mu \partial_\mu$ can be transformed into the following time dependent Schrödinger type equation

$$\ddot{\psi}_{\mathbf{k}}(t) + \left[Q_{\mathbf{k}}^2(t) + ik_\parallel(t) \right] \psi_{\mathbf{k}}(t) = 0 \tag{6.20}$$

---

[2] From equation (6.13) we derive

$$|R_{\mathbf{k}}|^2 = \frac{|\beta_{\mathbf{k}}|^2}{1 + |\beta_{\mathbf{k}}|^2} = \frac{N_{\mathbf{k}}}{1 + N_{\mathbf{k}}}.$$

[3] The fermionic anticommutation relations are

$$\{\hat{a}_{\mathbf{k},s}, \hat{a}_{\mathbf{k}',s'}\} = 0, \qquad \left\{\hat{a}^\dagger_{\mathbf{k},s}, \hat{a}^\dagger_{\mathbf{k}',s'}\right\} = 0, \qquad \left\{\hat{a}_{\mathbf{k},s}, \hat{a}^\dagger_{\mathbf{k}',s'}\right\} = \delta_{\mathbf{k},\mathbf{k}'}\delta_{s,s'}.$$

with

$$k_\parallel(t) \equiv k_\parallel - e\mathcal{A}(t).$$
(6.21)

Making an appropriate WKB ansatz for the solution, cf. [368], the associated Bogoliubov coefficients are determined by the following coupled first order differential equations

$$\dot{\alpha}_{\mathbf{k}}(t) = \frac{\dot{k}_\parallel(t)\varepsilon}{2Q_{\mathbf{k}}^2(t)}\beta_{\mathbf{k}}(t)e^{2i\int^t Q_{\mathbf{k}}}, \quad \dot{\beta}_{\mathbf{k}}(t) = -\frac{\dot{k}_\parallel(t)\varepsilon}{2Q_{\mathbf{k}}^2(t)}\alpha_{\mathbf{k}}(t)e^{-2i\int^t Q_{\mathbf{k}}}.$$
(6.22)

The corresponding unitarity condition is

$$|\alpha_{\mathbf{k}}(t)|^2 + |\beta_{\mathbf{k}}(t)|^2 = 1$$
(6.23)

which preserves the fermionic anticommutation relations for the resulting time dependent creation and annihilation operators. In contrast to the previous bosonic case the sign is changed. Accordingly, the number of produced pairs with momentum $\mathbf{k}$ is given by

$$N_{\mathbf{k}} = |\beta(t = +\infty)|^2 = \frac{|R_{\mathbf{k}}|^2}{1 + |R_{\mathbf{k}}|^2}.$$
(6.24)

Again, assuming that the reflection probability $|R_{\mathbf{k}}|^2$ is typically a small number, we may finally approximate

$$N_{\mathbf{k}} \approx |R_{\mathbf{k}}|^2.$$
(6.25)

6.2 Riccati equation

6.2.1 Bosons

It is possible to transform the quantum mechanical problem (6.8) into an appropriate differential equation. The latter is advantageous for the direct treatment via numerical integration techniques. The time evolution for the reflection probability for each mode $\mathbf{k}$ is described by the following Riccati equation

$$\dot{R}_{\mathbf{k}}(t) = \frac{\alpha_{\mathbf{k}}(t)\dot{\beta}_{\mathbf{k}}(t) - \dot{\alpha}_{\mathbf{k}}(t)\beta_{\mathbf{k}}(t)}{\alpha_{\mathbf{k}}^2(t)} = \frac{1}{2}\frac{\dot{\Omega}_{\mathbf{k}}(t)}{\Omega_{\mathbf{k}}(t)}\left[e^{-2i\int^t \Omega_{\mathbf{k}}} - R_{\mathbf{k}}^2(t)e^{2i\int^t \Omega_{\mathbf{k}}}\right]$$
(6.26)

where the second equality is obtained by inserting the derivatives from (6.11). For a given $k_\parallel$ and $\mathcal{A}(t)$ the Riccati equation can be solved with the initial condition

$$R_{\mathbf{k}}(-\infty) = 0.$$
(6.27)

The number of pairs is then given by $|R(t = +\infty)|^2$, see equation (6.17). This method is completely equivalent to the kinetic approach discussed in chapter 7.

6.2.2 Fermions

We can similarly proceed for the spinor case by transforming the problem (6.20) into a corresponding differential equation. The time evolution of the reflection coefficient $R_{\mathbf{k}} = \frac{\beta_{\mathbf{k}}}{\alpha_{\mathbf{k}}}$ leads to the following Riccati equation

$$\dot{R}_{\mathbf{k}}(t) = \frac{\alpha_{\mathbf{k}}(t)\dot{\beta}_{\mathbf{k}}(t) - \dot{\alpha}_{\mathbf{k}}(t)\beta_{\mathbf{k}}(t)}{\alpha_{\mathbf{k}}^2(t)} = -\frac{1}{2}\frac{\dot{k}_{\parallel}\epsilon_{\perp}}{\Omega_{\mathbf{k}}^2(t)}\left[e^{-2i\int^t \Omega_{\mathbf{k}}} + R_{\mathbf{k}}^2(t)e^{2i\int^t \Omega_{\mathbf{k}}}\right], \quad (6.28)$$

where the second equality is obtained by inserting the derivatives from (6.22). This equation can again be solved numerically after imposing the initial condition

$$R_{\mathbf{k}}(-\infty) = 0. \quad (6.29)$$

The number of pairs is then given by $|R(t = +\infty)|^2$.

6.3 Semiclassical approximation

In the following, we particularly focus on the scalar case. The derivative of the reflection coefficient is given in (6.26).

6.3.1 Dominant contribution

As mentioned before, we assume that $R_{\mathbf{k}}(t)$ is small for all t. This allows to neglect the nonlinear term $\propto R_{\mathbf{k}}^2$ on the right-hand side in equation (6.26). With the initial condition from (6.27), we get the following approximate expression in the asymptotic time limit

$$R_{\mathbf{k}}(\infty) \approx \frac{1}{2}\int_{-\infty}^{+\infty} dt\, \frac{\dot{\Omega}_{\mathbf{k}}(t)}{\Omega_{\mathbf{k}}(t)} \exp\left(-2i\int_{-\infty}^t dt'\, \Omega_{\mathbf{k}}(t')\right). \quad (6.30)$$

Let us remind that the present method does not lead to the correct prefactor [341, 369, 370] which stems from quantum fluctuations around the classical stationary worldline solutions as we have seen in chapter 5.

We assume the prefactor $\frac{\dot{\Omega}_{\mathbf{k}}}{\Omega_{\mathbf{k}}}$ and the integral $\int^t dt'\Omega_{\mathbf{k}}(t')$ to be analytic functions in the complex plane including the real axis. In order to perform the integration $\int_{-\infty}^{+\infty} dt\,(\cdots)$, we close the integration contour in the upper complex half plane, i.e. $\Im(t) > 0$. Since the exponential

$$e^{-2i\int_{-\infty}^t dt'\, \Omega_{\mathbf{k}}(t')} \quad (6.31)$$

in this region is highly suppressed, this will lead to a suppression of $R_\mathbf{k}$ as well. Thus, the integral (6.30) is dominated by the contributions of the poles determined by

$$\Omega_\mathbf{k} = 0 \tag{6.32}$$

which are the semiclassical turning points, in the following denoted as t_{TP}. From the latter condition we get

$$e\mathcal{A}(t_{\text{TP}}) = \pm im, \tag{6.33}$$

where we have neglected both the transversal momentum $\mathbf{k}_\perp$ as well as the parallel momentum $k_\parallel$. This approximation is in particular allowed for backgrounds which we consider. The reason is that for those the distribution for $N_\mathbf{k}$ is symmetrically peaked around $\mathbf{k} = 0$ [34, 151, 342]. Moreover, one should note that the number of produced pairs with momentum transversal to the external background are negligible compared to those with momentum pointing in the same direction as the background, cf. e.g. [34, 160].

According to Cauchy's theorem, the dominant solution of (6.30) can be estimated as

$$R_\mathbf{k}(t = +\infty) \sim \exp\left(-2i \int^{t_{\text{TP}}} dt' \, \tilde\Omega(t')\right), \qquad \tilde\Omega(t) \equiv \sqrt{m^2 + e^2 \mathcal{A}^2(t)}, \tag{6.34}$$

for details see the discussion below. In the low energy regime, we may further approximate [37],

$$R_\mathbf{k}(t = +\infty) \sim \exp\left(-2|imt_{\text{TP}}|\right). \tag{6.35}$$

For instance, the simplest case is the situation with a static electric background for which $\mathcal{A}(t) = Et$. Inserting this potential into (6.33), we get a pair of complex turning points $t_{\text{TP}} = \pm\frac{im}{eE}$ (where $k = 0$). Plugging t_{TP} into (6.35) gives the standard tunneling exponent $\sim \frac{E_{\text{S}}}{E}$.

6.3.2   Quantum interference

As we have seen in the previous part, there is only one pair of turning points present for the static electric background. In general, it is possible that many

turning points contribute to the exponential factor. Usually those which lead to the smallest imaginary part in (6.34) are the dominating one. However, it can happen that interference effects appear in momentum space if some have comparable contribution [34, 160, 340–342].

In the present semiclassical approach interference can be incorporated by taking into account all present turning points. In the following, we briefly sketch the general method for sQED. An analogous approach is possible for the spinor case [341].

For simplifying reason, let us assume that $\Omega_{\mathbf{k}}^2$ has a first order zero. In the vicinity of the turning point, we can write

$$\Omega_{\mathbf{k}} \sim \sqrt{t - t_{\text{TP}}}. \tag{6.36}$$

Introducing a function

$$x(t) = \int^t dt' \, \Omega_{\mathbf{k}}(t'), \tag{6.37}$$

we obtain from the latter approximate form

$$x \sim \frac{2}{3}(t - t_{\text{TP}})^{3/2} + x_{\text{TP}}. \tag{6.38}$$

Hence, inserting the relations

$$\frac{\dot{\Omega}_{\mathbf{k}}(t)}{\Omega_{\mathbf{k}}(t)} \sim \frac{1}{t - t_{\text{TP}}}, \qquad t - t_{\text{TP}} \sim (x - x_{\text{TP}})^{2/3}, \qquad \partial_t \sim \partial_x (x - x_{\text{TP}})^{1/3} \tag{6.39}$$

into the derivative expression (6.26) of the reflection coefficient (6.30), i.e. without the nonlinear term, results in

$$\frac{dR_{\mathbf{k}}}{dx} \sim \frac{1}{x - x_{\text{TP}}} e^{-2ix}. \tag{6.40}$$

Then, according to the residue theorem,[4] here multiplied with $-2\pi i$ due to negative orientation of the contour, we get

$$R_{\mathbf{k}}(\infty) \approx -2i\pi e^{-2ix_{\text{TP}}} \tag{6.41}$$

---

[4] For a positively oriented contour γ the solution to the integral

$$\oint_\gamma f(z)dz$$

is given by

$$2\pi i \sum_j \text{Res}_{a_j} f$$

where a_j are the poles. For a pole of order one the Residue is $\text{Res}_a f = \lim_{z \to a}(z - a)f(z)$ which is equivalent to Cauchy's integral theorem.

where

$$x_{\text{TP}} = \int_{-\infty}^{t_{\text{TP}}} \Omega_{\mathbf{k}}(t) \ dt. \tag{6.42}$$

Of course, the prefactor is not correct [371, 372]. However, taking into account the nonlinear term in (6.26) can help [373–375].

Now including all contributions arising from the turning points in the upper half plane of the complex domain, the approximate result for the reflection coefficient can be approximated as

$$R_{\mathbf{k}}(\infty) \approx \sum_{t_{\text{TP}}} e^{-2i \int_{-\infty}^{t_{\text{TP}}} \Omega_{\mathbf{k}}(t) dt}. \tag{6.43}$$

In order to compute the integral in the exponent we first separate it. Namely, integrals of $\Omega_{\mathbf{k}}(t)$ along the real axis are real, whereas integrations along the imaginary direction result in imaginary values. Thus, we may rewrite the exponential from above in the form

$$\begin{aligned}
R_{\mathbf{k}}(\infty) &\approx \exp\left(-2i \int_{-\infty}^{\Re(t_{\text{TP},1})} \Omega_{\mathbf{k}}(t) dt\right) \\
&\times \sum_j \exp\left(-2i \int_{\Re(t_{\text{TP},1})}^{\Re(t_{\text{TP},j})} \Omega_{\mathbf{k}}(t) dt\right) \exp\left(-2 \left| \int_{\Re(t_{\text{TP},j})}^{t_{\text{TP},j}} \Omega_{\mathbf{k}}(t) dt \right|\right).
\end{aligned} \tag{6.44}$$

The second exponent in the sum is real. The first exponent in the sum is the phase between neighboring turning points obtained by integrating $\Omega_{\mathbf{k}}$ along the real axis. Such phases are responsible for the interplay between different turning points and hence for interference effects. Taking the modulus squared,[5] the semiclassical approximation for the number of produced pairs with momentum $\mathbf{k}$ finally reads

$$N_{\mathbf{k}} = |R_{\mathbf{k}}(\infty)|^2 \approx \sum_j e^{-2K_{\mathbf{k},j}} + \sum_{j \neq l} 2\cos\left(2\Theta_{\mathbf{k},[j,l]}\right) e^{-K_{\mathbf{k},j}} e^{-K_{\mathbf{k},l}} \tag{6.45}$$

with

$$K_{\mathbf{k},j} := \left| \int_{t_{\text{TP},j}^*}^{t_{\text{TP},j}} \Omega_{\mathbf{k}}(t) \ dt \right|, \qquad \Theta_{\mathbf{k},[j,l]} := \int_{\Re(t_{\text{TP},j})}^{\Re(t_{\text{TP},l})} \Omega_{\mathbf{k}}(t) \ dt. \tag{6.46}$$

---

[5] Here, we use

$$\left[\sum_j (\cdots)_j\right]^2 = \sum_j (\cdots)_j^2 + \sum_{j \neq l} (\cdots)_j (\cdots)_l.$$

The first summation in (6.45) corresponds to contributions from independent turning points. The second sum includes the interference terms between different turning points. Due to the exponential suppression, it can be seen that the dominant contribution comes from turning points $t_{\text{TP},j}$ with smallest integral values $K_{\mathbf{k},j}$, as already discussed in section 6.3.1. Moreover, as the functions in the second sum in equation (6.45) indicate, interference effects become significant if the integrals $K_{\mathbf{k},j}$ are comparable for different pairs of turning points $\left(t_{\text{TP},j}, t_{\text{TP},j}^*\right)$ where the second is meant to be the complex conjugated complement.

Chapter 7

Quantum kinetic theory

7.1 Oscillating electric fields

WE consider VPP from the QED vacuum polarized by an electric background, spatially homogeneous, but time dependent. As in the previous chapters, we again omit the potential realization of avalanche processes [376] which may deplete the background. We note that the oscillatory background we will be assuming can be Fourier expanded in terms of the canonical momentum $\mathbf{p}$. In addition, we do not consider any magnetic field components. Let us remind that according to Noether's theorem the total momentum of each produced pair will always sum up to zero. Therefore, for a background in form of a purely time dependent oscillating electric field (OEF), producing an electron with momentum $\mathbf{p}$ will guarantee a produced positron with momentum $-\mathbf{p}$. This is similar to the assumptions in the quantum mechanical scattering approach introduced in chapter 6.

We choose the temporal gauge $\mathcal{A}_0(t) = 0$, where $\mathcal{A}^\mu = (\mathcal{A}_0, \boldsymbol{\mathcal{A}})$. The electric field we take to be $\mathbf{E}(t) = (0, E(t), 0)$ with $E(t) = -\partial_t \mathcal{A}(t)$. We again restrict ourselves to the subcritical regime, $E \ll E_\mathrm{S}$. We take into account neither the collision between the produced particles nor their inherent radiation fields. We want to emphasize that previous investigations have shown that such effects are irrelevant in the subcritical regime [44, 377, 378].

Here, only those Lorentz transformations that leave the background invariant describe the formal invariance of the vacuum in the presence of the field. This is in line with group theoretical studies developed for an external constant [379, 380]

and for a circularly polarized electromagnetic plane wave [381]. Since they form a subgroup of the full Lorentz symmetry group and the concept of one-particle states requires its irreducible representation [246], the standard classification of elementary particles is no longer applicable during the alterations of the external oscillatory background. The canonical quantization in QED with an OEF is possible [222].

7.2   Quantum Boltzmann-Vlasov equation

The main step is to diagonalize the underlying Hamiltonian in every time instant. As before in chapter 6, this we achieve by reformulating the problem in terms of time dependent Bogoliubov coefficients. Hence, the fermionic field operator can be expressed in terms of the background degrees of freedom,

$$
\begin{aligned}
\Psi(\boldsymbol{x}, t) &= \frac{1}{L^{\frac{3}{2}}} \sum_{\boldsymbol{p}} \Phi_{\boldsymbol{p}}(t) e^{i \boldsymbol{p} \cdot \boldsymbol{x}}, \\
\Phi_{\boldsymbol{p}}(t) &= \sum_{s} \left\{ a_{\boldsymbol{p}, s}(t) u_{\boldsymbol{p}, s}(t) + b_{-\boldsymbol{p}, s}^{\dagger}(t) v_{-\boldsymbol{p}, s}(t) \right\}.
\end{aligned}
\tag{7.1}
$$

This is called quasiparticle representation where $V = L^3$ denotes the normalization volume and

$$
\boldsymbol{p} = \frac{2\pi}{L} \boldsymbol{n}
\tag{7.2}
$$

is the discretized momentum with

$$
\boldsymbol{n} = (n_x, n_y, n_z), \quad n_i = 0, \pm 1, \pm 2, \ldots.
\tag{7.3}
$$

The time dependent bispinors $u_{\boldsymbol{p}, s}(t)$ and $v_{\boldsymbol{p}, s}(t)$ are eigenfunctions of the boost operator component along the y direction having eigenvalues $s = \pm \frac{1}{2}$. The time dependent operators

$$
\hat{a}_{\boldsymbol{p}, s}(t), \quad \hat{a}_{\boldsymbol{p}, s}^{\dagger}(t)
\tag{7.4}
$$

are the corresponding annihilator and creator for a quasiparticle, respectively. Similarly,

$$
\hat{b}_{-\boldsymbol{p}, s}(t), \quad \hat{b}_{-\boldsymbol{p}, s}^{\dagger}(t)
\tag{7.5}
$$

are the analogous operators for the antiquasiparticle. These instantaneous operators satisfy the fermionic anticommutation relations at equal time

$$
\begin{aligned}
\left\{ \hat{a}_{\boldsymbol{p}, s}(t), \hat{a}_{\boldsymbol{p}', s'}^{\dagger}(t) \right\} &= \delta_{\boldsymbol{p}, \boldsymbol{p}'} \delta_{s, s'}, \\
\left\{ \hat{b}_{\boldsymbol{p}, s}(t), \hat{b}_{\boldsymbol{p}', s'}^{\dagger}(t) \right\} &= \delta_{\boldsymbol{p}, \boldsymbol{p}'} \delta_{s, s'},
\end{aligned}
\tag{7.6}
$$

where all other commutations vanish identically.

Now, due to the temporal dependence of the operators, one can introduce quantities that are generically employed in the study of transport phenomena. A well example is the single particle distribution function (SPDF)

$$W(\boldsymbol{p}, t) = \sum_s \langle \text{vac}, \text{in}|a_{\boldsymbol{p},s}^\dagger(t) a_{\boldsymbol{p},s}(t)|\text{vac}, \text{in}\rangle. \tag{7.7}$$

The vacuum state $|\text{vac}, \text{in}\rangle$ is defined as usual by

$$\hat{a}_{\text{in}}|\text{vac}, \text{in}\rangle = \hat{b}_{\text{in}}|\text{vac}, \text{in}\rangle = 0 \tag{7.8}$$

where

$$\hat{a}_{\text{in}} := \hat{a}_{\boldsymbol{p},s}(t_{\text{in}}), \quad \hat{b}_{\text{in}} := \hat{b}_{-\boldsymbol{p},s}(t_{\text{in}}). \tag{7.9}$$

The relation between the in-operators (7.9) and the instantaneous one in (7.6) is determined by the corresponding Bogoliubov coefficients $f(\boldsymbol{p}, t)$ and $g(\boldsymbol{p}, t)$ whose explicit derivation can be found in appendix C.

The time evolution equations are

$$W(\boldsymbol{p}, t) = 2|f(\boldsymbol{p}, t)|^2. \tag{7.10}$$

Since the representation (7.1) has to satisfy the Dirac equation in the external background, this can be used to determine $f(\boldsymbol{p}, t)$. This procedure results in a system of coupled ordinary differential equation (ODE) which have been utilized in order to study various aspects of VPP [34, 340, 342, 382–384].

The equations of the mentioned ODE can be written in the form

$$\begin{aligned} i\dot{f}(\boldsymbol{p}, t) &= a_{\boldsymbol{p}}(t)f(\boldsymbol{p}, t) + b_{\boldsymbol{p}}(t)g(\boldsymbol{p}, t), \\ i\dot{g}(\boldsymbol{p}, t) &= b_{\boldsymbol{p}}^*(t)f(\boldsymbol{p}, t) - a_{\boldsymbol{p}}(t)g(\boldsymbol{p}, t) \end{aligned} \tag{7.11}$$

satisfying the following initial conditions

$$\begin{aligned} f(\boldsymbol{p}, -\infty) &= 0, \\ g(\boldsymbol{p}, -\infty) &= 1. \end{aligned} \tag{7.12}$$

Here, the dot corresponds to the time derivative. The remaining functions in (7.11) are given as

$$
\begin{aligned}
a_{\boldsymbol{p}}(t) &= w_{\boldsymbol{p}}(t) + \frac{eE(t)p_x}{2w_{\boldsymbol{p}}(t)(w_{\boldsymbol{p}}(t)+m)}, \\
b_{\boldsymbol{p}}(t) &= \frac{1}{2}\frac{eE(t)\epsilon_\perp}{w_{\boldsymbol{p}}^2(t)}\exp\left[-i\arctan\left(\frac{p_x q_\parallel}{\epsilon_\perp^2 + w_{\boldsymbol{p}}(t)m}\right)\right].
\end{aligned}
\tag{7.13}
$$

The kinetic momentum pointing in the same direction as the external field is

$$
q_\parallel(t) = p_\parallel - e\mathcal{A}(t).
\tag{7.14}
$$

Furthermore, we have

$$
\epsilon_\perp^2 = m^2 + \boldsymbol{p}_\perp^2
\tag{7.15}
$$

defined as the transverse energy squared and

$$
w_{\boldsymbol{p}}^2(t) = \epsilon_\perp^2 + q_\parallel^2(t)
\tag{7.16}
$$

which characterizes the total energy squared. Here, $\boldsymbol{p}_\perp = (p_x, 0, p_z)$ and $\boldsymbol{p}_\parallel = (0, p_y, 0)$ are the components of the canonical momentum being perpendicular and parallel to the external direction direction, respectively. Due to cylindrical symmetry with respect to the y axis, we may choose $p_z = 0$ without loss of generality.

The equations (7.11) including the functions (7.13) are already appropriate for a numerical treatment. For reasons of simplicity, they will be transformed so that we can work with an integrodifferential equation of the form

$$
\begin{aligned}
\dot{W}(\boldsymbol{p}, t) &= \partial_t W(\boldsymbol{p}, t) + eE(t)\partial_{q_\parallel} W(\boldsymbol{p}, t) \\
&= \frac{eE(t)\epsilon_\perp}{w_{\boldsymbol{p}}^2(t)}\int_{-\infty}^{t} dt' \frac{eE(t')\epsilon_\perp}{w_{\boldsymbol{p}}^2(t')}[1 - W(\boldsymbol{p}, t')]\cos\left[2\int_{t'}^{t} dt''\, w_{\boldsymbol{p}}(t'')\right].
\end{aligned}
\tag{7.17}
$$

This is known as the quantum Boltzmann-Vlasov equation (QBVE) which allows to extract some important quantities. This equation satisfies the initial vacuum condition $W(\boldsymbol{p}, -\infty) = 0$. Its derivation starting from the equations in (7.11) is shown in appendix D.

From the QBVE in (7.17), we already see that VPP is a nonequilibrium time dependent process. The appearance of the temporal nonlocality and the memory effects indicated by the quantum statistic factor $\propto [1 - W(\boldsymbol{p}, t)]$ shows that the

transport equation (7.17) possesses some non-Markovian feature [365, 377, 382]. Namely, the SPDF strictly depends on the initial number of degrees of freedom in the system. Here, we are interested in the asymptotically large time limits, $t \to \pm\infty$, where the OEF is switched off, $\boldsymbol{E}(\pm\infty) \to 0$. At these times the degrees of freedom in the OEF are relaxed to the single particle states. Therefore, the physically meaningful quantity we consider is the asymptotic SPDF $W(\boldsymbol{p}, \infty)$.[1]

The number of produced pairs per unit volume is then defined via the following momentum integral

$$\mathcal{N}_{e^-e^+} = \lim_{t\to\infty} \int \dd^3p \, W(\boldsymbol{p}, t) \tag{7.18}$$

where we have defined for simplicity

$$\dd \equiv d/(2\pi). \tag{7.19}$$

We should note that the corresponding VPP rate differs from the asymptotic expression of the vacuum decay rate $\Gamma_{\text{vac}}(t)$ per unit volume given in equation (C.20). Only if $|f(\boldsymbol{p}, \infty)|^2 \ll 1$, it is possible to take the approximate correspondence

$$\Gamma_{\text{vac}}(\infty) \approx -\dot{\mathcal{N}}_{e^-e^+}. \tag{7.20}$$

However, as we will see in the following, due to substantial resonance effects the former relation is not always satisfied in an OEF. Hence, in general one clearly has to distinguish between both concepts.

7.3 Resonances and Rabi frequencies

7.3.1 Multimode oscillating field

VPP in an OEF shows characteristic resonance effects basically due to the absorption of multiple energy packages, photons, resulting in Rabi-like oscillations, see [385] and [204, 384, 386, 387] for further developments in case of a single-mode OEF. In the present section, we provide a generalization of the underlying equations to the case of a multimode OEF within the described framework of

---

[1] The physical interpretation of quasiparticle states in the presence of a time dependent OEF has been discussed in [101].

nonequilibrium QFT, see [34]. We start with the following equations

$$
\begin{aligned}
\dot{\bar{f}}(\boldsymbol{p}, t) &= -\frac{eE(t)\epsilon_\perp}{2w_{\boldsymbol{p}}^2(t)} \bar{g}(\boldsymbol{p}, t) \exp\left[2i \int_{t_0}^t dt' \ w_{\boldsymbol{p}}(t')\right], \\
\dot{\bar{g}}(\boldsymbol{p}, t) &= \frac{eE(t)\epsilon_\perp}{2w_{\boldsymbol{p}}^2(t)} \bar{f}(\boldsymbol{p}, t) \exp\left[-2i \int_{t_0}^t dt' \ w_{\boldsymbol{p}}(t')\right]
\end{aligned}
\tag{7.21}
$$

which are equivalent to the equation in (7.17), see appendix D. The lower integration limit t_0 leads to an arbitrary phase at a given time instant. Moreover, we have again $W(\boldsymbol{p}, t) = 2|\bar{f}(\boldsymbol{p}, t)|^2$.

Next, we decompose the background consisting of periodic functions as follows

$$
\mathcal{A}_\mu(\eta_1, \ldots, \eta_k) = \sum_{i=1}^k \mathcal{A}_\mu^{(i)}(\eta_i), \quad \text{with} \quad \eta_i = \omega_i t.
\tag{7.22}
$$

Each mode $\mathcal{A}_\mu^{(i)}(\eta_i)$ is a 2π-periodic function in η_i. Of course $\mathcal{A}_\mu(\eta_1, \ldots, \eta_k)$ is not periodic. However, each of the functions are separately periodic in the corresponding variables $\eta_1, \eta_2, \ldots, \eta_k$. Hence, we can extract a periodic part $\tilde{\Theta}_{\boldsymbol{p}}(\eta_1, \ldots, \eta_k)$ in the dynamical phase

$$
\int_{t_0}^t dt' \ w_{\boldsymbol{p}}(t') = \bar{\varepsilon}_{\boldsymbol{p}} t + \tilde{\Theta}_{\boldsymbol{p}}(\eta_1, \ldots, \eta_k),
\tag{7.23}
$$

with $\bar{\varepsilon}_{\boldsymbol{p}}$ being the quasiparticle energy. The product of functions in equations (7.21) can be Fourier expanded,

$$
\begin{aligned}
\frac{eE(t)\epsilon_\perp}{w_{\boldsymbol{p}}^2(t)} \exp\left[2i \int_{t_0}^t dt' \ w_{\boldsymbol{p}}(t')\right] \simeq \sum_{n_1 \ldots n_k = -\infty}^\infty \Lambda_{n_1, \ldots, n_k}(\boldsymbol{p}) \\
\times \exp\left[2i\bar{\varepsilon}_{\boldsymbol{p}} t - i \sum_{j=1}^k n_j \eta_j\right].
\end{aligned}
\tag{7.24}
$$

The Fourier coefficients turn out to be k-fold parametric integral functions

$$
\begin{aligned}
\Lambda_{n_1, \ldots, n_k}(\boldsymbol{p}) = \int_{-\pi}^\pi \mathrm{d}^3 p\, \eta_1 \ldots \int_{-\pi}^\pi \mathrm{d}^3 p\, \eta_k \frac{eE(\eta_1, \ldots, \eta_k)\epsilon_\perp}{w_{\boldsymbol{p}}^2(\eta_1, \ldots, \eta_k)} \\
\times \exp\left[2i\tilde{\Theta}_{\boldsymbol{p}}(\eta_1, \ldots, \eta_k) + i \sum_{j=1}^k n_j \eta_j\right]
\end{aligned}
\tag{7.25}
$$

whose explicit form is not important for the generic nature of the process.

Now, the only time dependence in (7.24) appears in the complex exponent. This will result in enormous oscillations as soon as $t \to \pm\infty$. From this, the dominant

contribution is obtained when the exponent vanishes which immediately leads to the energy conservation

$$2\bar{\varepsilon}_{\boldsymbol{p}} = \sum_{j=1}^{k} n_j \omega_j, \tag{7.26}$$

denoting the Fourier indices by $n_1, \ldots, n_k$. Dropping the rapidly varying terms, equation (7.24) can be approximated by the most slowly altering Fourier mode[2]

$$\frac{eE(t)\epsilon_\perp}{w_{\boldsymbol{p}}^2(t)} \exp\left[2i \int_{t_0}^{t} dt' \; w_{\boldsymbol{p}}(t')\right] \approx \Lambda_{n_1,\ldots,n_k}(\boldsymbol{p}) \exp\left[i\Delta_{n_1,\ldots,n_k}(\boldsymbol{p})t\right] \tag{7.27}$$

with the detuning parameter

$$\Delta_{n_1,\ldots,n_k}(\boldsymbol{p}) \equiv 2\bar{\varepsilon}_{\boldsymbol{p}} - \sum_j n_j \omega_j. \tag{7.28}$$

Owing to the latter approximation, equation (7.21) reduces to a system of ODEs. The corresponding solutions can be found much easier. The resulting function $\bar{f}(\boldsymbol{p}, t)$ can be used to express the SPDF as

$$W_{n_1,\ldots,n_k}(\boldsymbol{p}, t) \approx \frac{1}{2} \frac{|\Lambda_{n_1,\ldots,n_k}(\boldsymbol{p})|^2}{\Omega_{\mathrm{Rabi}}^2(\boldsymbol{p})} \sin^2\left[\Omega_{\mathrm{Rabi}}(\boldsymbol{p})(t - t_{\mathrm{in}})\right], \tag{7.29}$$

assuming that the field is instantaneously switched on at t_{in} satisfying

$$\begin{aligned}
\bar{f}(\boldsymbol{p}, t_{\mathrm{in}}) &= 0, \\
\bar{g}(\boldsymbol{p}, t_{\mathrm{in}}) &= 1.
\end{aligned} \tag{7.30}$$

The Rabi-like frequency of the instantaneous vacuum is

$$\Omega_{\mathrm{Rabi}}(\boldsymbol{p}) \equiv \frac{1}{2}\left[|\Lambda_{n_1,\ldots,n_k}(\boldsymbol{p})|^2 + \Delta_{n_1,\ldots,n_k}^2(\boldsymbol{p})\right]^{\frac{1}{2}} \tag{7.31}$$

which clearly manifests the instability in a multimode OEF. This statement can be verified by supposing that the standing wave is instantaneously switched off after some finite interaction time

$$\tau \equiv t_{\mathrm{out}} - t_{\mathrm{in}}. \tag{7.32}$$

---

[2] Note that in case of commensurable field mode frequencies $\omega_1, \ldots, \omega_k$, there can exist more than one exact solution of equation (7.26). For several integer combinations of frequencies this can apply approximately as well, see section III-C of [34]. So in general it is possible to have more than one dominant Fourier mode.

7.3.2 Driven two-level system

Let us set for simplicity $\boldsymbol{p} = 0$ and consider equation (11.32) near the resonance[3] [34], means

$$\Delta_{n_1,\ldots,n_k} \simeq 0. \tag{7.33}$$

In this case, the Rabi-like frequency approaches

$$\Omega_{\mathrm{Rabi}}^{(0)} \equiv \Omega_{\mathrm{Rabi}}(0) \approx \frac{1}{2}|\Lambda_{n_1,\ldots,n_k}(0)| \tag{7.34}$$

which leads to the following approximation for the SPDF from equation (11.32)

$$W_{n_1,\ldots,n_k}(t) \approx \begin{cases} 2\sin^2\left[\Omega_{\mathrm{Rabi}}^{(0)}(t - t_{\mathrm{in}})\right], & t < t_{\mathrm{out}} \\[2em] 2\sin^2\left[\Omega_{\mathrm{Rabi}}^{(0)}\tau\right], & t \geqslant t_{\mathrm{out}} \end{cases}. \tag{7.35}$$

The latter indicates an oscillatory pattern due to continuous transitions characterized by a period

$$\mathcal{T} = \frac{2\pi}{\Omega_{\mathrm{Rabi}}^{(0)}}. \tag{7.36}$$

These continuous transitions resemble the Rabi oscillations associated with a driven two-level atomic system. Therefore, from (11.44) we deduce that in a multimode OEF the number of quasiparticles with $\boldsymbol{p} = 0$ is not stationary. For times larger than the interaction time, $t > \tau$, the SPDF for the asymptotic states is constant. This clearly indicates that both the quantum vacuum and the produced pairs approach the stability limit which is of course required for experimental measurements.

---

[3] Away from the resonance the oscillations are faster, but their amplitude is lowered substantially.

Part III

Quantum vacuum

Chapter 8

Dynamical enhancement via reflections

8.1 Outline

W$^{\text{E}}$ study the enhancement of the VPP rate via two mechanisms, the assisted mechanism and the assisted dynamical mechanism as described in section 1.4. Both mechanisms apply in a time dependent electric background that consists of a strong field superimposed with a weak field oscillating at a much shorter time scale. The main difference between both is that in the standard assisted mechanism the strong field is assumed to be (locally) static. A complete analytical treatment for such complex backgrounds is extremely challenging and has not been done so far.

We utilize the worldline instanton method to develop an effective reflection approach.[1] Based on this approach, the enhancement can simply be understood by means of certain critical points which can be directly obtained from the instanton equations introduced in (5.23). While one of the critical points is the closing point

---

[1] It is important to note that the effect of assistance generally requires the nonperturbative treatment of both the strong and the weak field and thus preserves the characteristic nonperturbative behavior of the Schwinger effect, see section 1.4. A nonperturbative treatment of the problem is automatically realized in the reflection approach. A characteristic property for backgrounds of the mentioned type is the appearance of a critical threshold. As we will show for various cases, below the threshold there are no substantial effects due to assistance. It should be mentioned that perturbation theory with respect to the weak dependence cannot account for the described critical behavior, see e.g. [31].

of the stationary worldline path, the other serves as an Euclidean mirror which reflects and squeezes the worldline instanton. We show that it is basically this reflection and shrinking which is responsible for an enormous enhancement of the VPP rate.

Specifically, we find that many properties and characteristic features can be explained by means of such reflections even when poles in the instanton plane do not exist. Particularly, we focus on the role of the assisting weak rapid field.

Consistent with previous studies, we first discuss the standard assisted mechanism with a static strong field and certain weak fields with a distinct pole structure in order to show that the reflection takes place exactly at the poles. We also discuss the effect of possible subcycle structures.

Then, in the first main part, we extend the reflection picture to weak fields which have no poles present and illustrate the effective reflections with explicit examples. We find that an additional field strength dependence for the rate occurs in such cases. We analytically compute the characteristic threshold in the standard assisted mechanism given by the critical combined Keldysh parameter. We discuss significant differences between these two types of weak fields. For various backgrounds, we present the contributing instantons and analytically predict the corresponding rates treating both fields nonperturbatively.

In the second main part, we study the case with a nonstatic strong field which gives rise to the assisted dynamical mechanism. For different strong field profiles we investigate the impact on the critical combined Keldysh parameter. As an explicit example, we analytically compute the rate by employing the exact reflection points. The validity of the predictions for both mechanisms is confirmed by numerical computations.[2]

---

[2] For the numerical treatment we use the results from the direct approach described in section 5.4, see also [37].

8.2 Stationary worldlines

We consider time dependent backgrounds oriented in the $\hat{x}_3$ direction. The instanton equations (5.23) then become

$$
\begin{aligned}
\ddot{x}_4 &= +\frac{iea}{m}\partial_4\mathcal{A}_3(x_4)\dot{x}_3, \\
\ddot{x}_3 &= -\frac{iea}{m}\partial_4\mathcal{A}_3(x_4)\dot{x}_4.
\end{aligned}
\tag{8.1}
$$

To allow only real instanton solutions, we consider electric backgrounds which are described by analytic even functions in Minkowskian time t. Note that, generally those can be complex as well [160]. The Euclidean vector potential ($x_4 = it$) can be written in the form

$$
\mathcal{A}_3(x_4) = -iEF(x_4),
\tag{8.2}
$$

where F is assumed to be an odd real function. The complex i in front of F guarantees that the equations (8.1) have real solutions.

It has been shown that time dependent inhomogeneous electric backgrounds can enhance the VPP rate even with field strengths E far below E_S [32, 141–143, 145, 146, 383, 388]. The physical picture is that the vacuum energy gap can effectively be lowered by the additional inhomogeneity in spacetime. Such an effect also applies in atomic ionization processes [358]. A geometric explanation based on worldline instantons has previously been discussed in section 5.8.

In the present case, we consider a linearly combined electric background of the form

$$
\mathbf{E}(t) = \left(Ef(t) + \tilde{E}g(t)\right)\hat{x}_3.
\tag{8.3}
$$

The weak rapid field, $\propto \tilde{E}$ with frequency $\tilde{\omega}$, is described by an analytic function $g(t)$, whereas the the strong slow field, $\propto E$ with frequency ω, is characterized by a function $f(t)$. We assume that

$$
\begin{aligned}
E_\mathrm{S} &\gg E \gg \tilde{E}, \\
m &\gg \tilde{\omega} \gg \omega
\end{aligned}
\tag{8.4}
$$

holds. Furthermore, both functions f and g are taken to be even in Minkowski time t. After analytic continuation to the complex domain the corresponding gauge

potential reads

$$\mathcal{A}_3(x_4) = -iEF(x_4) - i\tilde{E}G(x_4). \tag{8.5}$$

Here $F(x_4)$ and $G(x_4)$ denote the associated odd functions obtained after the integration of $f(t)$ and $g(t)$, respectively. Inserting the derivative of the gauge potential

$$\partial_4\mathcal{A}_3(x_4) = -i\left(EF'(x_4) + \tilde{E}G'(x_4)\right) \tag{8.6}$$

into the instanton equations (8.1), we find the following nonlinearly coupled system of differential equations

$$\begin{aligned}
\ddot{x}_4 &= +\frac{eaE}{m}\left(F'(x_4) + \epsilon G'(x_4)\right)\dot{x}_3, \\
\ddot{x}_3 &= -\frac{eaE}{m}\left(F'(x_4) + \epsilon G'(x_4)\right)\dot{x}_4,
\end{aligned} \tag{8.7}$$

where a dimensionless parameter $\epsilon := \tilde{E}/E$ is introduced for clarity.

8.3   Instanton reflections

For the seek of convenience, we first write down the following dimensionless Keldysh parameters [146, 357, 389],

$$\gamma = \frac{m\omega}{eE}, \qquad \tilde{\gamma} = \frac{m\tilde{\omega}}{eE}. \tag{8.8}$$

The strong field parameter γ interpolates between the adiabatic nonperturbative tunneling regime, $\gamma \ll 1$, and the antiadiabatic perturbative multiphoton regime, $\gamma \gg 1$ [256]. A background composed of a single inhomogeneous field with $\gamma > 0$ gives rise to the dynamical Schwinger mechanism without showing the effect of assistance. The assisted dynamical mechanism is discussed in section 8.6.

The second parameter $\tilde{\gamma}$ in (8.8) is usually called the combined or relative Keldysh parameter, respectively. It involves the strong field amplitude E and the weak field frequency $\tilde{\omega}$. In the limit $\tilde{\gamma} \to 0$ the standard Schwinger mechanism is approached. Notably, $\tilde{\gamma} \gg 1$ does not correspond to a pure perturbative multiphoton weak field. It includes both multiphotons with the energy $\tilde{\omega}$ as well as the dependence on the field strength E, see e.g. [32]. We will see that in cases where the weak field possesses a distinct pole structure, this parameter becomes the main

quantity in the standard assisted mechanism.[3]

In principal, we can integrate the second equation in (8.7)

$$\dot{x}_3 = -\frac{eaE}{m}\left(F(x_4) + \epsilon G(x_4)\right) \tag{8.9}$$

and by using the kinematic invariant $a = \sqrt{\dot{x}_3^2 + \dot{x}_4^2}$, see equation (5.22), we may write the equation for $\dot{x}_4$. However, the integral is generally difficult to solve analytically. In certain cases a reflection approach [32] provides a simplified way to tackle this problem approximately, see also [152].

Namely, since we are interested in the limit $\epsilon \ll 1$, we may omit the second term in equation (8.9). However, going back to the original instanton equations in (8.7), this is allowed as long as $G'(x_4)$ is sufficiently small. As soon as it becomes very large, which happens for sure at some pole determined by

$$[g(x_4^{\mathrm{p}})]^{-1} = 0, \tag{8.10}$$

we expect a substantial contribution from this term. For the moment, let us therefore assume that the weak field has a distinct pole structure. Note that due to symmetry reasons, which apply for the specific background configurations considered here, it is sufficient to do the present analysis with respect to the pole on the positive Euclidean time axis, x_4^{p}.

Thus, the weak field pole acts as an infinite wall where the instanton will be reflected with a nonvanishing velocity $\dot{x}_4$. Away from these Euclidean mirrors, as we call such reflection points, we neglect the second terms in the brackets and integrate the instanton equations approximately as

$$\dot{x}_3 \approx -a\frac{\omega}{\gamma}F(x_4),$$
$$\dot{x}_4 \approx \pm a\sqrt{1 - \left(\frac{\omega}{\gamma}F(x_4)\right)^2}. \tag{8.11}$$

Since at the reflection points we assume $\dot{x}_4 \neq 0$, the invariant a is expected to be modified. For the relevant limit $\epsilon \ll 1$, we then write the external part in the

---

[3] We discuss in detail that weak fields without a distinct pole structure lead in general to an additional ϵ dependence in the VPP rate, cf. section 8.5.

worldline action (5.12) as

$$\mathcal{W}_{\text{ext}} = ie \int_0^1 du \ \dot{x} \cdot \mathcal{A} \approx eE \int_0^1 du \ \dot{x}_3(u) F(x_4(u)), \tag{8.12}$$

Due to the instanton symmetry

$$\begin{aligned} x_3 &\to -x_3, \\ x_4 &\to -x_4 \end{aligned} \tag{8.13}$$

we may use the relation

$$\int_0^{1/4} du \ \dot{x}_3 = \int_0^{x_4^{\text{c}}} dx_4 \ \frac{\dot{x}_3}{\dot{x}_4}, \tag{8.14}$$

since the derivatives F' and G' are even functions. Here, x_4^{c} is the closing point at the intersection between the first and second quarter where $x_3 = 0$. Accordingly, we can deduce the external part of the stationary worldline action in equation (5.25),

$$\mathcal{W}_{0,\text{ext}} = 4eE \int_0^{x_4^{\text{c}}} dx_4 \ \frac{-\frac{\omega}{\gamma} F(x_4) F(x_4)}{\sqrt{1 - \left(\frac{\omega}{\gamma} F(x_4)\right)^2}}, \tag{8.15}$$

with x_4^{c} denoting the point where the instanton has to be closed.

At this stage we are confronted with the problem of choosing an appropriate closing point. One may think about the critical point

$$\frac{\omega}{\gamma} F(x_4^*) = 1, \tag{8.16}$$

that we can read off directly from the denominator in equation (8.15). This point, however, corresponds to $\dot{x}_4 = 0$ which cannot be allowed in the reflection picture with poles in the instanton plane present. If the instanton is reflected at the pole of the weak field, the path has to be closed there as well. Therefore, in case of reflection, means if the weak field assists the process of VPP, we have to set

$$x_4^{\text{c}} \stackrel{!}{=} x_4^{\text{p}}. \tag{8.17}$$

Otherwise, if

$$x_4^{\text{c}} = x_4^*, \tag{8.18}$$

the instanton path is closed much earlier, means no resizing of the instanton due to reflections will take place.
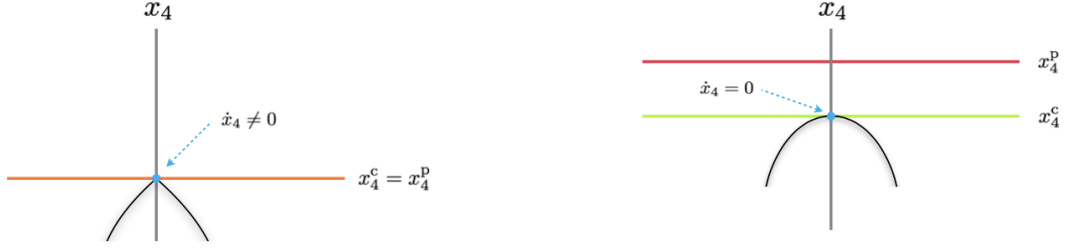
Figure 8.1: Comparison of assisted (left) and standard Schwinger mechanism (right) in time dependent inhomogeneous electric background. The former is characterized by the additional instanton reflection due to the additional weak, but rapid field.

The described behavior is schematically illustrated in figure 8.1. In the left panel, we have drawn the situation in the reflection case where $x_4^{\mathrm{c}} = x_4^{\mathrm{p}}$. In the right panel, the instanton is closed before reaching the pole, i.e. $x_4^{\mathrm{c}} < x_4^{\mathrm{p}}$. The reflection condition in equation (8.17) shows that the profile of the weak rapid field, which basically determines the position of the pole x_4^{p}, is crucial for the assisted mechanism. Moreover, the profile of the strong slow field, f, determines the form of the integrand in equation (8.15). Hence, the interplay between both contributions will be relevant. We still need to find the invariant a in order to compute the stationary kinetic term in (5.25),

$$\mathcal{W}_{0,\mathrm{kin}} = ma. \tag{8.19}$$

In fact, demanding the closing point x_4^{c} to be equal to x_4^{p}, cf. equation (8.17), leads to substantial modifications of the internal invariant a.

Now, we first rewrite the integration measure and set $x_4^{\mathrm{c}} = x_4^{\mathrm{p}}$ in order to find

$$\frac{1}{4} = \int_0^{1/4} du = \int_0^{x_4^{\mathrm{p}}} \frac{dx_4}{\dot{x}_4}. \tag{8.20}$$

From this equality we can easily determine the kinematic invariant in equation (5.22) after inserting $\dot{x}_4$ from (8.11) into the latter integrand on the right-hand side which yields the following integral representation

$$a = 4 \int_0^{x_4^{\mathrm{p}}} dx_4 \; \frac{1}{\sqrt{1 - \left(\frac{\omega}{\gamma} F(x_4)\right)^2}}. \tag{8.21}$$

Altogether, combining the relations in equations (8.15) and (8.21), we find the

following integral expression for the stationary worldline action

$$\mathcal{W}_0 = 4m \int_0^{x_4^{\mathrm{P}}} dx_4 \ \sqrt{1 - \left(\frac{\omega}{\gamma} F(x_4)\right)^2}. \tag{8.22}$$

8.4   Assisted mechanism: fields with poles

We begin by illustrating the previous modifications for some well known background configurations. We consider a static strong field, i.e.

$$f(t) = 1, \qquad F(x_4) = x_4, \tag{8.23}$$

which in the presence of a superimposed weak rapid field gives rise to the standard assisted mechanism [32]. We note that for $\gamma \gg 1$ the effect of assistance does not set in for relatively small $\tilde{\gamma}$. This is due to the mentioned occurrence of a threshold value for the latter which is characteristic for the assisted mechanism [32, 37]. In such a case, the strong field alone is sufficient to drive the enhancement. This corresponds to the standard dynamical mechanism which gives rise to the multi-photon process operating in the perturbative regime, see section 1.4.

Here, we focus on the static strong field case for which the integral in (8.21) can be solved analytically

$$a = 4 \int_0^{x_4^{\mathrm{P}}} dx_4 \ \frac{1}{\sqrt{1 - \left(\frac{\omega}{\gamma} x_4\right)^2}} = 4\frac{\gamma}{\omega} \arcsin\left(\frac{\omega}{\gamma} x_4\right) \Big|_{x_4=0}^{x_4^{\mathrm{P}}} \tag{8.24}$$

leading to the following kinematic invariant

$$a = 4\frac{\gamma}{\omega} \arcsin\left(\frac{\omega}{\gamma} x_4^{\mathrm{P}}\right) \tag{8.25}$$

that depends on the pole x_4^{P} that is not specified yet. The latter expression already signals the appearance of the mentioned critical value for $\tilde{\gamma}$ depending on x_4^{P}, since we need to satisfy

$$\frac{\omega}{\gamma} = \frac{\tilde{\omega}}{\tilde{\gamma}} \leq \frac{1}{x_4^{\mathrm{P}}}. \tag{8.26}$$

Accordingly, the instanton path in the right-half plane, i.e. $u \in \left[-\frac{1}{4}, \frac{1}{4}\right]$, see equation (5.7), is simply an arch-like curve and the large mass approximation condition from (5.10) becomes

$$4\gamma \frac{m}{\omega} \arcsin\left(\frac{\omega}{\gamma} x_4^{\mathrm{P}}\right) \gg 1. \tag{8.27}$$

After integrating the expression in (8.1) and inserting the modified invariant in (8.25), we obtain

$$
\begin{aligned}
x_4(u) &= \frac{m}{eE} \sin\left(4u \arcsin\left(\frac{\omega x_4^{\mathrm{p}}}{\gamma} \right) \right), \\
x_3(u) &= \frac{m}{eE} \cos\left(4u \arcsin\left(\frac{\omega x_4^{\mathrm{p}}}{\gamma} \right) \right) - \mathcal{C}.
\end{aligned}
\tag{8.28}
$$

The closed stationary worldline path is realized by the integration constant

$$
\mathcal{C} = x_3\left(u = \pm \frac{1}{4} \right) = \frac{m}{eE} \cos\left(\arcsin\left(\frac{\omega x_4^{\mathrm{p}}}{\gamma} \right) \right).
\tag{8.29}
$$

The latter shifts the instanton along the x_3 axis in order to guarantee the condition

$$
x_3\left(u = \pm \frac{1}{4} \right) = 0.
\tag{8.30}
$$

Finally, evaluating the stationary worldline action with the help of the previously derived integral form in equation (8.22) yields the following result

$$
\begin{aligned}
\mathcal{W}_0 &= 4m \int_0^{x_4^{\mathrm{p}}} dx_4 \ \sqrt{1 - (\omega x_4/\gamma)^2} \\
&= \frac{2m}{\omega} \left(x_4^{\mathrm{p}}\omega \sqrt{1 - \left(\frac{x_4^{\mathrm{p}}\omega}{\gamma} \right)^2} + \gamma \arcsin\left(\frac{x_4^{\mathrm{p}}\omega}{\gamma} \right) \right).
\end{aligned}
\tag{8.31}
$$

8.4.1   Examples

In the following, we demonstrate the described reflections for two different backgrounds consisting of a weak rapid field with poles in the instanton plane.

8.4.1.1   Weak Sauter

In the first example, we consider a weak field of Sauter type, i.e.

$$
g(t) = \mathrm{sech}^2(\tilde{\omega} t), \qquad G(x_4) = \frac{\tan(\tilde{\omega} x_4)}{\tilde{\omega}}.
\tag{8.32}
$$

The pole structure for this pulsed field is of multi type. However, the (first) relevant pole for $g(x_4) = \sec^2(\tilde{\omega} x_4)$ is placed at

$$
x_4^{\mathrm{p}} = \frac{\pi}{2\tilde{\omega}},
\tag{8.33}
$$

which leads to the following invariant

$$
a = 4\frac{m}{eE} \arcsin\left(\frac{\pi}{2\tilde{\gamma}} \right).
\tag{8.34}
$$
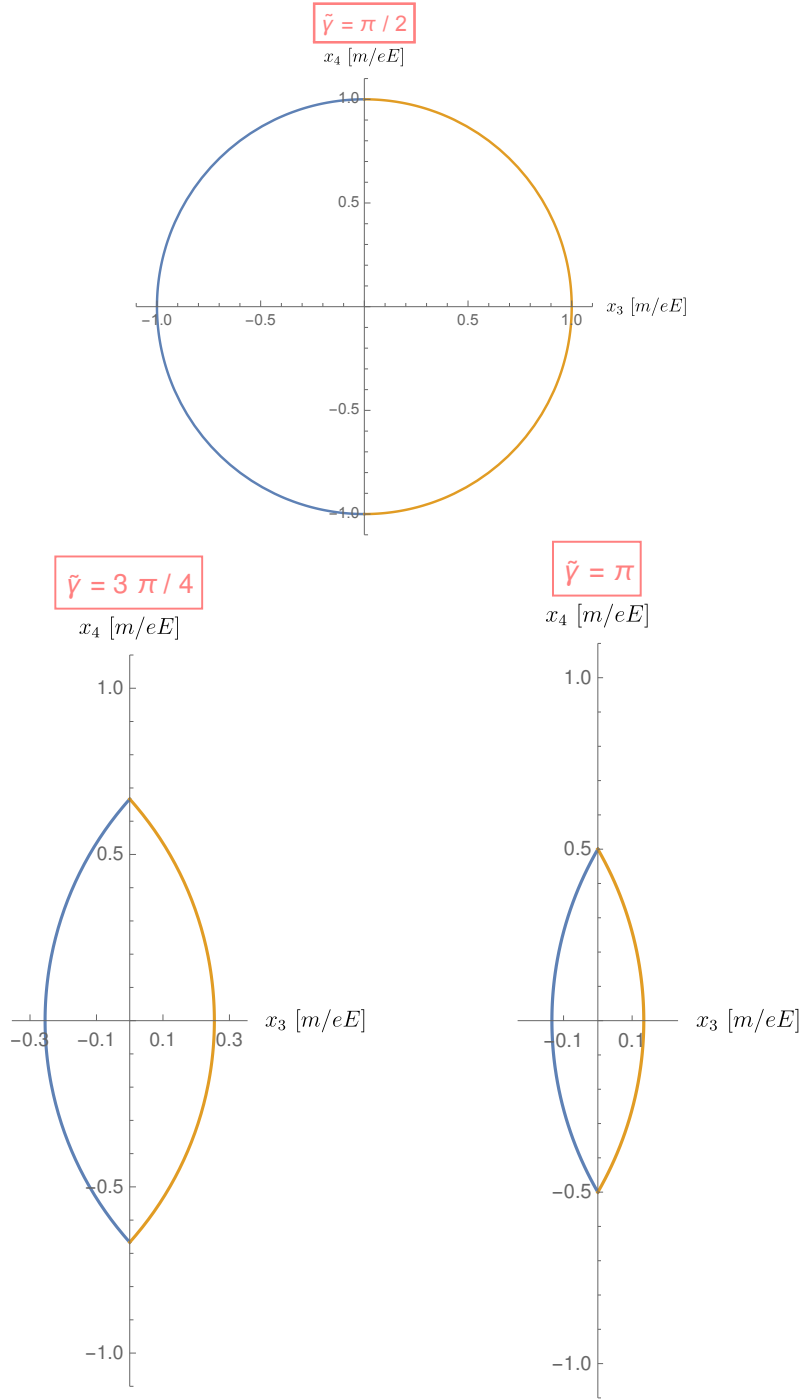
Figure 8.2: Instanton path for an electric background as superposition of a strong static and weak Sauter field is shown for different combined Keldysh parameters $\tilde{\gamma}$ given in the plot labels.

The latter invariant signals that the combined Keldysh parameter has to satisfy $\tilde{\gamma} > \pi/2$, otherwise we would end up with $a \in \mathbb{C}$. Below the critical value,

$$\tilde{\gamma}^{\text{crit}} = \frac{\pi}{2}, \tag{8.35}$$

there will be no effect of the weak field and we are left with the strong static field contribution, see [32]. Importantly, even the weak field does not contribute, there is still a nonzero, but small VPP rate due to the nonperturbative strong field. Here, the strong field can be in general assumed as locally static as it is seen by the weak but rapid field. It is clear that this can only be allowed for a large frequency difference. As soon as γ approaches larger values, it leads to substantial effects below the critical value $\tilde{\gamma}^{\text{crit}}$ as we discuss in section 8.6.

Coming back to the present example, inserting the pole x_4^{p} into the modified solutions in (8.28), we plot the instanton path for different frequencies $\tilde{\omega}$ as shown in figure 8.2. The size of the instanton decreases with larger $\tilde{\gamma}$. It is this shrinking which increases the VPP rate, since the stationary worldline action becomes smaller if the size of the instanton is reduced. These lens shaped instanton paths also apply if the strong field is a spatially inhomogeneous Sauter field [152].

After inserting the pole into the solution (8.31) we get

$$\mathcal{W}_0 = \frac{m^2}{eE} \left(\frac{\pi}{2\tilde{\gamma}^2} \sqrt{4\tilde{\gamma}^2 - \pi^2} + 2\arcsin\left(\frac{\pi}{2\tilde{\gamma}}\right) \right), \tag{8.36}$$

cf. e.g. [32]. Alternatively, this result can be obtained by plugging the instanton solution from (8.28) into the expression (8.22) and integrating over $u \in \left[0, \frac{1}{4}\right]$.

8.4.1.2 Weak Lorentzian

A second example we want to discuss is the case with a weak Lorentzian field described by

$$g(t) = \frac{1}{(1 + (\tilde{\omega}t)^2)^{3/2}}, \qquad G(x_4) = \frac{1}{\tilde{\omega}} \frac{\tilde{\omega}x_4}{\sqrt{1 - (\tilde{\omega}x_4)^2}}. \tag{8.37}$$

The function

$$g(x_4) = \frac{1}{(1 - (\tilde{\omega}x_4)^2)^{3/2}} \tag{8.38}$$

has the pole

$$x_4^{\text{p}} = \frac{1}{\tilde{\omega}}. \tag{8.39}$$
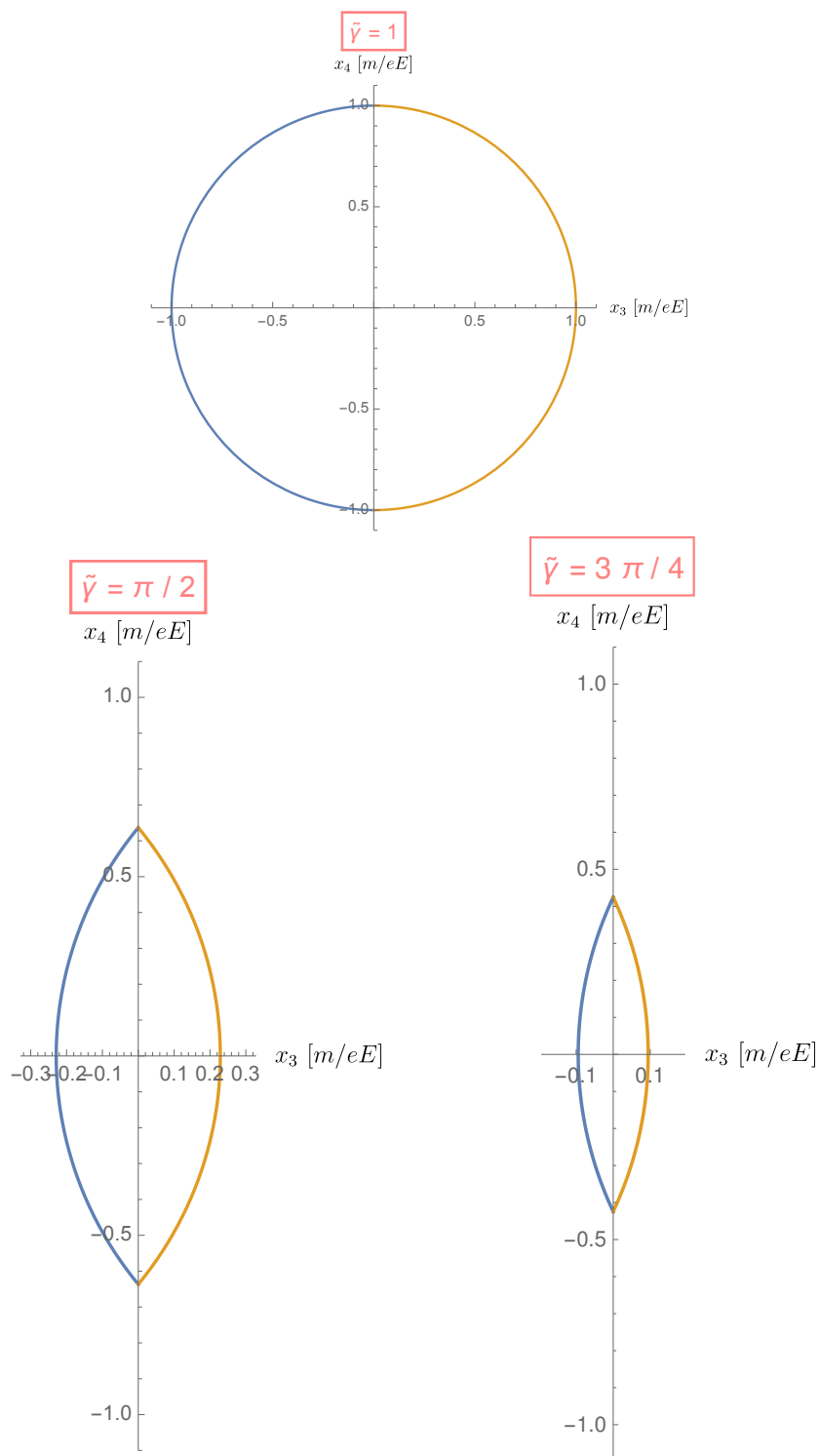
Figure 8.3: Instanton path for an electric background as superposition of a strong static and weak Lorentzian field is shown for different combined Keldysh parameters $\tilde{\gamma}$ given in the plot labels.

Except the factor $\pi/2$, this case resembles the example before and is therefore expected to lead to similar results. We should remark that not the visually indistinguishable bell shaped profiles of the fields is responsible for this similarity,[4] cf. [37]. This aspect is discussed in detail in section 8.5.

The modified invariant is given by

$$a = 4\frac{m}{eE}\arcsin\left(\frac{1}{\tilde{\gamma}}\right) \tag{8.40}$$

which leads to

$$\tilde{\gamma}^{\text{crit}} = 1, \tag{8.41}$$

cf. [390]. Consequently, the weak Lorentzian field will contribute much earlier compared to the previous Sauter field as it is illustrated in figure 8.3. Inserting the pole into (8.31), we find the stationary worldline action [390]

$$\mathcal{W}_0 = \frac{m^2}{eE}\left(\frac{2}{\tilde{\gamma}^2}\sqrt{\tilde{\gamma}^2 - 1} + 2\arcsin\left(\frac{1}{\tilde{\gamma}}\right)\right). \tag{8.42}$$

The comparison of $\mathcal{W}_0$ for both fields is shown in figure 8.4. The difference with respect to the critical threshold is clearly observable. Despite the relative difference
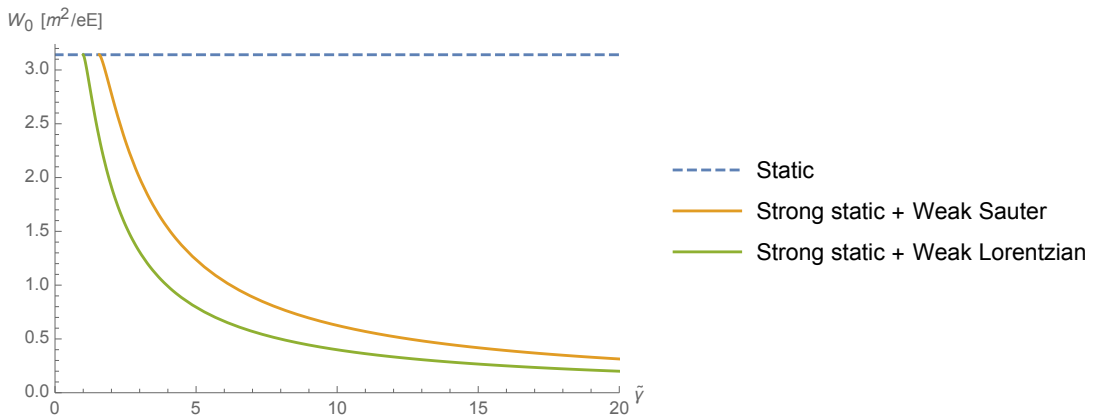
Figure 8.4: Stationary worldline action $\mathcal{W}_0$ in units of $\frac{m^2}{eE}$ is shown for an electric background as superposition of a strong static and weak Sauter/Lorentzian (yellow/green) field. The horizontal blue line corresponds to the static field case with $\mathcal{W}_0 = \pi\frac{m^2}{eE}$.

between the curves, we find that both follow similar trends. Identical results will apply, if we increase the frequency of the Sauter field by a factor $\frac{\pi}{2}$. This we can

---

[4] It is rather the distinct pole structure of the field which is responsible for such a similarity.

already observe directly by looking at figure 8.4. For instance, in the Lorentzian field case the value $\mathcal{W}_0 \approx 1.8 \times \frac{E_\mathrm{S}}{E}$ is reached at $\tilde{\gamma} \approx 2$. The same result applies for the Sauter field at $\tilde{\gamma} \approx 3.2$ which is just the mentioned factor $\frac{\pi}{2}$.

Now, suppose a general Lorentzian described by

$$g(t) = \frac{1}{(1 + (\tilde{\omega}t)^2)^{d/2}}, \tag{8.43}$$

where $d \in \mathbb{N}$. Apparently, we will obtain the same pole as before which is the inverse of $\tilde{\omega}$. It turns out that in the relevant regime $\epsilon \ll 1$ the pole is sufficient to predict the assistance. Namely, after the rotation in the complex plane the variation of d will have negligible effects on the rate.[5] It is the reflection at the pole from equation (8.39) that predominantly determines the strength of the enhancement.

8.4.2 Effects of subcycle structure

In the following, we discuss the possible impact of an additional oscillatory subcycle structure. This situation is reflected in laser setups where the field is usually a very short wave pulse.[6] Hence, the question is, how will the rate be influenced?

In order to get some insight, we consider a simple oscillatory pulse described by

$$g(t) = \frac{1 - 3(\tilde{\omega}t)^2 - 2(N\tilde{\omega}t)^2}{(1 + (N\tilde{\omega}t)^2)^{5/2}}, \qquad G(x_4) = \frac{1}{\tilde{\omega}} \frac{\tilde{\omega}x_4 + (\tilde{\omega}x_4)^3}{(1 - (N\tilde{\omega}x_4)^2)^{3/2}}, \quad N \geq 1. \tag{8.44}$$

Its comparison for $N = 1$ with the Lorentzian profile (8.37) is depicted in the top-left panel in figure 8.5. In the general case, we find the generalized Lorentzian pole

$$x_4^\mathrm{p} = \frac{1}{N\tilde{\omega}}. \tag{8.45}$$

For sufficiently small ϵ the subcycle structure is expected to be irrelevant, in some sense, analogous to the considerations before. This means that the pole structure

---

[5] Actually, the variation of d minimally alters the effective field strength. However, this contribution is small in comparison to effects caused by instanton reflections for $\tilde{\gamma} \geq \tilde{\gamma}^\mathrm{crit}$.

[6] Despite the fact that those are electromagnetic pulses, a pure electric field of this type is still a good approximation. It can be realized, for instance, through a collision of two counter-propagating pulses equal in their (linear) polarization and intensity. Usually, the spatial dependence in that case can be neglected due to delocalization effects in vacuum pair production, see chapter 10, particularly section 10.3.1, as well as chapter 11.

of the bell shaped Lorentzian mainly regulates the strength of the enhancement.

The expected behavior is indeed confirmed in figure 8.5. In the top-right panel we have plotted again $\mathcal{W}_0$ for the previous Lorentzian field, but now confronting it with numerical curves for different ϵ. For $\epsilon < 0.01$ the analytical prediction and the numerical result are almost identical. Only for $\epsilon = 0.01$ there appears a notable difference. Doing the same computation for the oscillatory pulse, equation (8.44), we identify a similar trend. Despite the fact, that for larger ϵ one observes a stronger deviation which is completely plausible, since the increased total effective field strength contributes as well, we observe that the prediction agrees very well with the numerical results.[7] Hence, having obtained the exact reflection point turns out to be sufficient to predict the stationary worldline action and hence the VPP rate in the interesting regime $\epsilon \ll 1$. For $\tilde{\gamma} \gg 1$ both curves merge with each other, independent of ϵ.

The previous observations are interesting, since pulsed fields can be described by an appropriate oscillatory function multiplied with some bell shaped envelope function. Usually such envelopes lead to poles which are closer to the origin than the effective reflection points for (infinitely extended) oscillating fields, see section 8.5. Thus, it is exactly the latter pole originating from the envelope function which will predominantly determine the reflection of the instanton. Note that an envelope function which can model such a pulsed field may also exist without a distinct pole structure. An example is the Gaussian field studied in section 8.5.

At least for $\epsilon \ll 1$, we therefore expect that the assistance is mainly determined by the pole structure of the envelope function and not by the encased oscillatory subcycle structure. However, this strictly applies for the total VPP rate, cf. e.g. [344]. Differences in the momentum spectrum due to the inner subcycle structure can still be visible. The latter turn out to be very decisive, basically in form of interference patterns, cf. e.g. [34, 340–342, 391]. The observed features will also change for fields which do not fulfill the symmetry properties we have assumed for the present studies.

---

[7] To compute $\mathcal{W}_0$ numerically we transform the worldline action as described in 5.4 making use of the underlying structure of the instanton equations (8.1), cf. e.g. [37]. The integration is done with the standard `Mathematica` routine.
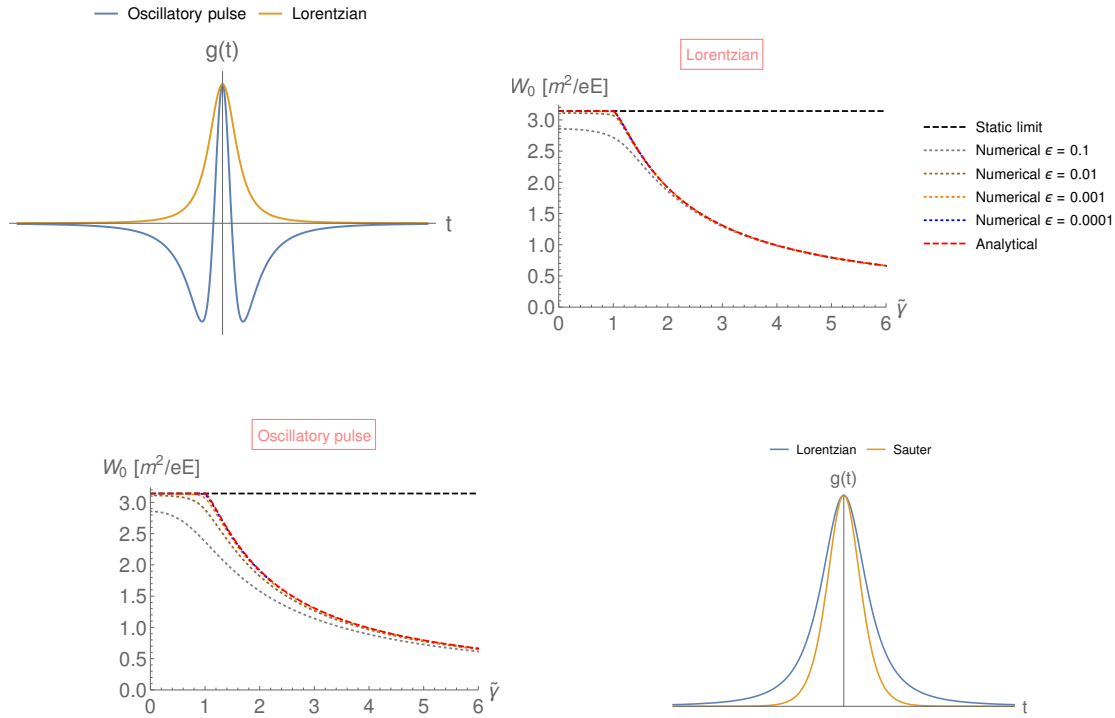
Figure 8.5: Analytically and numerically computed stationary worldline action $\mathcal{W}_0$ for the weak oscillatory pulse in (8.44) with $N = 1$ (bottom-left) and Lorentzian (8.37) (top-right) profile. The values for ϵ are given in the plot legend. The function $g(t)$ for the oscillatory pulse (blue) and Lorentzian field (yellow) is plotted in the top-left panel. The comparison between the Sauter and Lorentzian field is depicted in the bottom-right panel where the frequency for the former one is multiplied by $\pi/2$. This leads to the same reflection point x_4^{p}, see (8.33) and (8.39). Even though the profiles look different, the corresponding stationary worldline actions are identical for field strength ratios $\epsilon \lesssim 10^{-3}$.

Another point is that the critical pole for the Lorentzian field is obtained if we multiply the critical frequency for the Sauter field by a factor $\frac{\pi}{2}$. For a sufficiently small weak field, say $\epsilon = 10^{-3}$, the rate is identical for both cases, confirmed by numerical computations as well. However, the field profiles with this frequency ratio clearly differ, see bottom-right panel in figure 8.5. This is similar to the previous situation with the oscillatory pulse. Despite the visual differences in Minkowski spacetime, we find identical results caused due to same critical points in the instanton plane.

8.5 Assisted mechanism: fields without poles

We have so far illustrated the instanton reflections for backgrounds which lead to a distinct pole structure in the instanton plane. The assisted mechanism operates more general, namely also for nonstatic weak fields with a completely different profile [33–37, 41, 392, 393]. A much considered example is the case of a weak sinusoidal field which is extended to infinity and does not have poles.

As we have seen in the previous examples, instanton reflections at the weak field poles turn out to be the main mechanism behind assistance. Motivated by this observation, we come to the first main goal of the present chapter. After a brief sketch of the basic idea, we aim to find out analogous reflection points in order to generalize the picture from above even to the case where poles from the weak field do not exist.

8.5.1 Motivation
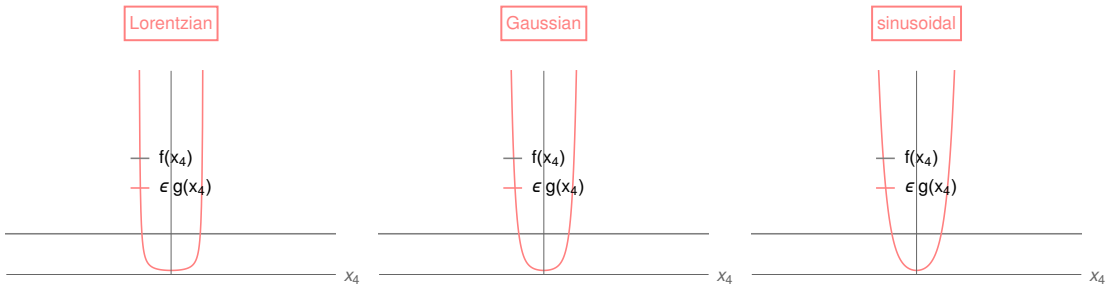
Figure 8.6: Intersection points between the strong and weak field as reflecting mirrors: The functions $f(x_4)$ (gray line) and $\epsilon g(x_4)$ (pink curves) are plotted schematically versus x_4. After rotation in the complex plane the strong static field becomes again static (gray line). The inhomogeneous weak field, however, becomes a positive monotonic function (pink curves). The weak field is assumed to be Lorentzian (left), Gaussian (center) and sinusoidal (right). Note that, in contrast to the Lorentzian field, the last two have not a distinct pole structure.

Let us consider the following case: in the limit $\tilde{\omega} \gg \omega$, the function g will be curved much stronger than the slower varying function f. For sufficiently large frequencies $\tilde{\omega}$ such a bending results in a wall-like potential confining a considerable region of the strong static curve f as sketched in figure 8.6. The left panel shows the case with a weak Lorentzian field. The infinite wall is formed at the poles x_4^{p}. In the remaining two other cases, the Gaussian (center) and sinusoidal (right) field,

we observe a similar picture. These fields as well seem to result in some effective reflectors located around the intersection points between f and ϵg. Thus, at least for a sufficiently large frequency $\tilde{\omega}$, we may expect that the intersection points, denoted in the following by x_4^{i}, will play a similar role as poles in the instanton plane. Of course this is a very rough picture. Later, we will show that improving the location of such effective reflection points is indeed necessary.

According to the described analogy, let us set as a first attempt

$$x_4^{\mathrm{p}} = x_4^{\mathrm{i}}. \tag{8.46}$$

Taking into account $f \sim F'$ and $g \sim G'$, except the prefactors in front, we have to solve the following conditional equation

$$F'(x_4^{\mathrm{i}}) \stackrel{!}{=} \epsilon G'(x_4^{\mathrm{i}}). \tag{8.47}$$

Note that the latter also arises from the original instanton equations in (8.7), namely, when we want to determine the point at which both fields contribute equally. Previously, it was the first expression in (8.7) where we have neglected the term proportional to ϵ away from the poles. So it is natural to look for critical points of the described type. Finding a solution for the equation (8.47) by assuming $F(x_4) = x_4$ is a straightforward task, see section 8.4.

On the other hand, integrating the spatial coordinate $\ddot{x}_3$, see equation (8.9), we obtain a second important conditional equation

$$F(x_4) = \epsilon G(x_4) \tag{8.48}$$

which basically determines the true critical Keldysh parameter. Indeed, it actually corresponds to some equivalent condition[8] in the semiclassical approach to the quantum mechanical scattering formulation discussed in chapter 6.

For weak poleless fields, the equation (8.48) is in general transcendental and cannot be solved directly. We will argue and demonstrate later that perturbing around x_4^{i}, which is much easier to obtain, proves very powerful in order to analytically derive an approximate solution for the equation (8.48). This will allow us to analytically

---

[8] Such a conditional equation will lead to a complex turning point which is equally determined by both fields.

predict the critical point where both the static strong field and the weak rapid field contribute equally.

Besides, applying x_4^{i} for the present purpose is additionally motivated by recent studies. Namely, the critical threshold can be estimated to a remarkable accuracy just by applying such intersection points which lead to the same predictions as in [37, 393]. Due to equation (8.47), it is evident that the effective reflector will
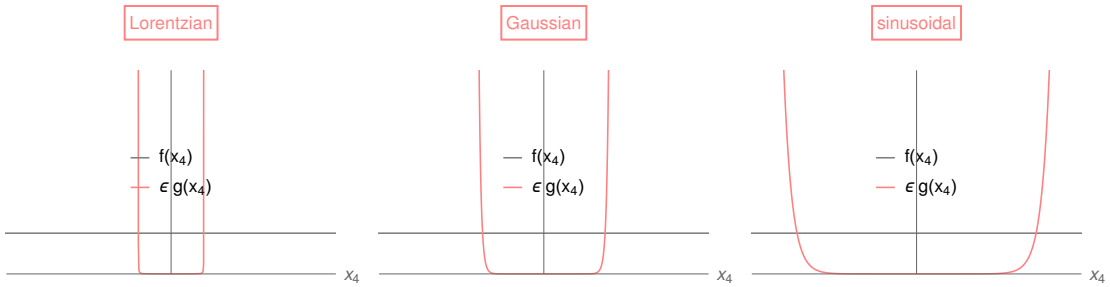
Figure 8.7: Similar plot as in figure 8.6. The strength of the weak field is decreased by 5 orders of magnitude compared to the latter plots. The poles for the Lorentzian field (left) do not change. However, the position of the intersection points for the Gaussian (center) and sinusoidal (right) field depend on the parameter ϵ.

depend on the strength parameter ϵ, another common observation recently discussed in [37]. Note that such an ϵ dependence will also apply for the quantum fluctuation prefactor discussed in section 5.5. This has been shown in numerical investigations [390].

The ϵ dependence is schematically demonstrated in figure 8.7. The location of true poles is fixed, i.e. independent of ϵ. However, for poleless fields a huge difference applies where the strength of the weak field is decreased by five orders of magnitude relatively to figure 8.6. One may expect that the prescribed procedure becomes more accurate as soon as $\epsilon \to 0$, since this would lead to a very fast increase of the weak field curve in the intersection points, similar as one finds in the vicinity of a true pole, cf. left plot in figure 8.7. For poleless weak fields we expect that the point at which the weak field contributes as much as the strong field will drift towards the intersection point.
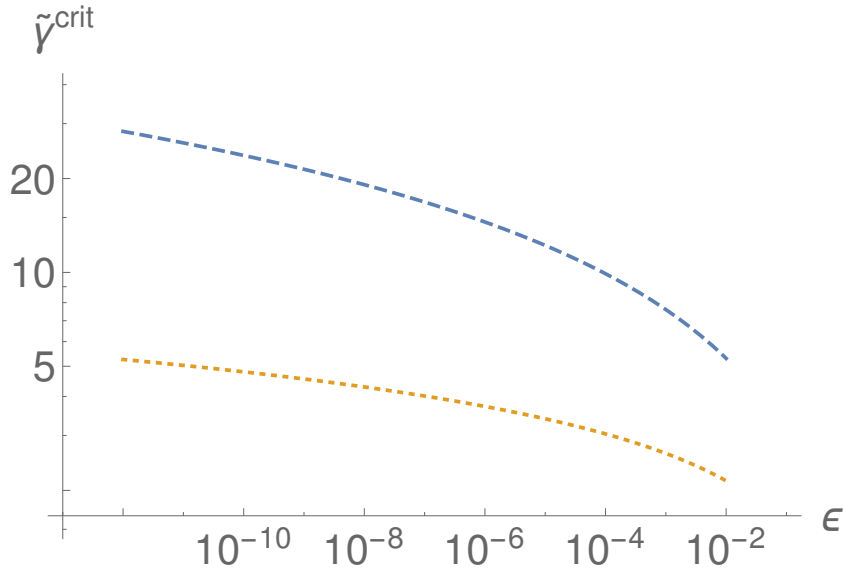
Figure 8.8: Critical combined Keldysh parameter $\tilde{\gamma}^{\mathrm{crit}}$ for the weak sinusoidal and Gaussian field, superimposed with a strong static field, is plotted versus ϵ, where $\tilde{\gamma}^{\mathrm{crit}}$ is evaluated assuming the critical point to be equal to the intersection point x_4^{i}.

8.5.2 Intersection points as reflectors

In the following two sections, we use the intersection points as effective reflectors in order to predict the VPP rate for $\tilde{\gamma}$ above the critical threshold. Improvements for parameters in the vicinity of the critical value are discussed in section 8.5.7.

8.5.2.1 Weak sinusoid

Assume a weak sinusoidal field described by

$$g(t) = \cos(\tilde{\omega}t), \qquad G(x_4) = \frac{\sinh(\tilde{\omega}x_4)}{\tilde{\omega}}. \tag{8.49}$$

Inserting the derivatives F' and G' into the equation (8.47) leads to the following intersection point

$$x_4^{\mathrm{i}} = \frac{\mathrm{arccosh}(1/\epsilon)}{\tilde{\omega}}. \tag{8.50}$$

Using the condition in equation (8.46), we can directly obtain the modified kinematic invariant by applying the relations in (8.25) and (8.8),

$$a \approx 4\frac{\gamma}{\omega}\arcsin\left(\frac{1}{\tilde{\gamma}}\mathrm{arccosh}(1/\epsilon)\right). \tag{8.51}$$

For the critical combined Keldysh parameter, we find from the latter expression, or alternatively by solving (8.112),

$$\tilde{\gamma}^{\mathrm{crit}} = \operatorname{arccosh}(1/\epsilon) \approx \ln(2/\epsilon) \approx |\ln(\epsilon)|, \qquad (8.52)$$

since $\epsilon \ll 1$. It is remarkable that this rough estimation already agrees with the WKB prediction found in [37]. The result from above is depicted in figure 8.8.

Subsequently, applying the findings in (8.28), we obtain the approximate instanton path described by

$$\begin{aligned} x_4(u) &\approx \frac{m}{eE} \sin\left(4u\arcsin\left(\frac{\operatorname{arccosh}(1/\epsilon)}{\tilde{\gamma}}\right)\right), \\ x_3(u) &\approx \frac{m}{eE} \cos\left(4u\arcsin\left(\frac{\operatorname{arccosh}(1/\epsilon)}{\tilde{\gamma}}\right)\right) - \mathcal{C} \end{aligned} \qquad (8.53)$$

with $\mathcal{C} = x_3(u = \pm 1/4)$. Inserting equation (8.50) into equation (8.31), we conclude

$$\mathcal{W}_0 \approx \frac{m^2}{eE}\left(\frac{2\operatorname{arccosh}(1/\epsilon)}{\tilde{\gamma}^2}\sqrt{\tilde{\gamma}^2 - \operatorname{arccosh}^2(1/\epsilon)} + 2\arcsin\left(\frac{\operatorname{arccosh}(1/\epsilon)}{\tilde{\gamma}}\right)\right). \qquad (8.54)$$

The resulting plots for the stationary worldline action from (8.54) are depicted in figure 8.9. Although the analytical prediction follows the trend of the exact numerical curve, both considerably differ from each other. There will be some region right after the intersection point which will surely have a non-negligible contribution to the VPP rate. This is completely neglected when we set $x_4^{\mathrm{p}} = x_4^{\mathrm{i}}$. An improvement of the effective reflection point is therefore needed. Before we proceed in that direction, let us first introduce a second example which shares similar features.

8.5.2.2   Weak Gaussian

We consider a Gaussian field described by

$$g(t) = \exp(-(\tilde{\omega}t)^2), \qquad G(x_4) = \frac{\sqrt{\pi}\operatorname{erfi}(\tilde{\omega}x_4)}{2\tilde{\omega}}. \qquad (8.55)$$

The intersection point is

$$x_4^{\mathrm{i}} = \frac{\sqrt{\ln(1/\epsilon)}}{\tilde{\omega}}. \qquad (8.56)$$
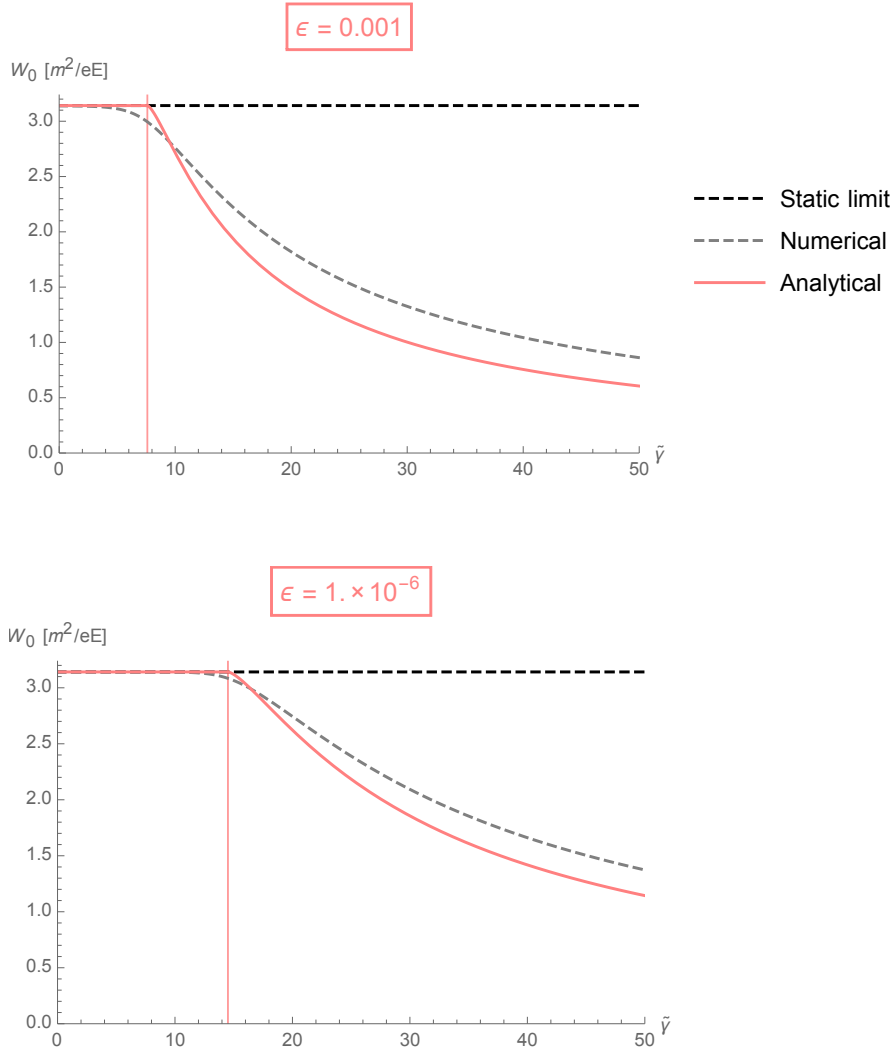
Figure 8.9: Stationary worldline action is plotted for the weak sinusoidal field as described in (8.49). The analytical prediction in equation (8.54) is compared with the exact numerical result for $\epsilon = \{10^{-3}, 10^{-6}\}$ (top,bottom) where we have assumed $x_4^{\mathrm{p}} = x_4^{\mathrm{i}}$.

Proceeding similarly, we get the approximate invariant using equation (8.25),

$$a \approx 4\frac{\gamma}{\omega}\arcsin\left(\frac{1}{\tilde{\gamma}}\sqrt{\ln(1/\epsilon)}\right),\tag{8.57}$$

which leads to the following critical combined Keldysh parameter

$$\tilde{\gamma}^{\mathrm{crit}} = \sqrt{\ln(1/\epsilon)} = \sqrt{|\ln(\epsilon)|}.\tag{8.58}$$

As in the previous case, this result again equals to the prediction obtained using the WKB approach [37]. The critical value is plotted in figure 8.8. Inserting the

intersection point into equation (8.28), we continue with

$$x_4(u) \approx \frac{m}{eE} \sin\left(4u \arcsin\left(\frac{\sqrt{\ln(1/\epsilon)}}{\tilde{\gamma}}\right)\right),$$

$$x_3(u) \approx \frac{m}{eE} \cos\left(4u \arcsin\left(\frac{\sqrt{\ln(1/\epsilon)}}{\tilde{\gamma}}\right)\right) - \mathcal{C}, \tag{8.59}$$

where the constant $\mathcal{C} = x_3(u = \pm 1/4)$ plays the same role as before. We can again plug equation (8.56) into equation (8.31), which results in the following approximate stationary worldline action

$$\mathcal{W}_0 \approx \frac{m^2}{eE}\left(\frac{2\sqrt{\ln(1/\epsilon)}}{\tilde{\gamma}^2}\sqrt{\tilde{\gamma}^2 - \ln(1/\epsilon)} + 2\arcsin\left(\frac{\sqrt{\ln(1/\epsilon)}}{\tilde{\gamma}}\right)\right). \tag{8.60}$$

The plots for (8.60) are shown in figure 8.10 where we still find a clear deviation. However, the discrepancy is significantly smaller than in the case before. This behavior agrees with the curve trends shown in figure 8.8.

8.5.3   Improved reflection points

We have seen that reflecting the instanton at x_4^i can mimic the reduction of the stationary worldline action for large $\tilde{\gamma}$. However, the predictions still considerably differ from the exact numerical curves. In the following, we improve the effective reflection points in order to confirm the validity of the reflection approach even for cases with a weak poleless field.

Before starting with actual calculations, let us emphasize that such an improvement will only affect the region in which $\tilde{\gamma}$ is considerably larger than the critical threshold. Strictly speaking, it will in general not allow a prediction at the critical point.[9] But, as will be discussed in section 8.5.7, an appropriate perturbation around the intersection point allows an analytical prediction for the critical point as well. This is a powerful method to find out when dynamical assistance sets in. Actually, to find this out is a highly challenging problem which has been not approached before analytically. Namely, for most field combinations as weak Gaussian fields, the relevant equation in (8.48) becomes transcendental. More details

---

[9] The critical point here is defined to be the point at which the weak field contribution to the VPP process starts to exceed the strong field contribution, i.e. effect of dynamical assistance, see also section 1.4.
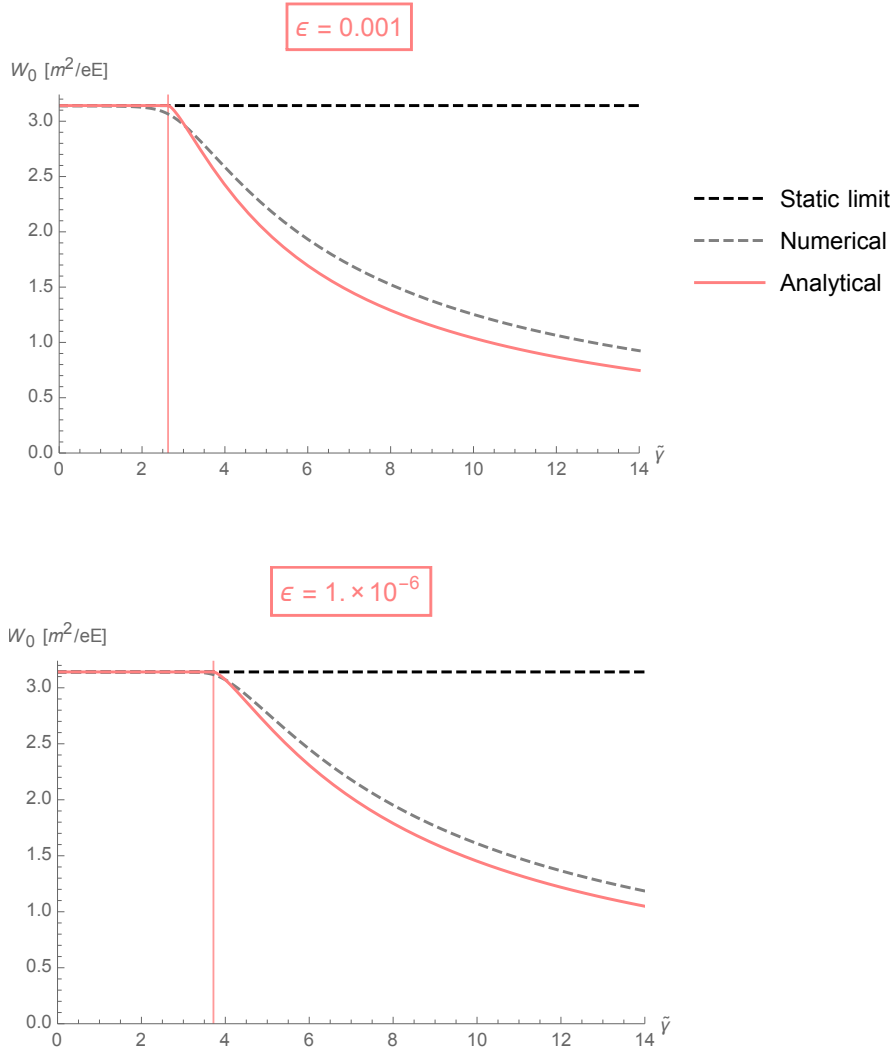
Figure 8.10: Stationary worldline action $\mathcal{W}_0$ for the weak Gaussian field described in (8.55). The analytical prediction in equation (8.60) is compared with the numerical result for $\epsilon = \{10^{-3}, 10^{-6}\}$ (top,bottom) where we have assumed $x_4^{\mathrm{p}} = x_4^{\mathrm{i}}$.

are discussed in section 8.5.7.

Let us first elaborate the first improvement mentioned above in order to predict the rate for sufficiently large $\tilde{\gamma}$. We argued before that some region after the intersection points will be necessary. Hence, we make a correction ansatz of the following form

$$x_4^{\mathrm{p}} \to x_4^{\mathrm{i}} + \frac{\delta}{\tilde{\omega}}, \tag{8.61}$$

where δ denotes some displacement parameter that we still have to specify. Once we have computed δ, the relevant parameter $\tilde{\gamma}$ in the final expressions has to be

modified as well, since $\tilde{\gamma}^{\text{crit}}$ will still be determined by the intersection point.[10] Here, we are interested in the behavior for $\tilde{\gamma} \gg \tilde{\gamma}^{\text{crit}}$. Therefore, we keep x_4^{i} as some approximate critical point.[11] The relevant modifications can be written as follows

$$x_4^{\text{p}} \to x_4^{\text{i}} + \frac{\delta}{\tilde{\omega}}, \qquad \tilde{\gamma} \to \tilde{\gamma} + \delta. \tag{8.62}$$

Such a shifted Keldysh parameter signals already that the impact of the weak rapid field on the VPP rate substantially differs for weak fields with and without poles. We have seen that weak fields with poles result in vertical reflecting walls. The position of these mirrors only depends on the weak field frequency. This fact basically explains why the VPP rate in the assisted mechanism should not alter with ϵ. Differently, in case of weak poleless fields, we need to increase the accuracy of the effective reflection points because of the explicit dependence on ϵ.

In order to accomplish this, let us recall some findings in the equivalent WKB approach introduced in chapter 6. The plan is to obtain conditions that we can combine with our previous analysis in the worldline instanton approach to improve our analytical predictions for $\tilde{\gamma}$ being much larger than the critical threshold. This will also illustrate the equivalence between both methods with respect to the tunneling exponential for which both approaches lead in general to the same result if the momentum spectrum is peaked around zero (canonical) momentum [151]. This is the case for backgrounds depending on one spacetime coordinate as considered here, see e.g. [341].

To be concrete, starting with the corresponding state equation in the presence of a temporal electric background, one can first identify the evolution of the corresponding time dependent Bogoliubov coefficients. Afterwards the resulting system, which is described by the Riccati equation in (6.26), can approximately be integrated and one obtains for $p = 0$, after continuing to the complex domain, the

---

[10] This is in general characteristic for fields without poles. There is always a difference between the effective reflection point and the critical point at which the weak field starts to be dominating. For fields with a distinct pole structure such a disagreeance is not present, at least in the highly weak limit $\epsilon \ll 1$.

[11] We assume the weak field contribution before reaching x_4^{i} as negligible, since, as will be shown, the enormous enhancement of the VPP rate is mainly triggered by instanton reflections.

approximate condition

$$eE\left(F(x_4^*) + \epsilon G(x_4^*)\right) = m \tag{8.63}$$

for the Euclidean versions of the complex turning points, x_4^*, see equation (6.33). This relation, for instance, can alternatively be read from the right-hand side of the integrated expression in (8.9). Analogously, the singularities x_4^* then determine the VPP rate, at least the correct tunneling exponential.[12] The solution of this equation then gives the poles of the fields. If $\epsilon \ll 1$ and G is sufficiently small, one gets the usual strong field pole $x_4^* = \frac{m}{eE}$ in case we assume $F(x_4) = x_4$. For the assisted mechanism, we have to consider the situation where the smallness of ϵ is counterbalanced by the reflection point. This happens in case if

$$\epsilon G(x_4^{\mathrm{p}}) \overset{!}{=} \frac{\tilde{\gamma}}{\tilde{\omega}} \tag{8.64}$$

is satisfied where F is taken to be negligible small in the reflection point, i.e.

$$F(x_4^{\mathrm{p}}) \ll \epsilon G(x_4^{\mathrm{p}}). \tag{8.65}$$

Note that from the previously mentioned conditional equation in (8.48) one deduces the point at which both fields contribute equally. This equation can be transcendental[13] and hence cannot be solved algebraically. In this case, we follow an alternative approach leading to a drastic simplification of the problem. Observe that deriving that equation after x_4 on both sides, leads to the intersection condition already introduced in (8.47).

Now, if the inverse of G does exist, the equation (8.64) can be solved directly having the solution

$$x_4^{\mathrm{p}} = G^{-1}\left(\frac{\tilde{\gamma}}{\epsilon\tilde{\omega}}\right). \tag{8.66}$$

This yields the improved effective reflection point. Reminding that we have started from the assumption $x_4^{\mathrm{p}} \approx x_4^{\mathrm{i}}$, we therefore try to find the displacement parameter in our ansatz in (8.61). Accordingly, the correcting parameter $\delta > 0$ is determined by

$$\delta = \tilde{\omega}G^{-1}\left(\frac{\tilde{\gamma}}{\epsilon\tilde{\omega}}\right) - \tilde{\omega}x_4^{\mathrm{i}}. \tag{8.67}$$

---

[12] As mentioned in chapter 6, the fluctuation prefactor cannot be correctly determined via the semiclassical WKB approach.

[13] For instance, this is the case for a weak (super) Gaussian pulse, cf. section 8.5.

It is important to note that according to the present approach x_4^{i} still has to be the corresponding point for the critical Keldysh parameter $\tilde{\gamma}^{\mathrm{crit}}$, i.e.

$$\gamma \overset{!}{=} \omega F(x_4^{\mathrm{i}}) \rightsquigarrow \tilde{\gamma}^{\mathrm{crit}}. \tag{8.68}$$

The true value that obeys the definition of the actual critical point[14] is discussed in section 8.5.7. According to the latter simplification, contributions from the weak field are neglected before the instanton reflection.[15]

However, the improved effective reflection point (8.61) will for sure modify $\tilde{\gamma}^{\mathrm{crit}}$ from above. This value we denote as $\tilde{\gamma}^{\mathrm{p,crit}}$ which follows from

$$\gamma \overset{!}{=} \omega F(x_4^{\mathrm{p}}) \rightsquigarrow \tilde{\gamma}^{\mathrm{p,crit}}. \tag{8.69}$$

Thus, in order to keep (8.68) as the critical threshold, one has to shift $\tilde{\gamma}$ in the final expressions via (8.67),

$$\tilde{\gamma} \to \tilde{\gamma} + \delta, \tag{8.70}$$

where δ can now be written as

$$\delta = \tilde{\gamma}^{\mathrm{p,crit}} - \tilde{\gamma}^{\mathrm{crit}}. \tag{8.71}$$

Because of $\delta > 0$ and $\epsilon \ll 1$, we assume

$$2\tilde{\gamma}^{\mathrm{crit}} > \tilde{\gamma}^{\mathrm{p,crit}} > \tilde{\gamma}^{\mathrm{crit}}. \tag{8.72}$$

Note that the last two steps are justified only if the weak field raises sufficiently fast in the vicinity of the intersection points which usually applies if $\tilde{\gamma} \gg 1$. Compared to equation (8.67), we will therefore neglect the explicit $\tilde{\gamma}$ dependence and rewrite $\tilde{\gamma}^{\mathrm{p,crit}}$ as

$$\tilde{\gamma}^{\mathrm{p,crit}} = (1 + \xi)\tilde{\gamma}^{\mathrm{crit}} \tag{8.73}$$

with $0 < \xi < 1$. With this, we obtain

$$\delta = \xi\tilde{\gamma}^{\mathrm{crit}}. \tag{8.74}$$

---

[14] The true critical point is defined to be the solution of equation (8.48).

[15] As mentioned before, this is a good approximation, since the enormous enhancement is mainly caused by instanton reflections.

Combining the equations (8.61) and (8.67), we deduce from (8.69)

$$\tilde{\gamma}^{\text{p,crit}} = \tilde{\omega} G^{-1} \left(\frac{\tilde{\gamma}^{\text{p,crit}}}{\epsilon \tilde{\omega}} \right), \tag{8.75}$$

where $F(x_4) = x_4$ applies for the static strong field. Subsequently, we use the relation in (8.73) to obtain

$$(\xi + 1)\tilde{\gamma}^{\text{crit}} = \tilde{\omega} G^{-1} \left(\frac{(\xi + 1)\tilde{\gamma}^{\text{crit}}}{\epsilon \tilde{\omega}} \right) \tag{8.76}$$

with $\tilde{\gamma}^{\text{crit}}$ known from previous analysis, see condition (8.68). The latter equation is difficult to solve in general, because of the nonlinear ξ dependence on the right-hand side. However, since we have $\xi < 1$, one may Taylor expand the nonlinearity in the lowest relevant order and compute ξ. This solution can be used to obtain the displacement parameter from the expression (8.74). This is a powerful way to compute δ, specifically, in situations where the inverse of G is difficult to find or does not exist at all, respectively. Finally, all relevant modifications we need for the improvement are the one given in (8.62).

8.5.4   Reflecting at improved points

Let us apply the ideas from above to the previously discussed examples to compute the VPP rate for parameters $\tilde{\gamma}$ above the critical threshold.

8.5.4.1   Weak sinusoid

We start with the weak sinusoidal field. According to the modifications in (8.62), we first need to compute δ. Applying the inverse function

$$G^{-1}(x_4) = \frac{\text{arcsinh}(\tilde{\omega} x_4)}{\tilde{\omega}} \tag{8.77}$$

to equation (8.67), we find

$$\delta = \text{arcsinh} \left(\frac{\tilde{\gamma}}{\epsilon} \right) - \text{arccosh} \left(\frac{1}{\epsilon} \right). \tag{8.78}$$

Inserting the corresponding replacements afterwards, i.e.

$$\text{arccosh}(1/\epsilon) \rightarrow \text{arccosh}(1/\epsilon) + \delta,$$
$$\tilde{\gamma} \rightarrow \tilde{\gamma} + \delta, \tag{8.79}$$

into the equations (8.51), (8.53) and (8.54), we obtain the improved invariant a, instanton path and stationary worldline action, respectively. The latter written out explicitly reads

$$
\mathcal{W}_0 \approx \frac{m^2}{eE} \left(\frac{2 \left(\operatorname{arccosh}(1/\epsilon) + \delta\right)}{(\tilde{\gamma} + \delta)^2} \sqrt{(\tilde{\gamma} + \delta)^2 - (\operatorname{arccosh}(1/\epsilon) + \delta)^2} \right.
$$
$$
\left. + 2\arcsin \left(\frac{\operatorname{arccosh}(1/\epsilon) + \delta}{\tilde{\gamma} + \delta} \right) \right).
\tag{8.80}
$$

The action (8.80) plotted in figure 8.11 for $\epsilon = \{10^{-3}, 10^{-6}\}$ clearly shows a substantial improvement of the approximate analytical result, cf. figure 8.9. As expected, despite the region around $\tilde{\gamma} = \tilde{\gamma}^{\mathrm{crit}}$ marked by the vertical dashed red line, the analytical curve is in good agreement with the exact numerical curve.

8.5.4.2   Weak Gaussian

Now, we can proceed similarly for the weak Gaussian field given in (8.55). The displacement parameter δ we expect to be smaller compared to the one for the sinusoidal field from (8.49). This is simply due to a stronger slope of the function g in the vicinity of the intersection point, cf. figure 8.7. Apart from this, there is another difference. The function G is the imaginary error function for which the inverse is difficult to express. However, as discussed in the previous section, in such a case we can first apply (8.76) and Taylor expand the nonlinearity in ξ introduced in (8.73), since $\xi < 1$. Proceeding in that way, we obtain the following result in leading order

$$
\xi \approx \frac{1}{\sqrt{2}} \sqrt{\frac{2}{\ln\left(\frac{1}{\epsilon}\right)} - \frac{\sqrt{\pi}\epsilon\,\mathrm{erfi}\left(\sqrt{\ln\left(\frac{1}{\epsilon}\right)}\right)}{\ln^{\frac{3}{2}}\left(\frac{1}{\epsilon}\right)}},
\tag{8.81}
$$

depending only on ϵ which is implicitly required due to the assumptions (8.72) and (8.73). Finally, using the approximate critical value (8.58), we get

$$
\delta = \xi\sqrt{\ln(1/\epsilon)}.
\tag{8.82}
$$

Inserting the replacements

$$
\sqrt{\ln(1/\epsilon)} \rightarrow \sqrt{\ln(1/\epsilon)} + \delta,
$$
$$
\tilde{\gamma} \rightarrow \tilde{\gamma} + \delta
\tag{8.83}
$$
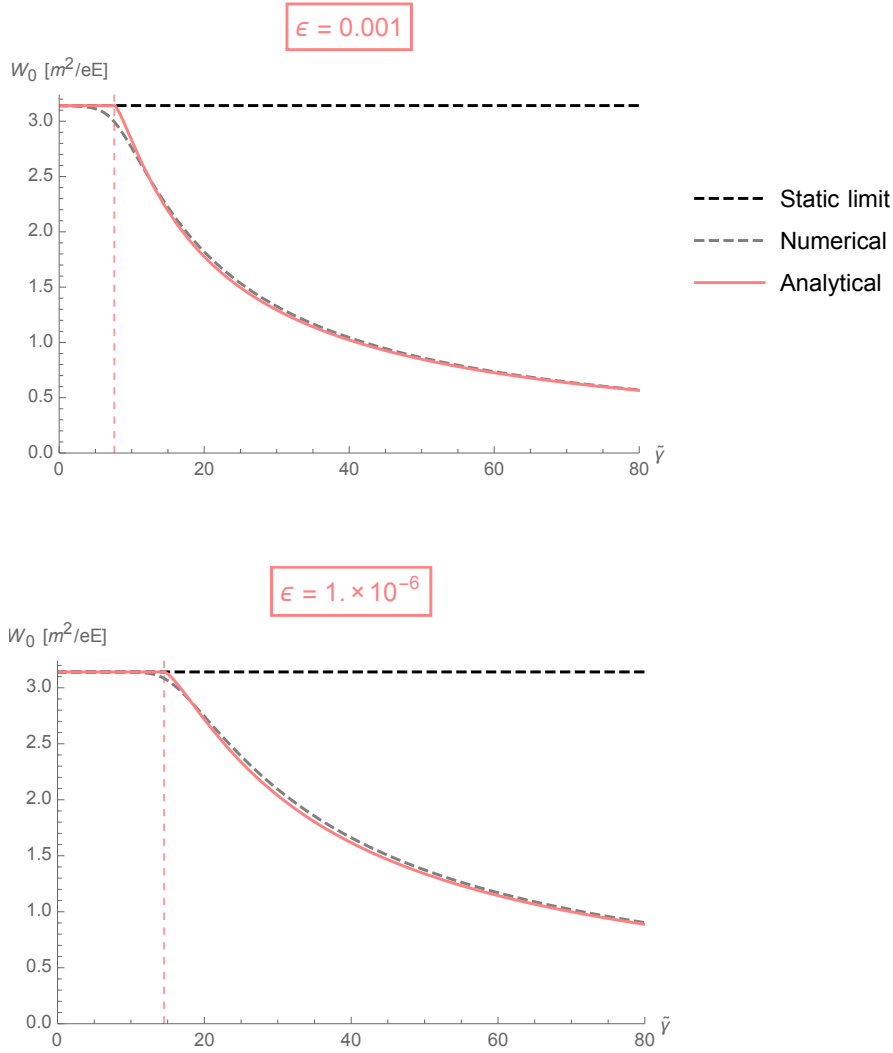
Figure 8.11: Stationary worldline action $\mathcal{W}_0$ plotted for the sinusoidal weak field described in (8.49). The analytical prediction in equation (8.80) is compared with the exact numerical result. The ratio between the strong and weak field strengths is set to $\epsilon = \{10^{-3}, 10^{-6}\}$ (top,bottom). The vertical dashed red lines are placed at $\tilde{\gamma} = \tilde{\gamma}^{\text{crit}}$. Here, we have applied the improved effective reflection point $x_4^{\text{p}} = x_4^{\text{i}} + \delta/\tilde{\omega}$.

into the equations (8.57), (8.59) and (8.60), we obtain again the improved invariant a, instanton path and the following stationary worldline action

$$
\begin{aligned}
\mathcal{W}_0 \approx \frac{m^2}{eE} \Bigg(& \frac{2\left(\sqrt{\ln(1/\epsilon)} + \delta\right)}{(\tilde{\gamma} + \delta)^2} \sqrt{(\tilde{\gamma} + \delta)^2 - \left(\sqrt{\ln(1/\epsilon)} + \delta\right)^2} \\
& + 2\arcsin\left(\frac{\sqrt{\ln(1/\epsilon)} + \delta}{\tilde{\gamma} + \delta}\right) \Bigg),
\end{aligned}
\tag{8.84}
$$

respectively. The comparison between the analytically approximated stationary worldline action in (8.84) and its exact numerical computation is depicted in figure
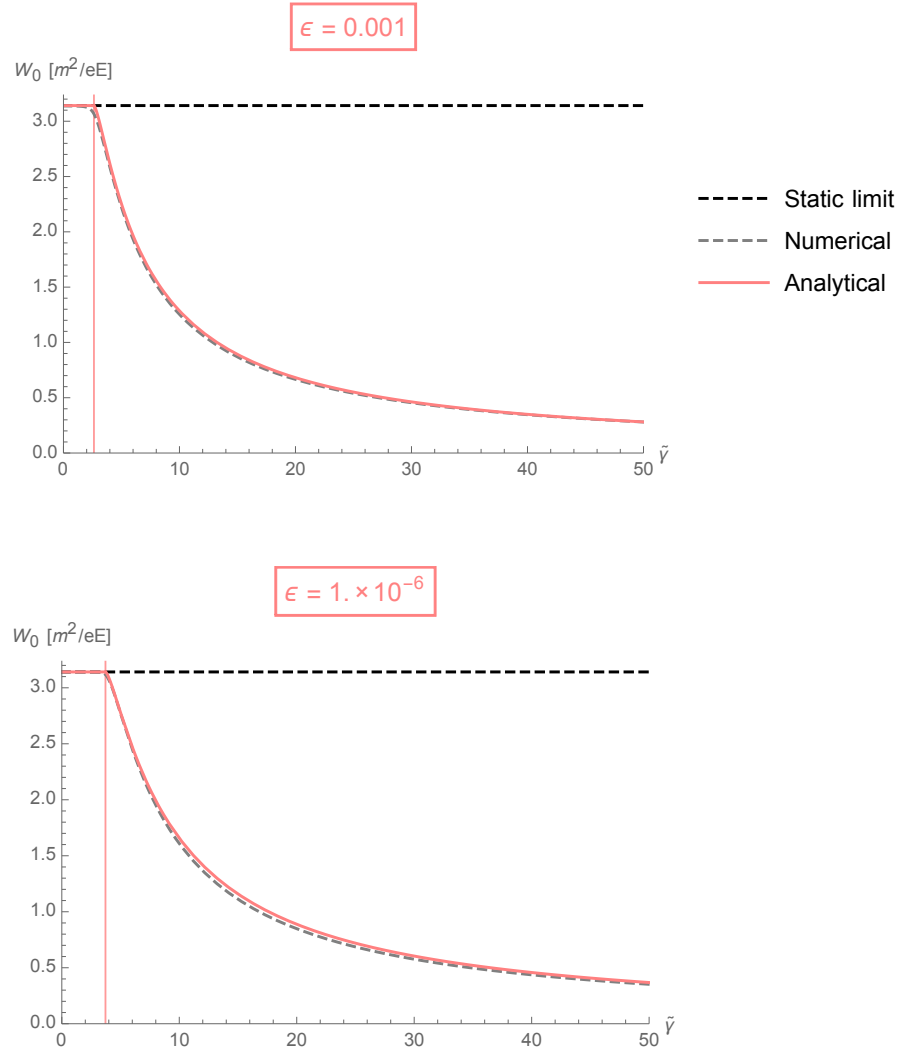
Figure 8.12: Stationary worldline action $\mathcal{W}_0$ for the weak Gaussian field described in (8.55). The analytical prediction in equation (8.84) is compared with the numerical result. The ratio between the strong and weak field strengths is set to $\epsilon = \{10^{-3}, 10^{-6}\}$ (top,bottom). The vertical red lines are placed at $\tilde{\gamma} = \tilde{\gamma}^{\mathrm{crit}}$. Here, we have applied the improved effective reflection point $x_4^{\mathrm{p}} = x_4^{\mathrm{i}} + \delta/\tilde{\omega}$.

8.12.   As in the previous example, the analytical curve is clearly improved for sufficiently large $\tilde{\gamma}$, cf. figure 8.10. The prediction is in good agreement with the exact numerical computation. This observation confirms again the validity of the reflection picture.

8.5.5   Weak super Gaussian

The standard Gaussian field (8.55) has led to more accurate results if the intersection point is taken as the effective reflector. A field with a stronger slope in
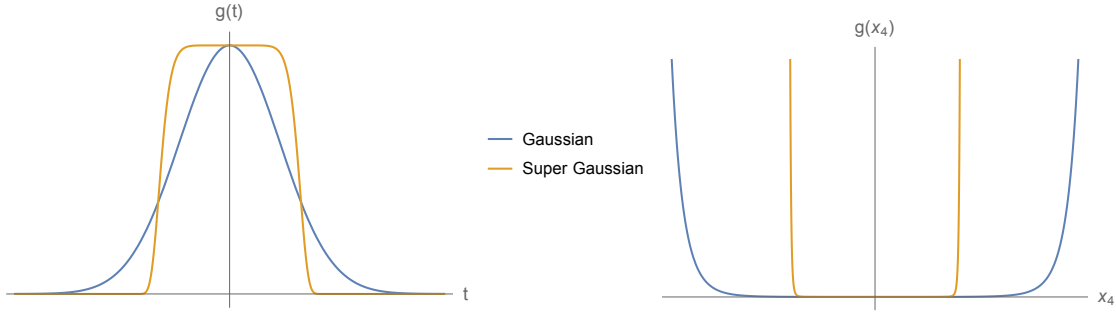
Figure 8.13: Comparison between the standard Gaussian pulse from (8.55) and the super Gaussian pulse from (8.85) shown in blue and yellow, respectively. In the left panel the function $g(t)$ in Lorentzian time is plotted. The right panel shows the analytic continued function $g(x_4)$ depending on Euclidean time.

the vicinity of the intersection points may even lead to more accurate predictions. For that reason, let us introduce a third example assuming a weak super Gaussian described by

$$g(t) = \exp(-(\tilde{\omega}t)^{10}), \qquad G(x_4) = -\frac{(\tilde{\omega}x_4)\mathbf{E}_{\frac{9}{10}}\left((-i\tilde{\omega}x_4)^{10}\right)}{10\tilde{\omega}} \tag{8.85}$$

where $\mathbf{E}_n(z)$ denotes the exponential integral function. The comparison with the standard Gaussian field in (8.55) is depicted in figure 8.13. The field profile resembles a rectangular potential wall with a flat top (left panel). Rotating the function g in the complex plane shows a large curve slope, similar to the situation with a weak Sauter-like field.

The intersection point for the super Gaussian fro above is

$$x_4^{\mathrm{i}} = \frac{\ln(1/\epsilon)^{1/10}}{\tilde{\omega}}. \tag{8.86}$$

Setting $x_4^{\mathrm{p}} = x_4^{\mathrm{i}}$ leads to the modified invariant

$$a \approx 4\frac{\gamma}{\omega}\arcsin\left(\frac{1}{\tilde{\gamma}}\ln(1/\epsilon)^{1/10}\right) \tag{8.87}$$

and critical Keldysh parameter

$$\tilde{\gamma}^{\mathrm{crit}} = \ln(1/\epsilon)^{1/10} \approx |\ln(\epsilon)|^{1/10}. \tag{8.88}$$

The large mass approximation condition in (5.10) becomes

$$ma \approx \frac{E_{\mathrm{S}}}{E}4\arcsin\left(\frac{1}{\tilde{\gamma}}\left(\ln(1/\epsilon)\right)^{1/10}\right) \gg 1. \tag{8.89}$$

For the worldline instanton path we obtain

$$x_4(u) \approx \frac{m}{eE} \sin\left(4u \arcsin\left(\frac{(\ln(1/\epsilon))^{1/10}}{\tilde{\gamma}} \right) \right),$$
$$x_3(u) \approx \frac{m}{eE} \cos\left(4u \arcsin\left(\frac{(\ln(1/\epsilon))^{1/10}}{\tilde{\gamma}} \right) \right) - \mathcal{C}, \tag{8.90}$$

where the constant $\mathcal{C}$ plays the same role as before, i.e. $\mathcal{C} = x_3(u = \pm 1/4)$.

The predicted instantons are plotted in figure 8.14 for $\epsilon = \{10^{-3}, 10^{-6}\}$. The paths
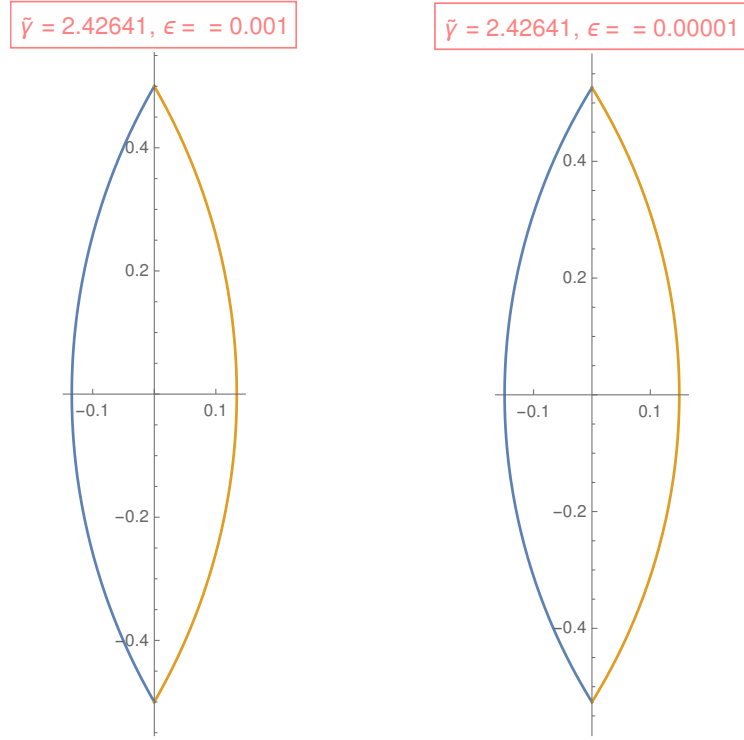
Figure 8.14: Instanton paths for an electric background as superposition of a strong static and weak super Gaussian field as described in (8.85) are plotted for $\epsilon = \{10^{-3}, 10^{-5}\}$ (left,right). The combined Keldysh parameter is set to $\tilde{\gamma} = 2\tilde{\gamma}^{\mathrm{crit}}(\epsilon = 0.001)$. Here, the instanton is reflected at the intersection point, i.e. $x_4^{\mathrm{p}} = x_4^{\mathrm{i}}$.

do not differ much from each other, in other words, the ϵ dependence has become weaker. This is basically in line with the situation for fields which have true poles. Because of the strong curve slope, the position of the intersection points is almost fixed and does not change with varying ϵ. Inserting equation (8.86) into (8.31), we get

$$\mathcal{W}_0 \approx \frac{m^2}{eE} \left(\frac{2 \left(\ln(1/\epsilon)\right)^{1/10}}{\tilde{\gamma}^2} \sqrt{\tilde{\gamma}^2 - (\ln(1/\epsilon))^{1/5}} + 2\arcsin\left(\frac{(\ln(1/\epsilon))^{1/10}}{\tilde{\gamma}} \right) \right) \tag{8.91}$$
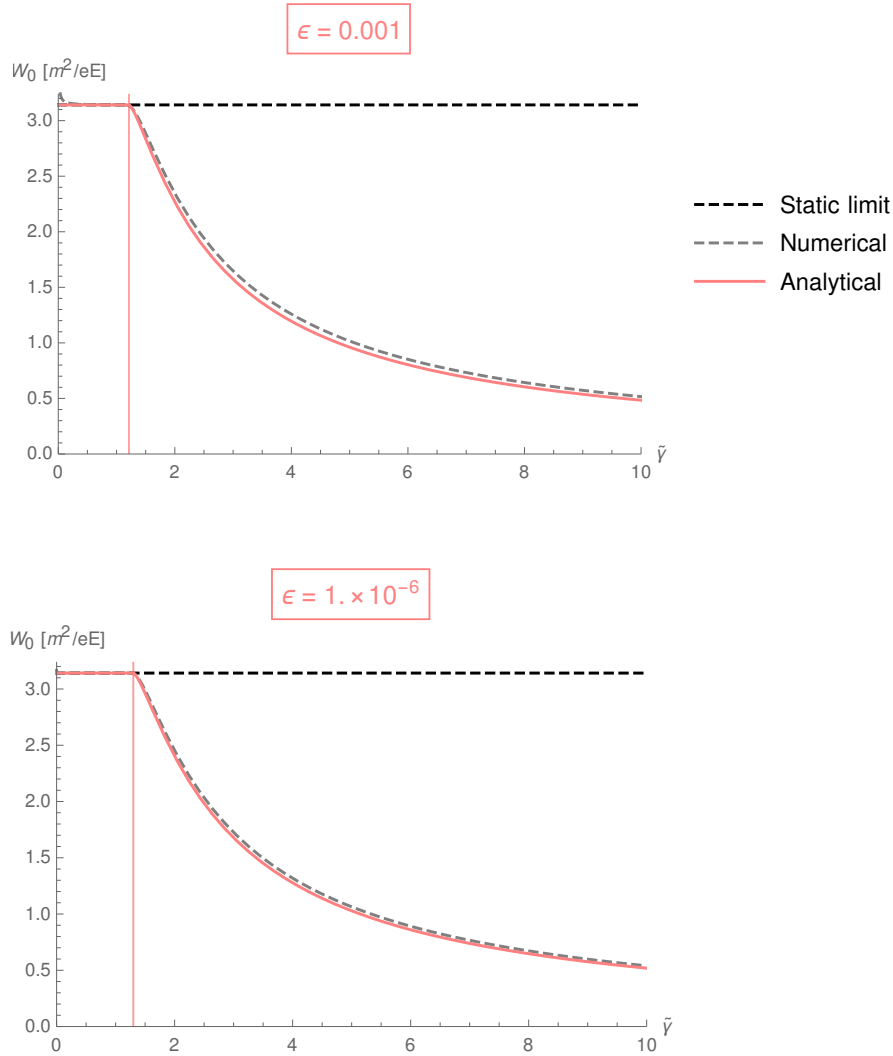
Figure 8.15: Stationary worldline action $\mathcal{W}_0$ for the weak super Gaussian field (8.85). The analytical prediction (8.91) is compared with the numerical result. The instanton is reflected at the intersection point, i.e. $x_4^{\mathrm{p}} = x_4^{\mathrm{i}}$. The vertical red lines are placed at $\tilde{\gamma} = \tilde{\gamma}^{\mathrm{crit}}$.

which is shown in figure 8.15. The result agrees well with the numerical curve. Hence, the discussed features from above lead indeed to a substantial improvement of the analytical estimation, namely, already with setting $x_4^{\mathrm{p}} = x_4^{\mathrm{i}}$.

These results can be generalized to the case with an arbitrary super Gaussian field of the form

$$g(t) = \exp(-(\tilde{\omega}t)^{(4N+2)}), \quad N \in \mathbb{N}. \tag{8.92}$$

The corresponding intersection point is

$$x_4^{\mathrm{i}} = \frac{\ln(1/\epsilon)^{\frac{1}{4N+2}}}{\tilde{\omega}}. \tag{8.93}$$

Thus, for $N > 2$ we may expect the prediction with $x_4^{\mathrm{p}} = x_4^{\mathrm{i}}$ to be even more accurate compared to the latter case with $N = 2$, means there is principally no need for any substantial correction δ. Therefore higher order super Gaussians as in (8.92) almost behave like fields with poles. The ϵ dependence becomes suppressed with increasing N regulating the order of the super Gaussian. Hence, the VPP rate will be enhanced even more, simply due to

$$\tilde{\omega} x_4^{\mathrm{i}} \to 1 \quad (N \to \infty). \tag{8.94}$$

It should be noted that the latter limit coincides with the reflection point for a weak Lorentzian field. More aspects related to this coincidence is discussed in chapter 9.

8.5.6 Comparison of stationary worldline actions

In this part, we compare the predicted stationary worldline actions from above. The results are plotted in figure 8.16 for $\epsilon = \{10^{-3}, 10^{-6}\}$. The fields without poles are marked with asterisks in the plot legend. For simplification, we take the critical Keldysh parameter to be determined by the approximate value $\tilde{\gamma}^{\mathrm{crit}}$, see section 8.5.7 regarding the true value.

We observe that the bell shaped fields enhance the rate much more than the infinitely extended sinusoidal field. Those among them with true poles tend to reduce the stationary action even more. This is shown upon the direct comparison with the Gaussian field which is a bell shaped field but has no poles.

Interestingly, the super Gaussian with $N = 2$ which does not have true poles as well leads to comparable enhancement, even much stronger than the Sauter field. This can be understood by rotating the field in the complex plane where a very strong slope in the vicinity of the relatively small intersection point applies, see section 8.5. The computed intersection point is almost equal to the improved effective reflection point and true critical point which on the other side differ considerably from each other if poles for the weak field are absent, see section 8.5.
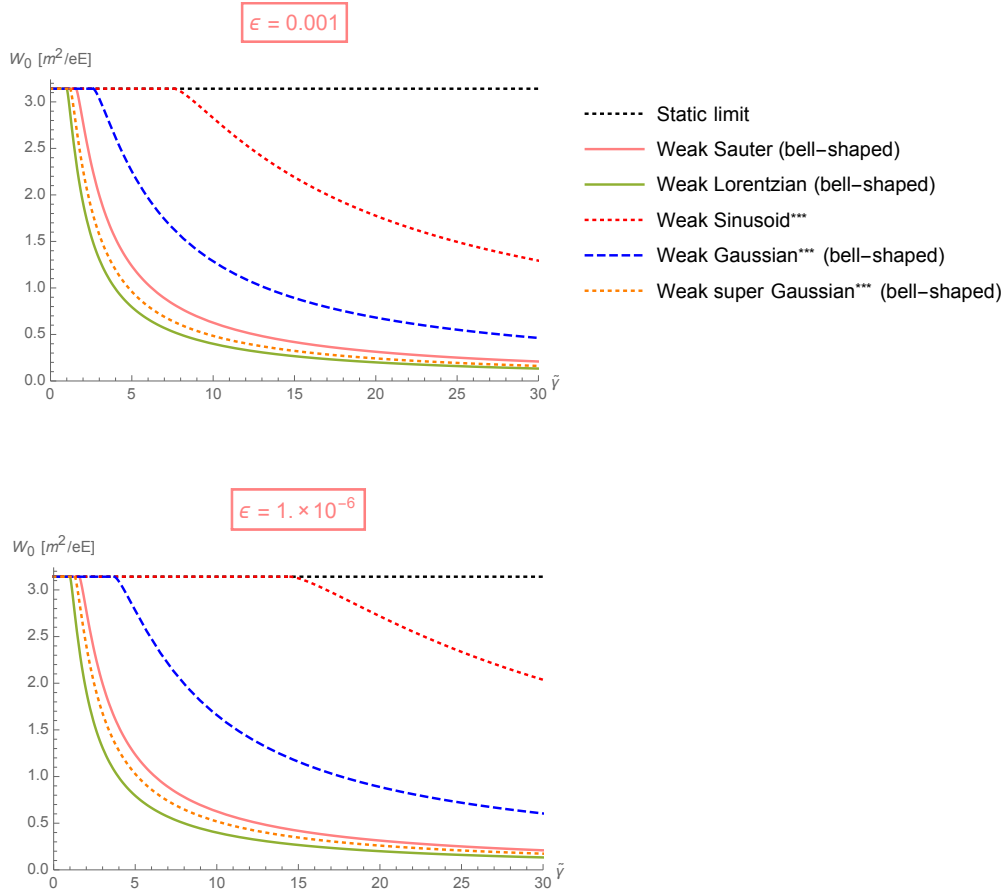
Figure 8.16: Comparison of the stationary worldline action $\mathcal{W}_0$ for different weak fields. The ratio between the strong and weak field strengths is set to $\epsilon = \{10^{-3}, 10^{-6}\}$ (top,bottom). The different field are labeled in the legend. Fields without poles are marked with asterisks in the legend. Note that the applied critical Keldysh parameter for those fields is approximated by $\tilde{\gamma}^{\mathrm{crit}}$. For more on the true critical value we refer to the discussion in the following section 8.5.7.

Bell shaped fields may have important consequences for oscillatory pulses. The latter may be described by multiplying, for instance, an infinitely extended sinusoidal field with a bell shaped envelope function. According to the presented results, a weak field of this form will predominantly trigger the assistance via instanton reflections at the poles of the envelope function. Varying the pulse width via the frequency of the latter is therefore expected to be dominating the enhancement.

However, as discussed in section 8.4, resolving the momentum spectrum of the produced pair may disclose interference effects which can be sensitive to the subcycle structure of a pulse. On the other hand, the total VPP rate is highly sensitive to the finite size of the weak pulse. This especially is substantial for laser experiments where pulses have very short duration. These insights can be, for instance, used

for optimization studies in order to enhance the VPP rate even more by choosing an appropriate field setup.

8.5.7 Improved critical point

In this part, we discuss how to derive the true critical Keldysh parameter. As shown in section 8.5.3, for improving the effective reflection point we have computed the displacement parameter δ. For the case, where the inverse of G is complicated, we have applied some advanced perturbation technique around the intersection point.

As stressed before, the critical point needs to be improved as well.[16] For this, we can generally assume a correction of the from

$$(1 - \Delta)x_4^{\mathrm{i}}, \tag{8.95}$$

resulting in the critical threshold

$$(1 - \Delta)\tilde{\gamma}^{\mathrm{crit}}. \tag{8.96}$$

In the following, we compute the correction Δ again via perturbing in the vicinity of x_4^{i}, since the relevant domain to look for is

$$x_4 \in (0, x_4^{\mathrm{i}}], \tag{8.97}$$

cf. figures 8.6 and 8.7. This will correct the previous estimations in (8.52) and (8.58). The relevant equation in the present case is (8.48). Inserting the ansatz (8.95) into equation (8.48) we write

$$(1 - \Delta)x_4^{\mathrm{i}} = \epsilon G\left((1 - \Delta)x_4^{\mathrm{i}}\right) \tag{8.98}$$

where we again have set $F(x_4) = x_4$. In contrast to the original equation in (8.48), the modified version in (8.98) can be Taylor expanded on the right-hand side for which we find the series

$$(1 - \Delta)x_4^{\mathrm{i}} \approx G(x_4^{\mathrm{i}}) - G'(x_4^{\mathrm{i}})\Delta - \frac{1}{2}G''(x_4^{\mathrm{i}})\Delta^2 + \mathcal{O}(\Delta^3). \tag{8.99}$$

Now, this equation can be solved by truncating after a sufficient order in Δ. This allows to solve the relevant equation (8.48) which in general is hard to tackle directly due to its transcendental form for various types of backgrounds. In the following, we explicitly compute Δ for the weak sinusoidal and Gaussian field.

---

[16] It is taken as the point where both the strong, slow and weak, rapid field contribute equally to the VPP process.

8.5.7.1 Weak sinusoid

The sinusoidal field is described in (8.49). Plugging into the corresponding function into the equation (8.98) yields

$$(1 - \Delta)x_4^{\mathrm{i}} = \frac{\epsilon}{\tilde{\omega}} \sinh((1 - \Delta)\tilde{\omega}x_4^{\mathrm{i}}). \tag{8.100}$$

With the intersection point (8.50), we obtain up to order $\mathcal{O}(\Delta^2)$,

$$\tilde{\gamma}^{\mathrm{crit}}(1 - \Delta) \approx \epsilon \left(\frac{1}{2}\tilde{\gamma}^{\mathrm{crit}^2}\Delta^2 \sinh(\tilde{\gamma}^{\mathrm{crit}}) - \tilde{\gamma}^{\mathrm{crit}}\Delta \cosh(\tilde{\gamma}^{\mathrm{crit}}) + \sinh(\tilde{\gamma}^{\mathrm{crit}}) \right). \tag{8.101}$$

Here, we have used the relation $\tilde{\omega}x_4^{\mathrm{i}} = \tilde{\gamma}^{\mathrm{crit}}$. The parameter Δ is then determined by

$$\Delta \approx -\frac{\mathrm{csch}(\tilde{\gamma}^{\mathrm{crit}})}{\tilde{\gamma}^{\mathrm{crit}}\epsilon} + \frac{\coth(\tilde{\gamma}^{\mathrm{crit}})}{\tilde{\gamma}^{\mathrm{crit}}} + \mathrm{csch}(\tilde{\gamma}^{\mathrm{crit}})$$

$$\times \frac{\sqrt{(2\tilde{\gamma}^{\mathrm{crit}} - 2\tilde{\gamma}^{\mathrm{crit}}\epsilon \cosh(\tilde{\gamma}^{\mathrm{crit}}))^2 - 4\tilde{\gamma}^{\mathrm{crit}^2}\epsilon \sinh(\tilde{\gamma}^{\mathrm{crit}})(2\epsilon \sinh(\tilde{\gamma}^{\mathrm{crit}}) - 2\tilde{\gamma}^{\mathrm{crit}})}}{2\tilde{\gamma}^{\mathrm{crit}^2}\epsilon}. \tag{8.102}$$

8.5.7.2 Weak Gaussian

The weak Gaussian field is given in (8.55) with the corresponding intersection point in (8.56). As before, we plug the associated quantities into the equation (8.98) and get

$$(1 - \Delta)\tilde{\omega}x_4^{\mathrm{i}} = \epsilon \frac{\sqrt{\pi}}{2}\mathrm{erfi}((1 - \Delta)\tilde{\omega}x_4^{\mathrm{i}}). \tag{8.103}$$

This equation can be written up to order $\mathcal{O}(\Delta^2)$ as

$$(1 - \Delta)\tilde{\gamma}^{\mathrm{crit}} \approx \epsilon \left(-\frac{2\left(e^{\tilde{\gamma}^{\mathrm{crit}^2}}\tilde{\gamma}^{\mathrm{crit}}\right)\Delta}{\sqrt{\pi}} + \frac{2e^{\tilde{\gamma}^{\mathrm{crit}^2}}\tilde{\gamma}^{\mathrm{crit}^3}\Delta^2}{\sqrt{\pi}} + \mathrm{erfi}(\tilde{\gamma}^{\mathrm{crit}}) \right) \tag{8.104}$$

so that we find

$$\Delta \approx \frac{e^{-\tilde{\gamma}^{\mathrm{crit}^2}}\sqrt{\left(\sqrt{\pi}\tilde{\gamma}^{\mathrm{crit}} - 2e^{\tilde{\gamma}^{\mathrm{crit}^2}}\tilde{\gamma}^{\mathrm{crit}}\epsilon\right)^2 - 8e^{\tilde{\gamma}^{\mathrm{crit}^2}}\tilde{\gamma}^{\mathrm{crit}^3}\epsilon\left(\sqrt{\pi}\epsilon\mathrm{erfi}(\tilde{\gamma}^{\mathrm{crit}}) - \sqrt{\pi}\tilde{\gamma}^{\mathrm{crit}}\right)}}{4\tilde{\gamma}^{\mathrm{crit}^3}\epsilon}$$

$$- \frac{\sqrt{\pi}e^{-\tilde{\gamma}^{\mathrm{crit}^2}}}{4\tilde{\gamma}^{\mathrm{crit}^2}\epsilon} + \frac{1}{2\tilde{\gamma}^{\mathrm{crit}^2}}. \tag{8.105}$$

8.5.7.3 Comparisons

In case of a distinct pole structure, we can compute $\tilde{\gamma}^{\mathrm{crit}}$ by solving the simple equation

$$x_4^{\mathrm{p}} = \frac{\gamma}{\omega}, \tag{8.106}$$

cf. equation (8.112). If poles are not present, we may set $x_4^{\mathrm{p}} = x_4^{\mathrm{i}}$. In order to consider $\tilde{\gamma}^{\mathrm{crit}}$ as the critical threshold, we can assume that the background after the rotation in the complex plane is approximated by f for $\tilde{\gamma} \leq \tilde{\gamma}^{\mathrm{crit}}$, cf. figures 8.6 and 8.7, respectively. This is for sure not the realistic situation, since there is some contribution from the weak field described by g which actually leads to an increased effective field strength. Nevertheless, the simplification has allowed to predict the stationary worldline action for $\tilde{\gamma}$ being larger than the critical threshold. In the absence of true poles simple arguments are not very clear. Therefore, the obtained agreements from above have helped to sort earlier observations into a more general picture. One should bear in mind, that further improvements with respect to the effective reflection points are needed, see equation (8.61).

Improving the estimations in (8.52) and (8.58), respectively, can be accomplished by starting from the ansatz in (8.96). We expect that the difference between the resulting true critical point (8.95) and the intersection point decreases for $\epsilon \to 0$, see figures 8.11 and 8.12.

On the other hand, if poles exist then intersection, critical and reflection point are just given by the pole itself, means $\delta \to 0$ and $\Delta \to 0$. This is the main reason why poleless weak fields assist less at the critical onset determined by the improved value (8.96). In contrast, for weak fields with true poles, the stationary worldline action decreases very rapidly as soon as $\tilde{\gamma}$ approaches the critical threshold, cf. figure 8.4. The difference between the intersection point and the true critical point from (8.95) is

$$x_4^{\mathrm{i}} - (8.95) = x_4^{\mathrm{i}} - (1 - \Delta)x_4^{\mathrm{i}} = \Delta x_4^{\mathrm{i}} = \Delta \frac{\tilde{\gamma}^{\mathrm{crit}}}{\tilde{\gamma}} \frac{m}{eE} \tag{8.107}$$

where Δ denotes the correction in (8.102) and (8.105), respectively, plotted in figure 8.17. In the limit $\epsilon \to 0$, we find that $\Delta \to 0$. This is consistent with our expectation and observations in the figures 8.11 and 8.12. The improved critical combined Keldysh parameter in (8.96) is plotted in the right panel of figure 8.17.
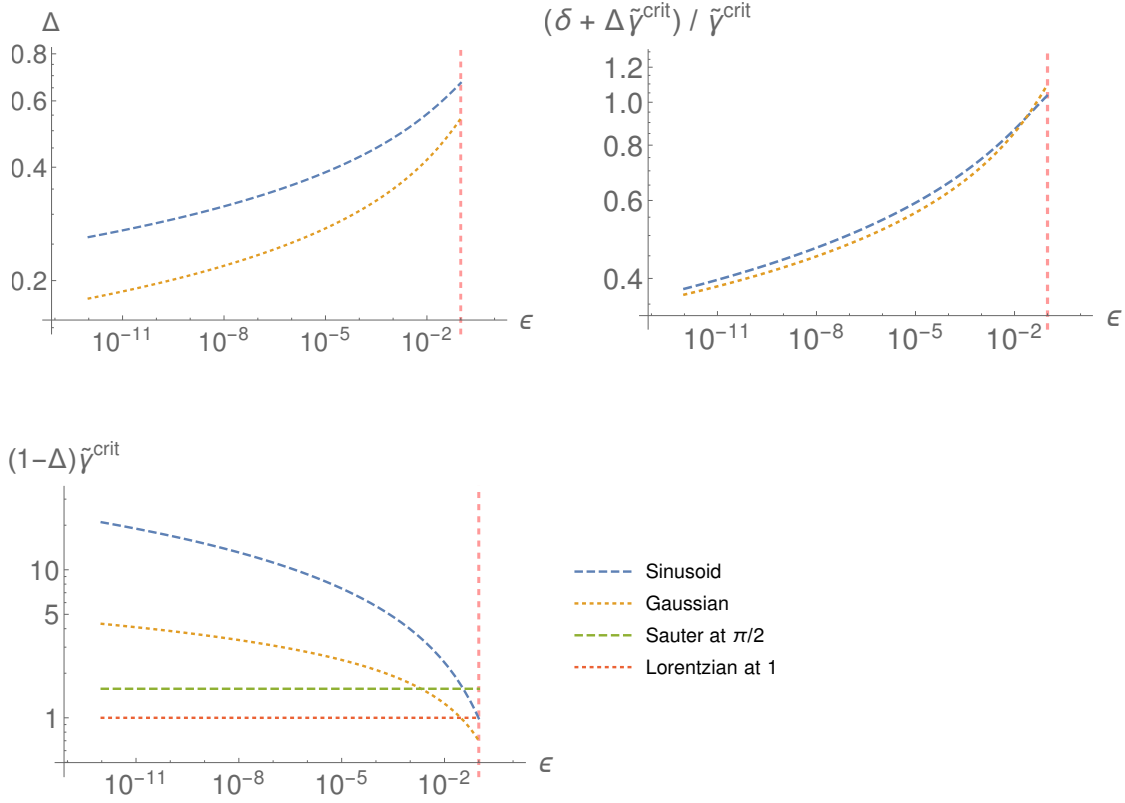
Figure 8.17: Comparison of Δ for the sinusoidal and Gaussian field (top-left). The difference, here with $\tilde{\gamma} = \tilde{\gamma}^{\text{crit}}$, between the improved effective reflection point from (8.61) and the true critical point from (8.95) is shown in units of $\frac{m}{eE}$ (top-right). Note that for fields with a distinct pole structure we find $\delta, \Delta \to 0$ in the relevant regime, $\epsilon \ll 1$. The true critical combined Keldysh parameter for fields without poles as introduced in (8.96) is plotted in the bottom panel. Note the difference compared to the previous estimations in figure 8.8. The correction Δ is computed up to order $\mathcal{O}(\Delta^2)$. For improvements, in particular, for the sinusoidal field due to a in general larger Δ, see top-left panel, we can simply truncate the Taylor series in equation (8.99) after higher orders in Δ. The vertical pink dashed line is placed at $\epsilon = 0.1$.

The found values coincide very well with the critical behavior in figures 8.11 and 8.12. The improved values are of high accuracy, although Δ has been computed only up to order $\mathcal{O}(\Delta^2)$, see equation (8.99).

A small deviation, however, occurs in case of the sinusoidal field where $\epsilon = 10^{-3}$. Namely, the analytically predicted value is $(1 - \Delta)\tilde{\gamma}^{\text{crit}} \approx 4$, blue dashed curve, while we observe $\tilde{\gamma} \approx 3$ in the left panel in figure 8.11, dashed gray curve. Such a difference originates due to $\Delta \lesssim 1$ as reflected in figure 8.17. To improve the analytical prediction, one can truncate the Taylor series in (8.99) after an appropriate higher order in Δ. The very well coincidence in the remaining other cases

confirm the validity of our predictions (8.102) and (8.105) obtained by solving the
conditional equation in (8.48). As mentioned, in may cases finding some analyt-
ical (approximate) solution for the latter equation can be highly challenging, see
e.g. [37, 390] for numerical investigations.

In addition, we also have plotted the constant lines in figure 8.17 (bottom) at $\frac{\pi}{2}$
and 1 for the Sauter and the Lorentzian field, respectively. For the remaining two
poleless fields we find the nonstatic dependence on ϵ. Increasing the parameter ϵ,
the critical threshold (8.96) turns out to be smaller compared to the first estima-
tions introduced in (8.52) and (8.58), see figures 8.8 and 8.17 (bottom) as well.
This is also in agreement with the presented plots in figures 8.11 and 8.12. For
sufficiently large ϵ, say $\sim 10^{-2}$, we even achieve values below $\frac{\pi}{2}$. However, although
in this case the Gaussian field starts to assist before the Sauter field, it reduces the
stationary worldline action much slower. This difference is a direct consequence of

$$(8.61) - (8.95) = \frac{\delta + \Delta\tilde{\gamma}^{\text{crit}}}{\tilde{\gamma}} > 0 \tag{8.108}$$

written in units of $\frac{m}{eE}$. Using the equations (8.78), (8.102) for the weak sinusoidal
field and (8.82), (8.105) for the weak Gaussian, respectively, we have plotted the
corresponding curves for $\tilde{\gamma} = \tilde{\gamma}^{\text{crit}}$ in figure 8.17. Differently, if the underlying weak
field has a pole we have (8.108) = 0.

We conclude that for $\epsilon \ll 1$ the critical combined Keldysh parameter for fields with
poles determines exactly the point where the weak field contribution becomes es-
sential and the reflection sets in. If poles are not present, the true critical point
of the form (8.95) does not generally correspond to the effective reflection point
(8.61). The latter is usually much larger. So we find a much larger range below
the critical Keldysh parameter where the dynamical assistance does not have any
effect on VPP, see for instance figure 8.11. Consequently, the reduction of the sta-
tionary worldline action progresses very slow. Nevertheless, a minimal reduction
is somewhat triggered. This is an effect of the minimally increased effective field
strength due to the superposition of the strong and weak field, see left and right
panels in figure 8.6. This somewhat resembles the standard dynamical mechanism
in a singlemode inhomogeneous electric background, see gray solid curve in figure
8.19. In this parameter range the effective reflection point is simply too far away
from the true critical point.

We note that as soon as (8.108) → 0, which applies for large $\tilde{\gamma}$ exceeding $\tilde{\gamma}^{\mathrm{crit}}$, the enhancement becomes much stronger due to a small effective reflection point. Consequently, the decrease of the stationary action evolves more quickly, similar to the case with true poles. We should note that $\tilde{\gamma} \gg \tilde{\gamma}^{\mathrm{crit}}$ is actually the regime where the instanton can be seen as reflected at the effective reflectors, see e.g. figures 8.11 and 8.12. A nonzero difference as in (8.108) turns out to be the characteristic attribute of poleless weak fields.

8.6 Assisted dynamical mechanism

As brought up in the beginning of this chapter, we now discuss the assisted dynamical mechanism again utilizing the reflection approach.

8.6.1 Impact on critical threshold

First, we want to find out the effect of the strong field on the critical combined Keldysh parameter. From equation (8.16), we can directly read off the critical point

$$x_4^* = F^{-1}\left(\frac{\gamma}{\omega}\right) \tag{8.109}$$

corresponding to $\dot{x}_3 = 0$. Closing the instanton in x_4^* results in the standard Schwinger mechanism. For dynamical assistance we need to satisfy (8.17). From the equality

$$x_4^* = x_4^{\mathrm{p}}, \tag{8.110}$$

we immediately obtain a critical frequency

$$\tilde{\omega}^{\mathrm{crit}} = \frac{eE}{m}\tilde{\gamma}^{\mathrm{crit}}. \tag{8.111}$$

Below this, there will be no assistance. In case a weak Sauter field is superimposed with a strong static field, the critical value is known from (8.35). For the case of a weak Lorentzian field see equation (8.41).

Note that the condition (8.110) clearly indicates that the critical combined Keldysh parameter basically depends on the strong field, which determines the left-hand

side of the equation (8.110), and on the weak field itself, which is responsible for the right-hand side of the equation. This is expected, since with increasing γ the closing point x_4^c drifts towards the origin along the complex time axis as sketched in the left panel of figure 8.18. Accordingly, the pole x_4^p has to become smaller as well, see condition (8.17). This is why the threshold depends on γ as well as on the strong field profile. Such a dependence has analytically been obtained for the case of a strong spatial Sauter field combined with a temporal Sauter field, treating both fields nonperturbatively [152]. Following analogous geometric arguments as discussed here, the present approach has been extended to spatiotemporal electric backgrounds with temporal sinusoidal or Gaussian dependence [2] resulting in highly accurate predictions for the critical Keldysh parameter. This extension to multidimensional backgrounds is discussed in chapter 10.

Coming back to the present example, for too large γ the strong field drives the enhancement in the VPP process alone, since the critical combined Keldysh parameter becomes too large. As noted Such a singlemode dynamical background gives rise to the usual antiadiabatic perturbative multiphoton process. For not too large γ, the assistance is expected to set in even for moderate $\tilde{\gamma}$. However, as soon as γ becomes much smaller than unity, the (locally) static strong field will again be a good approximation. An explicit example for which the strong field is assumed to be nonstatic is studied in the following section 8.6.2. Before we proceed with an explicit example, the question is whether the reflection approach is valid or not if one allows for γ values of order unity or larger. We should note that this situation may be not appropriate for current or planned experimental designs.

In order to resolve the latter question, let us bear in mind that the basic starting point for the reflection picture was based on the negligibility of the weak field contribution away from the reflection point in the original instanton equations (8.7). Therefore, even if we allow γ to be large, there will be always a reflector from the much more rapid weak field that will dominate above the critical threshold. Also for very weak fields, $\epsilon \ll 1$, such poles will be much closer to the origin than, if present, the strong field poles, simply because of $\tilde{\omega} \gg \omega$. In order to study the strong field profile dependence of the critical threshold, we use the relation in (8.109) which leads to the following criticality condition

$$\gamma = \omega F\left(x_4^p\right). \tag{8.112}$$

Figure 8.18: Left panel: condition for the assisted mechanism. In case of reflection both critical points, i.e. closing point of the instanton (red dots) and the weak field pole (yellow dot), have to coincide, see conditional equation in (8.110). For increasing γ the closing points drift towards the origin (red dots) and the instanton (solid lines) curves much stronger around its closing point. Right panel: critical combined Keldysh parameter $\tilde{\gamma}^{\text{crit}}$ for the case of a weak Lorentzian field superimposed with a strong field of different profiles. The profiles are listed in the legend. The relevant regime for the assisted mechanism, $\tilde{\gamma} > \tilde{\gamma}^{\text{crit}}$, is depicted by the colored region. The adiabatic nonperturbative regime, $\gamma \ll 1$, lies to the left of the vertical dashed red line where $\tilde{\gamma}^{\text{crit}} \approx 1$.

For illustrative reasons, let us assume the weak field of Lorentzian type described as in (8.37) with the corresponding pole given in equation (8.39). Using this setup, we can easily compute the critical combined Keldysh parameter for several strong field profiles starting from equation (8.112) and using the relation $\omega = \frac{m\gamma E}{E_{\text{S}}}$:

$$\textbf{Strong static field} \quad f(t) = 1, \quad F(x_4) = x_4,$$
$$\tilde{\omega}^{\text{crit}} = m\frac{E}{E_{\text{S}}}, \quad \tilde{\gamma}^{\text{crit}} = 1, \quad (8.113)$$

$$\textbf{Strong Lorentzian} \quad f(t) = \frac{1}{(1 + (\omega t)^2)^{3/2}}, \quad F(x_4) = \frac{x_4}{\sqrt{1 - (\omega x_4)^2}},$$
$$\tilde{\omega}^{\text{crit}} = m\frac{E}{E_{\text{S}}}\sqrt{1 + \gamma^2}, \quad \tilde{\gamma}^{\text{crit}} = \sqrt{1 + \gamma^2}, \quad (8.114)$$

$$\textbf{Strong sinusoid} \quad f(t) = \cos(\omega t), \quad F(x_4) = \frac{\sinh(\omega x_4)}{\omega},$$
$$\tilde{\omega}^{\text{crit}} = m\frac{E}{E_{\text{S}}}\frac{\gamma}{\text{arcsinh}(\gamma)}, \quad \tilde{\gamma}^{\text{crit}} = \frac{\gamma}{\text{arcsinh}(\gamma)}, \quad (8.115)$$

Strong Sauter $\qquad f(t) = \text{sech}^2(\omega t), \qquad F(x_4) = \dfrac{\tan(\omega x_4)}{\omega},$

$$\tilde{\omega}^{\text{crit}} = m \frac{E}{E_{\text{S}}} \frac{\gamma}{\arctan(\gamma)}, \qquad \tilde{\gamma}^{\text{crit}} = \frac{\gamma}{\arctan(\gamma)}. \qquad (8.116)$$

In the limit $\gamma \to 0$, we approach for all cases the static strong field, i.e. (8.113), corresponding to the adiabatic nonperturbative tunneling regime. However, for larger γ the critical value $\tilde{\gamma}^{\text{crit}}$ increases first parabolic then linear with γ, see right panel in figure 8.18. The relevant regime for the assisted mechanism, i.e. $\tilde{\gamma} > \tilde{\gamma}^{\text{crit}}$, is indicated by the colored patterns. For values $\gamma > 0.1$ which lie to the right of the vertical dashed red line, we leave the region with almost constant dependence on γ where $\tilde{\gamma}^{\text{crit}} \approx 1$. The latter is the nonperturbative regime for the strong field. The slope of the plotted curves turns out to be much stronger for fields that gives rise to small reflection points. This explains why for these the weak field inhomogeneity has to be much larger. Such studies exhibit the two types of mechanisms which basically lead to a substantial enhancement of the VPP rate in time dependent electric backgrounds:

1. The enhancement is driven by a singlemode field, i.e. antiadiabatic perturbative multiphoton regime. This is also known as the dynamical Schwinger mechanism. The role of a second weak field becomes negligible with increasing γ. A characteristic threshold in this case does not exist.

2. The electric background is composed of a strong static field in the adiabatic nonperturbative tunneling regime, superimposed with a weak, but rapid field. This situation corresponds to the assisted Schwinger mechanism. The contribution of the weak field is essential for the enhancement. It sets in for $\tilde{\gamma}$ above the characteristic threshold, the critical combined Keldysh parameter. Here, we have distinguished between the standard assisted mechanism and the assisted dynamical mechanism. The latter is characterized by an inhomogeneous strong field in addition to the weak rapid field.
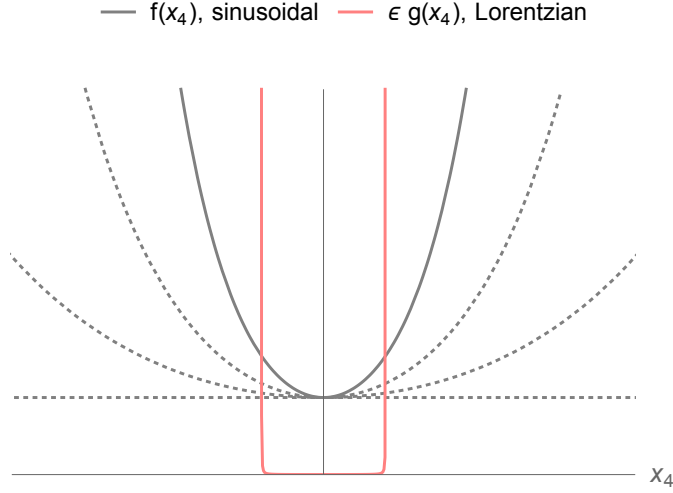
Figure 8.19: Combined electric background after rotation in the complex plane: the strong inhomogeneous field (without poles, grey solid curve) and weak inhomogeneous field (with poles, pink curve) for $\gamma/\tilde{\gamma} < 1$ are plotted separately. Dotted gray curves indicate the increase of γ starting at $\gamma = 0$ (horizontal dotted line).

8.6.2   Strong sinusoid and weak Lorentzian

To study the effects described in section 8.6.1, we consider the example with a strong sinusoidal field and a weak Lorentzian pulse,

$$f(t) = \cos(\omega t), \qquad F(x_4) = \frac{\sinh(\omega x_4)}{\omega},$$
$$g(t) = \frac{1}{(1 + (\omega t)^2)^{3/2}}, \qquad G(x_4) = \frac{x_4}{\sqrt{1 - (\omega x_4)^2}}. \tag{8.117}$$

The corresponding modification compared to a static strong field is shown schematically in figure 8.19. For increasing γ we leave the static limit by bending up the initial horizontal line, shown as dotted gray curves that represent the function $f(x_4)$. For $\gamma \neq 0$, there will be a substantial structure (solid gray curve) between the poles of the Lorentzian field (pink curve). The interplay between this parabolic strong field curve and the reflecting weak field poles has to be computed. The pole for the weak Lorentzian is $x_4^{\mathrm{p}} = \frac{1}{\tilde{\omega}}$. Using the expression in (8.21), we get

$$a = -i\frac{4}{\omega}\mathbf{F}\left(i\frac{\gamma}{\tilde{\gamma}}\,\middle|\,\frac{-1}{\gamma^2}\right), \tag{8.118}$$

where $\mathbf{F}(\cdot|\cdot)$ is the incomplete elliptic integral of the first kind. From the latter invariant (8.118), we can read off the critical combined Keldysh parameter $\tilde{\gamma}^{\mathrm{crit}}$ depending on γ which equals to the one given in (8.115). Using the modified
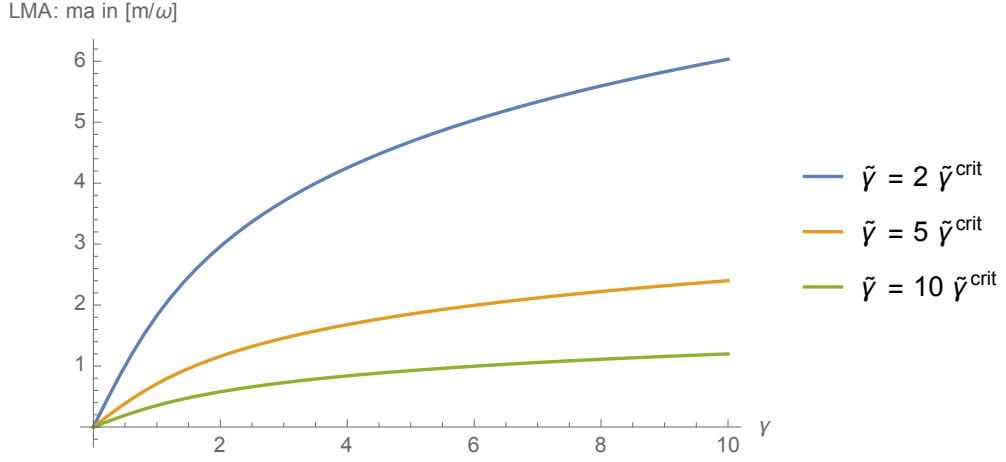
Figure 8.20: Relevant quantity ma expressed in units of $\frac{m}{\omega}$. The large mass approximation requires $ma \gg 1$. Curves are plotted for different $\tilde{\gamma}$. The values are depicted in the plot legend. The critical combined Keldysh parameter is given in (8.115).

invariant in (8.118), the large mass approximation condition in (5.10) reads

$$\frac{m}{\omega}\left(-i4\mathbf{F}\left(i\frac{\gamma}{\tilde{\gamma}}\bigg|\frac{-1}{\gamma^2}\right)\right) \gg 1 \qquad (8.119)$$

which is plotted in figure 8.20 versus γ and different Keldysh parameters $\tilde{\gamma}$. Very large $\tilde{\gamma}$ are excluded because of the latter condition. Using the equation (8.22), we obtain the stationary worldline action

$$\mathcal{W}_0 \approx \frac{m^2}{eE}\frac{4}{\gamma}\left(-i\mathbf{E}\left(i\frac{\gamma}{\tilde{\gamma}}\bigg|\frac{-1}{\gamma^2}\right)\right). \qquad (8.120)$$

The function $\mathbf{E}(\cdot|\cdot)$ denotes the incomplete elliptic integral of the second kind. The instanton solutions for the sinusoidal field are known [146]. Based on these, we can write the present modified solution in the right half plane, i.e. $u \in \left[-\frac{1}{4}, \frac{1}{4}\right]$, as

$$x_4 = \frac{m}{eE}\frac{1}{\gamma}\text{arcsinh}\left(\frac{\gamma}{\sqrt{1+\gamma^2}}\mathbf{sd}\left(-i\mathbf{F}\left(i\frac{\gamma}{\tilde{\gamma}}\bigg|\frac{-1}{\gamma^2}\right)\frac{\sqrt{1+\gamma^2}}{\gamma}u\bigg|\frac{\gamma^2}{1+\gamma^2}\right)\right), \qquad (8.121)$$

$$x_3 = \frac{m}{eE}\frac{1}{\gamma}\text{arcsin}\left(\frac{\gamma}{\sqrt{1+\gamma^2}}\mathbf{cd}\left(-i\mathbf{F}\left(i\frac{\gamma}{\tilde{\gamma}}\bigg|\frac{-1}{\gamma^2}\right)\frac{\sqrt{1+\gamma^2}}{\gamma}u\bigg|\frac{\gamma^2}{1+\gamma^2}\right)\right) - \mathcal{C}. \qquad (8.122)$$

The functions $\mathbf{sd}(\cdot|\cdot)$ and $\mathbf{cd}(\cdot|\cdot)$ denote Jacobi elliptic functions. The shifting constant along the x_3 axis is again determined by

$$\mathcal{C} = x_3\left(u = \pm\frac{1}{4}\right). \qquad (8.123)$$

The action above applies only for $\tilde{\gamma} \geq \tilde{\gamma}^{\text{crit}}$. Taking into account the case when the contribution of the weak field is absent, we can write the complete stationary

worldline action as

$$
\mathcal{W}_0 = \begin{cases} \frac{m^2}{eE} \frac{4}{\gamma} \left(-i\mathbf{E}\left(i\frac{\gamma}{\tilde{\gamma}} \,\middle|\, \frac{-1}{\gamma^2} \right) \right) & \tilde{\gamma} \geq \tilde{\gamma}^{\text{crit}} \\ 4\frac{m^2}{eE} \frac{\sqrt{\gamma^2+1}}{\gamma^2} \left(\mathbf{K}\left(\frac{\gamma^2}{\gamma^2+1} \right) - \mathbf{E}\left(\frac{\gamma^2}{\gamma^2+1} \right) \right) & \tilde{\gamma} < \tilde{\gamma}^{\text{crit}} \end{cases} . \tag{8.124}
$$

Here, $\mathbf{K}(\cdot)$ and $\mathbf{E}(\cdot)$ denote the complete elliptic integrals of the first and second kind, respectively.
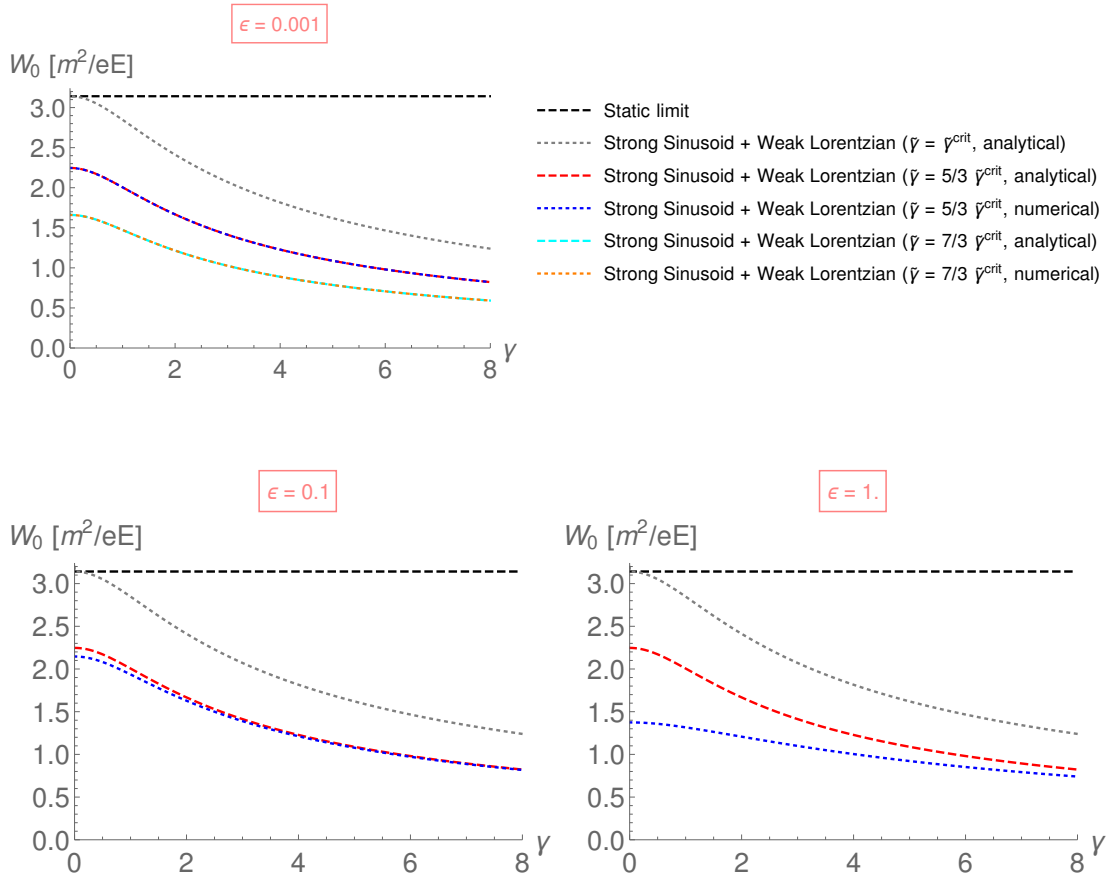
Figure 8.21: Stationary worldline action from (8.124) for a strong sinusoidal field superimposed with the weak Lorentzian field from (8.49) is plotted versus γ. The analytical prediction is compared with exact numerical computations. The ratio between the strong and weak field strengths is set to $\epsilon = \{10^{-3}, 10^{-1}, 10^0\}$ (top, bottom-left, bottom-right). The values for the combined Keldysh parameter are given in the plot legend with $\tilde{\gamma}^{\text{crit}}$ being computed according to the found relation in (8.115).

The stationary worldline action in (8.124) is plotted in figure 8.21. Setting $\tilde{\gamma} = \frac{5}{3}\tilde{\gamma}^{\text{crit}}$, we compare between the analytical prediction and the exact numerical computation. Both results do perfectly coincide as long as $\epsilon \ll 1$ which is the valid regime in the reflection picture. Only if relatively large values $\epsilon = \{0.1, 1.0\}$ are

applied, there appears a notable difference between both curves. The effect of the weak field is well indicated. A considerable decrease applies in contrast to the situation with $\tilde{\gamma} = \tilde{\gamma}^{\text{crit}}$, where the weak field contribution is absent. For $\gamma \to 0$, means $\tilde{\gamma} = \frac{5}{3}$, we again find the result previously depicted in figure 8.4.
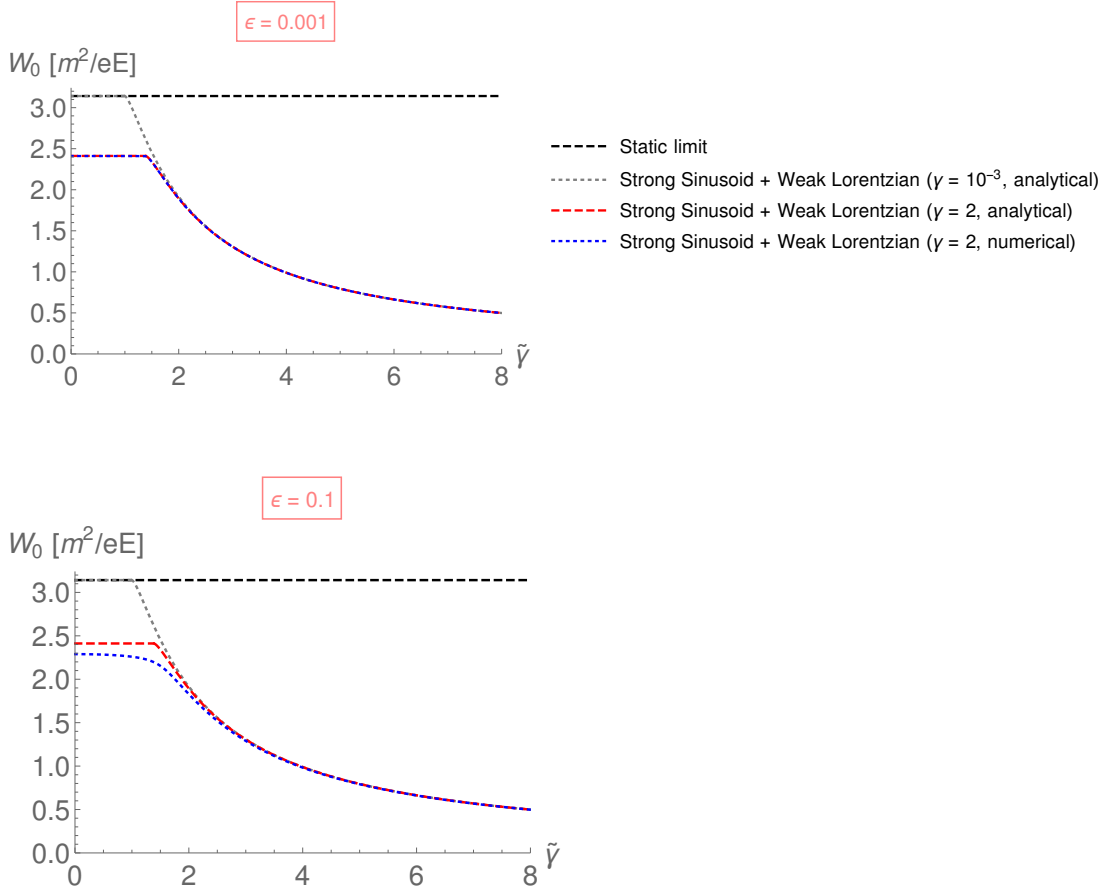
Figure 8.22: Same stationary worldline action as in figure 8.21, here, plotted versus the combined Keldysh parameter $\tilde{\gamma}$. The corresponding strong field inhomogeneities γ as well as the ratios ϵ between the field strengths are given in the plots. The gray dotted curve is the previous result in figure 8.4, i.e. green curve.

We have seen that the superposition of a strong field with $\gamma > 0$ and a weak faster field leads to a stronger enhancement compared to the case with a static strong dependence. However, this is only operative for $\tilde{\gamma}$ below the threshold $\tilde{\gamma}^{\text{crit}}$. For larger values, it is again the weak rapid field that mainly drives the enhancement, see figure 8.22.

In the latter case, we have set $\gamma = 2$ for the strong field. Technically, a very strong

pulsed field as at ELI together with a high frequency as, for instance, realizable with the European XFEL, are neither possible with current experimental facilities nor visioned for upcoming setups. One can alternatively think of the following more realistic situation. Assume we have a very strong field with strength E_1 and frequency $\omega_1 \to 0$. Superimposing this low frequent field with a second weak more rapid field, i.e. $\frac{E_2}{E_1} \ll 1$ and $\omega_2 \gg \omega_1$, resembles the strong field setup sketched in figure 8.19.

8.7   Summary

We have studied enhancement effects in VPP via two mechanisms; the assisted mechanism (sections 8.4 and 8.5) and the assisted dynamical mechanism (section 8.6). Based on the worldline instanton approach described in chapter 5, we have found two separate critical points. While one of them is responsible for the closing of the instanton path, the other serves as a reflecting mirror in the instanton plane. Developing an effective reflection approach, we have analyzed various characteristic features. Specifically, we have focused on the role of the assisting weak rapid field. Based on geometric considerations, we have explained the origin for substantial differences by distinguishing between two types of backgrounds.

The first type is characterized by weak fields which possess a distinct pole structure in Euclidean space. This is the case where geometrical arguments become very intuitive. Revisiting previous observations for the standard assisted mechanism, we have shown that the drastic enhancement is the direct consequence of instanton reflections at such poles (section 8.4). More precisely, this has been illustrated for weak fields of Sauter and Lorentzian type leading to similar behavior. We have shown that these findings are caused due to their similar pole structure. We have also discussed the impact of a possible subcycle structure. Performing explicit computations, we have seen that the assistance is primarily determined by the pole of the bell shaped envelope function. Only for sufficiently large ϵ, the encased subcycle structure of the considered oscillatory pulse leads to considerable deviations.

For the standard assisted mechanism, we then developed an extended reflection approach for backgrounds consisting of poleless weak fields (section 8.5). Based

on geometrical arguments, we have obtained specific conditions from combined analysis based on the instanton and the equivalent WKB approach described in chapter 6. By doing so, we have analytically computed corresponding effective reflection points.

In addition, we have predicted the critical point at which the weak field contribution starts to dominate so that dynamical assistance sets in. We have shown that the critical point deviates from the relatively large valued effective reflection point, even in the highly weak limit. This feature turns out to be the major difference between weak fields with and without poles. In the former case, reflection and critical point are equal to the pole itself. We have demonstrated that this discrepancy can be seen as the primary reason why poleless fields enhance less than fields with poles or pole-like behavior, respectively. We have also shown that an additional ϵ dependence occurs if the weak rapid field cannot be characterized by a distinct pole structure. However, for weak super Gaussian pulses such a dependence becomes increasingly suppressed.

In the second main part, we have studied the assisted dynamical mechanism where the strong field is assumed to be nonstatic in addition to the weak but more rapid variation (section 8.6). Again, applying the reflection approach, we have analytically computed the rate for an explicit example. The additional inhomogeneity has led to substantial enhancement effects compared to the standard assisted mechanism. Our analytical predictions in the relevant regime are in perfect agreement with numerical computations.

We conclude that the dynamical assistance is predominantly determined by instanton reflections, no matter whether poles are present or not. The location of critical points for the weak field determines the strength of the assistance. It is notable that reflection points close to the origin, that is along the imaginary time axis, basically lead to a stronger enhancement. Such insights may allow to pursue further optimization studies with respect to the weak field in order to maximize these effects.

The presented techniques can also be applied to the case of an additional spatially inhomogeneous field which allows an analytical treatment for electric backgrounds

with genuine spatiotemporal dependence. This can in particular facilitate the role of such backgrounds with regard to the nonlocal nature of nonperturbative VPP. Results in that direction have been presented in [2] which are discussed in chapter 10 of the present thesis.

Chapter 9

Nonperturbative and perturbative aspects

9.1 Outline

WE study the Schwinger mechanism in the presence of an additional uniformly oriented, weak super Gaussian of integer order $4N + 2$ (dynamical assisted mechanism) motivated by previous findings in section 8.5.5. Using the worldline instanton approach introduced in chapter 5, we determine the relevant critical points developed in section 8.5 in order to compute the leading order tunneling exponential analytically.

For $N = 2$, we already find a much stronger dynamical enhancement compared to a weak contribution of Sauter type. For higher orders, specifically for $N \to \infty$, we approach the same stationary worldline action as obtained for a weak Lorentzian. Even though such backgrounds significantly differ in Minkowski spacetime, we show that the found coincidence applies due to identical reflection points in the instanton plane.

In addition to this, we also treat the background in perturbation theory using the N photon master formula derived in section 4.4.3 within the framework of string-inspired WQFT, similar to the studies in [393]. We show that the parameter N and thus the background shape determines whether the weak contribution behaves perturbatively or nonperturbatively.

9.2   Nonperturbative approach

As before, we again consider spin zero particles and restrict ourselves to the adiabatic, nonperturbative regime where we neglect contributions from the dynamical gauge field, see discussion in section 5.1. As in section 5.3, the stationary worldline action in the tunneling exponential is obtained after evaluating the worldline action on the periodic instanton path, see equation (5.25). The stationary path is determined by the equations (5.23). Since the exponential factor is the dominant quantity for the present study, which generally strongly suppresses the VPP process, we set the quantum fluctuation prefactor again to unity and approximate the VPP rate according to (5.24).

As described above, we consider a purely electric background which is a uniformly oriented superposition described by

$$\boldsymbol{E}(t) = E\left(f + \epsilon g\right)\hat{x}_3 \tag{9.1}$$

where $\epsilon \ll 1$ and

$$f(t) = 1, \quad g(t) = e^{-(\omega t)^{4N+2}}, \quad N \in \mathbb{N}. \tag{9.2}$$

In figure 9.1 the function g is depicted for various N including the Sauter and Lorentzian cases considered in section 8.4.1. After the rotation in the complex plane we arrive at

$$\mathcal{A}_3(x_4) = -iE(F + \epsilon G), \tag{9.3}$$

where

$$\begin{aligned}
F(x_4) &= x_4, \\
G(x_4) &= -\frac{1}{\omega}\frac{(\omega x_4)\mathbf{E}_{\frac{4N+1}{4N+2}}(-(\omega x_4)^{4N+2})}{4N+2}.
\end{aligned} \tag{9.4}$$

Here, $\mathbf{E}_n$ denotes the exponential integral function. Inserting the vector potential in equation (9.3) into the instanton equations (5.23), we find the following coupled system of differential equations

$$\begin{aligned}
\ddot{x}_4 &= +\frac{aE}{m}\Big[F' + \epsilon G'\Big]\dot{x}_3, \\
\ddot{x}_3 &= -\frac{aE}{m}\Big[F' + \epsilon G'\Big]\dot{x}_4.
\end{aligned} \tag{9.5}$$
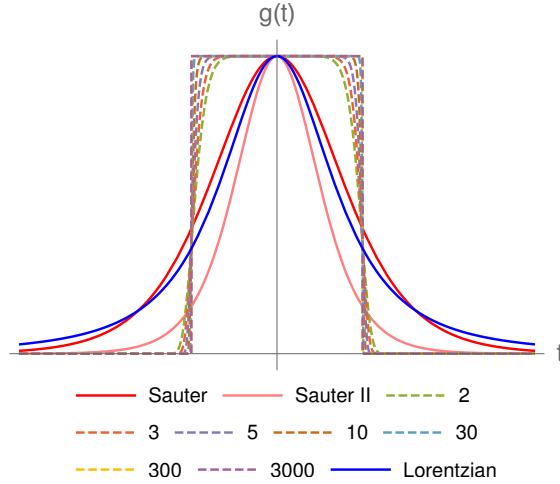
Figure 9.1: Comparison of function g plotted versus t. The numbers in the legend correspond to the integer N in (9.2). The pink curve corresponds to a modified Sauter pulse with frequency shift $\omega \to \omega\pi/2$ leading to the same $\mathcal{W}_0$ as the Lorentzian (blue). For $N \to \infty$ we approach the usual rectangular potential barrier.

The prime denotes the derivative with respect to x_4.

For conventional reasons, we again introduce the dimensionless combined Keldysh parameter [32]

$$\gamma = \frac{m\omega}{E}. \tag{9.6}$$

Moreover, due to simplifying reasons, we have absorbed the particle charge e into the field strength, $eE \to E$.

As presented in section 8.5 the idea again is to compute the points for which the strong contribution can be taken as negligible compared to the weak term, see in particular section 8.5.4. This can be done by using the additional condition that determines the complex turning points in the equivalent WKB approach; see chapter 6, more precisely section 6.3.

For one-dimensional temporal backgrounds these turning points lead to the correct tunneling exponent, see e.g. [37, 341, 394]. So starting on basis of the condition given in (6.33), the relevant equation we have to solve is of the form

$$\epsilon G(x_4^*) = \frac{\gamma}{\omega}. \tag{9.7}$$
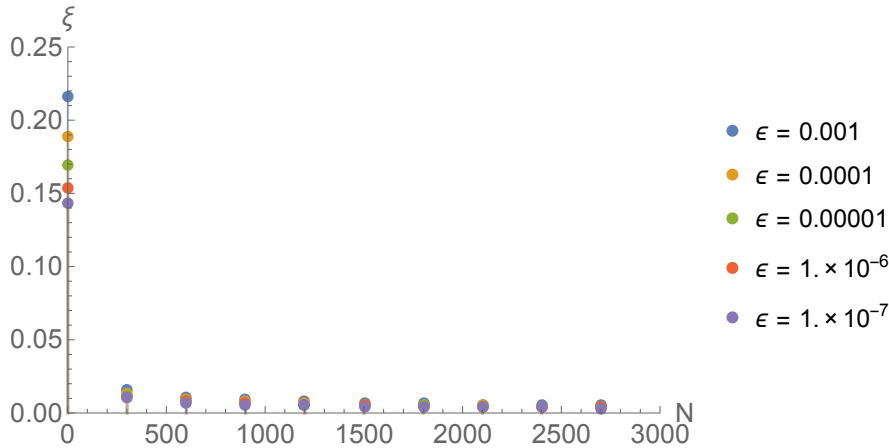
Figure 9.2: Comparison of $\xi = -\mathfrak{Z}/(\alpha\mathfrak{D})$ versus N (starting with $N = 1$) for various ϵ given in the plot legend. With increasing N the dependence on ϵ gets suppressed. For $N \to \infty$ we approach the Lorentzian case, i.e. $\delta = \xi\check{\gamma} \to 0$ (since $\xi \to 0$) and $\check{\gamma} \to 1$.

Once x_4^* has been computed, it can be applied as an effective reflection point in the instanton plane. This allows to find a sufficiently accurate analytical expression for the stationary worldline action. For more details, we refer to the previous chapter 8.

Interestingly, an appropriate modification of the background shape can lead to time scale reductions in driven quantum systems, see e.g. [395]. Therefore, one may think about analogies related to such reflection points placed on the Euclidean time axis.

Proceeding in the described way, we end up with the following stationary worldline action

$$\mathcal{W}_0 \simeq \frac{E_\mathrm{S}}{E} \begin{cases} \pi & \gamma < \check{\gamma} \\ 2\check{x}_4\sqrt{1 - \check{x}_4^2} + 2\arcsin(\check{x}_4) & \gamma \geq \check{\gamma} \end{cases}, \tag{9.8}$$

where

$$\check{x}_4 = \frac{\check{\gamma} + \delta}{\gamma + \delta}, \qquad \check{\gamma} = \left(\ln(1/\epsilon)\right)^{\frac{1}{4N+2}}, \qquad \delta = -\frac{\check{\gamma}}{\alpha}\frac{\mathfrak{Z}}{\mathfrak{D}}. \tag{9.9}$$

In order to compute the remaining quantities $\alpha, \mathfrak{Z}$ and $\mathfrak{D}$ appearing in the last expression of (9.9), we Taylor expand the associated function in $\xi < 1$, where $\delta \equiv \xi\check{\gamma}$, see section 8.5.4 for detailed discussion. The related steps have been established in [3].

By doing so, we then truncate the resulting series after the second order which leads to the following expressions

$$\mathfrak{D} := 2\epsilon(2N+1)(2\alpha\Omega_2 + 4\alpha N\Omega_2 + 4N\Omega_1 + 3\Omega_1),$$

$$\mathfrak{Z} := 2\alpha\Omega_1\epsilon + 4\alpha N\Omega_1\epsilon + 4N + \Omega\epsilon + 2 + \Big[(\epsilon(2\alpha\Omega_1 + \Omega) + 4N(\alpha\Omega_1\epsilon + 1) + 2)^2$$
$$- 4\alpha\epsilon(2N+1)(4N + \Omega\epsilon + 2)(2\alpha(2N+1)\Omega_2 + (4N+3)\Omega_1)\Big]^{1/2},$$

$$\Omega := \mathbf{E}_{\frac{4N+1}{4N+2}}(-\alpha), \quad \Omega_1 := \mathbf{E}_{\frac{4N+1}{4N+2}-1}(-\alpha), \quad \Omega_2 := \mathbf{E}_{\frac{4N+1}{4N+2}-2}(-\alpha), \quad \alpha := \check{\gamma}^{4N+2}.$$
$$(9.10)$$

We begin with the correction δ, which we expect to vanish for increasing N, here denoted as $N \uparrow$. The parameter ξ is plotted versus N in figure 9.2, where the field strength ratio ϵ varies between different values as given in the plot legend.

For $N = 1$ the points clearly differ. However, as soon as $N \uparrow$, they rapidly merge together and converge to zero. Thus, the ϵ dependence becomes strongly suppressed and we find $\xi \to 0$, see figure 9.2. Remarkably, such an ϵ independence applies usually for Sauter-like pulses which have a distinct pole structure in the instanton plane, see section 8.4.1 as well as [37]. Super Gaussians do not share such properties, even for very large N, which is therefore an interesting coincidence in itself. We will come back to this point later on.
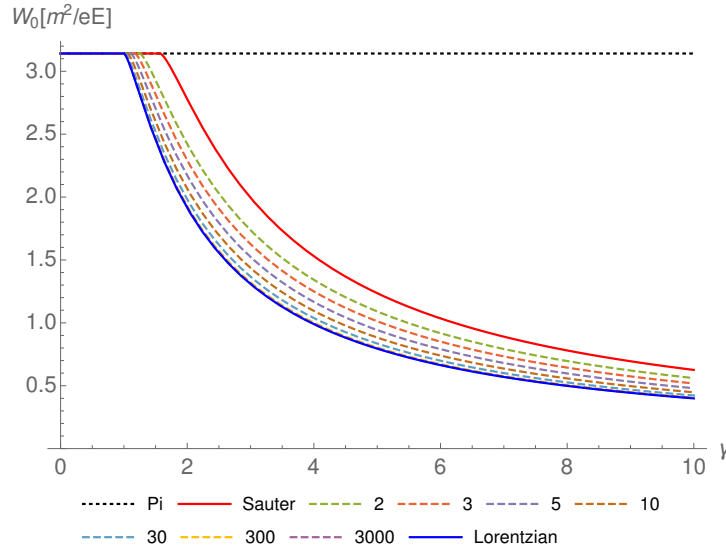
Figure 9.3: Stationary worldline action $\mathcal{W}_0$ in units of $[E_S/E]$. The integer values in the legend correspond to the parameter N in (9.2).

The nonperturbative prediction for the stationary worldline action in equation

([5.25](#)) is plotted in figure [9.3](#) versus the combined Keldysh parameter γ, again for different N as listed in the plot legend including the Sauter (red solid) and Lorentzian (blue solid) case. The dashed curves depict the predictions for the super Gaussian case. Starting with $N = 2$ (green), which already lies below the red solid curve, we find that as soon as $N \uparrow$, the curves converge to the blue solid one. For $N = 3000$ (magenta) both results are visually indistinguishable.

Moreover, the critical threshold[1], which can be approximated[2] by $\check{\gamma}$ for large N quite accurately, converges to $\gamma = 1$. Hence, for $N \to \infty$, corresponding to the usual rectangular potential barrier, we approach the blue solid curve as we have also seen in direct numerical computations.[3] The numerically found threshold matches with our prediction $\check{\gamma}$. We conclude that for parameters

$$N \in \mathbb{N}_{>1} \tag{9.11}$$

the corresponding curves for the stationary worldline action $\mathcal{W}_0$ lie within the throat-like region bounded by the red (Sauter) and blue (Lorentzian) one, see figure [9.3](#).

9.3 Perturbative expansion

For weak Sauter-like pulses the first order contribution in perturbation theory respective ϵ turns out to be sufficient to reproduce the leading order exponential factor in the VPP probability, $\mathcal{P}$. If their Fourier transform (FT) in the large frequency limit falls faster than exponentially, higher order contributions become relevant [393].

However, to find out whether two different weak fields lead to the same tunneling exponent are not directly visible via their FTs, even in the large frequency limit. Let us make this more concrete: for instance, both a Lorentzian and a Sauter pulse have FTs in the mentioned limit which decay exponentially, see expressions

---

[1] The critical point is defined as the point where both the strong and the weak contributions are equal, see [3].

[2] For this particular type of fields the Δ correction introduced in [3], see section [8.5.7](#), is negligible small, in particular for $N \gg 1$.

[3] The accuracy of the analytical prediction in ([9.8](#)) increases as soon as $N \uparrow$. A similar behavior applies for $\epsilon \downarrow$ with moderate N as discussed in [3] for $N = \{0, 1\}$.

(9.20) and (9.28) below. These functions are clearly distinguishable in form of a frequency shift by a factor $\frac{\pi}{2}$ and thus do not coincide.

So although for both the first order in the small parameter ϵ is sufficient to approach the nonperturbative result, the corresponding stationary worldline action $\mathcal{W}_0$ is distinct. According to previous findings [393], one may explain the mentioned frequency shift and hence the impact on $\mathcal{W}_0$ via the approximate FTs in the large frequency limit just by rescaling the large frequency estimate in (9.20), means $\omega \to \frac{2\omega}{\pi}$, or vice versa.

However, note that this case is very special. Namely, in section 9.2 we have shown hat the weak super Gaussian with $N \to \infty$ leads to the same stationary worldline action as one obtains for the Lorentzian, see figure 9.3. So it is reasonable to expect that for such a rectangular pulse the first order in ϵ will be sufficient.

Referring to the findings in [393], such a behavior can be anticipated, since the FT does not decay faster than an exponential. However, the obtained coincidence for the stationary worldline action cannot be unveiled just by working out the corresponding FTs which are indeed highly distinct, see equations (9.12) and (9.16) as well as figure 9.5. As shown in section 9.2, this result can be explained by means of the corresponding effective reflection points in the instanton plane. Nevertheless, not only in order to support our results, but also to demonstrate in particular the differences occurring for any finite parameter $N > 1$, which has not been analytically studied so far, we discuss in the following the super Gaussian from (9.2) in Fourier space.

9.3.1   Fourier space

Let $\widetilde{g}$ denote the FT of the weak pulse. As mentioned, the order by order contributions in ϵ can be written in terms of $\widetilde{g}$. For the Lorentzian we find

$$\widetilde{g}(\varpi) = \frac{1}{\omega}\sqrt{\frac{2}{\pi}}\frac{\varpi}{\omega}\mathbf{K}_1\left(\frac{\varpi}{\omega}\right) \tag{9.12}$$

with $\mathbf{K}_1$ being the first order modified Bessel function of the second kind. For super Gaussians as described in equation (9.2), the representation in Fourier space is much more difficult to obtain. Therefore, we need to introduce a slightly different strategy which may also be suitable for other backgrounds leading to similar

problems.

We construct the super Gaussian pulse (SG_{4N+2}), particularly in the (almost) rectangular potential barrier limit, i.e. $N \gg 1$, which is the interesting case here, via the convolution of an ordinary Gaussian,

$$G_{\sigma_g} \mathrel{\hat{=}} e^{-(t/\sigma_g)^2}, \tag{9.13}$$

with the standard rectangular function,

$$R_{\sigma_r} \mathrel{\hat{=}} \mathrm{rect}\left(\frac{t}{2\sigma_r}\right). \tag{9.14}$$

So in order to compute $\tilde{g}$, we proceed according to the following prescription

$$
\begin{array}{ccc}
SG_{4N+2} & \xdashrightarrow{\mathcal{FT}} & \widetilde{SG}_{4N+2} \\
\simeq \Big| & & \Big| \simeq \\
\frac{1}{C_{\sigma_g,\sigma_r}}\left(G_{\sigma_g} \otimes R_{\sigma_r}\right) & \xrightarrow{\mathcal{FT}} & \frac{1}{\widetilde{C}_{\sigma_g,\sigma_r}}\left(\widetilde{G}_{\sigma_g} \times \widetilde{R}_{\sigma_r}\right)
\end{array}
$$

where $\otimes$ denotes the convolution product and $C_{\sigma_g,\sigma_r}, \widetilde{C}_{\sigma_g,\sigma_r}$ are some normalization factors. Identifying

$$
\begin{aligned}
N &\leftrightarrow 1/\kappa, \\
\sigma_r &\leftrightarrow 1/\omega,
\end{aligned}
\tag{9.15}
$$

with $\kappa := \sigma_g/\sigma_r$, we can finally write (including the prefactor) the following FT

$$\tilde{g}(\varpi) = \frac{1}{\omega}\sqrt{\frac{2}{\pi}}\frac{\omega}{\varpi}\sin\left(\frac{\varpi}{\omega}\right)\exp\left(-\frac{\kappa^2\varpi^2}{4\omega^2}\right) \tag{9.16}$$

having assumed the condition $\kappa \ll 1$. It is important to keep the parameter κ for later purpose.

9.3.2 First order

The general expression after perturbing the interaction Hamiltonian in the (dressed) S-matrix approach gives [393]

$$\mathcal{P} = V_3 \int \frac{dp^3}{(2\pi)^3}\left|\ldots + \epsilon \int \frac{d\varpi}{2\pi}\,\tilde{g}\,\Pi_{\boldsymbol{p}} + \ldots\right|^2. \tag{9.17}$$

For simplifications we assume $\boldsymbol{p} = 0$ which is reasonable, since the spectrum for backgrounds considered here is symmetrically peaked around the origin. Then the matrix element at $\mathcal{O}(\epsilon)$ takes the form

$$\Pi_0(\varpi) = e^{\frac{E_{\mathrm{S}}}{E}\left(\left[\frac{\varpi}{2m}\sqrt{1-\left(\frac{\varpi}{2m}\right)^2}+\arcsin\left(\frac{\varpi}{2m}\right)\right]-\frac{\pi}{2}\right)} \tag{9.18}$$

which, not surprisingly, becomes unsuppressed for $\varpi = 2m$. We begin with the Lorentzian pulse,

$$g(t) = \left[1 + (\omega t)^2\right]^{-3/2}. \tag{9.19}$$

In order to perform a saddle point approximation to the ϖ integral in (9.17), we first assume $\varpi \gg \omega$ to estimate

$$\widetilde{g} \simeq \exp\left(-\frac{\varpi}{\omega}\right). \tag{9.20}$$

We insert the approximate expression (9.20) into equation (9.17) and find the corresponding saddle point [393]

$$\varpi_{\mathrm{sp}} = 2m\sqrt{1 - \frac{1}{\gamma^2}}. \tag{9.21}$$

The latter leads to the previously introduced threshold $\gamma \geq 1$ after plugging into the exponent in equation (9.18). For $\gamma = 1$ the contribution $\widetilde{g}(\varpi_{\mathrm{sp}})$ is maximal where the exponential $\Pi_0(\varpi_{\mathrm{sp}})$ approaches its minimum. Defining a variable

$$x := \frac{\varpi}{\omega}, \tag{9.22}$$

we find the following integral solution for the FT in (9.12)

$$\int d\varpi\ \widetilde{g} = \sqrt{\frac{2}{\pi}}\int_0^\infty dx\ x\mathbf{K}_1(x) = \sqrt{\frac{\pi}{2}}. \tag{9.23}$$

In case of the super Gaussian, we are particularly interested in the limit $\kappa \to 0$. For this, we cannot write an exponential expression for $\widetilde{g}$ just by assuming $x \gg 1$. However, according to the findings in section 9.2 we check whether $\varpi = \varpi_{\mathrm{sp}}$, see equation (9.21), solves the saddle point condition

$$\partial(\widetilde{g}\ \Pi_0)\Big|_{\kappa\to 0} = 0 \tag{9.24}$$
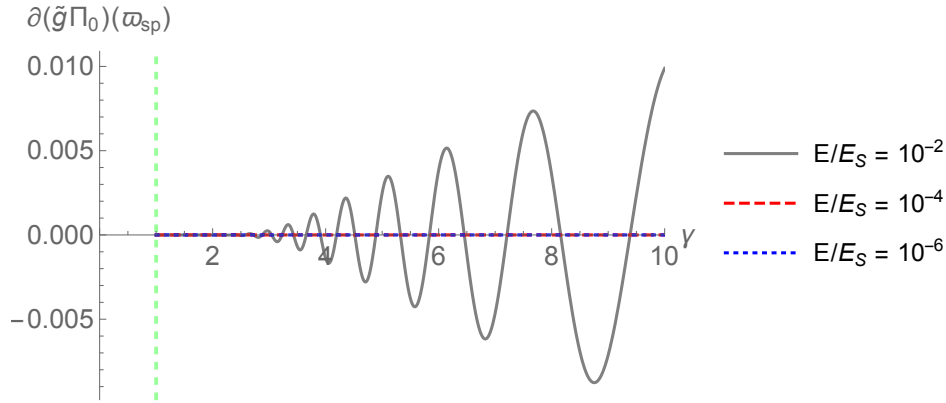
Figure 9.4: Saddle point condition (9.24) evaluated in ϖ_{sp} for different ratios E/E_{S} plotted versus γ. The vertical dashed line is placed at the critical threshold $\gamma = 1$.

where $\partial \equiv \frac{\partial}{\partial \varpi}$. It turns out that for the nonperturbative weak field regime, i.e. $\frac{E}{E_{\mathrm{S}}} \ll 1$ and $\omega \ll m$, the condition (9.24) is fulfilled, see figure 9.4. For $\frac{E}{E_{\mathrm{S}}} = 10^{-2}$ and $\gamma \gtrsim 2$ the curve becomes increasingly oscillating until it settles down at $\simeq 0.15$. Such a breakdown is reasonable, since according to $2\frac{E}{E_{\mathrm{S}}} = \frac{\omega}{m}$ the gray solid curve with $\frac{\omega}{m} > 2 \times 10^{-2}$ almost approaches the Compton scale. An approximate validity condition for ϖ_{sp} can therefore be given as

$$\gamma \frac{E}{E_{\mathrm{S}}} \lesssim 10^{-2} \tag{9.25}$$

which is obviously satisfied for $\frac{E}{E_{\mathrm{S}}} = 10^{-4}$, red dashed curve, and $\frac{E}{E_{\mathrm{S}}} = 10^{-6}$, blue dotted curve, as depicted in figure 9.4.

Now, applying again the previous variable substitution to the FT in equation (9.16), we obtain the same integral solution as in the Lorentzian case, see equation (9.23),

$$\int d\varpi\, \tilde{g} = \sqrt{\frac{2}{\pi}} \int_0^\infty dx\, \frac{\sin(x)}{x} e^{-\kappa^2 x^2/4} \overset{\kappa \to 0}{=} \sqrt{\frac{\pi}{2}}. \tag{9.26}$$

For large x the integrand oscillates around the function in equation (9.12), but asymptotically converges to zero. Therefore, since ϖ_{sp} works for any ω, at least for $\omega \ll m$, we may conclude that the threshold at $\gamma = 1$ applies for the super Gaussian in the limit $N \to \infty$ as well. This is exactly what we have found within the previous nonperturbative reflection approach, see section 9.2, which has also been confirmed in direct numerical computations. Note that, as soon as κ is taken to be sufficiently large, which basically corresponds to super Gaussians with finite

order N, the latter coincidence will not apply anymore.

For completeness, let us discuss the Sauter pulse, $g(t) = \text{sech}^2(\omega t)$, which has the following FT

$$\widetilde{g}(\varpi) = \frac{1}{\omega}\sqrt{\frac{\pi}{2}\frac{\varpi}{\omega}}\text{csch}\left(\frac{\pi}{2}\frac{\varpi}{\omega}\right). \tag{9.27}$$

Again, we can write an approximate expression assuming $x \gg 1$,

$$\widetilde{g} \simeq \exp\left(-\frac{\pi}{2}\frac{\varpi}{\omega}\right). \tag{9.28}$$

Inserting the expressions (9.28), (9.18) and the saddle point (9.21) into equation (9.17), results in the known critical threshold $\gamma \geq \pi/2$. Integrating the FT in (9.27) as before, we find

$$\int d\varpi\ \widetilde{g} = \sqrt{\frac{\pi}{2}}\int_0^\infty dx\ x\,\text{csch}\left(\frac{\pi}{2}x\right) = \sqrt{\frac{\pi}{2}}. \tag{9.29}$$

So the solution is identical to the previous one obtained for the Lorentzian and rectangular pulse in equations (9.23) and (9.26), respectively.

9.3.3   Integral coincidence
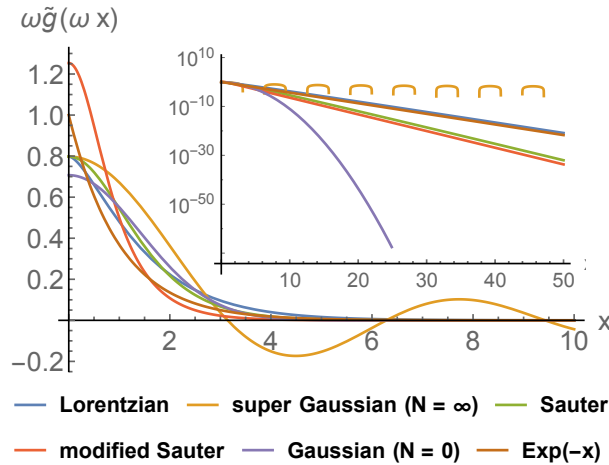
Figure 9.5: FTs, $\omega\widetilde{g}(\omega x)$, where $x := \varpi/\omega$ are plotted for the cases indicated in the plot legend. For the ordinary Gaussian ($N = 0$) we have $\sqrt{2}\omega\widetilde{g}(\omega x) = e^{-x^2/4}$. In the inset the same curves are shown with logarithmic scaling.

Evaluating first the exponential via a saddle point approximation using a large frequency estimation for $\widetilde{g}$, we consider the integral $\int d\varpi\ \widetilde{g}$ as a prefactor in front of the leading order exponential (9.18) in the perturbative expansion (9.17). Our

findings above suggest that this integral seems to incorporate useful information about the impact of the additional weak dependence.

Namely, we have seen that

$$\int_0^\infty dx\ \omega \widetilde{g}(\omega x) = \sqrt{\frac{\pi}{2}} \tag{9.30}$$

applies for all weak pulses, i.e. Lorentzian, super Gaussian with $N \to \infty$ and Sauter, which approach the nonperturbative result already at lowest order $\mathcal{O}(\epsilon)$. Notably, a Sauter pulse with frequency shift $\omega \to \omega \frac{\pi}{2}$ behaves similarly. We should note that the FTs as well as the condition in (9.30) do not carry sufficient information for unveiling whether the stationary worldline action from equation (5.25) matches for two different backgrounds.

On the other hand, we have seen in section 9.2 that even when two backgrounds crucially differ in Minkowski spacetime, see figure 9.1, they can result in the same tunneling exponential. These insights can be taken as a strong evidence that the mechanism of dynamical assistance is mainly triggered by the nonperturbative (effective) reflection points in the instanton plane, which, in contrast to $\widetilde{g}(\varpi)$ depicted in figure 9.5, do perfectly agree.

Coming back to the integral condition in (9.30), let us adduce an additional example. We consider a weak pulse of modified Sauter type described by

$$g(t) = \mathrm{sech}(\omega t), \qquad \widetilde{g}(\varpi) = \frac{1}{\omega}\sqrt{\frac{\pi}{2}}\mathrm{sech}\left(\frac{\pi}{2}\frac{\varpi}{\omega}\right). \tag{9.31}$$

In this case, we will find the same stationary worldline action for sufficiently small field strengths, usually $\epsilon < 10^{-2}$, as for the ordinary Sauter pulse (9.27). This coincidence is rooted in the same reflection point, cf. [3]. Therefore, we expect the same behavior with respect to ϵ. Indeed, as in the previous cases, computing the corresponding integral, the result obeys again the condition in (9.30),

$$\int d\varpi\ \widetilde{g} = \sqrt{\frac{\pi}{2}}\int_0^\infty dx\ \mathrm{sech}\left(\frac{\pi}{2}x\right) = \sqrt{\frac{\pi}{2}}. \tag{9.32}$$

We close this part by noting that for the super Gaussian with any finite order N we have

$$\int_0^\infty dx\ \omega \widetilde{g}(\omega x) < \sqrt{\frac{\pi}{2}}, \tag{9.33}$$

since $\kappa > 0$, see (9.16). For such pulses, as will be shown in the following, higher orders in ϵ generally become relevant. It is an interesting coincidence that in such a situation the condition (9.30) is not fulfilled anymore.

9.3.4   Higher orders

To compute higher order contributions we rely on the general expansion

$$\mathcal{P} \simeq \mathcal{P}_0 + \epsilon \mathcal{P}_1 + \epsilon^2 \mathcal{P}_2 + \mathcal{O}(\epsilon^3). \tag{9.34}$$

According to Furry's theorem, all odd orders in ϵ should vanish, see section 3.4.1.3. Here, in the presence of a static background such contributions are included as well [329, 396–398]. The zeroth order term stems again only from the strong background dependence. At a given order $\mathfrak{N}$, the perturbative probabilities $\mathcal{P}_{\mathfrak{N}}$ in the expansion (9.34) can be written as

$$\mathcal{P}_{\mathfrak{N}} \simeq \int d\varpi_1 \; \widetilde{g}(\varpi_1) \dots \int d\varpi_{\mathfrak{N}} \; \widetilde{g}(\varpi_{\mathfrak{N}}) \; \mathcal{F}_{\mathfrak{N}} \tag{9.35}$$

where $\widetilde{g}$ again denotes the FT of the weak pulse.

The functions $\mathcal{F}_{\mathfrak{N}}$ can be computed by using the $\mathfrak{N}$ photon master formula from section 4.4.3. Let us remind that the latter exactly describes the situation where a single particle loop in a static background is perturbatively coupled to $\mathfrak{N}$ photons. Therefore, we can use it for the present purpose.

The starting point is equation (4.4.3) where the initial polarization vectors ϵ_j^{μ} are replaced by $\widetilde{g}(\varpi)$ and the background is assumed to be a static electric one, cf. [393]. This exactly results in the introduced perturbative expansion as in (9.34) given above. Setting $k_j^{\mu} = (\omega_j, 0, 0, 0)$ for all $j = 1, \dots, \mathfrak{N}$, the functions $\mathcal{F}_{\mathfrak{N}}$, in particular the exponential dependence, reads

$$\mathcal{F}_{\mathfrak{N}} \simeq \delta \left(\sum_{j=1}^{\mathfrak{N}} \omega_j \right) \int_0^{\infty} ds \int_0^1 \prod_{j=1}^{\mathfrak{N}} d\tau_j \; (\dots)$$
$$\times \exp \left(-\frac{m^2}{E} \left[s + \frac{1}{2} \sum_{j,i=1}^{N} E\omega_j \mathcal{G}_{\mathrm{B}ji} \omega_i \right] \right) \tag{9.36}$$

where

$$\mathcal{G}_{\mathrm{B}ji} = \frac{\cos(s\dot{G}_{\mathrm{B}ji}) - \cos(s)}{2E \sin(s)},$$
$$\dot{G}_{\mathrm{B}ji} = \mathrm{sign}(\tau_j - \tau_i) - 2(\tau_j - \tau_i), \tag{9.37}$$

see [329]. The latter bosonic worldline correlator $G_{\mathrm{B}ji}$ has been introduced in section 4.2.4. The prefactors in (9.36) represented by $(\ldots)$ which depend on the integration variables have no influence on the exponential contribution. So as done before, we focus on the exponential in order to study the behavior with respect to higher orders in ϵ. The leading order contribution can be obtained by determining those integration variables for which the dominant exponential suppression is minimized.

Proceeding in this way, means performing a saddle point approximation with respect to the proper time, s, and worldline time, τ, see equation (5.5) in [393], the leading order approximation for $\mathcal{P}_{\mathfrak{N}}$ reads

$$\mathcal{P}_{\mathfrak{N}} \simeq \int d\varpi_1 \, \widetilde{g}(\varpi_1) \ldots \int d\varpi_{\mathfrak{N}} \, \widetilde{g}(\varpi_{\mathfrak{N}})$$
$$\times \exp\left(\frac{2m^2}{E} \left[\Sigma\sqrt{1 - \Sigma^2} + \arcsin(\Sigma) - \frac{\pi}{2} \right] \right) \tag{9.38}$$

where $0 < \Sigma < 1$ is defined as

$$\Sigma := \frac{1}{2m} \sum_{i=1}^{J} \varpi_i, \tag{9.39}$$

and

$$\sum_{l \in \{1,\ldots,J,\ldots,\mathfrak{N}\}} \varpi_l = 2m\Sigma + \sum_{j=J+1}^{\mathfrak{N}} \varpi_j = 0 \tag{9.40}$$

which applies due to energy conservation. Note that the exponential in (9.38) is of the same form as in (9.18).

Without loss of generality let us assume $2m\Sigma \gg \omega$. So for the Lorentzian we use again the approximate expression (9.20) and compute the ϖ_l integrals via (9.40). Carrying out a saddle point approximation with respect to Σ results in

$$\mathcal{P}_{\mathfrak{N}} \simeq \exp\left(-\frac{4m^2}{E} \frac{\Sigma_{\mathrm{sp}}}{\gamma} \right)$$
$$\times \exp\left(\frac{2m^2}{E} \left[\Sigma_{\mathrm{sp}}\sqrt{1 - \Sigma_{\mathrm{sp}}^2} + \arcsin(\Sigma_{\mathrm{sp}}) - \frac{\pi}{2} \right] \right) \tag{9.41}$$

where $\Sigma_{\mathrm{sp}} = \sqrt{1 - 1/\gamma^2}$. For the super Gaussian in the rectangular potential barrier limit, i.e. $\kappa \to 0$, the situation is not much different. First, we solve the ϖ_l integrals using condition (9.40).

The prefactor in front of the exponential in (9.38) takes the form

$$\prod_i \frac{\omega}{\varpi_i} \sin\left(\frac{\varpi_i}{\omega}\right) \prod_j \frac{\omega}{\varpi_j} \sin\left(\frac{\varpi_j}{\omega}\right) \tag{9.42}$$

with

$$
\begin{aligned}
\varpi_i &= \frac{2m\Sigma}{J-1}, \quad i \in \{2, \ldots, J\}, \\
\varpi_j &= \frac{-2m\Sigma}{\mathfrak{N}-J-1}, \quad j \in \{J+1, \ldots, \mathfrak{N}-1\}.
\end{aligned}
\tag{9.43}
$$

In case of $2m\Sigma \gg \omega$, we may use again the approximate form in equation (9.20), since in the relevant regime it leads to the correct leading order contribution as we have seen before, see figure 9.4.

So the prefactors (9.42) in equation (9.38) reduce then to an exponential that yields the following expression

$$
\begin{aligned}
\mathcal{P}_{\mathfrak{N}} &\simeq \exp\left(-\frac{4m\Sigma}{\omega}\right) \\
&\times \exp\left(\frac{2m^2}{E}\left[\Sigma\sqrt{1-\Sigma^2} + \arcsin(\Sigma) - \frac{\pi}{2}\right]\right).
\end{aligned}
\tag{9.44}
$$

Rescaling $2m\Sigma \to \Sigma$ subsequently, the saddle point is simply given by $\Sigma_{\mathrm{sp}} = \frac{\varpi_{\mathrm{sp}}}{2m}$. This gives the same exponential factor as in equation (9.41) which remains unchanged for any $\mathfrak{N} \geq 1$. We conclude that similar as in the Sauter-like cases, the first order contribution in ϵ will be sufficient to approach the nonperturbative result. Of course, this is quite different from the ordinary Gaussian, i.e. $N = 0$, which behaves nonperturbatively, since higher orders in ϵ turn out to be necessarily relevant [393].

9.4   Summary

In this chapter we have studied the Schwinger mechanism in the presence of an additional, uniformly oriented super Gaussian of integer order $4N+2$, the dynamical assisted mechanism. In the first part, section 9.2, we have treated the background nonperturbatively utilizing the reflection approach. We have shown that already for $N = 2$ a much stronger dynamical enhancement applies in comparison to a weak contribution of Sauter type.

Taking the limit $N \to \infty$, which corresponds to the usual rectangular potential barrier, results in the same leading order exponential factor as one finds for the bell shaped Lorentzian. Although both setups are highly distinct in Minkowski spacetime, the found coincidence applies due to identical effective reflection points in the instanton plane which turn out to be the main regulator in this dynamical mechanism.

In the second part, section 9.3, we have studied the impact of the weak super Gaussian in perturbation theory and found that in the rectangular potential barrier limit it shares the same higher order behavior as Sauter-like pulses. We have argued that the leading order contribution in ϵ already approaches the nonperturbative result, although a distinct pole structure, as one finds in the latter cases, is not present. In addition, we have seen that for any finite N a found integral condition is not fulfilled which indicates the relevance of higher order terms in the strength parameter ϵ.

The results clearly demonstrate that tunneling in such complex backgrounds can lead to nontrivial physics. The fact whether the weak pulse behaves perturbatively or nonperturbatively depends on its microscopic details determined by the parameter N.

Chapter 10

Instantons in multidimensions

10.1 Outline

WE study the VPP process in multidimensions. We focus on electric backgrounds as a linear combination of a spatial Sauter field and, interchangeably, certain weaker time dependent fields without poles in the complex plane such as the sinusoidal and Gaussian cases. Based on geometric considerations within the worldline formalism, as discussed in section 8.5, we employ the relevant critical points in order to analytically estimate a characteristic threshold for the temporal inhomogeneity.

We set appropriate initial conditions and apply additional symmetry constraints in order to determine the classical periodic paths in spacetime. Using these worldline instantons, we compute the corresponding leading order exponential factors showing large dynamical enhancement in general. We work out the main differences caused by the analytic structure of such composite backgrounds and also discuss the case with a strong temporal variation of Sauter type.

10.2 Tunneling instantons

10.2.1 Stationary points

We consider a purely electric background oriented in $\hat{x}_3$ direction where the spatial part is represented by the scalar potential $\mathcal{A}_4(x_3)$ and the temporal part by a vector potential $\mathcal{A}_3(t)$. Due to simplifying reasons, both parts shall be described by even

functions in t and x_3, respectively. After the rotation in the complex plane, we derive

$$\begin{aligned}
\mathcal{A}_3(x_4) &= -i\frac{E_\omega}{\omega}\mathcal{T}(\omega x_4), \\
\mathcal{A}_4(x_3) &= i\frac{E_k}{k}\mathcal{S}(kx_3),
\end{aligned} \tag{10.1}$$

where $\mathcal{T}$ and $\mathcal{S}$ are odd functions in the corresponding spacetime coordinates. Here, E_k and E_ω denote the field strengths and k and ω the wave number and frequency, respectively. Inserting the expressions from (10.1) into the instanton equations (5.23), we end up with the following system of differential equations

$$\begin{aligned}
\ddot{x}_4 &= +\frac{aE_k}{m}\left[\epsilon\frac{\partial_4\mathcal{T}(\omega x_4)}{\omega} + \frac{\partial_3\mathcal{S}(kx_3)}{k}\right]\dot{x}_3, \\
\ddot{x}_3 &= -\frac{aE_k}{m}\left[\epsilon\frac{\partial_4\mathcal{T}(\omega x_4)}{\omega} + \frac{\partial_3\mathcal{S}(kx_3)}{k}\right]\dot{x}_4,
\end{aligned} \tag{10.2}$$

where $\ddot{x}_1 = \ddot{x}_2 = 0$. As in the previous chapters, we define for the sake of convenience the dimensionless field strength ratio parameter $\epsilon := \frac{E_\omega}{E_k}$.

Next, we specify the spatial part as a Sauter pulse described by

$$\mathcal{S}_{\text{Sauter}}(kx_3) = \tanh(kx_3) \tag{10.3}$$

and introduce the following dimensionless quantities

$$\gamma_k = \frac{mk}{E_k}, \qquad \gamma_\omega = \frac{m\omega}{E_k}, \tag{10.4}$$

which in the present case are referred to as the spatial and temporal Keldysh parameter, respectively. Note that, as in chapter 9, the particle charge e is absorbed into the spatial field strength, $eE_k \to E_k$.

For the temporal dependence we choose between two different profiles that are described by

$$\begin{aligned}
\mathcal{T}_{\text{sinusoid}}(\omega x_4) &= \sinh(\omega x_4), \\
\mathcal{T}_{\text{Gaussian}}(\omega x_4) &= \frac{\sqrt{\pi}\,\text{erfi}(\omega x_4)}{2}.
\end{aligned} \tag{10.5}$$

A temporal Sauter field,

$$\mathcal{T}_{\text{Sauter}}(\omega x_4) = \tan(\omega x_4), \tag{10.6}$$

has been both analytically and numerically investigated in the weak limit $\epsilon \ll 1$, leading to an enormous enhancement due to instanton reflections at poles in the complex plane [152]. Of course, as we have seen in the previous chapters, such an enhancement is not restricted to this specific case and is expected to apply in general for any time dependent field with a distinct pole structure in the instanton plane [3].

We aim to extend such considerations for poleless fields as introduced in (10.5). Laser fields have an oscillatory structure leading to substantial interference effects in phase space [34, 341, 342]. Such setups motivate investigations for time dependent backgrounds entailing an oscillatory subcycle structure such as the sinusoidal field. For the field examples introduced above, a spatially inhomogeneous field is closely related to a temporal one by the analytic continuation

$$\gamma_\omega \to i\gamma_k. \tag{10.7}$$

This correspondence is automatically included in the worldline instanton approach [146, 159]. In the remaining part the dimensional quantities x_3, x_4 and a will be given in units of $\frac{m}{E_k}$.

10.2.2 Symmetries

For backgrounds composed of fields as introduced in equations (10.3) and (10.5), the closed instanton paths preserve (discrete) reflection symmetry,[1]

$$\begin{aligned}
x_3 &\to -x_3, \\
x_4 &\to -x_4,
\end{aligned} \tag{10.8}$$

i.e. isomorphic with C_2. In this case, one can set the starting point on the solution path satisfying, for instance,

$$\begin{aligned}
x_3(0) &\neq 0, \\
x_4(0) &= 0.
\end{aligned} \tag{10.9}$$

Afterwards, from the symmetry properties (10.8) we get $\dot{x}_3(0) = 0$ and therefore $\dot{x}_4(0) = a$, which is a direct consequence of the instanton periodicity. We may

---

[1] Let us remind that the static field instanton in the two-dimensional plane is maximally symmetric with C_∞, see section 5.7.

therefore conclude

$$
\begin{aligned}
x_3(0) = x_3(1) = -x_3(1/2) \neq 0, \\
x_3(1/4) = x_3(3/4) = 0, \\
x_4(0) = x_4(1/2) = x_4(1) = 0, \\
x_4(1/4) = -x_4(1/4) \neq 0.
\end{aligned}
\tag{10.10}
$$

As we will see, such relations lead to very powerful constraints improving numerical methods in order to find the correct instanton solutions, see section 10.3.3.

10.3 Strong spatial dependence

10.3.1 Analytical approximations

We suppose a dominant spatial dependence, $\epsilon \ll 1$, such that the terms proportional to ϵ in the instanton equations (10.2) can be neglected, except the cases where the contribution from $\mathcal{T}$ counterbalances the smallness of the field strength ratio parameter ϵ. For $\mathcal{T}_{\text{Sauter}}$ this happens at the pole

$$
x_4^{\text{ref}} = \frac{\pi}{2\gamma_\omega}
\tag{10.11}
$$

which serves as a reflection point. For the sinusoidal and Gaussian fields the situation is not so obvious.

However, if the Keldysh parameter of the weak field is much larger than the critical threshold, whose presence is characteristic for the dynamically assisted mechanism [31, 32, 152], a similar criterion applies even for poleless fields, as discussed in chapter 8. Here, we show, among others, that such effective reflection points apply for backgrounds depending on space and time as well.

We start by observing that for $k \to 0$ the spatial part has the largest contribution. This follows due to the field's Euclidean form that remains bounded from above. Therefore, we fix $k = 0$ and determine the critical point x_4^{ref} for which the spatial contribution becomes negligible compared to the weak time dependent one. Since in this static limit the maximal contribution from the spatial part is reached, x_4^{ref}

may also apply for $k > 0$. The effective reflection points read as

$$\textbf{sinusoidal} \quad x_4^{\text{ref}}(\gamma_\omega, \epsilon) \approx \frac{\text{arcsinh}(\gamma_\omega/\epsilon)}{\gamma_\omega},$$

$$\textbf{Gaussian} \quad x_4^{\text{ref}}(\gamma_\omega, \epsilon) \approx \frac{\sqrt{\ln(1/\epsilon)}(1 + \xi)}{\gamma_\omega}, \tag{10.12}$$

revealing an additional ϵ dependence which has interesting consequences for the tunneling rate as we also have seen before in the case with purely time dependent electric backgrounds. The detailed derivation of ξ has been accomplished in [3] which is revisited in chapter 8.

Following this reflection picture, one can analytically integrate the approximated instanton equations in order to get

$$\dot{x}_4 \approx a\frac{\mathcal{S}_{\text{Sauter}}(kx_3)}{\gamma_k} + a\mathcal{R},$$

$$\dot{x}_3 \approx a\sqrt{1 - \left(\frac{\mathcal{S}_{\text{Sauter}}(kx_3)}{\gamma_k} + \mathcal{R}\right)^2} \tag{10.13}$$

after applying the relation

$$a^2 = \dot{x}_3^2 + \dot{x}_4^2. \tag{10.14}$$

Here, $\mathcal{R}$ represents a dimensionless reflection constant (it is not the vacuum decay rate in section 3.3) which determines the velocity $\dot{x}_4(\pm 1/4)$ where $x_3 = 0$, see also [152].

Using the relation

$$\frac{1}{4} = \int_0^{x_3^{\text{turn}}} dx_3 \ \frac{1}{\dot{x}_3}, \tag{10.15}$$

which is justified due to the underlying instanton symmetry in (10.8), and inserting the second expression in (10.13) into the latter integral, the invariant a satisfies

$$a \approx 4 \int_0^{x_3^{\text{turn}}} dx_3 \ \frac{1}{\sqrt{1 - \left(\frac{\mathcal{S}_{\text{Sauter}}(kx_3)}{\gamma_k} + \mathcal{R}\right)^2}} \tag{10.16}$$

where the upper integration limit, the spatial turning point, is determined by

$$\mathcal{S}_{\text{Sauter}}(kx_3^{\text{turn}}) + \gamma_k\mathcal{R} = \gamma_k. \tag{10.17}$$

The constant $\mathcal{R}$ can be computed employing the relation

$$x_4^{\text{ref}} = \int_0^{x_3^{\text{turn}}} dx_3 \, \frac{\dot{x}_4}{\dot{x}_3} \tag{10.18}$$

and inserting the expressions (10.13) into the latter integral which results in the following implicit condition

$$x_4^{\text{ref}} \overset{!}{=} \int_0^{x_3^{\text{turn}}} dx_3 \, \frac{\mathcal{S}_{\text{Sauter}}(kx_3) + \gamma_k \mathcal{R}}{\sqrt{\gamma_k^2 - (\mathcal{S}_{\text{Sauter}}(kx_3) + \gamma_k \mathcal{R})^2}}. \tag{10.19}$$

In case of reflection one has $\mathcal{R} \neq 0$. However, setting $\mathcal{R} = 0$ and replacing x_4^{ref} on the left-hand side by the corresponding critical point x_4^{crit},[2] we can straightforwardly compute $\gamma_\omega^{\text{crit}}$. As shown in section 8.5, such critical points can be obtained via perturbations around certain intersection points which, in the present case, read

$$\begin{aligned} \textbf{sinusoidal} \quad & x_4^{\text{int}}(\gamma_\omega, \epsilon) = \frac{\text{arccosh}(1/\epsilon)}{\gamma_\omega}, \\ \textbf{Gaussian} \quad & x_4^{\text{int}}(\gamma_\omega, \epsilon) = \frac{\sqrt{\ln(1/\epsilon)}}{\gamma_\omega}. \end{aligned} \tag{10.20}$$

Accordingly, we may write

$$x_4^{\text{crit}} = x_4^{\text{int}}(1 - \Delta) \tag{10.21}$$

with the corresponding correction Δ which we explicitly have computed for the time dependent fields under consideration up to order $\mathcal{O}(\Delta^2)$, see section 8.5.7.

For fields with a pole structure both x_4^{ref} and x_4^{crit} are identical in the limit $\epsilon \ll 1$, so $\Delta = 0$. For the sinusoidal and Gaussian fields which have no poles present, these two points are not equal, $\Delta > 0$. Generally, the values for the effective reflection points are much larger. Due to the intersection points in (10.20), we find that the threshold depends on ϵ which has been discussed in the purely time dependent case [3, 37, 152], but needs some further modifications for the present spatiotemporal setup, see appendix E.

---

[2] The critical temporal Keldysh parameter is determined by the critical point denoted as x_4^{crit} which we take as the point where the weak field contribution starts to become dominating, i.e. $\mathcal{S} = \epsilon \mathcal{T}$.

Namely, the effective field strength ratio for $\gamma_k > 0$ is

$$\tilde{\epsilon} = \epsilon \cosh^2 \left(\text{arcsinh} \left(\frac{\gamma_k}{\sqrt{1 - \gamma_k^2}} \right) \right).$$ (10.22)

Here, one may only consider the spatial Sauter field where the right-hand side follows from $\max\{x_3\}$ determined by the corresponding exact instanton solution, see appendix E. With these modifications and applying the integral result from [152], the critical temporal Keldysh parameter can be generalized to

$$\gamma_\omega^{\text{crit}} = \gamma_\omega x_4^{\text{int}}(1 - \Delta) \frac{\gamma_k \sqrt{1 - \gamma_k^2}}{\arcsin(\gamma_k)}$$ (10.23)

with

$$x_4^{\text{int}} \equiv x_4^{\text{int}}(\gamma_\omega, \tilde{\epsilon}), \qquad \Delta \equiv \Delta(\tilde{\epsilon}), \qquad \tilde{\epsilon} \equiv \tilde{\epsilon}(\gamma_k, \epsilon).$$ (10.24)

Inserting the pole for the Sauter field, $x_4^{\text{int}} = \frac{\pi}{2\gamma_\omega}$ and $\Delta = 0$, leads to the threshold in [152].
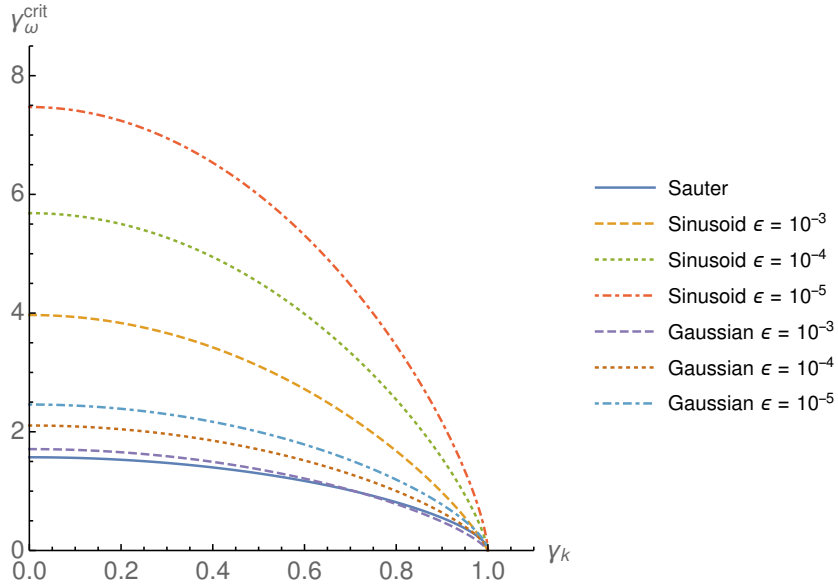
Figure 10.1: Critical temporal Keldysh parameter $\gamma_\omega^{\text{crit}}$ from (10.23) is plotted versus the spatial Keldysh parameter γ_k. The values for ϵ are listed in the plot legend.

The analytically predicted critical Keldysh parameters for all three weak fields are plotted in figure 10.1 where for the poleless cases we have used $\epsilon \in \{10^{-3}, 10^{-4}, 10^{-5}\}$. In the case $\gamma_k = 0$, the critical threshold $\gamma_\omega^{\text{crit}}$ increases as soon as $\epsilon \to 0$. In this

limit, the Gaussian field leads to a much smaller value for $\gamma_\omega^{\mathrm{crit}}$ in comparison to the sinusoidal case, being in accordance with previous findings in a purely temporal background.

In the limit $\gamma_k \to 1$, the threshold in the deeply weak regime, $\epsilon \ll 1$, behaves as $\gamma_\omega^{\mathrm{crit}} \to 0$. This clearly reflects delocalization effects which are generally inherent to finitely extended spatial fields.[3] To be more precise, for $\gamma_k \geq 1$ the width of the spatial field falls down below the Compton wavelength. Consequently, without additional assistance, that is $\gamma_\omega = 0$, the delocalized virtual pair cannot absorb sufficient energy to become a real pair. However, it is expected that the threshold at $\gamma_k = 1$ [23, 146, 388] will be shifted to larger values for increasing time variations approaching the Compton scale [57]. This would result in additional energetic multiphoton contributions leading to a substantial support.

A similar effect also applies for $\epsilon \to 1$, see e.g. [154, 162, 399]. On the other hand, if $\epsilon > 1$ and $\gamma_\omega \to 0$, there will be no critical value present for γ_k at all. In the latter scenario the tunneling can entirely be driven by the strong time dependent term even if the electrostatic energy provided by the weaker spatial term alone is incapable to produce the pair. More details on this are discussed in section 10.4.

Coming back to the present case, the remaining quantities can be computed according to the following prescription

$$
\begin{aligned}
x_4^{\mathrm{ref}} \ \& \ (10.19) \ \& \ (10.17) &\rightsquigarrow \mathcal{R}, \\
\mathcal{R} \ \& \ (10.17) \ \& \ (10.16) &\rightsquigarrow a, \\
\mathcal{R} \ \& \ (10.17) &\rightsquigarrow x_3^{\mathrm{turn}}.
\end{aligned}
\tag{10.25}
$$

Let us remind that due to restrictions regarding the derivation of x_4^{ref} stressed above, we expect the predictions in (10.25) to be valid if

$$
\gamma_\omega \gg \gamma_\omega^{\mathrm{crit}}
\tag{10.26}
$$

which is the condition for dynamical assistance [32]. For more details of the approach, we again refer to section 8.5.

---

[3] It is worth mentioning that the worldline instanton approach automatically accounts for such interesting effects.

10.3.2   Comparison with numerical results
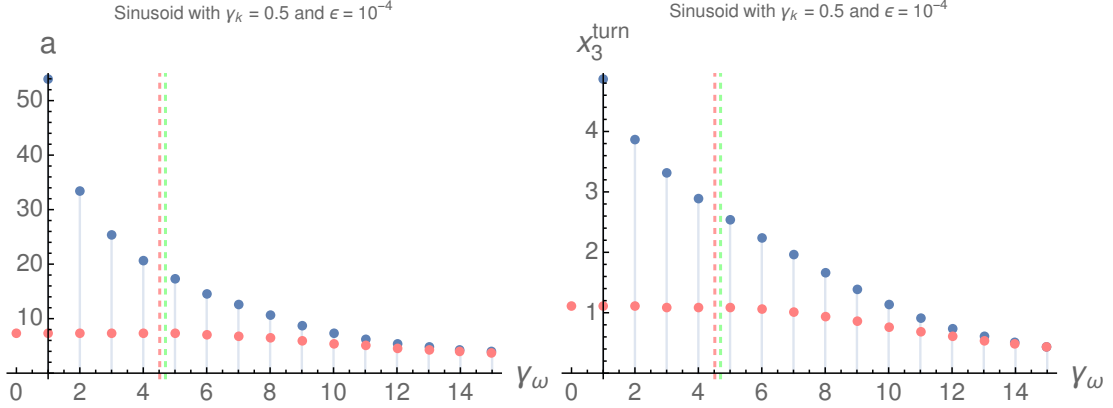
Figure 10.2: a (top) and x_3^{turn} (bottom) for time dependent sinusoidal field plotted versus $\gamma_\omega \in \{0, 1, \dots, 15\}$: values are computed via numerical shooting (red dots), where starting points $(a^{\mathrm{start}}, x_3^{\mathrm{start}})$ have been set by hand, and via the prescription in (10.25) (blue dots). Remaining field parameters are given as $\gamma_k = 0.5$ and $\epsilon = 10^{-4}$. The vertical, dashed, red line is located at $\gamma_\omega^{\mathrm{crit}}$ from (10.23), whereas the dashed, green line has been obtained without replacing ϵ by the modified parameter $\tilde{\epsilon}$ from (10.22).

In this part, we compare the predictions in (10.25) with directly obtained numerical results. For solving the system in (5.23), having closed periodic paths as solutions, we transform an appropriate boundary value problem via constructing a convenient multivariate function of an initial condition set by a and x_3^{turn} which we treat via the shooting technique, see also [400].

The idea is to reduce the whole task to the problem of finding the root of the multivariate function. This can be easily carried out, for instance, with standard computational tools for which we first estimate the required starting point

$$\left(a^{\mathrm{start}}, x_3^{\mathrm{start}}\right) \tag{10.27}$$

by hand.

Taking into account the instanton symmetry from (10.8), we first set

$$\begin{aligned} \dot{x}_3(0) &= 0, \\ x_4(0) &= 0. \end{aligned} \tag{10.28}$$
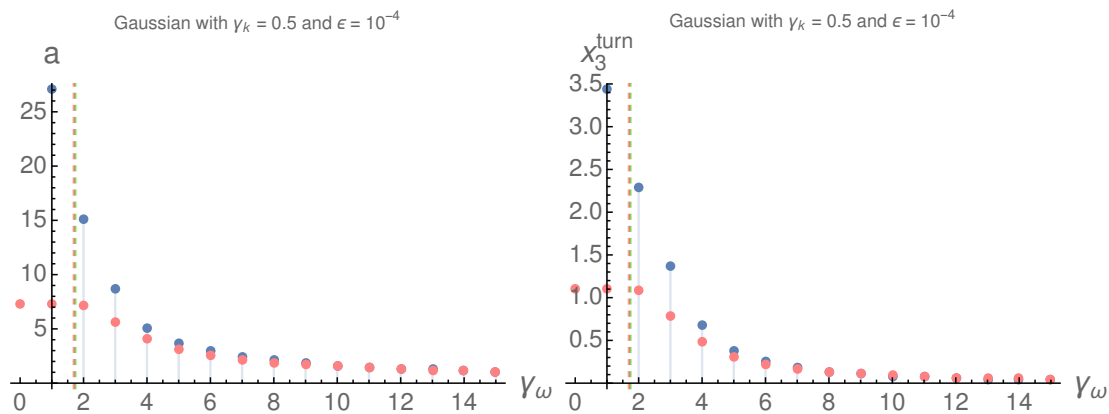
Figure 10.3: a (top) and x_3^{turn} (bottom) for time dependent Gaussian field plotted versus $\gamma_\omega \in \{0, 1, \ldots, 15\}$. Remaining parameters and colors are set as in figure 10.2.

Using the relation for the invariant a, we end up with the following initial conditions

$$
\begin{aligned}
x_3(0) &= \check{x}_3, \\
\dot{x}_3(0) &= 0, \\
x_4(0) &= 0, \\
\dot{x}_4(0) &= \check{a}.
\end{aligned}
\tag{10.29}
$$

The function, whose root we have to determine, then can be defined, for instance, as

$$
\boldsymbol{\Omega}_1(\check{a}, \check{x}_3) := \begin{pmatrix} x_3(1) - \check{x}_3 \\ x_4(1) \end{pmatrix} \in \mathbb{R}^2.
\tag{10.30}
$$

Note that $\boldsymbol{\Omega}_1$ basically includes only information about the periodicity of the stationary path. Having done this, we can evolute the solution for the pair $(\check{a}, \check{x}_3)$ solving the system of differential equations in (10.2) by imposing the initial conditions in (10.29) until a numerical root of the function $\boldsymbol{\Omega}_1$ is found, which then provides a solution, so that

$$
(a, x_3^{\mathrm{turn}}) \in \{(\check{a}, \check{x}_3) \mid \boldsymbol{\Omega}_1(\check{a}, \check{x}_3) = 0\}.
\tag{10.31}
$$

Even though this is an efficient way to find a solution, the result is very sensitive to the initial starting point which has to be preset for the root finder very carefully. One should note that restricting the solution via $\boldsymbol{\Omega}_1$ may lead to closed paths which, however, cannot be accepted as a correct solution simply due to violation of (10.8). Modifications needed in order to avoid such inconsistencies are discussed

in section 10.3.3. Nevertheless, apart from these technicalities, we can adjust the starting points for any setting by hand until an appropriate solution is found.

Proceeding in this way, the obtained results are depicted in figures 10.2 and 10.3, respectively, fixing the parameters $\gamma_k = 0.5$, $\epsilon = 10^{-4}$ and varying γ_ω as given in the figure captions. As one can clearly observe, the analytical approximations approach the numerical results for sufficiently large temporal inhomogeneities being in line with our expectation (10.26). Furthermore, the critical threshold (10.23), both with and without the replacement $\epsilon \to \tilde{\epsilon}$, turns out to be remarkably accurate. For $\gamma_\omega < \gamma_\omega^{\mathrm{crit}}$ both a and x_3^{turn} behave almost constant, reflecting the absence of substantial contributions from the weak field.

10.3.3   Starting points and symmetry constraints

Finding the worldline instantons directly, that is, without tweaking the starting point by hand, requires some refining of the previous strategy. The starting point has to be set accurately in order to find the correct root of $\mathbf{\Omega}_1$. This is actually very difficult to control, since the algorithm is highly sensitive to the initial starting points and also to numerical inaccuracies. However, once the correct invariant and spatial turning point is determined, solving the resulting system by incorporating the found root will supply the closed instanton path.

The previous comparisons show that we cannot benefit from (10.25), in particular, for values in the vicinity of $\gamma_\omega^{\mathrm{crit}}$. A possible approach can be pursued as follows: for $\gamma_\omega \le \gamma_\omega^{\mathrm{crit}}$ one simply assesses the starting point as the one that is obtained only for the strong spatial background term, which we denote as $(a_0, x_{0,3}^{\mathrm{turn}})$, whereas for $\gamma_\omega > \gamma_\omega^{\mathrm{crit}}$ one decides whether the prediction via (10.25) is smaller or larger than $(a_0, x_{0,3}^{\mathrm{turn}})$. In the former case, the analytical approximation can be taken as the corresponding starting point. These steps can be put together as

$$
\begin{aligned}
a^{\mathrm{start}} &= \begin{cases} a_0, & a_0 \le a \\ a, & a_0 > a \end{cases}, \\
x_3^{\mathrm{start}} &= \begin{cases} x_3^{0,\mathrm{turn}}, & x_3^{0,\mathrm{turn}} \le x_3^{\mathrm{turn}} \\ x_3^{\mathrm{turn}}, & x_3^{0,\mathrm{turn}} > x_3^{\mathrm{turn}} \end{cases}
\end{aligned}
\tag{10.32}
$$

where

$$a_0 = \frac{2\pi}{\sqrt{1 - \gamma_k^2}}, \quad x_{0,3}^{\text{turn}} = \frac{1}{\gamma_k}\text{arcsinh}\left(\frac{\gamma_k}{\sqrt{1 - \gamma_k^2}}\right), \quad (10.33)$$

see appendix E. As a last and crucial step, we replace the previous function by

$$\boldsymbol{\Omega}_2(\breve{a}, \breve{x}_3) := \begin{pmatrix} x_3(1/4) + x_3(3/4) + x_4(1/2) - x_4(1) \\ x_4(1/4) + x_4(3/4) + x_3(1/4) - x_3(3/4) \end{pmatrix} \quad (10.34)$$

for which we have explicitly imposed the constraints from (10.10). Due to the symmetry of the instanton, both components of the latter function have to be zero. The solution to the problem is then

$$(a, x_3^{\text{turn}}) \in \{(\breve{a}, \breve{x}_3) \mid \boldsymbol{\Omega}_2(\breve{a}, \breve{x}_3) = 0\}. \quad (10.35)$$

It turns out that searching for a numerical root of the function $\boldsymbol{\Omega}_2$ is much more robust and accurate for finding the correct solution which leads to closed paths keeping the instanton symmetry preserved.

10.3.4   Worldline instantons

Following the strategy described in section 10.3.3, we find the corresponding instanton paths for any field parameters of interest. The new results for a spatial Sauter field, superimposed with a time dependent sinusoidal and Gaussian field, are shown in figures 10.5 and 10.6, respectively. Here, we have fixed $\gamma_k = 0.5$ and varied only γ_ω and ϵ where the corresponding numerical values are listed in the figure captions.

For backgrounds with a weak temporal Sauter-like dependence, instantons admit a lens shape with cusped turning sections [3, 152], see figure 10.4. However, for pole-less fields, reflections turn out to be softened and the paths curve much smoother. For $\gamma_\omega \gg 1$ they tend to become increasingly lens shaped but still remain smoothly curved. This effect seems to be much stronger for the Gaussian field, see figures 10.5 and 10.6.

Furthermore, due to the additional ϵ dependence, there appear significant differences among the paths, independent from the field profile. The described effects are much more pronounced for the oscillatory sinusoidal field.
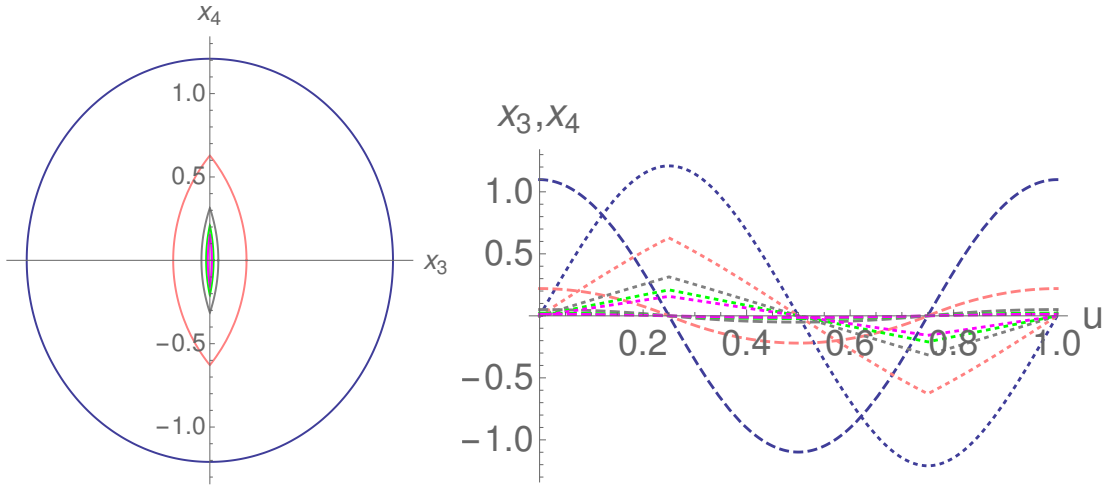
Figure 10.4: Worldline instantons for superimposed temporal Sauter field with $\gamma_\omega \in \{0.001, 2.5, 5, 7.5, 10\}$ (from blue, outer path, to magenta, inner path). In the right panel the components x_3 (dashed) and x_4 (dotted) are separately plotted. Remaining field parameters are chosen as $\gamma_k = 0.5$ and $\epsilon = 10^{-4}$.

The presence of poles for Sauter-like fields is basically responsible for the ϵ independence and the seemingly related cusps. This may explain why the leading order exponential factor in $\mathcal{P}$ can be accurately approached already at $\mathcal{O}(\epsilon)$ in perturbation theory [1, 393], see chapter 9. Since the stationary worldline action $\mathcal{W}_0$ does not feature any ϵ dependence, at least in the limit $\epsilon \ll 1$, the same exponent has to apply at any higher order in ϵ. Therefore, the first order contribution stemming from the weak field should indeed be capable to approximate $\mathcal{W}_0$. Note that we treat the background nonperturbatively.

For time dependent fields, such as of sinusoidal and Gaussian type, poles are not present. In these cases, since the stationary worldline action does in general depend on ϵ, we may expect different exponents in the perturbative expansion of $\mathcal{P}$. Hence, the effective reflection picture already elucidates the relevance of higher orders in ϵ for poleless fields as found in [1, 393]. For super Gaussians of the form

$$E_\omega e^{-(\omega t)^{4N+2}}, \ N \in \mathbb{N}, \tag{10.36}$$

which do not have poles in the instanton plane, such aspects have been extensively discussed in chapter 9.

Coming back to the worldline instantons in figures 10.5 and 10.6, the advantage for treating the system with the help of $\mathbf{\Omega}_2$ and rearranging the starting points
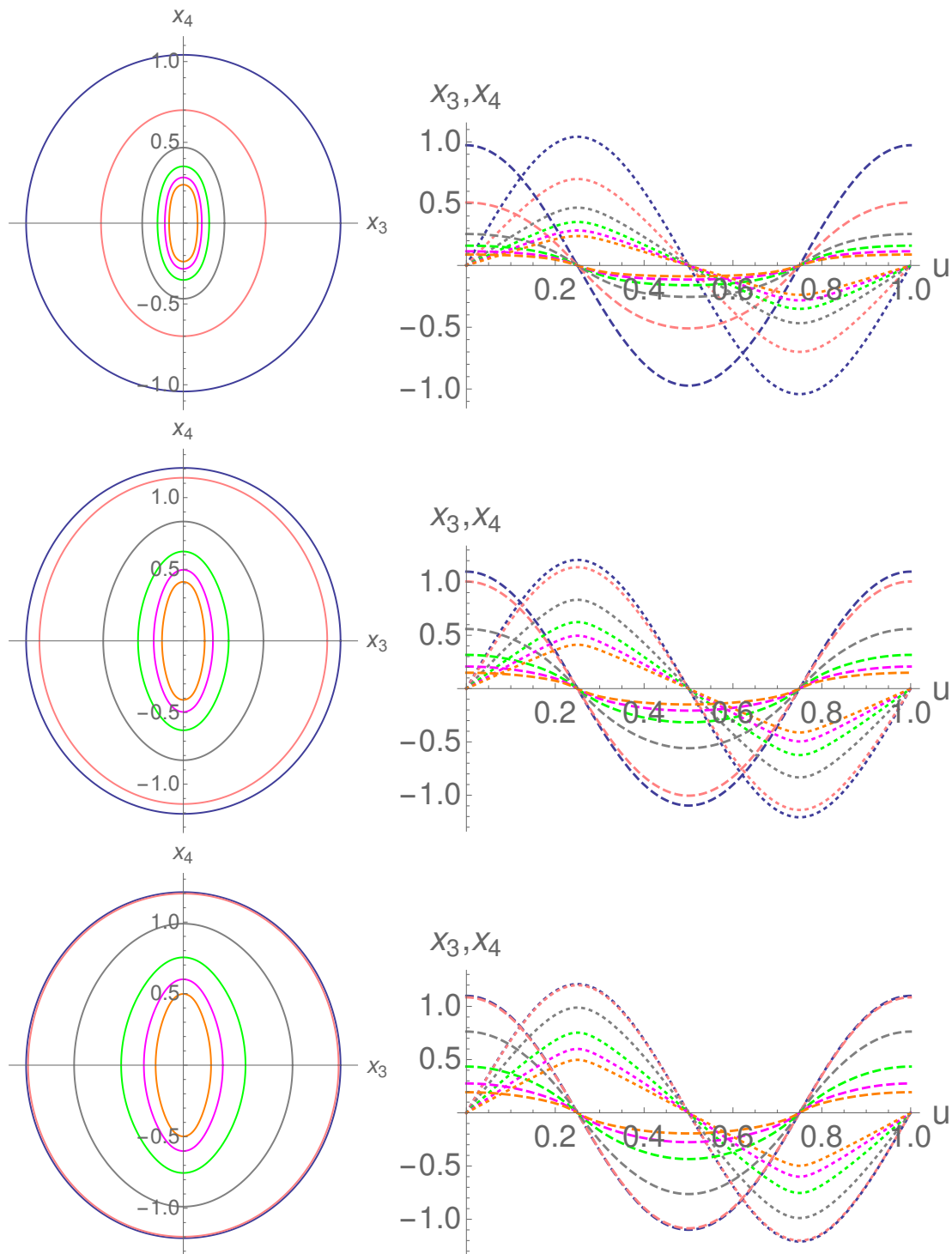
Figure 10.5: Worldline instantons for superimposed temporal sinusoidal field with $\gamma_\omega \in \{0.001, 5, 10, 15, 20, 25\}$, from blue outer path to orange inner path. In the right panel the components x_3 (dashed) and x_4 (dotted) are separately plotted. Remaining field parameters are chosen as $\gamma_k = 0.5$ and $\epsilon \in \{10^{-1}, 10^{-3}, 10^{-4}\}$, from top to bottom.
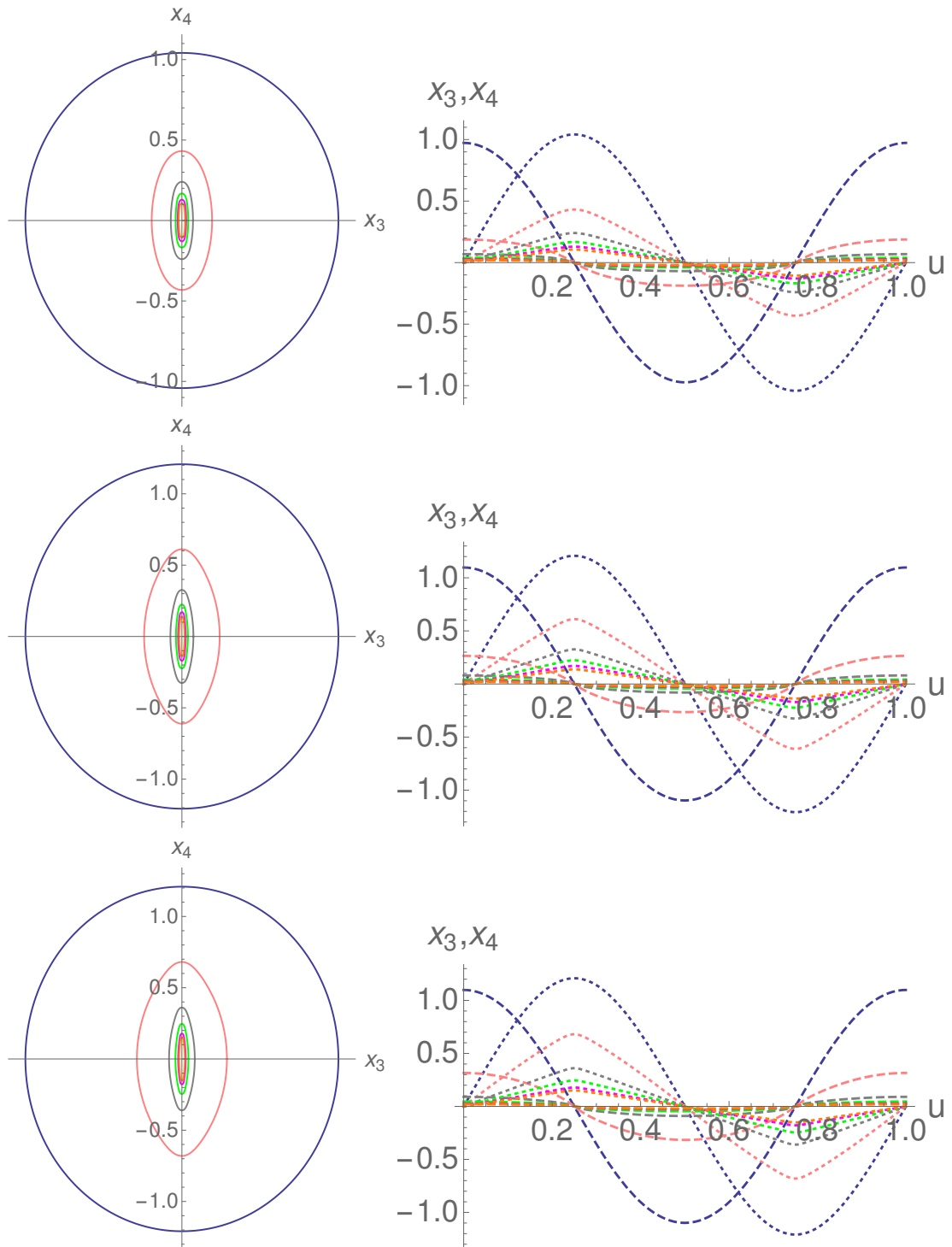
Figure 10.6: Worldline instantons for superimposed temporal Gaussian field with $\gamma_\omega \in \{0.001, 5, 10, 15, 20, 25\}$, from blue outer path to orange inner path. In the right panel the components x_3 (dashed) and x_4 (dotted) are separately plotted. Remaining field parameters are chosen as $\gamma_k = 0.5$ and $\epsilon \in \{10^{-1}, 10^{-3}, 10^{-4}\}$, from top to bottom.

is clearly reflected. The root finding works very robustly and provides the correct paths independently from the chosen field parameters which was not possible with $\mathbf{\Omega}_1$. Additional constraints resulting from the underlying instanton symmetry improve the root finding routine substantially.

10.3.5 Stationary worldline actions

What still remains to be done is the computation of the stationary worldline action, $\mathcal{W}_0$. This can be directly performed following the previous recipe in section 10.3.3. First, we numerically find the worldline instantons for a set of parameters and take the data afterwards to evaluate the worldline action $\mathcal{W}$ on these paths. For this, let us fix the field strength ratio as $\epsilon = 10^{-4}$. The spatial as well as Keldysh parameter is varied in a convenient range.

The results for the stationary worldline action are depicted in figures 10.7 and 10.8, respectively. In the top panels, $\mathcal{W}_0$ has been plotted versus γ_ω for different γ_k listed in the corresponding captions. In both cases, one finds that $\mathcal{W}_0 \uparrow$ if $\gamma_k \uparrow$ as long as $\gamma_\omega \ll \gamma_\omega^{\mathrm{crit}}$. If the weak field starts to assist, i.e. $\gamma_\omega > \gamma_\omega^{\mathrm{crit}}$, we find $\mathcal{W}_0 \downarrow$ for $\gamma_\omega \uparrow$. For $\gamma_\omega \gg \gamma_\omega^{\mathrm{crit}}$ the different curves converge to a single curve which one would obtain for $\gamma_k = 0$. This is in agreement with our expectation, since a static spatial field provides the largest contribution to the effective total field strength.

Interestingly, the critical threshold for the weak sinusoidal field applies much later compared to the Gaussian case. Moreover, for the former field all curves drop much slower for temporal Keldysh parameters $\gamma_\omega > \gamma_\omega^{\mathrm{crit}}$. This is consistent with the observations in chapter 8. There, such differences have been argued to be caused by the relatively large effective reflection point. Indeed, this has been presumed to be the key reason why a weak time dependent sinusoidal field assists less than a Sauter pulse for which the reflection point is much smaller and, even more important, ϵ independent [3, 32, 37, 152, 390]. As a consequence, in the latter case, worldline instantons are reflected and squeezed already for relatively small γ_ω leading to the mentioned faster decrease of the stationary worldline action. The effective reflection picture, as presented in chapter 8, helps to understand such differences in a quite intuitive way in terms of instanton reflections.
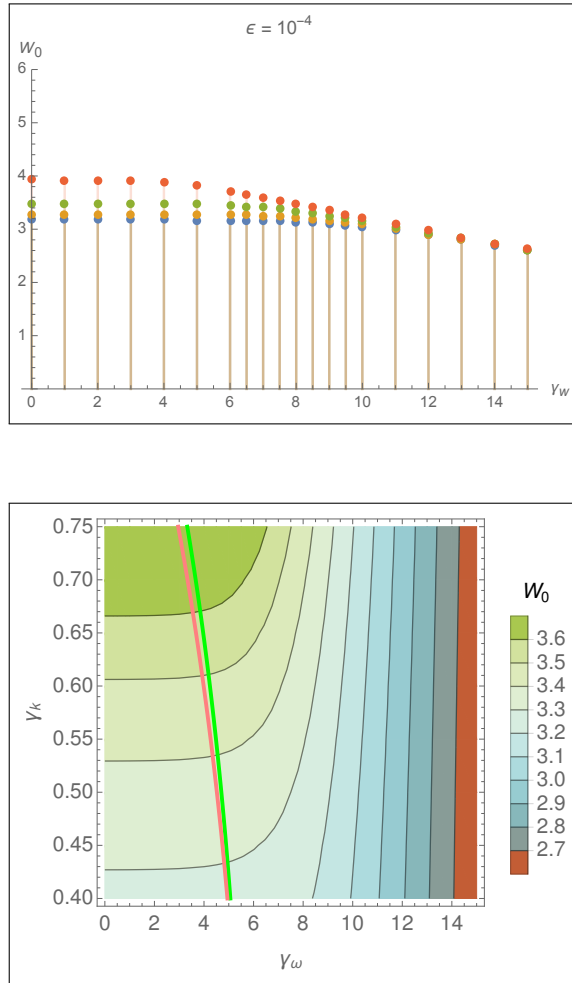
Figure 10.7: Top panel: stationary worldline action $\mathcal{W}_0 \, [E_{\mathrm{S}}/E_k]$ plotted versus γ_ω for the temporal sinusoidal field for fixed $\gamma_k \in \{0.2, 0.4, 0.6, 0.8\}$, from blue to red, and $\epsilon = 10^{-4}$. Bottom panel: $\mathcal{W}_0$ is depicted as a contour plot. The thick lines are the analytically predicted $\gamma_\omega^{\mathrm{crit}}$ from (10.23) with (pink) and without (green) the modified field strength parameter $\tilde{\epsilon}$, see (10.22), included.

In the bottom panels of figures 10.7 and 10.8, the separate curves are combined in a contour plot where the associated stationary worldline action is plotted versus γ_k and γ_ω. The color maps on the right-hand side are scaled according to the numerical values of the stationary worldline action. The previously described trends are again clearly reflected. However, in addition, we have now included the analytically predicted critical threshold $\gamma_\omega^{\mathrm{crit}}$ from (10.23) as well. The difference between the shown two critical curves, one in green and the other in pink, is that the former has been generated without incorporating the modified field strength parameter $\tilde{\epsilon}$ from (10.22) in (10.23).
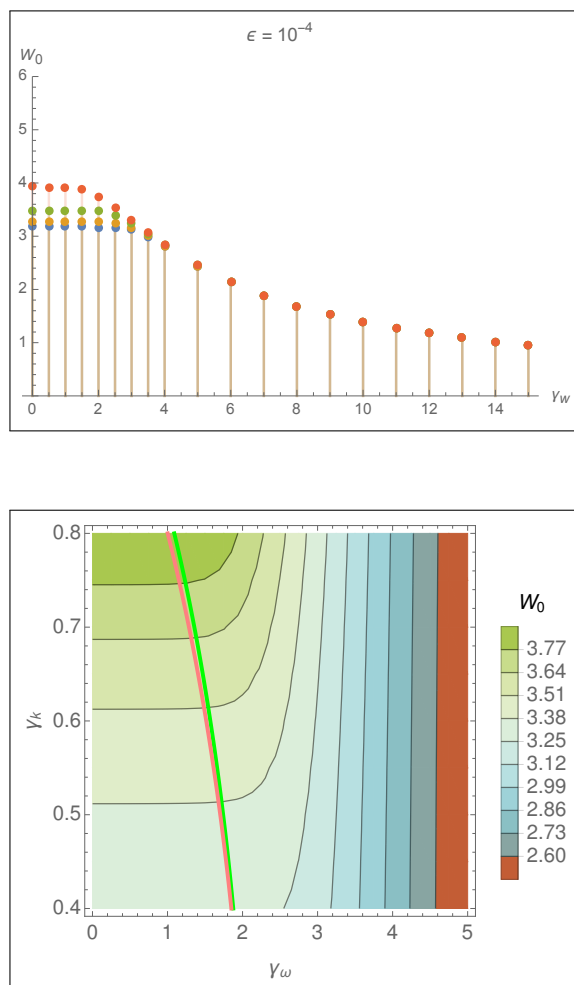
Figure 10.8: Top panel: stationary worldline action $\mathcal{W}_0 \, [E_S/E_k]$ plotted versus γ_ω for the temporal Gaussian field for fixed $\gamma_k \in \{0.2, 0.4, 0.6, 0.8\}$, from blue to red, and $\epsilon = 10^{-4}$. Bottom panel: $\mathcal{W}_0$ is depicted as a contour plot. The thick lines are the analytically predicted $\gamma_\omega^{\mathrm{crit}}$ from (10.23) with (pink) and without (green) the modified field strength parameter $\tilde{\epsilon}$, see (10.22), included.

For $\gamma_k \uparrow$, the curve with $\tilde{\epsilon}$ included is much more accurate being in agreement with the discussion in section 10.3.1. To the right of this critical curve, we find strong evidence for dynamical assistance indicated by the strongly bent gray, solid contour lines. Hence, the analytical approximations match very well with the exact numerical results. Such remarkable agreements suggest that the present approach serves as an efficient way to get some analytical insights even in cases with such complex backgrounds.

10.4 Strong time dependence

In an electric background being too localized in space, $\gamma_k \geq 1$, tunneling of virtual dipole pairs is not possible for $\epsilon \ll 1$ and $\gamma_\omega \to 0$. This corresponds to the nonexistence of a periodic path in spacetime, see e.g. [146, 388]. However, for the present type of backgrounds this effect will be absent if $\epsilon > 1$.

In the following, we assume the background to be the linear combination of two Sauter pulses. The numerical computation strategy is the same as discussed in section 10.3.3 which works very robust even for the present purpose. The obtained worldline instantons are depicted in the left panel of figure 10.9, whereas in the right panel, both space and time components, x_3 and x_4, are plotted separately. Chosen field parameters are given in the figure caption. In case of $\gamma_\omega \uparrow$ the instanton paths tend to shrink smoothly, means no appearance of discontinuities in form of cusped turning sections. More importantly, for $\gamma_k \uparrow$ instantons are real [146], since the dominant contribution comes from the stronger temporal dependence, see discussion in section 10.3.1. Thus, there will be no additional instanton reflections and, consequently, no dynamical assistance. For $\gamma_k \gg 1$ the spatial contribution will become increasingly negligible.

As soon as $\gamma_k \to 0$, the strength of the spatial Sauter field approaches its peak value and maximally contributes to the total effective field strength. This shrinks the instanton paths even more.

10.5 Summary

We have investigated the tunneling process of virtual pairs from the quantum vacuum in the presence of certain multidimensional (1+1) electric backgrounds which depend on space as well as on time.

Going beyond the case of two linearly combined Sauter pulses as considered in [152], we have studied a weak time dependence of sinusoidal and Gaussian type, respectively, which do not have poles in the complex plane. Using the worldline formalism, the resulting background has been treated nonperturbatively. The underlying equations have been simplified by applying certain effective critical points
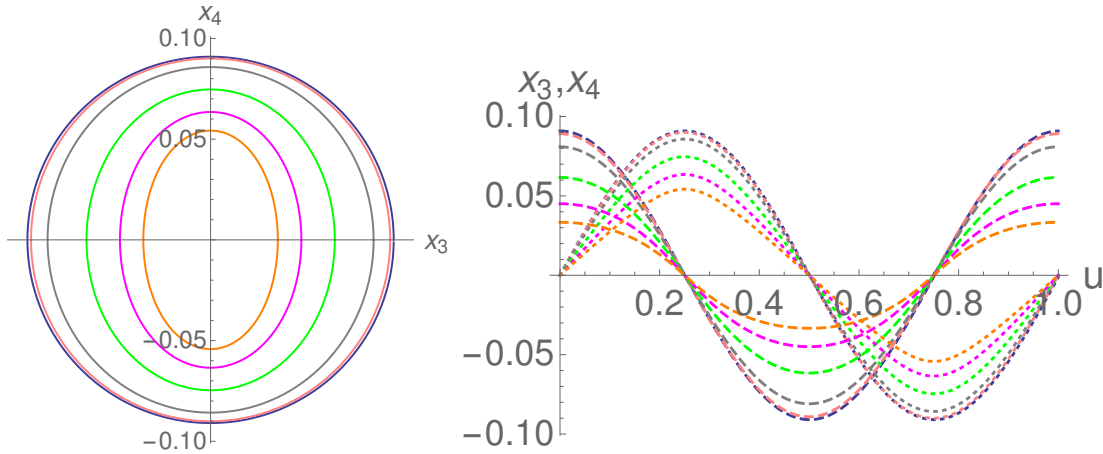
Figure 10.9: Worldline instantons for a spatial Sauter field combined with a stronger temporal Sauter field. The field parameters are $\gamma_k = 0.5$, $\epsilon = 10$ and $\gamma_\omega \in \{0.001, 2, 5, 10, 15, 20\}$, from blue outer path to orange inner path. The two components x_3 (dashed) and x_4 (dotted) are separately plotted in the right panel. The values are given in units of $[m/E_k]$.

as discussed in chapter 8. On this basis we have analytically predicted a threshold $\gamma_\omega^{\mathrm{crit}}$ for the temporal inhomogeneity γ_ω depending on both the field strength ratio ϵ and the spatial inhomogeneity γ_k.

We have set appropriate initial conditions and applied additional symmetry constraints present due to the assumed background structure in order to establish an efficient algorithm. Using the latter allowed us to find the corresponding worldline instantons for any parameters of interest. Then taking these closed paths in spacetime, the leading order exponential factors for both backgrounds have been computed for which we have found a large dynamical enhancement in general. We have seen that below the predicted threshold $\gamma_\omega^{\mathrm{crit}}$ there is no substantial contribution from the weak term.

Furthermore, we have found that such backgrounds lead in general to a smaller enhancement compared to the case with a Sauter-like time variation. This applies due to the fact that for $\gamma_k \to 0$, the limit where the spatial term maximally contributes to the delocalization of the virtual pair, the critical threshold $\gamma_\omega^{\mathrm{crit}}$ becomes relatively large. This effect is much more likely in the oscillatory sinusoidal case.

On the other hand, for $\gamma_k \to 1$ the width of the spatial Sauter pulse decreases towards the critical Compton region with the consequence that $\gamma_\omega^{\mathrm{crit}} \to 0$. In this

case, even arbitrarily small time variations are not negligible. The tunneling rate, however, decreases due to a large exponential suppression which slows down the enhancement even more compared to the Sauter case.

Finally, we have also discussed the $1+1$ dimensional double Sauter background for $\epsilon > 1$ and figured out the main differences found for the instanton paths compared to earlier studies in [152] with $\epsilon \ll 1$.

Part IV

Graphene

Chapter 11

Dynamical Schwinger mechanism in QED$_{2+1}$ and graphene

11.1 Outline

W$^{\text{E}}$ study the production of pairs of massive Dirac particles from the quantum field theoretic ground state in an external time dependent oscillating electric field. Starting from the quantum kinetic description in $3 + 1$ dimensions, we obtain the corresponding equations in lower dimensionality by spatial compactification. We apply the resulting descriptions to bandgapped graphene layers with charge carriers behaving like light massive Dirac fermions.

By doing so, we show that the production of electron-hole pairs in a vicinity of the Dirac points is described by a kinetic equation reflecting a characteristic non-Markovian nature. We compute the production rate and the momentum distribution of created particles developing numerical techniques. We demonstrate that the process closely resembles electron-positron VPP by the dynamical Schwinger mechanism. In addition, we describe suitable field parameters for the experimental observation of this effect.

11.2 Quantum kinetic approach

11.2.1 Assumptions in $3+1$ dimensions

The study of VPP in fields which may be generated with appropriate lasers is in general a major task due to both analytic and numerical reasons. Difficulties, introduced by the naturally complicated shape of such fields, are usually simplified for the sake of having a concise analytical access to the problem.[1]

As studied in the previous chapters, assuming a purely electric background can simplify the problem.[2] Even more specific, many of the results developed in the literature focus on more simple cases where the background instead is a spatially homogeneous, but temporally oscillating electric field [23, 142, 385, 402–405].

For fields of that type, for instance $\boldsymbol{E}(t) = (0, E(t), 0)$,[3] one may also utilize the S-matrix formalism [23, 142, 203, 353, 385, 386, 403, 404] or use ideas from transport theory as introduced in chapter 7 [34, 39, 340, 365, 377, 378, 382, 387, 406, 407]. Both formulations are equivalent and complement each other.

Here, we will focus on the latter quantum kinetic description which particularly highlights the nonequilibrium nature of VPP. As introduced in chapter 7, studies are carried out in terms of the SPDF from (7.7) to which the degrees of freedom in the external field are relaxed at asymptotically large times at which the field is

---

[1] We note that such descriptions cannot include an external plane wave background which has internal symmetries that can indeed crucially simplify the underlying problem. However, for such a background the invariants $\mathcal{F}$ and $\mathcal{G}$ vanish identically, see section 3.4.2, and therefore nonlinear phenomena as VPP cannot exist [22, 135, 222].

[2] This can be obtained to a good approximation through the head-on collision of two linearly polarized laser pulses with equal intensities, frequencies and polarizations. The resulting field will be a spatially inhomogeneous standing wave with time dependence. For treating the problem numerically the dependence on the space coordinates is still hard to deal with. However, this complication is mostly avoided, even though there exist some results including their effects [136, 401].

[3] We again treat the external background field as being not affected during the formation of the pair. Hence, we disregard the potential appearance of avalanche processes [376]. It is believed that these already set in below E_S which may rapidly deplete the applied external field by emitting hard photons producing the pair production avalanche. Similar depletion effects are generally expected due to backreaction as well. There, the number of produced pairs becomes so large that their total rest energy is comparable with the energy of the applied field. This eventually confirms Bohr's conjecture which states that an electric field with E_S may be never generated [376].

switched off. The time evolution of this quantity is prescribed by a QBVE showing a remarkable non-Markovian behavior,[4] see equation (7.17),

$$\dot{W}(\boldsymbol{p},t) = \frac{eE(t)\epsilon_\perp c}{w_{\boldsymbol{p}}^2(t)} \int_{-\infty}^t dt' \frac{eE(t')\epsilon_\perp c}{w_{\boldsymbol{p}}^2(t')}[1-W(\boldsymbol{p},t')]\cos\left[2\int_{t'}^t dt'' \, w_{\boldsymbol{p}}(t'')\right], \quad (11.1)$$

where $W(\boldsymbol{p},-\infty)=0$. We remind that the latter equation represents a semiclassical approximation in the sense that the external field is not quantized while the equation itself results from the quantization of the Dirac field. The SPDF involves a sum over both spin states, providing an overall factor two. The corresponding energy functions, see equations (7.14) and (7.16), are given by

$$\epsilon_\perp^2 = m^2 c^4 + \boldsymbol{p}_\perp^2 c^2, \tag{11.2}$$

$$w_{\boldsymbol{p}}^2(t) = \epsilon_\perp^2 + [p_\parallel - e\mathcal{A}(t)/c]^2 c^2 \tag{11.3}$$

with $\boldsymbol{p}_\perp$ and $\boldsymbol{p}_\parallel$ as in chapter 7. For the four potential we again chose the temporal gauge.

As mentioned, equation (7.17) or (11.1), respectively, does not take into account neither the collision between the created particles nor their inherent radiation fields. In the presence of a constant electric field (CEF) both phenomena are predicted to become relevant as the field strength E reaches E_S [44, 377, 378], see discussion in section 3.4.2.1.

So the solution of equation (11.1) is expected to be valid in the subcritical regime $E \ll E_S$ where the number of produced pairs per unit volume reads

$$\mathcal{N}_{3+1} = \lim_{t\to\infty} \int d^3 p \, W(\boldsymbol{p},t), \tag{11.4}$$

see chapter 7.

For a time dependent OEF with frequency ω and strength E, the resulting $\mathcal{N}_{3+1}$ should be much smaller than the maximum density

$$\mathcal{N}_{max} \sim \frac{E^2}{2\omega} \tag{11.5}$$

that can be created from it, otherwise the external field approach is no longer justified.

---

[4] In contrast to chapter 7, here we only set the Planck constant equal to unity, $\hbar = 1$, and keep the speed of light, c, in the equations for later purpose.

11.2.2 Dimensional reduction: compactification

Quantum kinetic theory turns out to be very advantageous for investigating VPP in a time dependent OEF in low dimensional spacetimes. The associated quantum QBVEs can be derived from the dressed Dirac equation following a similar path as considered in the $3 + 1$ dimensional case leading to equation (7.17), for details see [365, 406]. Alternatively, a dimensional reduction *à la* Kaluza-Klein [408, 409] can be applied with respect to the coordinates perpendicular to the field.[5] Indeed, using the latter approach, the corresponding formulations with different dimensionality can be obtained.

We consider VPP in $2 + 1$-dimensional Minkowski spacetime, M_{2+1}. For this, we treat the dimension in excess x^i as curled up in form of a circle S^1 with radius $\mathcal{R}$ such that the motion of the Dirac fermions is confined within the interval

$$0 \leqslant x^i \leqslant 2\pi\mathcal{R}. \tag{11.6}$$

Since this compactified coordinate is periodic and the applied OEF is homogeneous, we can Fourier expand the Dirac field in terms of the corresponding quantized momentum, see equation (7.1),

$$p_n^i = n\mathcal{R}^{-1}, \quad n \in \mathbb{Z}. \tag{11.7}$$

The exponentials in the expansion, $\exp\left(inx^i/\mathcal{R}\right)$, undergo large oscillations as soon as $\mathcal{R} \to 0$. In this limit only, the fundamental mode $n = 0$ that corresponds to a vanishing momentum along the compactified direction dominates. Accordingly, once the momentum $\boldsymbol{p}$ is locked up to a plane perpendicular to x^i, spontaneous pair production induced by an OEF in a $2+1$-dimensional spacetime is effectively described by the QBVE in (11.1). However, compared to the QED case in M_{3+1}, the SPDF in M_{2+1} does not involve a summation over the double valued spin indices. This sum is canceled out by dividing the resulting expression for $W(\boldsymbol{p}, t)$ by a factor 2 [34, 401].

It is important to say that this effective description will be valid as long as the typical energy of the problem is much smaller than the characteristic energy scale

$$\varepsilon_0 \simeq c\mathcal{R}^{-1}. \tag{11.8}$$

---

[5] This is $2 + 1$ dimensional QED where the external field lives in the plane spanned by the space coordinates.

The final expression for the number of produced pairs per unit area in M_{2+1} follows from equation (11.4) after making the transition to the discrete limit

$$\int \mathrm{d}p \to \frac{1}{2\pi\mathcal{R}} \sum_{p^i} . \tag{11.9}$$

As noted, we only consider the contribution of the vanishing mode. So, accordingly, we conclude

$$\mathcal{N}_{2+1} \equiv \frac{1}{2} \lim_{\mathcal{R}\to 0} 2\pi\mathcal{R}\ \mathcal{N}_{3+1} = \lim_{t\to\infty} \int \mathrm{d}^2p\, W_{2+1}(\boldsymbol{p}, t), \tag{11.10}$$

where $W_{2+1}(\boldsymbol{p}, t)$ corresponds to $W(\boldsymbol{p}, t)$ $[\equiv W_{3+1}(\boldsymbol{p}, t)]$ divided by 2 for which the momentum component p^i is set to zero due to the dominance of the fundamental mode $n = 0$,

$$W_{2+1}(\boldsymbol{p}, t) = \left.\frac{W_{3+1}(\boldsymbol{p}, t)}{2}\right|_{p^i=0}, \tag{11.11}$$

see (11.7).

Following the steps made in the previous case allows to apply equation (11.1) for the $1 + 1$-dimensional case as well. For this, accordingly, two spatial coordinates need to be compactified on a torus $\text{S}^1 \times \text{S}^1$. So we have to set the respective components of the quantized momentum to zero as the characteristic radii of the torus $\tilde{\mathcal{R}}$ and $\mathcal{R}$ vanish identically. Hence, the resulting expression based on the QBVE including the division by a factor 2 gives the produced pair density

$$\mathcal{N}_{1+1} = \lim_{t\to\infty} \int \mathrm{d}p\, W_{1+1}(\boldsymbol{p}, t). \tag{11.12}$$

Let us consider the procedure described above for a CEF, means

$$\mathcal{A}(t) = -cEt, \tag{11.13}$$

in M_{2+1}. We can use the known asymptotic expression for the SPDF in M_{3+1} given by [401]

$$W_{3+1}(\boldsymbol{p}, \infty) \simeq 2\exp\left(-\frac{\pi\epsilon_\perp^2}{|e|Ec}\right). \tag{11.14}$$

After compactifying the axis being perpendicular to the CEF and taking into account the fundamental mode, $n = 0 \Rightarrow p_z = 0$, we find that the VPP rate, $\propto \mathcal{P}$, per unit area is

$$\dot{\mathcal{N}}_{2+1} \approx \frac{(|e|E)^{3/2}}{4\pi^2 c^{1/2}} \exp\left(-\pi \frac{E_{\mathrm{S}}}{E}\right),\tag{11.15}$$

for field strengths $E \ll E_{\mathrm{S}}$.

A similar result appears in M_{1+1} for which we find that the asymptotic expression of the SPDF is momentum independent,

$$W_{1+1}(\infty) \simeq \exp\left(-\frac{\pi E_{\mathrm{S}}}{E}\right).\tag{11.16}$$

The related VPP rate per unit length is of the form

$$\dot{\mathcal{N}}_{1+1} \approx \frac{|e|E}{2\pi} \exp\left(-\pi \frac{E_{\mathrm{S}}}{E}\right).\tag{11.17}$$

The results in equations (11.15) and (11.17) are in agreement with previous expressions obtained by utilizing other methods, see e.g. [126, 339, 353, 410]. As we can see, a direct comparison between both formulas indicates a clear dependence on the respective spacetime dimensionality. Interestingly, this difference only occurs in the quantum fluctuation prefactor, see section 5.5, and not for the tunneling exponent which reveals the sensitivity of such fluctuations with respect to the corresponding dimensionality of the system under consideration.

11.2.3 Dirac fermions in graphene layers

The procedure described above can be applied to the production of Dirac fermions in graphene layers, since, as introduced in section 1.5, these basically approach a $2+1$-dimensional system. However, inherent features of this material require some modifications. Namely, while some of the seen characteristics can be used directly, there exist some other attributes which must be treated with certain carefulness.

For instance, the previous formulas do not take into account finite temperature effects. Due to this, their applicability will only be valid in the zero temperature limit. In addition, we suppose that the electron-hole symmetry in the graphene layer is preserved. This has been theoretically verified within the nearest neighbor tight binding model, see section 5.5. However, it is no longer valid as soon as the next to nearest neighbor interactions are taken into account as well [184].

Here, we assume for the charge carriers a tiny mass m that gives rise to a corresponding energy gap $\Delta\varepsilon = 2mv_f^2$ in contrast to earlier investigations [112, 115, 203, 204]. Later, for numerical calculations presented in section 11.3, the specific value $\Delta\varepsilon = 0.26$ eV is chosen for practical purposes. Such an energy gap, for instance, can originate from the epitaxial growth of graphene on SiC substrates [205], see figure 11.1.
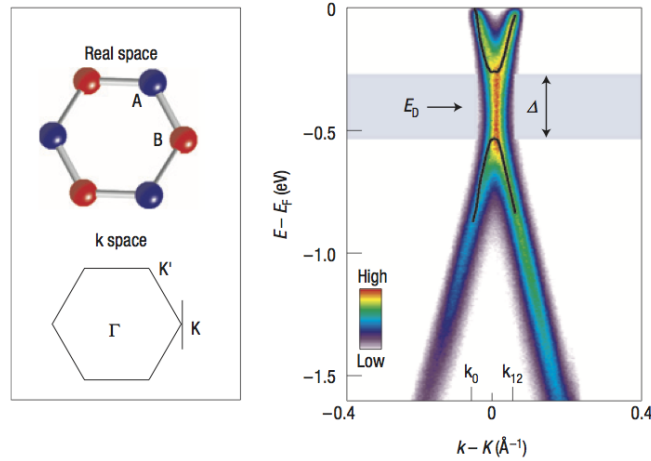
Figure 11.1: Left panel: sublattices in graphene in real (top) and $\boldsymbol{K}_{\pm}$ space (bottom). Right panel: gap opening in graphene via epitaxial growth on the Si face of SiC substrates. Angle-resolved photoemission spectroscopy (ARPES) dispersion close to the Dirac point shows a gap of $\Delta\epsilon = 0.26$ eV. Black triangles indicate the positions of the peaks in the energy distribution curves. The plots are taken from [205].

In order to make a comparison an energy gap $\Delta\varepsilon = 0.12$ eV is considered in addition to the latter value. We should emphasize that also other values for the energy gap can be realized in graphene [206].

Another important point is the following: when adapting the $2+1$-dimensional analogue of equation (11.1), one has to take into account that the Fermi velocity $v_f \approx c/300$ as introduced in section 1.5 cannot be exceeded in graphene. The inclusion of this material induced constraint requires that one slightly has to modify the corresponding QBVEs in M$_{2+1}$ which previously described the situation in vacuum where c, the speed of light, is the appropriate velocity in the equations.

These modifications can be implemented just by making the following replacements

$$mc^2 \to mv_f^2,$$
$$p_i c \to p_i v_f,$$
$$eEc \to eE v_f,$$
$$\mathcal{A}c \to \mathcal{A} v_f.$$
(11.18)

Consequently, the production of quasiparticle-hole pairs in graphene will be governed by the following equation

$$\dot{W}_g(\boldsymbol{p}, t) = Q(\boldsymbol{p}, t) \int_{-\infty}^{t} dt' Q(\boldsymbol{p}, t') \left[\frac{1}{2} - W_g(\boldsymbol{p}, t') \right] \cos\left[2 \int_{t'}^{t} dt'' \, w_{\boldsymbol{p}}(t'') \right]. \quad (11.19)$$

Here, we have introduced the function

$$Q(\boldsymbol{p}, t) \equiv \frac{eE(t) v_f \epsilon_\perp}{w_{\boldsymbol{p}}^2(t)}. \quad (11.20)$$

The expression

$$\epsilon_\perp^2 = m^2 v_f^4 + p_x^2 v_f^2 \quad (11.21)$$

is the squared transverse energy of the Dirac fermions and

$$w_{\boldsymbol{p}}^2(t) = \epsilon_\perp^2 + [p_y - e\mathcal{A}(t)/c]^2 v_f^2 \quad (11.22)$$

denotes their total energy squared. Of course, for zero mass and vanishing external field we find the characteristic pseudo-relativistic dispersion relation $w_{\boldsymbol{p}}^2 = |\boldsymbol{p}|^2 v_f^2$ with $|\boldsymbol{p}|^2 = p_x^2 + p_y^2$ depicted in figure 11.2 compared to other charged carriers in condensed matter systems.

From equation (11.19) we already deduce that the production of electron-hole pairs in graphene turns out to be a nonequilibrium phenomenon. As seen in QED, the combination of the nonlocality in time and the memory effects associated with the quantum statistic factor, $\sim \left[1/2 - W_g(\boldsymbol{p}, t) \right]$, shows that equation (11.19) has a pronounced non-Markovian behavior [365, 377, 382]. So analogous to the ordinary QED case discussed in chapter 7, the SPDF $W_g(\boldsymbol{p}, t)$ depends on the number of pairs that are already present in the system under consideration.

We should mention that the spectral information encoded in (11.19) is only valid in the vicinity of any of the two inequivalent lattice points in the reciprocal space $\boldsymbol{K}_\pm$,
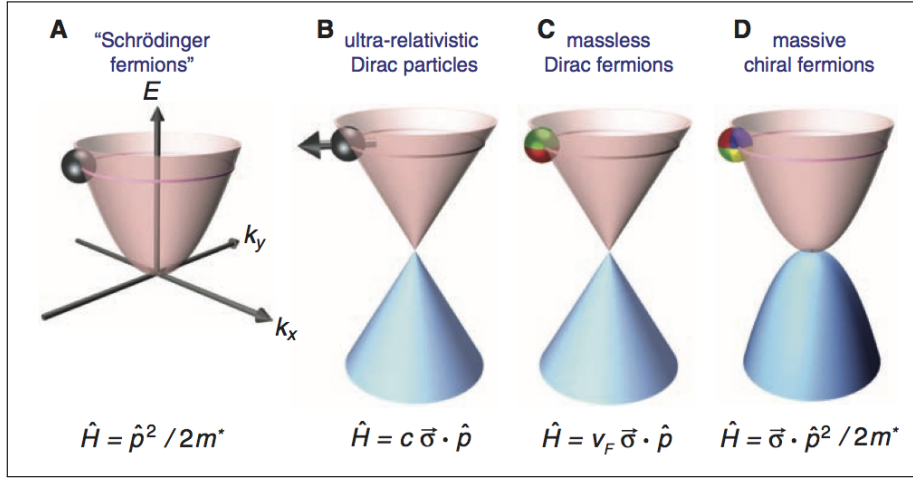
Figure 11.2: Dispersion relation of massless Dirac fermions in graphene compared to other quasiparticles: **A** charge carriers described by the Schrödinger equation with an effective mass m^* different from the free electron mass m are often considered in condensed matter physics. Here, $\hat{p}$ denotes the momentum operator. **B** Relativistic particles with zero rest mass are described by the Dirac equation, where c is the speed of light in vacuum and $\vec{\sigma}$ is the Pauli matrix. **C** Massless Dirac fermions are described by a two dimensional analogy of the Dirac equation, with the characteristic Fermi velocity $v_f \approx c/300 \approx 1 \times 10^6$ m/s replacing c and a pseudospin matrix $\vec{\sigma}$ due to the two sublattices of the honeycomb, see section 1.5. Similar to the fermionic spin that can be up and down oriented, the pseudospin is an index indicating location of the quasiparticle on the two sublattices. The pseudospin can be indicated by a color index, here, red and green. **D** Bilayer graphene allows the identification of another type of quasiparticles without any known analogies. These are described as massive Dirac fermions obeying a mixed Hamiltonian which has both Dirac and Schrödinger behavior. For these the pseudospin changes its color index four times (red, green, yellow, purple), since it moves among four carbon sublattices. The plots are taken from [411].

see section 1.5. Thus, the momentum of the quasiparticle, $\boldsymbol{p}$, has to be understood as relative to $\boldsymbol{K}_\pm$ with

$$|\boldsymbol{p}| \ll |\boldsymbol{K}_\pm| = \frac{4\pi}{3\sqrt{3}a_0} \tag{11.23}$$

and $a_0 = 0.142$ nm [177]. This upper bound in fact does guarantee the relativistic-like behavior of the charge carriers in graphene. Therefore, in order to compute the density of pairs per unit area, see equation (11.15), the respective integral has to be evaluated over a surface limited by

$$p_{\max} \ll |\boldsymbol{K}_\pm| \sim 3 \text{ eV}/v_f. \tag{11.24}$$

Note that the existence of the two inequivalent Dirac points together with the spin degeneracy leads to four different types of quasiparticles. Therefore, the total

number density of produced pairs in graphene is basically taken to be

$$\mathcal{N}_g = \lim_{t \to \infty} 4 \int_{|\boldsymbol{p}| \ll |\boldsymbol{K}_\pm|} \mathrm{d}^2p \; W_g(\boldsymbol{p}, t) \tag{11.25}$$

after the mentioned cutoff in the reciprocal space.

Applying the result (11.25) to the system that is driven by a CEF results in a $\mathcal{N}_g$ which differs from the expression one would derive from equation (11.15),[6]

$$\mathcal{N}_g \approx \frac{2p_{\max}}{\pi^2} \left(\frac{|e|E}{v_f} \right)^{1/2} \exp\left(-\pi \frac{E_g}{E} \right). \tag{11.26}$$

Note that

$$E_g = \frac{m^2 v_f^3}{|e|} \tag{11.27}$$

is the corresponding critical field strength analogy in graphene.

For instance, setting an energy gap $\Delta\varepsilon = 0.26$ eV, gives

$$E_g \simeq 2.6 \times 10^5 \text{ V/cm} \tag{11.28}$$

which arises in some sense from the break down of the chiral symmetry due to the mass m. Interestingly, the critical field strength $E_g \simeq 2.6 \times 10^7$ V/m turns out to be enormously smaller than the critical Schwinger limit in QED, E_S, namely by eleven orders of magnitude.

The density of produced pairs in equation (11.26) can be seen as a saturation density of Dirac-like pairs. It is approached when the interaction time with the CEF becomes of the order

$$T_{\text{sat}} \sim \frac{p_{\max}}{eE}. \tag{11.29}$$

For much longer interactions, particles with momenta larger than $p_{\max}$ will be created as well. However, these are not properly described by the Dirac equation [115, 203].

We should note that the effective description via the QBVEs describing the spontaneous production of electron-hole pairs is valid as long as the external field strength

---

[6] For more details regarding the integration, we would like to refer to section V of [203].

obeys the corresponding weak field condition, $E \ll E_g$. As in the vacuum case, the kinetic equation (11.19) does not take into account neither the contributions due to the inherent radiation of the charge carriers nor the possible collisions between the produced pairs.

11.3   Numerical results

11.3.1   Resonant approach and numerical aspects

The similarity between pair production in graphene described by the kinetic equation in (11.19) and the situation in QED, see equation (7.17), allows to extrapolate interesting outcomes associated with the production process in bandgapped graphene.

Namely, as discussed in chapter 7, for an electric field periodically oscillating in time, we expect that $W_g(\boldsymbol{p}, t)$ gives rise to the characteristic resonances associated with the absorption of energy packages, photons, from the external field [384–387, 412, 413] which takes place when the following resonance condition

$$2\bar{\varepsilon}_{\boldsymbol{p}} \simeq n\omega \tag{11.30}$$

is satisfied, cf. section 7.3. Here, n denotes the number of absorbed photons whereas

$$\bar{\varepsilon}_{\boldsymbol{p}} = \frac{1}{\tau} \int_0^\tau dt\, w_{\boldsymbol{p}}(t) \tag{11.31}$$

is the quasienergy of the produced particles, more precisely it is the energy averaged over the total pulse length τ. The behavior of the distribution function $W_{3+1}(\boldsymbol{p}, t)$ near a resonance characterized by n is known. Referring to the results obtained in [34, 386, 412] and discussed in chapter 7, and following the procedure described in the previous section, we can write

$$W_{g,n}(\boldsymbol{p}, t) \approx \frac{1}{4} \frac{|\Lambda_n(\boldsymbol{p})|^2}{\Omega_{\mathrm{Rabi}}^2(\boldsymbol{p})} \sin^2\left[\Omega_{\mathrm{Rabi}}(\boldsymbol{p})(t - t_{\mathrm{in}})\right]. \tag{11.32}$$

This expression is obtained by assuming that field is suddenly switched on at t_{in} and instantaneously switched off after some interaction time. Here, the explicit expression for the complex time independent function $\Lambda_n(\boldsymbol{p})$ is not important. In

equation (11.32), the quantity

$$\Omega_{\mathrm{Rabi}}(\boldsymbol{p}) = \frac{1}{2}\left[|\Lambda_n(\boldsymbol{p})|^2 + \Delta_n^2(\boldsymbol{p})\right]^{1/2} \tag{11.33}$$

is referred to as the Rabi-like frequency of the vacuum where

$$\Delta_n(\boldsymbol{p}) \equiv 2\bar{\varepsilon}_{\boldsymbol{p}} - n\omega \tag{11.34}$$

denotes the so-called detuning parameter. Here, we should note that the resonant condition (11.30) from above is only valid if the latter frequency is slow compared to the field frequency, $\Omega_{\mathrm{Rabi}}(\boldsymbol{p}) \ll \omega$ [384, 413].

Now, let us consider an explicit example for which we numerically evaluate the relevant kinetic equation in (11.19). We assume an OEF described by the following potential

$$\boldsymbol{A}(t) = -\frac{cE}{\omega}\mathscr{F}(\phi)\sin(\phi)\hat{\boldsymbol{n}}, \tag{11.35}$$

where ω and E denote the frequency and the electric field strength, respectively. Moreover, we abbreviate $\phi = \omega t$ and set the polarization direction of the field assuming $\hat{\boldsymbol{n}}^T = (0,1,0)$. The envelope function $\mathscr{F}$ in (11.35) is chosen with sine-squared shaped switch-on and switch-off segments enclosing a plateau region of constant field strength in between. Explicitly, such an envelope function can be written as

$$\mathscr{F}(\phi) = \begin{cases} \sin^2\left(\frac{1}{2}\phi\right) & 0 \leqslant \phi < \pi \\ 1 & \pi \leqslant \phi \leqslant 2\pi\mathcal{K} \\ \sin^2\left(N\pi - \frac{1}{2}\phi\right) & 2\pi\mathcal{K} < \phi \leqslant 2\pi N \\ 0 & \text{otherwise} \end{cases}, \tag{11.36}$$

where

$$\begin{aligned} N &= N_{\mathrm{plateau}} + 1, \\ \mathcal{K} &= N - \frac{1}{2}. \end{aligned} \tag{11.37}$$

The equations (11.35) and (11.36) guarantee that the OEF with zero amplitude starts at $t = 0$.

Even though equation (11.19) already allows various physical insights inherent to pair production in graphene, its numerical evaluation turns out to be much easier

when we reformulate the problem in form of an equivalent system of ODEs written as

$$
\begin{aligned}
i\dot{f}(\boldsymbol{p}, t) &= a_{\boldsymbol{p}}(t)f(\boldsymbol{p}, t) + b_{\boldsymbol{p}}(t)g(\boldsymbol{p}, t), \\
i\dot{g}(\boldsymbol{p}, t) &= b_{\boldsymbol{p}}^{*}(t)f(\boldsymbol{p}, t) - a_{\boldsymbol{p}}(t)g(\boldsymbol{p}, t)
\end{aligned}
\tag{11.38}
$$

cf. equations (7.11). As in chapter 7, according to this reformulation the distribution function is given by

$$
W_{g}(\boldsymbol{p}, t) = |f(\boldsymbol{p}, t)|^{2}
\tag{11.39}
$$

and the initial conditions are

$$
f(\boldsymbol{p}, -\infty) = 0, \qquad g(\boldsymbol{p}, -\infty) = 1.
\tag{11.40}
$$

The remaining parameters in (11.38) are given as

$$
a_{\boldsymbol{p}}(t) = w_{\boldsymbol{p}}(t) + \frac{eE(t)p_{x}v_{f}^{2}}{2w_{\boldsymbol{p}}(t)[w_{\boldsymbol{p}}(t) + mv_{f}^{2}]},
$$

$$
b_{\boldsymbol{p}}(t) = \frac{1}{2}\frac{eE(t)v_{f}\epsilon_{\perp}}{w_{\boldsymbol{p}}^{2}(t)}\exp\left[-i\arctan\left(\frac{p_{x}q_{\parallel}v_{f}^{2}}{\epsilon_{\perp}^{2} + mv_{f}^{2}w_{\boldsymbol{p}}(t)}\right)\right],
$$

where again, now inserting c,

$$
q_{\parallel} = p_{y} - \frac{e\mathcal{A}(t)}{c}
\tag{11.41}
$$

denotes the longitudinal kinetic momentum. The equivalence between equation (11.19) and the ODEs in (11.38) is shown in several references, see for instance [34, 365, 401]. However, various other formulations of the QBVE can be found in the literature. These are mainly motivated for optimizing the underlying numerics.

11.3.2   Results and discussions

In the following, we take the mass of the Dirac fermions as $m = \Delta\varepsilon/2v_{f}^{2}$. For $\Delta\varepsilon = 0.12$ eV this corresponds to $m = 0.06$ eV$/v_{f}^{2}$ or $m \approx 5.4$ keV$/c^{2}$, respectively. For $\Delta\varepsilon = 0.26$ eV we find $m \approx 11.7$ keV$/c^{2}$. The field frequency is set $\omega = 24.032$ meV. The length of the plateau region of the pulse is characterized by $N_{\text{plateau}} = 241$ cycles such that the total pulse duration is $\tau = 2\pi N/\omega \simeq 41.625$ ps. For the field strength we choose $E = 6.6 \times 10^{4}$ V/cm corresponding to a peak laser intensity of the order $I = cE^{2} \simeq 1.1 \times 10^{7}$ W/cm^{2}. These parameters have been
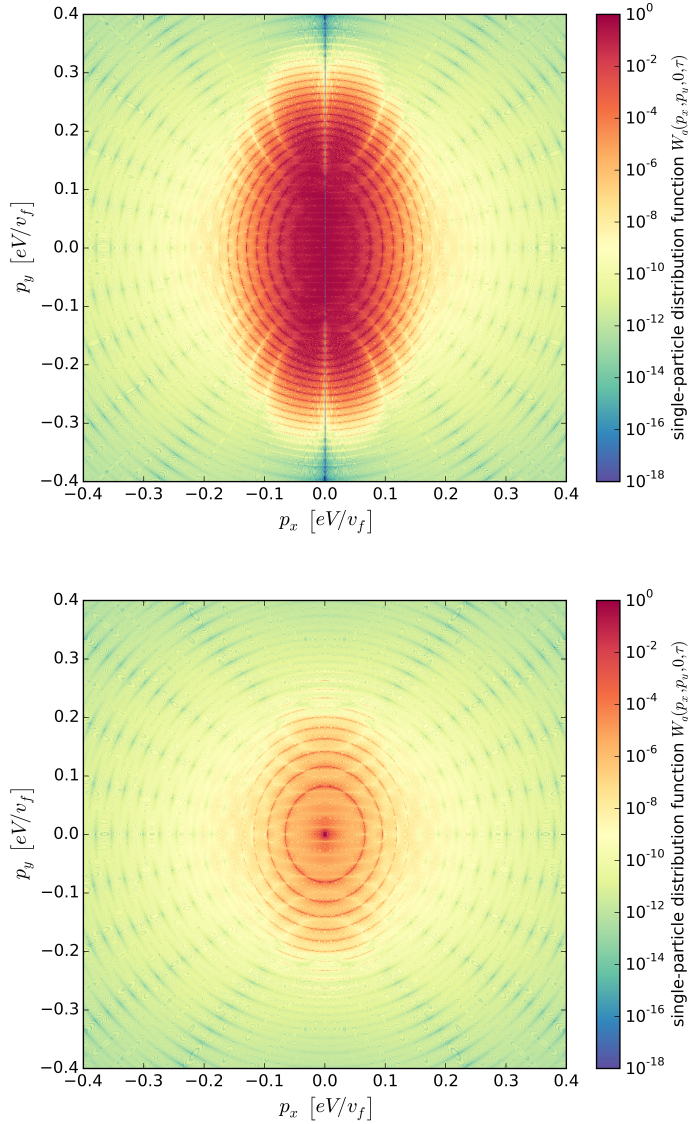
Figure 11.3: Logarithmic plots of the SPDFs for massless (top) and massive ($\Delta\varepsilon = 0.26$ eV, bottom) charged carriers are shown. In both cases the OEF parameters are chosen as $E = 6.6 \times 10^4$ V/cm, $\tau \simeq 41.625$ ps and $\omega = 24.032$ meV.

chosen, since in case of massive particles with $\Delta\varepsilon = 0.26$ eV the SPDF $W_g(\mathbf{0}, t)$ sits in a resonance which corresponds to the absorption of $n \approx 15$ photons from the strong OEF, see equation (11.30). Similar field parameters are easily attainable with terahertz laser pulses with picosecond duration [414, 415]. Moreover, the mentioned critical field E_g in graphene establishes a typical field strength $I_g = cE_g^2$ which corresponds to $I_g \simeq 1.8 \times 10^8$ W/cm^2 for $\Delta\varepsilon = 0.26$ eV. This intensity bound can be easily approached and exceeded with the current laser technology.

The system of ODEs in (11.38) has been solved for particle momenta chosen in the range -0.4 eV $\leqslant p_{x,y} v_f \leqslant 0.4$ eV. The results are depicted in figure 11.3 in form of a density plot with a color scheme scaling corresponding to $\log_{10}[W_g(\boldsymbol{p}, \tau)]$.

The upper panel shows the data associated with the massless case, $m = 0$. In the bottom panel the effects resulting from the chiral symmetry breaking are plotted. As can be clearly observed, the spectral density for the massive particles is highly distinct from the case with massless charge carriers. For instance, for zero momenta, $\boldsymbol{p} = 0$, the SPDF for the massive charge carriers hits the maximum value $W_g(0, \tau) = 1$. For the same momenta, the analogous result for the massless case results in a minimum $W_g(0, \tau) = 0$. Importantly, this minimum extends along the whole vertical line located at $p_x = 0$. This is an inherent feature of the present scenario. Its occurrence can already be anticipated by looking on equation (11.19). Namely, the right-hand side of this equation is proportional to the transverse energy squared,

$$Q(\boldsymbol{p}, t) Q(\boldsymbol{p}, t') \propto \epsilon_{\perp}^2 = p_x^2 v_f^2 + m^2 v_f^4. \tag{11.42}$$

The latter vanishes if we set the mass of the charge carriers and their momentum p_x to zero. In this case, the kinetic equation just reads $\dot{W}_g(p_y, t) = 0$ which has the only conceivable solution $W_g(p_y, t) = 0$ that is in accordance with our initial condition.

The ring-like patterns present in both panels correspond to isocontours of the quasienergy $\bar{\varepsilon}_{\boldsymbol{p}}$ which obey the resonance condition (11.30). The number of photons participating in each of the resonant processes can be obtained. Further insights regarding $W_g(\boldsymbol{p}, \tau)$ can be obtained by contrasting the numerical results with the approximate behavior near a resonance ring found in (11.32). For this, $W_{g,n}(\boldsymbol{p}, t)$ is computed for times t larger than the interaction time τ after it approaches constant values. At the resonance where equation (11.30) is fulfilled, means $\Delta_n \simeq 0$, the Rabi-like frequency can be approximated like

$$\Omega_{\text{Rabi}}(\boldsymbol{p}) \approx \frac{1}{2} |\Lambda_n(\boldsymbol{p})| \tag{11.43}$$

and therefore we may write

$$W_{g,n}(\boldsymbol{p}, \infty) \approx \sin^2 \left[\Omega_{\text{Rabi}}(\boldsymbol{p}) \tau \right]. \tag{11.44}$$
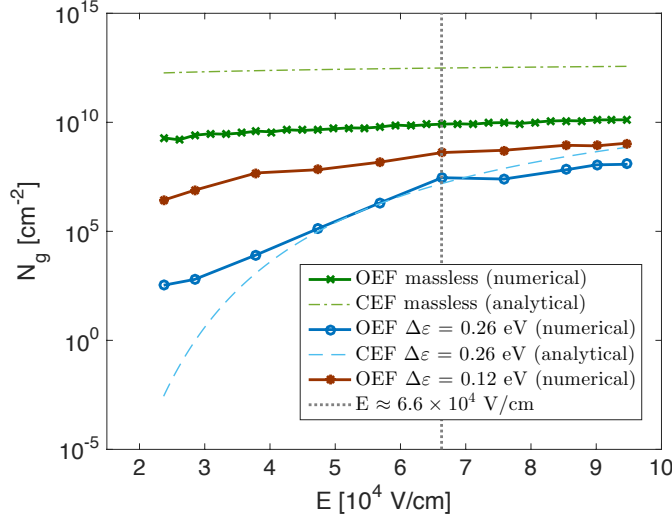
Figure 11.4: Number of electron-hole pairs produced per cm^2 in an OEF is plotted. The result for massless carriers is shown in green. The outcome for massive charges is shown in red and blue, with the data points connected by straight lines. The curves corresponding to the cases driven by a CEF, see equation (11.26), are displayed in green dashed dotted line for massless and blue dashed line for massive carriers. The vertical grey dashed line indicates the electric field strength which is used in figure 11.3. The same benchmark values and notation of figure 11.3 must be understood.

At a given interaction time τ, the equation (11.44) reaches its maximum value giving $W_{g,n}(\boldsymbol{p}_0, \tau) = 1$ for a certain pair of momenta $\boldsymbol{p}_0 = (p_{x_0}, p_{y_0})$. So, accordingly, the condition

$$\Omega_{\mathrm{Rabi}}(\boldsymbol{p}_0) = \frac{(2k+1)\pi}{\tau}, \quad k \in \mathbb{Z} \tag{11.45}$$

must hold. The previous setting has shown that τ has been chosen such that the maximum applies for $\boldsymbol{p} = 0$. Note that, away from the resonance, means for $\Delta_n \neq 0$, the amplitude of $W_{g,n}(\boldsymbol{p}, \tau)$ decreases, see equation (11.32). This can be observed in both panels around each of the isocontours in form of light red, sometimes orange, valleys. Additionally, these trends gradually decrease in the SPDF as soon as the momentum components increase.

Furthermore, we should emphasize that the isocontours have ellipse-like shapes with the long axis lying along the y direction. Such an elongation along that axis reflects the asymmetry due to the pointing direction of the external field in equation (11.19), see the term $p_y - e\mathcal{A}(t)/c$. This clearly indicates that the creation of a particle/hole with large momentum p_y is more likely to happen than with a large

transverse momentum. This observation resembles the pattern seen for a CEF where the SPDF is homogeneous along the longitudinal direction but suppressed by a Gaussian profile transversally.

In addition, comparing both panels reveals that the red colored region in the massless case is drastically larger than for the massive charge carriers for which only a few resonances appear. This already shows that the volume below the surface $W_g(p_x, p_y)$ with zero mass exceeds the one seen for massive carriers. Since these volumes are directly connected to the integrations over momenta, they determine the number of pairs for each case in the vicinity of a Dirac point. Accordingly, the plots depicted in figure 11.3 already make clear that the density of produced pairs in the massless case will be substantially larger than for the massive case.

The previous expectation is perfectly reflected in figure 11.4 showing the trend for (11.25) with respect to the electric field strength E. The green curve corresponds to the number of pairs per cm^2 for the massless case. The blue line is the corresponding curve for the massive charge carriers with $\Delta\varepsilon = 0.26$ eV. The respective results for a CEF have been included as well. From figure 11.4 we can see that the production efficiency for massive particles is reduced by several orders of magnitude. This mainly illustrates the effect of the tunneling exponential in equation (11.26) which is absent in the massless limit. So the outcomes for the latter case are more flat. The curves in the massive case have a stronger dependence on the electric field strength E.

For massive particles with a gap $\Delta\varepsilon = 0.26$ eV our numerical results for an OEF and the analytical prediction for a CEF are quite close to each other for field strengths above $E \gtrsim 4 \times 10^4$ V/cm. This may be understood by taking into account that the field oscillations are slow $\omega \ll m$. So as a result, the OEF locally resembles a CEF. The dimensionless intensity parameter[7]

$$\xi_g = \frac{|e|E}{m\omega v_f} \tag{11.46}$$

is of order unity for $E \approx 4.7 \times 10^4$ V/cm. For field strengths below $E \lesssim 3 \times 10^4$ V/cm the pair density for the OEF is significantly larger than for a CEF. This

---

[7] Note that this is just the inverse of the Keldysh parameter. Due to the same subscript, ξ_g shall not be confused with the critical field strength E_g.

can be understood due to the fact that in an OEF pairs can be generated both by the field amplitude and additionally by the time dependence of the field, i.e. dynamical Schwinger mechanism [115, 204]. It is clear that the latter channel is absent in a CEF which is the standard Schwinger mechanism, see section 1.4 for comparison. So for $\xi_g < 1$ the production by multiphoton absorption can be dominating which leads to an enhancement in an OEF compared to a static field.

For massless particles our numerical results for an OEF and the analytical prediction for a CEF shown in figure 11.4 turn out to be running almost parallel to each other. Here, the CEF curve which describes the saturation density in accordance with equation (11.26) is larger by a few orders of magnitude. We argue that the reason lies in the field oscillations which can be considered as very fast in this case, since $\omega \gg m = 0$. Therefore, the effective field strength present during the pair formation time is reduced by a corresponding time average. This explains the suppression shown in figure 11.4. We should note that this behavior is different from a nonoscillating, bell shaped Sauter-like field. For the latter, the pair production efficiency of massless charge carriers approaches the CEF result to within a factor of order unity [203].

As a comparison, our estimates for the number of produced massive pairs with $\Delta\varepsilon = 0.12$ eV are shown in figure 11.4 as well. In accordance with the naive expectation, the values turn out to be significantly larger than for $\Delta\varepsilon = 0.26$ eV and approaches the massless limit. For this, the critical field strength only amounts to $E_g \simeq 5.5 \times 10^4$ V/cm. Since this turns out to be comparable with the values encompassed in the picture, the curve for analytical result associated with a CEF is not shown here.

11.4 Summary

We have investigated VPP in low dimensional spacetimes by carrying out dimensional compactifications. The resulting effective descriptions have shown that the process in the 2+1 and 1+1 cases can be described by appropriate kinetic QBVEs.

The results for the former case have been applied to massive Dirac fermions in bandgapped graphene layers. We have studied the case where the system is driven

by an OEF. Similarly, as for the QED vacuum, we have found a pronounced resonant behavior reflected in the momentum distribution of produced quasiparticle-hole pairs. The total number density of pairs strongly depends on the applied field strength which is caused due to the tunneling exponential factor in the Schwinger effect involving the critical field strength analogue in graphene. This goes back to the massive quasiparticles in bandgapped graphene layers compared to the massless charge carriers in ordinary gap free graphene. Differences between the pair densities could be traced back to effects of the oscillatory structure of the background.

Our numerical findings have shown that terahertz laser pulses in combination with the substrate induced bandgap technique for graphene might provide a feasible scenario in which the creation of light quasiparticle-hole pairs could be realized. This may allow to simulate strong field induced vacuum decay in QED.

Conclusion

In the present thesis, we have addressed nonperturbative pair creation from the quantum field theoretic ground state (Schwinger effect). Particular focus has been placed on the impact of the corresponding background properties. We have considered purely electric time dependent as well as spatiotemporal backgrounds which give rise to substantial enhancement effects. In addition, we have investigated the pair creation process in lower dimensional spacetimes. The effective descriptions have been applied to bandgapped graphene layers.

Beginning with a comprehensive overview describing basic aspects and introducing the underlying concepts, we have discussed in detail different approaches such as the worldline formalism in quantum field theory, semiclassical instanton and WKB techniques as well as quantum kinetic descriptions. Combining these approaches has helped to advance the corresponding methods which allowed to obtain new and more general insights.

The first main part focuses on the quantum vacuum. In the first chapter, we have studied the enhancement via two mechanisms; the assisted mechanism and the assisted dynamical mechanism. Reformulating the problem using worldline methods, we have found two critical points where one is responsible for the closing of the instanton and the other serves as a reflecting mirror in the configuration plane. Developing an effective approach, we have analyzed characteristic features of different backgrounds with particular focus on the role of the dynamically assisting weak field. Making the extension to more general backgrounds, namely even for those which consist of poleless weak fields, it has been demonstrated that the effect of dynamical assistance is predominantly determined by instanton reflections, no matter whether poles are present or not. We have seen that reflection points located close to the origin lead to a stronger enhancement. In addition, we have

analytically calculated a characteristic critical threshold below which the effect of assistance is absent. The predictions have been confirmed by numerical computations. Our analytical findings have shown that the explicit shape of both strong and weak field is crucial for the strength of the assistance.

In the second chapter, we have studied the assisted mechanism for a certain class of weak fields. We have shown that two different setups that are highly distinct in Minkowski spacetime can surprisingly lead to the same leading order exponential factor in the vacuum pair production rate. It has been found that such a coincidence applies due to identical effective reflection points in the instanton plane. In addition, using the N coupling master formula, we have treated the weak field in perturbation theory and found that in the mentioned coincidence limit the leading order contribution in the field strength ratio parameter already approaches the nonperturbative result.

In the third chapter, we have investigated the tunneling process in multidimensional backgrounds. For doing so, we have determined the corresponding critical points and used them in order to simplify the underlying equations. This has allowed to analytically predict the critical threshold for the effect of assistance. We further have established an efficient algorithm by setting appropriate initial conditions and using additional symmetry constraints which we have implemented to find the corresponding worldline instantons. Utilizing the latter, the leading order tunneling exponential has been computed. We have seen that backgrounds which genuinely depend on space and on time give rise to substantial delocalization effects.

In the second main part, we have studied condensed matter analogs of the Schwinger effect. First, we have described vacuum pair production in lower dimensional spacetimes. In order to do so, we have derived effective quantum kinetic descriptions by employing compactification techniques. The resulting equations have been applied to Dirac fermions in bandgapped graphene layers in the presence of time dependent oscillatory backgrounds. We have found a pronounced resonant behavior reflected in the momentum distribution of the produced quasiparticle-hole pairs. In contrast to the vacuum case, the tunneling exponential factor depends on the critical field strength analogue in graphene. Differences between the pair densi-

ties could be traced back to effects of the background oscillations. We have shown that terahertz laser pulses applied to bandgapped graphene layers may simulate vacuum decay by the Schwinger effect.

Appendix A

Proof of overcompleteness

In the following, we proof the overcompleteness

$$\mathbf{1} = \frac{1}{\pi} \int d^2z \ |z\rangle\langle z| \tag{A.1}$$

for the normalized coherent state $|z\rangle$ in (2.13) where we have introduced the notation $d^2z \equiv dzdz^*$. Expressing the coherent state in form of an exact expansion in Fock space, see equation (2.16), we first rewrite the right-hand side as

$$\frac{1}{\pi} \int d^2z \ |z\rangle\langle z| = \frac{1}{\pi} \sum_{n,m} \frac{1}{\sqrt{n!m!}} |n\rangle\langle m| \int d^2z \ e^{-|z|^2} z^n z^{*m}. \tag{A.2}$$

In order to compute the integral, we first introduce polar coordinates $z = re^{i\varphi}$ where $r \equiv |z|$. Then the integral can be transformed as

$$\int d^2z \ e^{-|z|^2} z^n z^{*m} = \int_{r=0}^{\infty} rdr \ e^{-r^2} r^{n+m} \int_{\varphi=0}^{2\pi} d\varphi \ e^{i(n-m)\varphi}. \tag{A.3}$$

The φ integral yields $2\pi\delta_{nm}$ which results in

$$\begin{aligned}
\text{(A.2)} &= \frac{1}{\pi} \sum_{n,m} \frac{2\pi\delta_{nm}}{\sqrt{n!m!}} |n\rangle\langle m| \int_{r=0}^{\infty} rdr \ e^{-r^2} r^{n+m} \\
&= \sum_{n} \frac{|n\rangle\langle n|}{n!} 2 \int_{0}^{\infty} rdr \ e^{-r^2} r^{2n}.
\end{aligned} \tag{A.4}$$

For the remaining r integral we make the variable substitution $r^2 = t$ such that

$$2 \int_{0}^{\infty} rdr \ e^{-r^2} r^{2n} = \int_{0}^{\infty} dt \ t^n e^{-t} \tag{A.5}$$

which exactly corresponds to the definition of the standard Gamma function

$$\int_{0}^{\infty} dt \ t^n e^{-t} = \Gamma(n+1). \tag{A.6}$$

Now, using (A.5) and inserting the relation $\Gamma(n+1) = n!$ into the second line in (A.4) leads to the condition in (A.1).

Appendix B

Effective action from the path integral

We start with the most general representation in the path integral formulation from (3.24). We consider sQED without any external background field for which the corresponding integral in Minkowski spacetime reads

$$\int \mathcal{D}A \ e^{i\Gamma[A]} = \int \mathcal{D}A\mathcal{D}\phi\mathcal{D}\phi^* \ e^{i\int d^4x\left(-\frac{1}{4}F_{\mu\nu}^2 - \phi^*\left(D^2+m^2\right)\phi\right)}. \tag{B.1}$$

Because of the quadratic dependence on the scalar field ϕ, this integral is Gaussian and can be computed exactly. Using the standard formula[1] we arrive at

$$\int \mathcal{D}A \ e^{i\Gamma[A]} = \int \mathcal{D}A \ e^{-i\int d^4x\frac{1}{4}F_{\mu\nu}^2} \frac{\mathcal{N}}{\mathrm{Det}\left(-D^2 - m^2\right)} \tag{B.2}$$

which is of course fulfilled only if

$$e^{i[\Gamma[A]+\int d^4x\frac{1}{4}F_{\mu\nu}^2]} = \frac{\mathcal{N}}{\mathrm{Det}\left(-D^2 - m^2\right)}. \tag{B.3}$$

Taking the logarithm on both sides of the latter equation, we get

$$i\Gamma[A] + i\int d^4x \ \frac{1}{4}F_{\mu\nu}^2 - \ln\mathcal{N} = -\ln\mathrm{Det}\left(-D^2 - m^2\right). \tag{B.4}$$

If we now neglect the contribution of the dynamical gauge field and introduce an external background field $\mathcal{A}^\mu$ which dresses the correlation functions in the usual

---

[1] The standard result we use is

$$\int \mathcal{D}\phi\mathcal{D}\phi^* e^{i\int d^4x(\phi^* M\phi + J\phi)} = \mathcal{N}\left(\det M\right)^{-1} e^{iJM^{-1}J}$$

where M denotes a matrix and $\mathcal{N}$ is a normalization constant.

way, that means in form of the following covariant derivative $D_\mathcal{A}^\mu = \partial^\mu - ie\mathcal{A}^\mu$, we immediately obtain the formal expression for the one-loop EH effective action,

$$\Gamma[\mathcal{A}] = i \ln \text{Det} \left(-D_\mathcal{A}^2 - m^2 \right). \tag{B.5}$$

For the case without any external background field, but exact in the coupling to the dynamical gauge field A^μ, we can evaluate the trace in position space by resorting to the quantum mechanical formulation,

$$i\Gamma[A] = \int d^4x \left[-i\frac{1}{4}F_{\mu\nu}^2 - \langle x| \ln \left(-D^2 - m^2 \right) |x\rangle \right] + \ln \mathcal{N}. \tag{B.6}$$

Using the relation in footnote 7 and ignoring the normalization constant, we can write the corresponding effective Lagrangian

$$\mathcal{L}_{\text{eff}} = -\frac{1}{4}F_{\mu\nu}^2 - i \int_0^\infty \frac{ds}{s} \, e^{-s\epsilon} e^{-ism^2} \langle x| e^{-i\hat{H}s} |x\rangle \tag{B.7}$$

where the usual $i\epsilon$ constant has been included, see equation (3.27). This is the formal expression introduced in equation (3.44). Notably, this expression is even fully exact if both the dynamical photon field and the external background are taken into account.

Appendix C

Derivation of Bogoliubov coefficients

As in chapter 7, we consider a time dependent electric field of the form $\boldsymbol{E}(t) = (0, E(t), 0)$. The initial ground state $|\text{vac}, \text{in}\rangle$, that is at time the field is switched on, is defined as

$$\hat{a}_{\text{in}}|\text{vac}, \text{in}\rangle = \hat{b}_{\text{in}}|\text{vac}, \text{in}\rangle = 0 \tag{C.1}$$

with

$$\hat{a}_{\text{in}} \equiv a_{\boldsymbol{p},s}(t_{\text{in}}), \quad \hat{b}_{\text{in}} \equiv b_{-\boldsymbol{p},s}(t_{\text{in}}). \tag{C.2}$$

In an analogous way, the instantaneous vacuum state $|\text{vac}, t\rangle$ can then be defined according to

$$\hat{a}_{\boldsymbol{p},s}(t)|\text{vac}, t\rangle = \hat{b}_{-\boldsymbol{p},s}(t)|\text{vac}, t\rangle = 0, \tag{C.3}$$

where $\hat{a}_{\boldsymbol{p},s}(t)$ and $\hat{b}_{-\boldsymbol{p},s}(t)$ denote the annihilation operators for the quasiparticle and the antiquasiparticle, respectively, which together with the creation operators $\hat{a}^\dagger_{\boldsymbol{p},s}(t)$ and $\hat{b}^\dagger_{-\boldsymbol{p},s}(t)$ build up the corresponding Fock space. A connection between the operators in (C.2) and the instantaneous one in (C.3) is possible via a canonical unitary evolution operator $\mathcal{U}(t, t_{\text{in}})$, see [222, 403, 404], allowing

$$|\text{vac}, t\rangle = \mathcal{U}(t, t_{\text{in}})|\text{vac}, \text{in}\rangle. \tag{C.4}$$

Using the latter relations, we can find

$$\hat{a}_{\boldsymbol{p},s}(t) = \mathcal{U}(t, t_{\text{in}})\hat{a}_{\text{in}}\mathcal{U}^\dagger(t, t_{\text{in}}), \quad \hat{b}^\dagger_{-\boldsymbol{p},s}(t) = \mathcal{U}^\dagger(t, t_{\text{in}})\hat{b}^\dagger_{\text{in}}\mathcal{U}(t, t_{\text{in}}). \tag{C.5}$$

The evolution operator above can be constructed similar to the procedure as followed in the Bardeen-Cooper-Schrieffer (BCS) theory, see [416] and references therein. Following the ansatz in [222, 403, 404], we express $\mathcal{U}(t, t_{\text{in}})$ as

$$\mathcal{U}(t, t_{\text{in}}) = \exp[\Lambda(t, t_{\text{in}})], \tag{C.6}$$

where

$$\begin{aligned}
\Lambda(t, t_{\text{in}}) &= \sum_{\boldsymbol{p},s} \Lambda_{\boldsymbol{p},s}(t, t_{\text{in}}), \\
\Lambda_{\boldsymbol{p},s}(t, t_{\text{in}}) &= \alpha \hat{a}_{\text{in}}^{\dagger} \hat{b}_{\text{in}}^{\dagger} - \alpha^* \hat{b}_{\text{in}} \hat{a}_{\text{in}} + i\beta \hat{a}_{\text{in}}^{\dagger} \hat{a}_{\text{in}} - i\beta \hat{b}_{\text{in}} \hat{b}_{\text{in}}^{\dagger}
\end{aligned} \tag{C.7}$$

depend on functions

$$\alpha \equiv \alpha(\boldsymbol{p}, t) \in \mathbb{C}, \tag{C.8}$$

$$\beta \equiv \beta(\boldsymbol{p}, t) \in \mathbb{R}. \tag{C.9}$$

Note that the constructed evolution operator in (C.6) is unitary and has canonical features. In order to find the relation between the function α and the coefficient arising from the Bogoliubov transformations, we Taylor expand $\mathcal{U}(t, t_{\text{in}})$ in (C.5) which formally gives

$$\begin{aligned}
\hat{a}_{\boldsymbol{p},s}(t) &= \sum_{n=0}^{\infty} \frac{1}{n!} \left[\Lambda, [\Lambda, \dots [\Lambda, \hat{a}_{\text{in}}] \dots]\right], \\
\hat{b}_{-\boldsymbol{p},s}^{\dagger}(t) &= \sum_{n=0}^{\infty} \frac{1}{n!} \left[\Lambda, \left[\Lambda, \dots \left[\Lambda, \hat{b}_{\text{in}}^{\dagger}\right] \dots\right]\right].
\end{aligned} \tag{C.10}$$

Using the following commutation relations iteratively

$$\begin{aligned}
[\Lambda, \hat{a}_{\text{in}}] &= -\alpha \hat{b}_{\text{in}}^{\dagger} - i\beta \hat{a}_{\text{in}}, \\
\left[\Lambda, \hat{b}_{\text{in}}\right] &= \alpha \hat{a}_{\text{in}}^{\dagger} - i\beta \hat{b}_{\text{in}}, \\
[\Lambda, \hat{a}_{\text{in}}^{\dagger}] &= -\alpha^* \hat{b}_{\text{in}} + i\beta \hat{a}_{\text{in}}^{\dagger}, \\
[\Lambda, \hat{b}_{\text{in}}^{\dagger}] &= \alpha^* \hat{a}_{\text{in}} + i\beta \hat{b}_{\text{in}}^{\dagger},
\end{aligned} \tag{C.11}$$

we can write the relations in (C.10) in the following compact form

$$\begin{bmatrix} \hat{a}_{\boldsymbol{p},s}(t) \\ \hat{b}_{-\boldsymbol{p},s}^{\dagger}(t) \end{bmatrix} = \begin{bmatrix} g^*(\boldsymbol{p}, t) & f(\boldsymbol{p}, t) \\ -f^*(\boldsymbol{p}, t) & g(\boldsymbol{p}, t) \end{bmatrix} \begin{bmatrix} \hat{a}_{\text{in}} \\ \hat{b}_{\text{in}}^{\dagger} \end{bmatrix}, \tag{C.12}$$

where the Bogoliubov coefficients read

$$\begin{aligned}
f(\boldsymbol{p}, t) &= -\frac{\alpha}{\sqrt{|\alpha|^2 + \beta^2}} \sin(\sqrt{|\alpha|^2 + \beta^2}), \\
g(\boldsymbol{p}, t) &= \cos(\sqrt{|\alpha|^2 + \beta^2}) + i\frac{\beta}{\alpha} f(\boldsymbol{p}, t),
\end{aligned} \tag{C.13}$$

satisfying the condition

$$|g(\boldsymbol{p}, t)|^2 + |f(\boldsymbol{p}, t)|^2 = 1. \tag{C.14}$$

According to equation (C.4) which connects the initial and the instantaneous ground state, Taylor expanding $\mathcal{U}(t, t_{\text{in}})$ and acting on $|\text{vac}, \text{in}\rangle$ leads to many complicated combinations of the operators $\hat{a}_{\text{in}}$, $\hat{b}_{\text{in}}$, $\hat{a}_{\text{in}}^\dagger$, $\hat{b}_{\text{in}}^\dagger$. These operations can be simplified by noting that the evolution operator can be disentangled as

$$\mathcal{U}(t, t_{\text{in}}) = \prod_{\boldsymbol{p}, s} \exp[\Lambda_{\boldsymbol{p}, s}(t, t_{\text{in}})] \tag{C.15}$$

which is allowed, since two arbitrary elements $\Lambda_{\boldsymbol{p}, s}(t, t_{\text{in}})$ and $\Lambda_{\boldsymbol{p}', s'}(t, t_{\text{in}})$ commute with each other. Taking this into account, we expand $\exp[\Lambda_{\boldsymbol{p}, s}(t, t_{\text{in}})]$ and write the identities

$$\begin{aligned}
\Lambda_{\boldsymbol{p}, \sigma}^{2n+1}(t, t_{\text{in}}) &= (-1)^n (|\alpha|^2 + \beta^2)^n \Lambda_{\boldsymbol{p}, \sigma}(t, t_{\text{in}}), \\
\Lambda_{\boldsymbol{p}, \sigma}^{2n}(t, t_{\text{in}}) &= (-1)^{n-1} (|\alpha|^2 + \beta^2)^{n-1} \Lambda_{\boldsymbol{p}, \sigma}^2(t, t_{\text{in}})
\end{aligned} \tag{C.16}$$

where

$$\Lambda_{\boldsymbol{p}, \sigma}^2(t, t_{\text{in}}) = -(|\alpha|^2 + \beta^2)(\hat{b}_{\text{in}}^\dagger \hat{b}_{\text{in}} \hat{a}_{\text{in}}^\dagger \hat{a}_{\text{in}} + \hat{b}_{\text{in}} \hat{b}_{\text{in}}^\dagger \hat{a}_{\text{in}} \hat{a}_{\text{in}}^\dagger). \tag{C.17}$$

Using the latter equations (C.13) and (C.16), we can express the instantaneous ground state as a two-mode squeezed state of the in-particle states,

$$|\text{vac}, t\rangle = \prod_{\boldsymbol{p}, s} g^*(\boldsymbol{p}, t) \exp\left[\frac{f(\boldsymbol{p}, t)}{g^*(\boldsymbol{p}, t)} \hat{b}_{\text{in}}^\dagger \hat{a}_{\text{in}}^\dagger\right] |\text{vac}, \text{in}\rangle. \tag{C.18}$$

Based on this expression, one can verify that the vacuum persistence probability is given by

$$\begin{aligned}
\mathcal{P}_{\text{vac}}(t) = |\langle \text{vac}, t | \text{vac}, \text{in}\rangle|^2 &= \exp \sum_{\boldsymbol{p}, s} \ln\left[g(\boldsymbol{p}, t)^2\right] \\
&= \exp\left[(t - t_{\text{in}}) V \Gamma_{\text{vac}}(t)\right].
\end{aligned} \tag{C.19}$$

Here, $\Gamma_{\text{vac}}(t)$ is the instantaneous vacuum decay rate per unit volume V given as

$$\Gamma_{\text{vac}}(t) = \frac{\ln[\mathcal{P}_{\text{vac}}(t)]}{(t - t_{\text{in}}) V} = \frac{2}{t - t_{\text{in}}} \int d^3 p \, \ln\left(1 - |f(\boldsymbol{p}, t)|^2\right) \tag{C.20}$$

which is obtained after taking the infinite volume continuum limit where

$$\frac{1}{V} \sum_{\boldsymbol{p}} \to \int d^3 p. \tag{C.21}$$

The factor 2 in equation (C.20) is again the result of the summation over the discrete spin variable s. This is the spin statistics factor discussed before for the bosonic and fermionic Schwinger formulas, cf. (3.66) and (3.65). In the subcritical regime $E \ll E_{\mathrm{S}}$ and for a static electric background, the expression (C.20) gives the known vacuum decay probability, $\mathcal{P} \propto \mathcal{R} = \Gamma_{\mathrm{vac}}(\infty)$, [44]

$$\mathcal{P} \simeq \Im(\Gamma_{\mathrm{EH}}) = \frac{(eE)^2}{(2\pi)^3} \sum_{n=1}^{\infty} \frac{1}{n^2} \exp\left(-\pi n \frac{E_{\mathrm{S}}}{E}\right), \qquad (\text{C.22})$$

see equations (3.22) and (3.65).

Appendix D

Derivation of the quantum Boltzmann-Vlasov equation

In the following, we derive the integrodifferential representation of the quantum kinetic equation in (7.17) by using the equations (7.11). For this, we consider the temporal equations of the functions $\bar{f}(\boldsymbol{p}, t)$ and $\bar{g}(\boldsymbol{p}, t)$ which are related to the original Bogoliubov coefficients $f(\boldsymbol{p}, t)$ and $g(\boldsymbol{p}, t)$ through the following unitary transformations

$$
\begin{aligned}
\bar{f}(\boldsymbol{p}, t) &= -if(\boldsymbol{p}, t) \exp\left[i \int_{t_0}^{t} dt'\, a_{\boldsymbol{p}}(t')\right], \\
\bar{g}(\boldsymbol{p}, t) &= ig(\boldsymbol{p}, t) \exp\left[-i \int_{t_0}^{t} dt'\, a_{\boldsymbol{p}}(t')\right].
\end{aligned}
\tag{D.1}
$$

Taking the latter equations, together with the equations in (7.11), allows to derive the following system of ODEs

$$
\begin{aligned}
\dot{\bar{f}}(\boldsymbol{p}, t) &= -\frac{1}{2} Q_{\boldsymbol{p}}(t) \bar{g}(\boldsymbol{p}, t) \exp\left[2i\Theta_{\boldsymbol{p}}(t)\right], \\
\dot{\bar{g}}(\boldsymbol{p}, t) &= \frac{1}{2} Q_{\boldsymbol{p}}(t) \bar{f}(\boldsymbol{p}, t) \exp\left[-2i\Theta_{\boldsymbol{p}}(t)\right]
\end{aligned}
\tag{D.2}
$$

with $Q_{\boldsymbol{p}}(t)$ and $\Theta_{\boldsymbol{p}}(t)$ defined as

$$
Q_{\boldsymbol{p}}(t) := \frac{eE(t)\epsilon_{\perp}}{w_{\boldsymbol{p}}^2(t)}, \quad \Theta_{\boldsymbol{p}}(t) := \int_{t_0}^{t} dt'\, w_{\boldsymbol{p}}(t').
\tag{D.3}
$$

Here, the initial conditions

$$
\begin{aligned}
\bar{f}(\boldsymbol{p}, -\infty) &= 0, \\
\bar{g}(\boldsymbol{p}, -\infty) &= 1
\end{aligned}
\tag{D.4}
$$

ensure the pure vacuum condition. Now, we recall the time evolution equation (7.10) with (7.7) and introduce the quasiparticle correlation function

$$O(\boldsymbol{p}, t) = \sum_s \langle \text{vac}, \text{in} | b^\dagger_{-\boldsymbol{p},s}(t) a^\dagger_{\boldsymbol{p},s}(t) | \text{vac}, \text{in} \rangle = 2 f(\boldsymbol{p}, t) g^*(\boldsymbol{p}, t). \qquad (\text{D.5})$$

Using the equations in (D.2), we find

$$
\begin{aligned}
\dot{W}(\boldsymbol{p}, t) &= -Q_{\boldsymbol{p}}(t) \Re \left\{ O(\boldsymbol{p}, t) \exp\left[-2i\Theta_{\boldsymbol{p}}(t) \right] \right\}, \\
\dot{O}(\boldsymbol{p}, t) &= -Q_{\boldsymbol{p}}(t) \left[1 - W(\boldsymbol{p}, t) \right] \exp\left[2i\Theta_{\boldsymbol{p}}(t) \right].
\end{aligned}
\qquad (\text{D.6})
$$

Now, we first perform the time integration from $-\infty$ to t in the second expression in (D.6). Afterwards, we insert the resulting function $O(\boldsymbol{p}, t)$ into the first expression in (D.6). This leads to the QBVE introduced in (7.17).

Appendix E

Critical Keldysh parameter

The critical temporal Keldysh parameter $\gamma_\omega^{\mathrm{crit}}$ in case of $\gamma_k > 0$ requires a modification of the (effective) spatial field strength. This modification goes back to the observation in [3] where

$$\gamma_k \uparrow \, \Rightarrow \, \Delta \uparrow \, \Rightarrow \, \gamma_\omega^{\mathrm{crit}} \downarrow \tag{E.1}$$

holds in general. The corresponding value can be obtained by taking $\max\{x_3\}$ minimizing the field strength for a fixed γ_k. This maximum may be computed only for the spatial Sauter field, since we are interested in the critical threshold where the contribution of the temporal field may still be assumed as negligible. Note that the enormous enhancement applies for values above the threshold $\gamma_\omega^{\mathrm{crit}}$. In this case, the additional contribution for sure decreases $\max\{x_3\}$ which is, however, irrelevant for the present purpose. For the spatial Sauter field, the exact instanton solution reads

$$x_3(u) = \frac{1}{\gamma_k} \mathrm{arcsinh}\left(\frac{\gamma_k}{\sqrt{1-\gamma_k^2}}\cos(2\pi n u)\right),$$

$$x_4(u) = \frac{1}{\gamma_k\sqrt{1-\gamma_k^2}}\arcsin\left(\gamma_k \sin(2\pi n u)\right). \tag{E.2}$$

Taking the leading worldline instanton with winding number $n = 1$ [146, 158], the maximum of the spatial component is reached at (rescaled) proper time $u = 0$,

$$x_{3,\mathrm{max}} = \frac{1}{\gamma_k}\mathrm{arcsinh}\left(\frac{\gamma_k}{\sqrt{1-\gamma_k^2}}\right), \tag{E.3}$$

which subsequently results in

$$\min_{\text{fixed } k, E_k} \left\{ E_k \operatorname{sech}^2(kx_3) \right\} = E_k \operatorname{sech}^2(kx_{3,\max})$$
$$= E_k \operatorname{sech}^2 \left(\operatorname{arcsinh} \left(\frac{\gamma_k}{\sqrt{1 - \gamma_k^2}} \right) \right). \tag{E.4}$$

Hence, the effective field strength ratio for the general case $0 \leq \gamma_k < 1$ takes the form

$$\tilde{\epsilon} = \epsilon \cosh^2 \left(\operatorname{arcsinh} \left(\frac{\gamma_k}{\sqrt{1 - \gamma_k^2}} \right) \right) \tag{E.5}$$

which, accordingly, has to be plugged into equation (10.23), replacing the initial parameter ϵ.

References

[1] I. Akal, *Super Gaussian enhancers in the Schwinger mechanism*, `arXiv:1712.05368`.

[2] I. Akal and G. Moortgat-Pick, *Quantum tunnelling from vacuum in multidimensions*, *Phys. Rev.* **D96** (2017), no. 9 096027, [`arXiv:1710.04646`].

[3] I. Akal and G. Moortgat-Pick, *Euclidean mirrors: enhanced vacuum decay from reflected instantons*, *J. Phys.* **G45** (2018), no. 5 055007, [`arXiv:1706.06447`].

[4] I. Akal, R. Egger, C. Müller, and S. Villalba-Chávez, *Low-dimensional approach to pair production in an oscillating electric field: Application to bandgap graphene layers*, *Phys. Rev.* **D93** (2016), no. 11 116006, [`arXiv:1602.08310`].

[5] S. L. Glashow, *Partial-symmetries of weak interactions*, *Nuclear Physics* **22** (1961), no. 4 579–588.

[6] S. Weinberg, *A model of leptons*, *Physical review letters* **19** (1967), no. 21 1264.

[7] A. Salam, *Weak and electromagnetic interactions.*, tech. rep., Imperial Coll. of Science and Tech., London. International Centre for Theoretical Physics, Trieste, Italy, 1969.

[8] H. Fritzsch and M. Gell-Mann, *Current algebra: Quarks and what else?*, in *Murray Gell-Mann: Selected Papers*, pp. 241–261. World Scientific, 2010.

[9] G. Aad, T. Abajyan, B. Abbott, J. Abdallah, S. A. Khalek, A. Abdelalim, O. Abdinov, R. Aben, B. Abi, M. Abolins, et al., *Observation of a new particle in the search for the standard model higgs boson with the atlas detector at the lhc*, *Physics Letters B* **716** (2012), no. 1 1–29.

[10] S. Chatrchyan, V. Khachatryan, A. M. Sirunyan, A. Tumasyan, W. Adam, E. Aguilo, T. Bergauer, M. Dragicevic, J. Erö, C. Fabjan, et al., *Observation of a new boson at a mass of 125 gev with the cms experiment at the lhc*, *Physics Letters B* **716** (2012), no. 1 30–61.

[11] J. Goldstone, *Field theories with «superconductor» solutions*, *Il Nuovo Cimento (1955-1965)* **19** (1961), no. 1 154–164.

[12] J. Goldstone, A. Salam, and S. Weinberg, *Broken symmetries*, *Physical Review* **127** (1962), no. 3 965.

[13] P. W. Higgs, *Broken symmetries and the masses of gauge bosons*, *Physical Review Letters* **13** (1964), no. 16 508.

[14] F. Englert and R. Brout, *Broken symmetry and the mass of gauge vector mesons*, *Physical Review Letters* **13** (1964), no. 9 321.

[15] G. S. Guralnik, C. R. Hagen, and T. W. Kibble, *Global conservation laws and massless particles*, *Physical Review Letters* **13** (1964), no. 20 585.

[16] B. G. Sidharth and M. Altaisky, *Frontiers of Fundamental Physics 4*. Springer Science & Business Media, 2012.

[17] Y. Fukuda, T. Hayakawa, E. Ichihara, K. Inoue, K. Ishihara, H. Ishino, Y. Itow, T. Kajita, J. Kameda, S. Kasuga, et al., *Evidence for oscillation of atmospheric neutrinos*, *Physical Review Letters* **81** (1998), no. 8 1562.

[18] G. Hooft, *Magnetic monopoles in unified gauge theories*, *Nuclear Physics: B* **79** (1974), no. 2 276–284.

[19] J. Jaeckel and A. Ringwald, *The Low-Energy Frontier of Particle Physics*, *Ann. Rev. Nucl. Part. Sci.* **60** (2010) 405–437, [arXiv:1002.0329].

[20] J. L. Hewett et al., *Fundamental physics at the intensity frontier*, arXiv:1205.2671.

[21] D. Hanneke, S. Fogwell, and G. Gabrielse, *New measurement of the electron magnetic moment and the fine structure constant*, *Physical Review Letters* **100** (2008), no. 12 120801.

[22] J. Schwinger, *On Gauge Invariance and Vacuum Polarization*, *Physical Review* **82** (June, 1951) 664–679.

[23] A. Nikishov, *Barrier scattering in field theory removal of klein paradox*, *Nuclear Physics B* **21** (1970), no. 2 346–358.

[24] T. D. Cohen and D. A. McGady, *The schwinger mechanism revisited*, *Phys. Rev.* **D78** (2008) 036008, [arXiv:0807.1117].

[25] H. Gies, *Strong laser fields as a probe for fundamental physics*, *Eur. Phys. J.* **D55** (2009) 311–317, [arXiv:0812.0668].

[26] G. V. Dunne, *New Strong-Field QED Effects at ELI: Nonperturbative Vacuum Pair Production*, *Eur. Phys. J.* **D55** (2009) 327–340, [arXiv:0812.3163].

[27] G. Dunne, *New strong-field qed effects at extreme light infrastructure*, *The European Physical Journal D* **55** (2009), no. 2 327.

[28] G. V. Dunne, *Extreme quantum field theory and particle physics with IZEST*, *Eur. Phys. J. ST* **223** (2014), no. 6 1055–1061.

[29] B. M. Hegelich, G. Mourou, and J. Rafelski, *Probing the quantum vacuum with ultra intense laser pulses*, *Eur. Phys. J. ST* **223** (2014), no. 6 1093–1104, [arXiv:1412.8234].

[30] F. Gelis and N. Tanji, *Schwinger mechanism revisited*, *Prog. Part. Nucl. Phys.* **87** (2016) 1–49, [arXiv:1510.05451].

[31] G. V. Dunne, H. Gies, and R. Schützhold, *Catalysis of Schwinger Vacuum Pair Production*, *Phys. Rev.* **D80** (2009) 111301, [arXiv:0908.0948].

[32] R. Schützhold, H. Gies, and G. Dunne, *Dynamically assisted Schwinger mechanism*, *Phys. Rev. Lett.* **101** (2008) 130404, [arXiv:0807.0754].

[33] A. Nuriman, B.-S. Xie, Z.-L. Li, and D. Sayipjamal, *Enhanced electron-positron pair creation by dynamically assisted combinational fields*, *Phys. Lett.* **B717** (2012) 465–469.

[34] I. Akal, S. Villalba-Chávez, and C. Müller, *Electron-positron pair production in a bifrequent oscillating electric field*, *Physical Review D* **90** (Dec., 2014) 113004, [arXiv:1409.1806].

[35] A. Otto, D. Seipt, D. Blaschke, B. Kämpfer, and S. A. Smolyansky, *Lifting shell structures in the dynamically assisted Schwinger effect in periodic fields*, *Phys. Lett.* **B740** (2015) 335–340, [arXiv:1412.0890].

[36] A. Otto, D. Seipt, D. Blaschke, S. A. Smolyansky, and B. Kämpfer, *Dynamical Schwinger process in a bifrequent electric field of finite duration: survey on amplification*, *Phys. Rev.* **D91** (2015), no. 10 105018, [arXiv:1503.08675].

[37] M. F. Linder, C. Schneider, J. Sicking, N. Szpak, and R. Schützhold, *Pulse shape dependence in the dynamically assisted Sauter-Schwinger effect*, *Phys. Rev.* **D92** (2015), no. 8 085009, [arXiv:1505.05685].

[38] S. S. Bulanov, V. D. Mur, N. B. Narozhny, J. Nees, and V. S. Popov, *Multiple colliding electromagnetic pulses: a way to lower the threshold of e^+e^- pair production from vacuum*, *Phys. Rev. Lett.* **104** (2010) 220404, [arXiv:1003.2623].

[39] C. Kohlfürst, M. Mitter, G. von Winckel, F. Hebenstreit, and R. Alkofer, *Optimizing the pulse shape for Schwinger pair production*, *Physical Review D* **88** (Aug., 2013) 045028, [arXiv:1212.1385].

[40] A. Gonoskov, I. Gonoskov, C. Harvey, A. Ilderton, A. Kim, M. Marklund, G. Mourou, and A. M. Sergeev, *Probing nonperturbative QED with optimally focused laser pulses*, *Phys. Rev. Lett.* **111** (2013) 060404, [arXiv:1302.4653].

[41] F. Hebenstreit and F. Fillion-Gourdeau, *Optimization of Schwinger pair production in colliding laser pulses*, *Phys. Lett.* **B739** (2014) 189–195, [arXiv:1409.7943].

[42] F. Hebenstreit, *The inverse problem for Schwinger pair production*, *Phys. Lett.* **B753** (2016) 336–340, [arXiv:1509.08693].

[43] F. Fillion-Gourdeau, F. Hebenstreit, D. Gagnon, and S. MacLean, *Pulse shape optimization for electron-positron production in rotating fields*, *Phys. Rev.* **D96** (2017), no. 1 016012, [arXiv:1704.08919].

[44] N. Tanji, *Dynamical view of pair creation in uniform electric and magnetic fields*, *Annals of Physics* **324** (Aug., 2009) 1691–1736, [arXiv:0810.4429].

[45] C. K. Dumlu, *Multidimensional quantum tunneling in the Schwinger effect*, *Phys. Rev.* **D93** (2016), no. 6 065045, [arXiv:1507.07005].

[46] P. Copinger and K. Fukushima, *Spatially Assisted Schwinger Mechanism and Magnetic Catalysis*, *Phys. Rev. Lett.* **117** (2016), no. 8 081603, [arXiv:1605.05957]. [Erratum: Phys. Rev. Lett.118,no.9,099903(2017)].

[47] E. Bavarsad, S. P. Kim, C. Stahl, and S.-S. Xue, *Effect of a magnetic field on Schwinger mechanism in de Sitter spacetime*, *Phys. Rev.* **D97** (2018), no. 2 025017, [arXiv:1707.03975].

[48] P. Elmfors and B.-S. Skagerstam, *Electromagnetic fields in a thermal background*, *Physics Letters B* **348** (1995), no. 1 141 – 148.

[49] H. Gies, *QED effective action at finite temperature: Two loop dominance*, *Phys. Rev.* **D61** (2000) 085021, [hep-ph/9909500].

[50] S. P. Kim, H. K. Lee, and Y. Yoon, *Schwinger Pair Production at Finite Temperature in QED*, *Phys. Rev.* **D79** (2009) 045024, [arXiv:0811.0349].

[51] W. Dittrich and H. Gies, *Probing the quantum vacuum. Perturbative effective action approach in quantum electrodynamics and its application*, *Springer Tracts Mod. Phys.* **166** (2000) 1–241.

[52] B. King, H. Gies, and A. Di Piazza, *Pair production in a plane wave by thermal background photons*, *Phys. Rev.* **D86** (2012) 125007, [arXiv:1204.2442]. [Erratum: Phys. Rev.D87,no.6,069905(2013)].

[53] S. Ozaki, T. Arai, K. Hattori, and K. Itakura, *Euler-Heisenberg-Weiss action for QCD+QED*, *Phys. Rev.* **D92** (2015), no. 1 016002, [arXiv:1504.07532].

[54] A. R. Brown, *Schwinger pair production at nonzero temperatures or in compact directions*, arXiv:1512.05716.

[55] L. Medina and M. C. Ogilvie, *Schwinger Pair Production at Finite Temperature*, *Phys. Rev.* **D95** (2017), no. 5 056006, [`arXiv:1511.09459`].

[56] O. Gould and A. Rajantie, *Thermal Schwinger pair production at arbitrary coupling*, *Phys. Rev.* **D96** (2017), no. 7 076002, [`arXiv:1704.04801`].

[57] H. Gies and G. Torgrimsson, *Critical Schwinger pair production*, *Phys. Rev. Lett.* **116** (2016), no. 9 090406, [`arXiv:1507.07802`].

[58] H. Gies and G. Torgrimsson, *Critical Schwinger pair production II - universality in the deeply critical regime*, *Phys. Rev.* **D95** (2017), no. 1 016001, [`arXiv:1612.00635`].

[59] G. L. Pimentel, A. M. Polyakov, and G. M. Tarnopolsky, *Vacua on the Brink of Decay*, pp. 399–417. 2018. `arXiv:1803.09168`.

[60] A. Casher, H. Neuberger, and S. Nussinov, *Chromoelectric Flux Tube Model of Particle Production*, *Phys. Rev.* **D20** (1979) 179–188.

[61] G. C. Nayak, *Non-perturbative quark-antiquark production from a constant chromo-electric field via the Schwinger mechanism*, *Phys. Rev.* **D72** (2005) 125010, [`hep-ph/0510052`].

[62] G. C. Nayak and P. van Nieuwenhuizen, *Soft-gluon production due to a gluon loop in a constant chromo-electric background field*, *Phys. Rev.* **D71** (2005) 125001, [`hep-ph/0504070`].

[63] N. Tanji and K. Itakura, *Schwinger mechanism enhanced by the Nielsen–Olesen instability*, *Phys. Lett.* **B713** (2012) 117–121, [`arXiv:1111.6772`].

[64] G. W. Semenoff and K. Zarembo, *Holographic Schwinger Effect*, *Phys. Rev. Lett.* **107** (2011) 171601, [`arXiv:1109.2920`].

[65] S. Bolognesi, F. Kiefer, and E. Rabinovici, *Comments on Critical Electric and Magnetic Fields from Holography*, *JHEP* **01** (2013) 174, [`arXiv:1210.4170`].

[66] Y. Sato and K. Yoshida, *Potential Analysis in Holographic Schwinger Effect*, *JHEP* **08** (2013) 002, [`arXiv:1304.7917`].

[67] K. Hashimoto, T. Oka, and A. Sonoda, *Magnetic instability in AdS/CFT: Schwinger effect and Euler-Heisenberg Lagrangian of supersymmetric QCD*, *JHEP* **06** (2014) 085, [arXiv:1403.6336].

[68] K. Bitaghsir Fadafan and F. Saiedi, *Holographic Schwinger effect in non-relativistic backgrounds*, *Eur. Phys. J.* **C75** (2015), no. 12 612, [arXiv:1504.02432].

[69] D. Kawai, Y. Sato, and K. Yoshida, *Schwinger pair production rate in confining theories via holography*, *Phys. Rev.* **D89** (2014), no. 10 101901, [arXiv:1312.4341].

[70] Y. Sato and K. Yoshida, *Holographic description of the Schwinger effect in electric and magnetic fields*, *JHEP* **04** (2013) 111, [arXiv:1303.0112].

[71] Y. Sato and K. Yoshida, *Universal aspects of holographic Schwinger effect in general backgrounds*, *JHEP* **12** (2013) 051, [arXiv:1309.4629].

[72] Y. Sato and K. Yoshida, *Holographic Schwinger effect in confining phase*, *JHEP* **09** (2013) 134, [arXiv:1306.5512].

[73] D. D. Dietrich, *Worldline holographic Schwinger effect*, *Phys. Rev.* **D90** (2014), no. 4 045024, [arXiv:1405.0487].

[74] K. Hashimoto, T. Oka, and A. Sonoda, *Electromagnetic instability in holographic QCD*, *JHEP* **06** (2015) 001, [arXiv:1412.4254].

[75] M. Ghodrati, *Schwinger Effect and Entanglement Entropy in Confining Geometries*, *Phys. Rev.* **D92** (2015), no. 6 065015, [arXiv:1506.08557].

[76] J. Maldacena and L. Susskind, *Cool horizons for entangled black holes*, *Fortsch. Phys.* **61** (2013) 781–811, [arXiv:1306.0533].

[77] J. Sonner, *Holographic Schwinger Effect and the Geometry of Entanglement*, *Phys. Rev. Lett.* **111** (2013), no. 21 211603, [arXiv:1307.6850].

[78] W. Fischler, P. H. Nguyen, J. F. Pedraza, and W. Tangarife, *Holographic Schwinger effect in de Sitter space*, *Phys. Rev.* **D91** (2015), no. 8 086015, [arXiv:1411.1787].

[79] M. Van Raamsdonk, *Building up spacetime with quantum entanglement*, *Gen. Rel. Grav.* **42** (2010) 2323–2329, [`arXiv:1005.3035`]. [Int. J. Mod. Phys.D19,2429(2010)].

[80] S. Ryu and T. Takayanagi, *Holographic derivation of entanglement entropy from AdS/CFT*, *Phys. Rev. Lett.* **96** (2006) 181602, [`hep-th/0603001`].

[81] S. Ryu and T. Takayanagi, *Aspects of Holographic Entanglement Entropy*, *JHEP* **08** (2006) 045, [`hep-th/0605073`].

[82] R. Ruffini, G. Vereshchagin, and S.-S. Xue, *Electron-positron pairs in physics and astrophysics: from heavy nuclei to black holes*, *Phys. Rept.* **487** (2010) 1–140, [`arXiv:0910.0974`].

[83] A. Di Piazza, C. Müller, K. Hatsagortsyan, and C. Keitel, *Extremely high-intensity laser interactions with fundamental quantum systems*, *Reviews of Modern Physics* **84** (2012), no. 3 1177.

[84] P. N. Arendt, Jr. and J. A. Eilek, *Pair creation in the pulsar magnetosphere*, *Astrophys. J.* **581** (2002) 451–469, [`astro-ph/0207638`].

[85] A. Levinson, D. Melrose, A. Judge, and Q.-h. Luo, *Large-amplitude, pair-creating oscillations in pulsar and black hole magnetospheres*, *Astrophys. J.* **631** (2005) 456–465, [`astro-ph/0503288`].

[86] T. Harko and K. S. Cheng, *Electron-positron pair production in the electrosphere of quark stars*, *Astrophys. J.* **643** (2006) 318–331, [`astro-ph/0601564`].

[87] A. Stebbins and H. Yoo, *Are Crab Nanoshots Schwinger Sparks?*, `arXiv:1505.06400`.

[88] B. i. Cerutti and A. Beloborodov, *Electrodynamics of pulsar magnetospheres*, *Space Sci. Rev.* **207** (2017), no. 1-4 111–136, [`arXiv:1611.04331`].

[89] R. P. Mignani, V. Testa, D. G. Caniulef, R. Taverna, R. Turolla, S. Zane, and K. Wu, *Evidence for vacuum birefringence from the first optical-polarimetry measurement of the isolated neutron star RX J1856.5-3754*, *Mon. Not. Roy. Astron. Soc.* **465** (2017), no. 1 492–500, [`arXiv:1610.08323`].

[90] I. Yu. Kobzarev, L. B. Okun, and M. B. Voloshin, *Bubbles in Metastable Vacuum, Sov. J. Nucl. Phys.* **20** (1975) 644–646. [Yad. Fiz.20,1229(1974)].

[91] S. R. Coleman, *The Fate of the False Vacuum. 1. Semiclassical Theory, Phys. Rev.* **D15** (1977) 2929–2936. [Erratum: Phys. Rev.D16,1248(1977)].

[92] C. G. Callan, Jr. and S. R. Coleman, *The Fate of the False Vacuum. 2. First Quantum Corrections, Phys. Rev.* **D16** (1977) 1762–1768.

[93] I. K. Affleck and F. De Luccia, *Induced Vacuum Decay, Phys. Rev.* **D20** (1979) 3168.

[94] S. R. Coleman and F. De Luccia, *Gravitational Effects on and of Vacuum Decay, Phys. Rev.* **D21** (1980) 3305.

[95] A. D. Linde, *Decay of the False Vacuum at Finite Temperature, Nucl. Phys.* **B216** (1983) 421. [Erratum: Nucl. Phys.B223,544(1983)].

[96] V. A. Rubakov, *Particle creation during vacuum decay, Nucl. Phys.* **B245** (1984) 481–516.

[97] M. B. Fröb, J. Garriga, S. Kanno, M. Sasaki, J. Soda, T. Tanaka, and A. Vilenkin, *Schwinger effect in de sitter space, Journal of Cosmology and Astroparticle Physics* **2014** (2014), no. 04 009.

[98] B. Pioline and J. Troost, *Schwinger pair production in ads2, Journal of High Energy Physics* **2005** (2005), no. 03 043.

[99] S. P. Kim and D. N. Page, *Schwinger pair production in ds_2 and ads_2, Physical Review D* **78** (2008), no. 10 103517.

[100] J. Martin, *Inflationary perturbations: The cosmological schwinger effect*, in *Inflationary Cosmology*, pp. 193–241. Springer, 2008.

[101] R. Dabrowski and G. V. Dunne, *Superadiabatic particle number in Schwinger and de Sitter particle production, Phys. Rev.* **D90** (2014), no. 2 025021, [`arXiv:1405.0302`].

[102] T. Kobayashi and N. Afshordi, *Schwinger Effect in 4D de Sitter Space and Constraints on Magnetogenesis in the Early Universe, JHEP* **10** (2014) 166, [`arXiv:1408.4141`].

[103] S. P. Kim, *Hawking Radiation as Quantum Tunneling in Rindler Coordinate*, *JHEP* **11** (2007) 048, [arXiv:0710.0915].

[104] L. Vanzo, G. Acquaviva, and R. Di Criscienzo, *Tunnelling Methods and Hawking's radiation: achievements and prospects*, *Class. Quant. Grav.* **28** (2011) 183001, [arXiv:1106.4153].

[105] K. Umetsu, *Hawking Radiation from Kerr-Newman Black Hole and Tunneling Mechanism*, *Int. J. Mod. Phys.* **A25** (2010) 4123–4140, [arXiv:0907.1420].

[106] D.-Y. Chen, Q.-Q. Jiang, and X.-T. Zu, *Hawking radiation of Dirac particles via tunnelling from rotating black holes in de Sitter spaces*, *Phys. Lett.* **B665** (2008) 106–110, [arXiv:0804.0131].

[107] D.-Y. Chen, Q.-Q. Jiang, S.-Z. Yang, and X.-T. Zu, *Fermions tunnelling from the charged dilatonic black holes*, *Class. Quant. Grav.* **25** (2008) 205022, [arXiv:0803.3248].

[108] R. Li and J.-R. Ren, *Hawking radiation of Dirac particles via tunneling from Kerr black hole*, *Class. Quant. Grav.* **25** (2008) 125016, [arXiv:0803.1410].

[109] C. K. Dumlu, *Hawking Radiation via Complex Geodesics*, arXiv:1710.07644.

[110] F. Dowker, J. P. Gauntlett, S. B. Giddings, and G. T. Horowitz, *On pair creation of extremal black holes and Kaluza-Klein monopoles*, *Phys. Rev.* **D50** (1994) 2662–2679, [hep-th/9312172].

[111] E. Keski-Vakkuri and P. Kraus, *Tunneling in a time dependent setting*, *Phys. Rev.* **D54** (1996) 7407–7420, [hep-th/9604151].

[112] D. Allor, T. D. Cohen, and D. A. McGady, *The Schwinger mechanism and graphene*, *Phys. Rev.* **D78** (2008) 096009, [arXiv:0708.1471].

[113] M. I. Katsnelson and G. E. Volovik, *Quantum electrodynamics with anisotropic scaling: Heisenberg-Euler action and Schwinger pair production in the bilayer graphene*, *JETP Lett.* **95** (2012) 411–415, [arXiv:1203.1578]. [Pisma Zh. Eksp. Teor. Fiz.95,457(2012)].

[114] M. A. Zubkov, *Schwinger pair creation in multilayer graphene*, *Pisma Zh. Eksp. Teor. Fiz.* **95** (2012) 540, [`arXiv:1204.0138`].

[115] F. Fillion-Gourdeau and S. MacLean, *Time-dependent pair creation and the Schwinger mechanism in graphene*, *Physical Review B* **92** (July, 2015) 035401.

[116] M. F. Linder and R. Schützhold, *Analog Sauter-Schwinger effect in semiconductors*, `arXiv:1503.07108`.

[117] F. Fillion-Gourdeau, D. Gagnon, C. Lefebvre, and S. MacLean, *Time-domain quantum interference in graphene*, *Phys. Rev.* **B94** (2016), no. 12 125423.

[118] T. Oka and H. Aoki, *Ground-state decay rate for the zener breakdown in band and mott insulators*, *Phys. Rev. Lett.* **95** (Sep, 2005) 137601.

[119] N. Szpak and R. Schützhold, *Optical lattice quantum simulator for QED in strong external fields: Spontaneous pair creation and the Sauter-Schwinger effect*, *New J. Phys.* **14** (2012) 035001, [`arXiv:1109.2426`].

[120] F. Dreisow, S. Longhi, S. Nolte, A. Tunnermann, and A. Szameit, *Vacuum Instability and Pair Production in an Optical Setting*, *Phys. Rev. Lett.* **109** (2012) 110401.

[121] V. Kasper, F. Hebenstreit, M. Oberthaler, and J. Berges, *Schwinger pair production with ultracold atoms*, *Phys. Lett.* **B760** (2016) 742–746, [`arXiv:1506.01238`].

[122] V. Kasper, F. Hebenstreit, F. Jendrzejewski, M. K. Oberthaler, and J. Berges, *Implementing quantum electrodynamics with ultracold atomic systems*, *New J. Phys.* **19** (2017), no. 2 023030, [`arXiv:1608.03480`].

[123] R. A. Abramchuk and M. A. Zubkov, *Schwinger pair creation in Dirac semimetals in the presence of external magnetic and electric fields*, *Phys. Rev.* **D94** (2016), no. 11 116012, [`arXiv:1605.02379`].

[124] M. J. Strassler, *Field theory without Feynman diagrams: One loop effective actions*, *Nucl. Phys.* **B385** (1992) 145–184, [`hep-ph/9205205`].

[125] C. Schubert, *Perturbative quantum field theory in the string inspired formalism*, *Phys. Rept.* **355** (2001) 73–234, [`hep-th/0101036`].

[126] F. Hebenstreit, J. Berges, and D. Gelfand, *Simulating fermion production in 1+1 dimensional QED*, *Physical Review D* **87** (May, 2013) 105006, [`arXiv:1302.5537`].

[127] V. Kasper, F. Hebenstreit, and J. Berges, *Fermion production from real-time lattice gauge theory in the classical-statistical regime*, *Phys. Rev.* **D90** (2014), no. 2 025016, [`arXiv:1403.4849`].

[128] G. V. Dunne and M. Ünsal, *Uniform WKB, Multi-instantons, and Resurgent Trans-Series*, *Phys. Rev.* **D89** (2014), no. 10 105009, [`arXiv:1401.5202`].

[129] G. V. Dunne and M. Ünsal, *What is QFT? Resurgent trans-series, Lefschetz thimbles, and new exact saddles*, *PoS* **LATTICE2015** (2016) 010, [`arXiv:1511.05977`].

[130] G. V. Dunne and M. Ünsal, *New Nonperturbative Methods in Quantum Field Theory: From Large-N Orbifold Equivalence to Bions and Resurgence*, *Ann. Rev. Nucl. Part. Sci.* **66** (2016) 245–272, [`arXiv:1601.03414`].

[131] M. Cristoforetti, F. Di Renzo, A. Mukherjee, and L. Scorzato, *Quantum field theories on the Lefschetz thimble*, *PoS* **LATTICE2013** (2014) 197, [`arXiv:1312.1052`].

[132] A. Alexandru, G. Başar, and P. Bedaque, *Monte Carlo algorithm for simulating fermions on Lefschetz thimbles*, *Phys. Rev.* **D93** (2016), no. 1 014504, [`arXiv:1510.03258`].

[133] S. P. Kim and D. N. Page, *Schwinger pair production via instantons in strong electric fields*, *Physical Review D* **65** (May, 2002) 105002, [`hep-th/0005078`].

[134] S. P. Kim and D. N. Page, *Schwinger pair production in electric and magnetic fields*, *Phys. Rev.* **D73** (2006) 065020, [`hep-th/0301132`].

[135] G. V. Dunne, *Heisenberg-Euler effective Lagrangians: Basics and extensions*, in *From fields to strings: Circumnavigating theoretical physics.*

Ian Kogan memorial collection (3 volume set) (M. Shifman, A. Vainshtein, and J. Wheater, eds.), pp. 445–522. 2004. `hep-th/0406216`.

[136] M. Ruf, G. R. Mocken, C. Müller, K. Z. Hatsagortsyan, and C. H. Keitel, *Pair production in laser fields oscillating in space and time*, *Phys. Rev. Lett.* **102** (2009) 080402, [`arXiv:0810.4047`].

[137] F. Hebenstreit, R. Alkofer, and H. Gies, *Schwinger pair production in space- and time-dependent electric fields: Relating the Wigner formalism to quantum kinetic theory*, *Physical Review D* **82** (Nov., 2010) 105026, [`arXiv:1007.1099`].

[138] F. Hebenstreit, R. Alkofer, and H. Gies, *Particle self-bunching in the Schwinger effect in spacetime-dependent electric fields*, *Phys. Rev. Lett.* **107** (2011) 180403, [`arXiv:1106.6175`].

[139] I. A. Aleksandrov, G. Plunien, and V. M. Shabaev, *Electron-positron pair production in external electric fields varying both in space and time*, *Phys. Rev.* **D94** (2016), no. 6 065024, [`arXiv:1606.06313`].

[140] I. A. Aleksandrov, G. Plunien, and V. M. Shabaev, *Dynamically assisted Schwinger effect beyond the spatially-uniform-field approximation*, `arXiv:1805.07579`.

[141] V. S. Popov, *Production of e+e- Pairs in an Alternating External Field*, *JETP Lett.* **13** (1971) 185–187. [Pisma Zh. Eksp. Teor. Fiz.13,261(1971)].

[142] E. Brezin and C. Itzykson, *Pair production in vacuum by an alternating field*, *Phys. Rev.* **D2** (1970) 1191–1199.

[143] M. S. Marinov and V. S. Popov, *Electron-Positron Pair Creation from Vacuum Induced by Variable Electric Field*, *Fortsch. Phys.* **25** (1977) 373–400.

[144] X. Bai-Song, M. Melike, and D. Sayipjamal, *Electron-positron pair production in an elliptic polarized time varying field*, *Chinese Physics Letters* **29** (2012), no. 2 021102.

[145] D. D. Dietrich, *Fermion production in time dependent fields*, *Phys. Rev.* **D68** (2003) 105005, [`hep-th/0302229`].

[146] G. V. Dunne and C. Schubert, *Worldline instantons and pair production in inhomogeneous fields*, Phys. Rev. **D72** (2005) 105004, [`hep-th/0507174`].

[147] H. Kleinert, R. Ruffini, and S.-S. Xue, *Electron-Positron Pair Production in Space- or Time-Dependent Electric Fields*, Phys. Rev. **D78** (2008) 025011, [`arXiv:0807.0909`].

[148] S. P. Kim and C. Schubert, *Non-adiabatic Quantum Vlasov Equation for Schwinger Pair Production*, Phys. Rev. **D84** (2011) 125028, [`arXiv:1110.0900`].

[149] A. Chervyakov and H. Kleinert, *Exact Pair Production Rate for a Smooth Potential Step*, Phys. Rev. **D80** (2009) 065010, [`arXiv:0906.1422`].

[150] H. Kleinert and S.-S. Xue, *Electron-positron pair productions in classical electric field and electromagnetic wave*, Annals Phys. **333** (2013) 104–126, [`arXiv:1207.0401`].

[151] E. Strobel and S.-S. Xue, *Semiclassical pair production rate for time-dependent electrical fields with more than one component: WKB-approach and world-line instantons*, Nucl. Phys. **B886** (2014) 1153–1176, [`arXiv:1312.3261`].

[152] C. Schneider and R. Schützhold, *Dynamically assisted Sauter-Schwinger effect in inhomogeneous electric fields*, JHEP **02** (2016) 164, [`arXiv:1407.3584`].

[153] T. C. Adorno, S. P. Gavrilov, and D. M. Gitman, *Exactly solvable cases in QED with t-electric potential steps*, Int. J. Mod. Phys. **A32** (2017), no. 18 1750105, [`arXiv:1512.01288`].

[154] A. Ilderton, G. Torgrimsson, and J. Wårdh, *Nonperturbative pair production in interpolating fields*, Phys. Rev. **D92** (2015), no. 6 065001, [`arXiv:1506.09186`].

[155] T. C. Adorno, S. P. Gavrilov, and D. M. Gitman, *Particle creation by peak electric field*, Eur. Phys. J. **C76** (2016), no. 8 447, [`arXiv:1605.09072`].

[156] T. C. Adorno, R. Ferreira, S. P. Gavrilov, and D. M. Gitman, *Role of switching-on and -off effects in the vacuum instability*, Int. J. Mod. Phys. **A33** (2018), no. 11 1850060, [`arXiv:1802.08850`].

[157] A. Goriely, *Integrability and nonintegrability of dynamical systems*, vol. 19. World Scientific, 2001.

[158] I. K. Affleck, O. Alvarez, and N. S. Manton, *Pair Production at Strong Coupling in Weak External Fields*, *Nucl. Phys.* **B197** (1982) 509–519.

[159] G. V. Dunne, Q.-h. Wang, H. Gies, and C. Schubert, *Worldline instantons. II. The Fluctuation prefactor*, *Phys. Rev.* **D73** (2006) 065028, [hep-th/0602176].

[160] C. K. Dumlu and G. V. Dunne, *Complex Worldline Instantons and Quantum Interference in Vacuum Pair Production*, *Phys. Rev.* **D84** (2011) 125023, [arXiv:1110.1657].

[161] J. Gordon and G. W. Semenoff, *World-line instantons and the Schwinger effect as a Wentzel-Kramers-Brillouin exact path integral*, *J. Math. Phys.* **56** (2015) 022111, [arXiv:1407.0987].

[162] A. Ilderton, *Localisation in worldline pair production and lightfront zero-modes*, *JHEP* **09** (2014) 166, [arXiv:1406.1513].

[163] J. Gordon and G. W. Semenoff, *Schwinger pair production: Explicit Localization of the world-line instanton*, arXiv:1612.05909.

[164] E. Silverstein, *Duality, compactification, and $e^{-1/lambda}$ effects in the heterotic string theory*, *Phys. Lett.* **B396** (1997) 91–96, [hep-th/9611195].

[165] G. Başar and G. V. Dunne, *Resurgence and the Nekrasov-Shatashvili limit: connecting weak and strong coupling in the Mathieu and Lamé systems*, *JHEP* **02** (2015) 160, [arXiv:1501.05671].

[166] M. C. Gutzwiller, *Periodic orbits and classical quantization conditions*, *J. Math. Phys.* **12** (1971) 343–358.

[167] R. G. Littlejohn, *Semiclassical structure of trace formulas*, *Journal of Mathematical Physics* **31** (Dec., 1990) 2952–2977.

[168] R. Aurich and F. Steiner, *On the Periodic Orbits of a Strongly Chaotic System*, *Physica* **D32** (1988) 451–460.

[169] M. Sieber and F. Steiner, *Generalized periodic-orbit sum rules for strongly chaotic systems*, *Physics Letters A* **144** (1990), no. 3 159 – 163.

[170] P. Richens and M. Berry, *Pseudointegrable systems in classical and quantum mechanics*, *Physica D: Nonlinear Phenomena* **2** (1981), no. 3 495 – 512.

[171] S. Müller, S. Heusler, P. Braun, F. Haake, and A. Altland, *Semiclassical foundation of universality in quantum chaos*, *Physical review letters* **93** (2004), no. 1 014103.

[172] S. Müller, S. Heusler, A. Altland, P. Braun, and F. Haake, *Periodic-orbit theory of universal level correlations in quantum chaos*, *New Journal of Physics* **11** (2009), no. 10 103025.

[173] D. D. Dietrich and G. V. Dunne, *Gutzwiller's trace formula and vacuum pair production*, *J. Phys.* **A40** (2007) F825–F830, [`arXiv:0706.4006`].

[174] M. V. Berry and M. Tabor, *Closed orbits and the regular bound spectrum*, .

[175] P. Muratore-Ginanneschi, *Path integration over closed loops and Gutzwiller's trace formula*, *Phys. Rept.* **383** (2003) 299–397, [`nlin/0210047`].

[176] B. K. Shivamoggi, *Nonlinear dynamics and chaotic phenomena: An introduction*, vol. 103. Springer, 2014.

[177] A. H. Castro Neto, F. Guinea, N. M. R. Peres, K. S. Novoselov, and A. K. Geim, *The electronic properties of graphene*, *Reviews of Modern Physics* **81** (Jan., 2009) 109–162, [`arXiv:0709.1163`].

[178] T. Wehling, A. M. Black-Schaffer, and A. V. Balatsky, *Dirac materials*, *Advances in Physics* **63** (2014), no. 1 1–76.

[179] K. S. Novoselov, A. K. Geim, S. V. Morozov, D. Jiang, Y. Zhang, S. V. Dubonos, I. V. Grigorieva, and A. A. Firsov, *Electric Field Effect in Atomically Thin Carbon Films*, *Science* **306** (Oct., 2004) 666–669, [`cond-mat/0410550`].

[180] K. S. Novoselov, D. Jiang, F. Schedin, T. J. Booth, V. V. Khotkevich, S. V. Morozov, and A. K. Geim, *Two-dimensional atomic crystals*, *Proceedings of the National Academy of Science* **102** (July, 2005) 10451–10453, [`cond-mat/0503533`].

[181] K. S. Novoselov, A. K. Geim, S. V. Morozov, D. Jiang, M. I. Katsnelson, I. V. Grigorieva, S. V. Dubonos, and A. A. Firsov, *Two-dimensional gas of massless Dirac fermions in graphene*, Nature **438** (Nov., 2005) 197–200, [cond-mat/0509330].

[182] V. N. Kotov, B. Uchoa, V. M. Pereira, F. Guinea, and A. H. Castro Neto, *Electron-Electron Interactions in Graphene: Current Status and Perspectives*, Reviews of Modern Physics **84** (July, 2012) 1067–1125, [arXiv:1012.3484].

[183] D. N. Basov, M. M. Fogler, A. Lanzara, F. Wang, and Y. Zhang, *Colloquium: Graphene spectroscopy*, Reviews of Modern Physics **86** (July, 2014) 959–994, [arXiv:1407.6721].

[184] P. R. Wallace, *The Band Theory of Graphite*, Physical Review **71** (May, 1947) 622–634.

[185] M. Katsnelson and K. Novoselov, *Graphene: New bridge between condensed matter physics and quantum electrodynamics*, Solid State Communications **143** (2007), no. 1-2 3–13.

[186] M. Franz and Z. Tešanović, *Algebraic fermi liquid from phase fluctuations:"topological" fermions, vortex "berryons," and qed 3 theory of cuprate superconductors*, Physical Review Letters **87** (2001), no. 25 257003.

[187] S. Cahangirov, M. Topsakal, E. Aktürk, H. Şahin, and S. Ciraci, *Two-and one-dimensional honeycomb structures of silicon and germanium*, Physical review letters **102** (2009), no. 23 236804.

[188] M. Hasan, *Mz hasan and cl kane, rev. mod. phys. 82, 3045 (2010).*, Rev. Mod. Phys. **82** (2010) 3045.

[189] C. L. Kane and E. J. Mele, *Z 2 topological order and the quantum spin hall effect*, Physical review letters **95** (2005), no. 14 146802.

[190] J. E. Moore and L. Balents, *Topological invariants of time-reversal-invariant band structures*, Physical Review B **75** (2007), no. 12 121306.

[191] M. König, S. Wiedmann, C. Brüne, A. Roth, H. Buhmann, L. W. Molenkamp, X.-L. Qi, and S.-C. Zhang, *Quantum spin hall insulator state in hgte quantum wells*, *Science* **318** (2007), no. 5851 766–770.

[192] Y. Xia, D. Qian, D. Hsieh, L. Wray, A. Pal, H. Lin, A. Bansil, D. Grauer, Y. S. Hor, R. J. Cava, et al., *Observation of a large-gap topological-insulator class with a single dirac cone on the surface*, *Nature physics* **5** (2009), no. 6 398.

[193] X.-L. Qi and S.-C. Zhang, *The quantum spin hall effect and topological insulators*, *arXiv preprint arXiv:1001.1602* (2010).

[194] P. Soltan-Panahi, J. Struck, P. Hauke, A. Bick, W. Plenkers, G. Meineke, C. Becker, P. Windpassinger, M. Lewenstein, and K. Sengstock, *Multi-component quantum gases in spin-dependent hexagonal lattices*, *Nature Physics* **7** (2011), no. 5 434.

[195] L. Tarruell, D. Greif, T. Uehlinger, G. Jotzu, and T. Esslinger, *Creating, moving and merging dirac points with a fermi gas in a tunable honeycomb lattice*, *Nature* **483** (2012), no. 7389 302.

[196] M. I. Katsnelson, K. S. Novoselov, and A. K. Geim, *Chiral tunnelling and the Klein paradox in graphene*, *Nature Physics* **2** (Sept., 2006) 620–625, [cond-mat/0604323].

[197] A. De Martino, D. Klöpfer, D. Matrasulov, and R. Egger, *Electric-Dipole-Induced Universality for Dirac Fermions in Graphene*, *Physical Review Letters* **112** (May, 2014) 186603, [arXiv:1401.5992].

[198] M. Lewkowicz and B. Rosenstein, *Dynamics of Particle-Hole Pair Creation in Graphene*, *Physical Review Letters* **102** (Mar., 2009) 106802, [arXiv:0901.1476].

[199] M. Lewkowicz, H. C. Kao, and B. Rosenstein, *Signature of the Schwinger pair creation rate via radiation generated in graphene by a strong electric current*, *Physical Review B* **84** (July, 2011) 035414, [arXiv:1105.3489].

[200] N. Yokomizo, *Radiation from electrons in graphene in strong electric field*, *Annals of Physics* **351** (Dec., 2014) 166–199, [arXiv:1405.1070].

[201] B. Dóra and R. Moessner, *Nonlinear electric transport in graphene: Quantum quench dynamics and the Schwinger mechanism*, *Physical Review B* **81** (Apr., 2010) 165431, [`arXiv:0909.2528`].

[202] B. Dóra and R. Moessner, *Dynamics of the spin Hall effect in topological insulators and graphene*, *Physical Review B* **83** (Feb., 2011) 073403, [`arXiv:1008.0531`].

[203] G. L. Klimchitskaya and V. M. Mostepanenko, *Creation of quasiparticles in graphene by a time-dependent electric field*, *Physical Review D* **87** (June, 2013) 125011, [`arXiv:1305.5700`].

[204] H. K. Avetissian, A. K. Avetissian, G. F. Mkrtchian, and K. V. Sedrakian, *Creation of particle-hole superposition states in graphene at multiphoton resonant excitation by laser radiation*, *Physical Review B* **85** (Mar., 2012) 115443, [`arXiv:1112.2905`].

[205] S. Y. Zhou, G.-H. Gweon, A. V. Fedorov, P. N. First, W. A. de Heer, D.-H. Lee, F. Guinea, A. H. Castro Neto, and A. Lanzara, *Substrate-induced bandgap opening in epitaxial graphene*, *Nature Materials* **6** (Oct., 2007) 770–775.

[206] G. Giovannetti, P. A. Khomyakov, G. Brocks, P. J. Kelly, and J. van den Brink, *Substrate-induced band gap in graphene on hexagonal boron nitride: Ab initio density functional calculations*, *Physical Review B* **76** (Aug., 2007) 073103, [`arXiv:0704.1994`].

[207] A. Varykhalov, J. Sánchez-Barriga, A. M. Shikin, C. Biswas, E. Vescovo, A. Rybkin, D. Marchenko, and O. Rader, *Electronic and Magnetic Properties of Quasifreestanding Graphene on Ni*, *Physical Review Letters* **101** (Oct., 2008) 157601.

[208] Z. Fried and J. H. Eberly, *Scattering of a high-intensity, low-frequency electromagnetic wave by an unbound electron*, *Physical Review* **136** (1964), no. 3B B871.

[209] J. H. Eberly and H. R. Reiss, *Electron self-energy in intense plane-wave field*, *Physical Review* **145** (1966), no. 4 1035.

[210] J. H. Eberly, *Vii interaction of very intense light with free electrons*, in *Progress in Optics*, vol. 7, pp. 359–415. Elsevier, 1969.

[211] R. Neville and F. Rohrlich, *Quantum electrodynamics on null planes and applications to lasers*, *Physical Review D* **3** (1971), no. 8 1692.

[212] F. Rohrlich, *Null plane field theory*, in *Concepts in Hadron Physics*, pp. 277–322. Springer, 1971.

[213] W. Furry, *On bound states and scattering in positron theory*, *Physical Review* **81** (1951), no. 1 115.

[214] E. Fradkin and D. Gitman, *Furry picture for quantum electrodynamics with pair-creating external field*, *Fortschritte der Physik* **29** (1981), no. 9 381–411.

[215] A. Nikishov and V. Ritus, *Quantum processes in the field of a plane electromagnetic wave and in a constant field*, *Sov. Phys. JETP* **19** (1964), no. 529 1191.

[216] A. Nikishov and V. Ritus, *Quantum processes in the field of a plane electromagnetic wave and in a constant field 1*, *Zh. Eksp. Teor. Fiz.* **19** (1964) 529–541.

[217] A. Nikishov and V. Ritus, *Quantum processes in the field of a plane electromagnetic wave and in a constant field 2*, *Zh. Eksp. Teor. Fiz.* **19** (1964) 1768–1781.

[218] T. Kibble, *Frequency shift in high-intensity compton scattering*, *Physical Review* **138** (1965), no. 3B B740.

[219] T. Heinzl and A. Ilderton, *Superintegrable relativistic systems in spacetime-dependent background fields*, *J. Phys.* **A50** (2017), no. 34 345204, [arXiv:1701.09168].

[220] H. Mitter, *Quantum electrodynamics in laser fields*, in *Electromagnetic Interactions and Field Theory*, pp. 397–468. Springer, 1975.

[221] V. Ritus, *Quantum effects of the interaction of elementary particles with an intense electromagnetic field*, *Journal of Soviet Laser Research* **6** (1985), no. 5 497–617.

[222] E. S. Fradkin, D. M. Gitman, and S. M. Shvartsman, *Quantum electrodynamics with unstable vacuum.* Springer, 1991.

[223] R. J. Glauber, *Coherent and incoherent states of the radiation field,* *Physical Review* **131** (1963), no. 6 2766.

[224] R. J. Glauber, *The quantum theory of optical coherence,* *Physical Review* **130** (1963), no. 6 2529.

[225] T. Kibble, *Coherent soft-photon states and infrared divergences. i. classical currents,* *Journal of Mathematical Physics* **9** (1968), no. 2 315–324.

[226] T. Kibble, *Coherent soft-photon states and infrared divergences. ii. mass-shell singularities of green's functions,* *Physical Review* **173** (1968), no. 5 1527.

[227] W.-M. Zhang, R. Gilmore, et al., *Coherent states: theory and some applications,* *Reviews of Modern Physics* **62** (1990), no. 4 867.

[228] E. Schrödinger, *Der stetige übergang von der mikro-zur makromechanik,* *Naturwissenschaften* **14** (1926), no. 28 664–666.

[229] M. D. Schwartz, *Quantum field theory and the standard model.* Cambridge University Press, 2014.

[230] J.-P. Gazeau, *Coherent states in quantum physics.* Wiley, 2009.

[231] T. Lee, F. Low, and D. Pines, *The motion of slow electrons in a polar crystal,* *Physical Review* **90** (1953), no. 2 297.

[232] J. Valatin and D. Butler, *On the collective properties of a boson system,* *Il Nuovo Cimento (1955-1965)* **10** (1958), no. 1 37–54.

[233] P. W. Anderson, *Coherent excited states in the theory of superconductivity: Gauge invariance and the meissner effect,* *Physical review* **110** (1958), no. 4 827.

[234] J. Schwinger, *On the green's functions of quantized fields. i,* *Proceedings of the National Academy of Sciences* **37** (1951), no. 7 452–455.

[235] J. Schwinger, *On the green's functions of quantized fields. ii,* *Proceedings of the National Academy of Sciences* **37** (1951), no. 7 455–459.

[236] J. Schwinger, *The theory of quantized fields. iii*, *Physical Review* **91** (1953), no. 3 728.

[237] J. Schwinger, *The theory of quantized fields. vi*, *Physical Review* **94** (1954), no. 5 1362.

[238] P. K. Rashevskii, *On the mathematical foundations of quantum electrodynamics*, *Uspekhi Matematicheskikh Nauk* **13** (1958), no. 3 3–110.

[239] J. R. Klauder, *The action option and a feynman quantization of spinor fields in terms of ordinary c-numbers*, *Annals of Physics* **11** (1960), no. 2 123–168.

[240] E. Sudarshan, *Equivalence of semiclassical and quantum mechanical descriptions of statistical light beams*, *Physical Review Letters* **10** (1963), no. 7 277.

[241] S. Bo-sture et al., *Coherent states: applications in physics and mathematical physics.* World scientific, 1985.

[242] A. Perelomov, *Generalized coherent states and their applications.* Springer Science & Business Media, 2012.

[243] J. R. Klauder and E. C. G. Sudarshan, *Fundamentals of quantum optics.* Courier Corporation, 2006.

[244] M. O. Scully and M. S. Zubairy, *Quantum optics.* Cambridge university press, 1997.

[245] D. Feng, J. Klauder, and M. Strayer, *Coherent states: Past, present and future*, in *Proceedings of the 1993 Oak Ridge Conference. World Scientific, Singapore*, 1994.

[246] S. Weinberg, *The quantum theory of fields*, vol. 1. Cambridge university press, 1995.

[247] M. E. Peskin and D. V. Schroeder, *An introduction to quantum field theory.* Westview press, 1995.

[248] S. N. Gupta, *Theory of longitudinal photons in quantum electrodynamics*, *Proceedings of the Physical Society. Section A* **63** (1950), no. 7 681.

[249] K. Bleuler, *Eine neue methode zur behandlung der longitudinalen und skalaren photonen*, *Helvetica Physica Acta* **23** (1950), no. 5 567–586.

[250] C. Itzykson and J.-B. Zuber, *Quantum field theory*. Courier Corporation, 2006.

[251] M. Srednicki, *Quantum field theory*. Cambridge University Press, 2007.

[252] M. Kaku, *Quantum field theory: a modern introduction*. Oxford Univ. Press, 1993.

[253] W.-M. Zhang, *Coherent states in field theory, arXiv preprint hep-th/9908117* (1999).

[254] V. Yanovsky, V. Chvykov, G. Kalinchenko, P. Rousseau, T. Planchon, T. Matsuoka, A. Maksimchuk, J. Nees, G. Cheriaux, G. Mourou, et al., *Ultra-high intensity-300-tw laser at 0.1 hz repetition rate.*, *Optics Express* **16** (2008), no. 3 2109–2114.

[255] A. V. Korzhimanov, A. A. Gonoskov, E. A. Khazanov, and A. M. Sergeev, *Horizons of petawatt laser technology*, *Physics-Uspekhi* **54** (2011), no. 1 9–28.

[256] A. Ringwald, *Pair production from vacuum at the focus of an X-ray free electron laser*, *Phys. Lett.* **B510** (2001) 107–116, [hep-ph/0103185].

[257] A. Hewish, *Pulsars*, *Annual Review of Astronomy and Astrophysics* **8** (1970), no. 1 265–296.

[258] C. Kouveliotou, S. Dieters, T. Strohmayer, J. Van Paradijs, G. Fishman, C. Meegan, K. Hurley, J. Kommers, I. Smith, D. Frail, et al., *An x-ray pulsar with a superstrong magnetic field in the soft γ-ray repeater sgr1806-20*, *Nature* **393** (1998), no. 6682 235.

[259] S. Mereghetti, *The strongest cosmic magnets: soft gamma-ray repeaters and anomalous x-ray pulsars*, *The Astronomy and Astrophysics Review* **15** (2008), no. 4 225–287.

[260] A. K. Harding, *The physics of gamma-ray bursts*, *Physics Reports* **206** (1991), no. 6 327–391.

[261] T. Behnke, J. E. Brau, B. Foster, J. Fuster, M. Harrison, J. M. Paterson, M. Peskin, M. Stanitzki, N. Walker, and H. Yamamoto, *The International Linear Collider Technical Design Report - Volume 1: Executive Summary*, `arXiv:1306.6327`.

[262] A. Hartin, G. Moortgat-Pick, and S. Porto, *Strong field effects on physics processes at the Interaction Point of future linear colliders*, *PoS* **ICHEP2012** (2013) 480, [`arXiv:1304.2632`].

[263] J. Esberg, U. I. Uggerhoj, B. Dalena, and D. Schulte, *Strong field processes in beam-beam interactions at the Compact Linear Collider*, *Phys. Rev. ST Accel. Beams* **17** (2014), no. 5 051003.

[264] J. Rafelski, J. Kirsch, B. Müller, J. Reinhardt, and W. Greiner, *Probing QED Vacuum with Heavy Ions*, *FIAS Interdisc. Sci. Ser.* **9783319441658** (2017) 211–251, [`arXiv:1604.08690`].

[265] G. Soff, B. Müller, and J. Rafelski, *Precise values for critical fields in quantum electrodynamics*, *Zeitschrift für Naturforschung A* **29** (1974), no. 9 1267–1275.

[266] W. Greiner, B. Müller, and J. Rafelski, *Quantum Electrodynamics of Strong Fields: With an Introduction into Modern Relativistic Quantum Mechanics*. Theoretical and Mathematical Physics. Springer Berlin Heidelberg, 2012.

[267] C. D. Roberts and S. M. Schmidt, *Dyson-Schwinger equations: Density, temperature and continuum strong QCD*, *Prog. Part. Nucl. Phys.* **45** (2000) S1–S103, [`nucl-th/0005064`].

[268] F. Sauter, *Über das verhalten eines elektrons im homogenen elektrischen feld nach der relativistischen theorie diracs*, *Zeitschrift für Physik* **69** (1931), no. 11-12 742–764.

[269] W. Heisenberg and H. Euler, *Consequences of Dirac's theory of positrons*, *Z. Phys.* **98** (1936) 714–732, [`physics/0605038`].

[270] J. Schwinger, *On gauge invariance and vacuum polarization*, *Physical Review* **82** (1951), no. 5 664.

[271] W. Dittrich and M. Reuter, *Effective Lagrangians In Quantum Electrodynamics*, *Lect. Notes Phys.* **220** (1985) 1–244.

[272] J. Schwinger, *Quantum electrodynamics. ii. vacuum polarization and self-energy*, *Physical Review* **75** (1949), no. 4 651.

[273] C. Schubert, *Qed in the worldline representation*, in *AIP Conference Proceedings*, vol. 917, pp. 178–194, AIP, 2007.

[274] C. Schubert, *Schwinger pair creation of particles and strings*, *arXiv preprint arXiv:1103.0243* (2011).

[275] H. Euler and B. Köckel, *On the scattering of light by light in dirac's theory*, *Naturwiss* **23** (1935) 246.

[276] V. Weisskopf, *The electrodynamics of the vacuum based on the quantum theory of the electron*, *Kong. Dan. Vid. Sel. Mat. Fys. Med.* **14N6** (1936) 1–39.

[277] C. Schubert, *An introduction to the worldline technique for quantum field theory calculations*, *arXiv preprint hep-th/9610108* (1996).

[278] G. V. Dunne, *The heisenberg–euler effective action: 75 years on*, *International Journal of Modern Physics A* **27** (2012), no. 15 1260004.

[279] I. Huet, D. McKeon, and C. Schubert, *Euler-heisenberg lagrangians and asymptotic analysis in 1+ 1 qed. part i: two-loop*, *Journal of High Energy Physics* **2010** (2010), no. 12 36.

[280] I. Huet, M. R. de Traubenberg, and C. Schubert, *The euler-heisenberg lagrangian beyond one loop*, in *International Journal of Modern Physics: Conference Series*, vol. 14, pp. 383–393, World Scientific, 2012.

[281] G. V. Dunne and C. Schubert, *Multiloop information from the qed effective lagrangian*, in *Journal of Physics: Conference Series*, vol. 37, p. 59, IOP Publishing, 2006.

[282] H. Gies and F. Karbstein, *An Addendum to the Heisenberg-Euler effective action beyond one loop*, *JHEP* **03** (2017) 108, [arXiv:1612.07251].

[283] J. P. Edwards and C. Schubert, *One-particle reducible contribution to the one-loop scalar propagator in a constant field*, *Nucl. Phys.* **B923** (2017) 339–349, [arXiv:1704.00482].

[284] N. Ahmadiniaz, F. Bastianelli, O. Corradini, J. P. Edwards, and C. Schubert, *One-particle reducible contribution to the one-loop spinor propagator in a constant field*, Nucl. Phys. **B924** (2017) 377–386, [arXiv:1704.05040].

[285] W. H. Furry, *A symmetry theorem in the positron theory*, Physical Review **51** (1937), no. 2 125.

[286] A. Ringwald, *Fundamental physics at an x-ray free electron laser*, in *Electromagnetic Probes Of Fundamental Physics: (With CD-ROM)*, pp. 63–74. World Scientific, 2003.

[287] A. Ringwald, *Boiling the vacuum with an x-ray free electron laser*, in *Quantum Aspects of Beam Physics 2003*, pp. 149–163. World Scientific, 2004.

[288] G. V. Dunne and T. M. Hall, *Borel summation of the derivative expansion and effective actions*, Physical Review D **60** (1999), no. 6 065002.

[289] G. Dunne and T. Hall, *Qed effective action in time dependent electric backgrounds*, Physical Review D **58** (1998), no. 10 105022.

[290] L. Sriramkumar and T. Padmanabhan, *Does a nonzero tunneling probability imply particle production in time independent classical electromagnetic backgrounds?*, Phys. Rev. **D54** (1996) 7599–7606, [hep-th/9604111].

[291] V. Popov, *Pis' ma zh. eksp. teor. fiz. 18 453 (1973)*, JETP Lett **18** (1973) 255.

[292] R. P. Feynman, *Mathematical formulation of the quantum theory of electromagnetic interaction*, Phys. Rev. **80** (1950) 440–457.

[293] A. M. Polyakov, *Gauge fields and strings*, Physics Today **42** (1989) 100.

[294] Z. Bern and D. A. Kosower, *The Computation of loop amplitudes in gauge theories*, Nucl. Phys. **B379** (1992) 451–561.

[295] J. Scherk, *An introduction to the theory of dual models and strings*, Reviews of Modern Physics **47** (1975), no. 1 123.

[296] R. Metsaev and A. A. Tseytlin, *On loop corrections to string theory effective actions*, Nuclear Physics B **298** (1988), no. 1 109–132.

[297] R. I. Nepomechie, *Remarks on quantized yang-mills theory in 26 dimensions*, *Physics Letters B* **128** (1983), no. 3-4 177–178.

[298] Z. Bern, L. Dixon, D. C. Dunbar, and D. A. Kosower, *One-loop n-point gauge theory amplitudes, unitarity and collinear limits*, *Nuclear Physics B* **425** (1994), no. 1-2 217–260.

[299] Z. Bern, L. Dixon, D. C. Dunbar, and D. A. Kosower, *Fusing gauge theory tree amplitudes into loop amplitudes*, *Nuclear Physics B* **435** (1995), no. 1-2 59–101.

[300] K. Daikouji, M. Shino, and Y. Sumino, *Bern-kosower rule for scalar qed*, *Physical Review D* **53** (1996), no. 8 4598.

[301] Z. Bern and D. C. Dunbar, *A mapping between feynman and string motivated one-loop rules in gauge theories*, *Nuclear Physics B* **379** (1992), no. 3 562–601.

[302] Z. Bern, D. C. Dunbar, and T. Shimada, *String-based methods in perturbative gravity*, *Physics Letters B* **312** (1993), no. 3 277–284.

[303] K. Roland, *Multiloop gluon amplitudes in pure gauge theories*, *Physics Letters B* **289** (1992), no. 1-2 148–152.

[304] P. Di Vecchia, L. Magnea, A. Lerda, R. Marotta, and R. Russo, *Two-loop scalar diagrams from string theory*, *Physics Letters B* **388** (1996), no. 1 65–76.

[305] E. Fradkin and A. A. Tseytlin, *Non-linear electrodynamics from quantized strings*, *Physics Letters B* **163** (1985), no. 1-4 123–130.

[306] M. G. Schmidt and C. Schubert, *Worldline green functions for multiloop diagrams*, *Physics Letters B* **331** (1994), no. 1-2 69–76.

[307] M. G. Schmidt and C. Schubert, *Multiloop calculations in the string-inspired formalism: The single spinor loop in qed*, *Physical Review D* **53** (1996), no. 4 2150.

[308] M. Reuter, M. G. Schmidt, and C. Schubert, *Constant external fields in gauge theory and the spin 0, $\frac{1}{2}$, 1 path integrals*, *Annals of Physics* **259** (1997), no. 2 313–365.

[309] M. G. Schmidt and C. Schubert, *On the calculation of effective actions by string methods*, *Physics Letters B* **318** (1993), no. 3 438–446.

[310] H. Kleinert, *Path integrals in quantum mechanics, statistics, polymer physics, and financial markets*. World scientific, 2009.

[311] W. Dittrich and M. Reuter, *Classical and quantum dynamics*, vol. 20. Springer, 1994.

[312] R. P. Feynman and M. Gell-Mann, *Theory of the fermi interaction*, *Physical Review* **109** (1958), no. 1 193.

[313] A. O. Barut and I. H. Duru, *Path integral formulation of quantum electrodynamics from classical particle trajectories*, *Physics Reports* **172** (1989), no. 1 1–32.

[314] E. D'Hoker and D. G. Gagne, *Worldline path integrals for fermions with general couplings*, *Nuclear Physics B* **467** (1996), no. 1-2 297–312.

[315] E. D'Hoker and D. G. Gagne, *Worldline path integrals for fermions with scalar, pseudoscalar and vector couplings*, *Nuclear Physics B* **467** (1996), no. 1-2 272–296.

[316] Y. Ohnuki and T. Kashiwa, *Coherent states of fermi operators and the path integral*, *Progress of Theoretical Physics* **60** (1978), no. 2 548–564.

[317] J. Henty, P. S. Howe, and P. Townsend, *Quantum mechanics of the relativistic spinning particle*, *Classical and Quantum Gravity* **5** (1988), no. 5 807.

[318] E. Fradkin, *Application of functional methods in quantum field theory and quantum statistics (ii)*, *Nuclear Physics* **76** (1966), no. 3 588–624.

[319] R. Casalbuoni, *The classical mechanics for bose-fermi systems*, *Il Nuovo Cimento A (1965-1970)* **33** (1976), no. 3 389–431.

[320] A. Barducci, F. Bordi, and R. Casalbuoni, *Path integral quantization of spinning particles interacting with crossed external electromagnetic fields*, *Il Nuovo Cimento B (1971-1996)* **64** (1981), no. 2 287–315.

[321] J. Van Holten, *Propagators and path integrals*, *Nuclear Physics B* **457** (1995), no. 1-2 375–407.

[322] M. G. Schmidt and C. Schubert, *The worldline path integral approach to feynman graphs, arXiv preprint hep-ph/9412358* (1994).

[323] D. Fliegner, P. Haberl, M. Schmidt, and C. Schubert, *The higher derivative expansion of the effective action by the string inspired method, ii*, Annals of Physics **264** (1998), no. 1 51–74.

[324] V. Y. Fainberg and A. V. Marshakov, *Local supersymmetry and dirac particle propagator as a path integral*, Nuclear Physics B **306** (1988), no. 3 659–676.

[325] L. Brink, P. Di Vecchia, and P. Howe, *A lagrangian formulation of the classical and quantum dynamics of spinning particles*, Nuclear Physics B **118** (1977), no. 1-2 76–94.

[326] P. Di Vecchia and F. Ravndal, *Supersymmetric dirac particles*, Physics Letters A **73** (1979), no. 5-6 371–373.

[327] L. Brink, S. Deser, B. Zumino, P. D. Vecchia, and P. Howe, *Local supersymmetry for spinning particles*, in *Supergravities in Diverse Dimensions: Commentary and Reprints (In 2 Volumes)*, pp. 743–746. World Scientific, 1989.

[328] M. A. Shifman, *ITEP lectures in particle physics and field theory*, vol. 62. World Scientific, 1999.

[329] C. Schubert, *Vacuum polarisation tensors in constant electromagnetic fields: Part i*, Nuclear Physics B **585** (2000), no. 1-2 407–428.

[330] G. V. Dunne, *Worldline instantons, vacuum pair production and gutzwiller's trace formula*, Journal of Physics A: Mathematical and Theoretical **41** (2008), no. 16 164041.

[331] S. Levit and U. Smilansky, *A new approach to gaussian path integrals and the evaluation of the semiclassical propagator*, Annals of Physics **103** (1977), no. 1 198–207.

[332] M. Morse, *The calculus of variations in the large*, vol. 18. American Mathematical Soc., 1934.

[333] I. M. Gel'fand and A. M. Yaglom, *Integration in functional spaces and its applications in quantum physics*, *Journal of Mathematical Physics* **1** (1960), no. 1 48–69.

[334] S. Levit and U. Smilansky, *A theorem on infinite products of eigenvalues of sturm-liouville type operators*, *Proceedings of the American Mathematical Society* **65** (1977), no. 2 299–302.

[335] K. Kirsten and A. J. McKane, *Functional determinants for general sturm–liouville problems*, *Journal of Physics A: Mathematical and General* **37** (2004), no. 16 4649.

[336] G. V. Dunne, Q.-h. Wang, H. Gies, and C. Schubert, *Worldline instantons and the fluctuation prefactor*, *Physical Review D* **73** (2006), no. 6 065028.

[337] M. Gutzwiller, *Chaos in Classical and Quantum Mechanics.* Interdisciplinary Applied Mathematics. Springer New York, 2013.

[338] S. Lebedev and V. Ritus, *Virial representation of the imaginary part of the lagrangian of an electromagnetic field*, *Zh. Eksp. Teor. Fiz.* **86** (1984), no. 2 408–422.

[339] T. D. Cohen and D. A. McGady, *Schwinger mechanism revisited*, *Physical Review D* **78** (Aug., 2008) 036008, [`arXiv:0807.1117`].

[340] F. Hebenstreit, R. Alkofer, G. V. Dunne, and H. Gies, *Momentum Signatures for Schwinger Pair Production in Short Laser Pulses with a Subcycle Structure*, *Physical Review Letters* **102** (Apr., 2009) 150404, [`arXiv:0901.2631`].

[341] C. K. Dumlu and G. V. Dunne, *Interference Effects in Schwinger Vacuum Pair Production for Time-Dependent Laser Pulses*, *Phys. Rev.* **D83** (2011) 065028, [`arXiv:1102.2899`].

[342] M. Orthaber, F. Hebenstreit, and R. Alkofer, *Momentum Spectra for Dynamically Assisted Schwinger Pair Production*, *Phys. Lett.* **B698** (2011) 80–85, [`arXiv:1102.2182`].

[343] N. Abdukerim, Z.-L. Li, and B.-S. Xie, *Effects of laser pulse shape and carrier envelope phase on pair production*, *Phys. Lett.* **B726** (2013) 820–826.

[344] I. A. Aleksandrov, G. Plunien, and V. M. Shabaev, *Pulse shape effects on the electron-positron pair production in strong laser fields*, *Phys. Rev.* **D95** (2017), no. 5 056013, [`arXiv:1701.01058`].

[345] I. K. Affleck and N. S. Manton, *Monopole pair production in a magnetic field*, *Nuclear Physics B* **194** (1982), no. 1 38–64.

[346] V. Ritus, *Method of eigenfunctions and mass operator in quantum electrodynamics of a constant field*, tech. rep., CM-P00067532, 1978.

[347] V. Ritus, *Lagrangian of an intense electromagnetic field and quantum electrodynamics at short distances*, *Zh. Eksp. Teor. Fiz* **69** (1975), no. 151 7.

[348] M. Krasnansky, *Two-loop vacuum diagrams in background field and heisenberg-euler effective action*, *arXiv preprint hep-th/0607230* (2006).

[349] I. Huet, M. Rausch de Traubenberg, and C. Schubert, *Asymptotic behaviour of the qed perturbation series*, *Advances in High Energy Physics* **2017** (2017).

[350] R. P. Feynman, *The theory of positrons*, *Physical Review* **76** (1949), no. 6 749.

[351] V. Bagrov, D. Gitman, S. Gavrilov, and S. M. Shvartsman, *Creation of boson pairs from vacuum*, *Soviet Physics Journal* **18** (1975), no. 3 351–354.

[352] D. Gitman and S. Gavrilov, *Quantum processes in a strong electromagnetic field producing pairs. 3*, *Izvestiya Vysshikh Uchebnykh Zavedenij, Fizika* (1977) 94–99.

[353] S. P. Gavrilov and D. M. Gitman, *Vacuum instability in external fields*, *Physical Review D* **53** (1996), no. 12 7162.

[354] V. S. Popov, *Schwinger mechanism of electron-positron pair production by the field of optical and x-ray lasers in vacuum*, *Journal of Experimental and Theoretical Physics Letters* **74** (2001), no. 3 133–138.

[355] V. Popov, *On schwinger mechanism of e+ e- pair production from vacuum by the field of optical and x-ray lasers*, *Physics Letters A* **298** (2002), no. 2-3 83–90.

[356] S. P. Kim and D. N. Page, *Improved approximations for fermion pair production in inhomogeneous electric fields*, *Physical Review D* **75** (2007), no. 4 045013.

[357] L. Keldysh et al., *Ionization in the field of a strong electromagnetic wave*, *Sov. Phys. JETP* **20** (1965), no. 5 1307–1314.

[358] M. V. Fedorov, *L. v. keldysh's "ionization in the field of a strong electromagnetic wave" and modern physics of atomic interaction with a strong laser field*, *Journal of Experimental and Theoretical Physics* **122** (2016), no. 3 449–455.

[359] Y. Kluger, J. Eisenberg, B. Svetitsky, F. Cooper, and E. Mottola, *Pair production in a strong electric field*, *Physical Review Letters* **67** (1991), no. 18 2427.

[360] Y. Kluger, J. Eisenberg, B. Svetitsky, F. Cooper, and E. Mottola, *Fermion pair production in a strong electric field*, *Physical Review D* **45** (1992), no. 12 4659.

[361] J. Rau, *Pair production in the quantum boltzmann equation*, *Physical Review D* **50** (1994), no. 11 6911.

[362] J. Rau and B. Müller, *From reversible quantum microdynamics to irreversible quantum transport*, *Physics Reports* **272** (1996), no. 1 1–59.

[363] Y. Kluger, E. Mottola, and J. M. Eisenberg, *Quantum vlasov equation and its markov limit*, *Physical Review D* **58** (1998), no. 12 125015.

[364] S. Smolyansky, G. Roepke, S. Schmidt, D. Blaschke, V. Toneev, and A. Prozorkevich, *Dynamical derivation of a quantum kinetic equation for particle production in the schwinger mechanism*, *arXiv preprint hep-ph/9712377* (1997).

[365] S. M. Schmidt, D. Blaschke, G. Ropke, S. A. Smolyansky, A. V. Prozorkevich, and V. D. Toneev, *A Quantum kinetic equation for particle production in the Schwinger mechanism*, *Int. J. Mod. Phys.* **E7** (1998) 709–722, [`hep-ph/9809227`].

[366] S. M. Schmidt, D. Blaschke, G. Ropke, A. V. Prozorkevich, S. A. Smolyansky, and V. D. Toneev, *NonMarkovian effects in strong field pair creation*, Phys. Rev. **D59** (1999) 094005, [hep-ph/9810452].

[367] R. Alkofer, M. B. Hecht, C. D. Roberts, S. M. Schmidt, and D. V. Vinnik, *Pair creation and an x-ray free electron laser*, Phys. Rev. Lett. **87** (2001) 193902, [nucl-th/0108046].

[368] C. K. Dumlu, *On the Quantum Kinetic Approach and the Scattering Approach to Vacuum Pair Production*, Phys. Rev. **D79** (2009) 065027, [arXiv:0901.2972].

[369] L. Baird, *New integral formulation of the schrödinger equation*, Journal of Mathematical Physics **11** (1970), no. 8 2235–2242.

[370] J. P. Davis and P. Pechukas, *Nonadiabatic transitions induced by a time-dependent hamiltonian in the semiclassical/adiabatic limit: The two-state case*, The Journal of Chemical Physics **64** (1976), no. 8 3129–3137.

[371] V. Pokrovskli, S. Savvinykh, and F. Ulinich, *Reflection from the barrier in the semi-classical approximation*, Zh. Eksper. Teoret. Piz **34** (1958) 1272–1277.

[372] V. Pokrovskii and I. Khalatnikov, *On the problem of above-barrier reflection of high-energy particles*, Soviet Phys. JETP **13** (1961) 1207–1210.

[373] M. V. Berry and K. Mount, *Semiclassical approximations in wave mechanics*, Reports on Progress in Physics **35** (1972), no. 1 315.

[374] M. Berry, *Semiclassically weak reflections above analytic and non-analytic potential barriers*, Journal of Physics A: Mathematical and General **15** (1982), no. 12 3693.

[375] J. Hu and M. Kruskal, *Reflection coefficient beyond all orders for singular problems. i: Separated critical points on the nearest critical level line*, Journal of mathematical physics **32** (1991), no. 9 2400–2405.

[376] A. M. Fedotov, N. B. Narozhny, G. Mourou, and G. Korn, *Limitations on the Attainable Intensity of High Power Lasers*, Physical Review Letters **105** (Aug., 2010) 080402, [arXiv:1004.5398].

[377] J. C. R. Bloch, V. A. Mizerny, A. V. Prozorkevich, C. D. Roberts, S. M. Schmidt, S. A. Smolyansky, and D. V. Vinnik, *Pair creation: Back reactions and damping*, *Physical Review D* **60** (Dec., 1999) 116011, [nucl-th/9907027].

[378] D. Vinnik, A. Prozorkevich, S. Smolyansky, V. Toneev, M. Hecht, C. D. Roberts, and S. Schmidt, *Plasma production and thermalisation in a strong field*, *The European Physical Journal C-Particles and Fields* **22** (2001), no. 2 341–349.

[379] H. Bacry, P. Combe, and J. Richard, *Group-theoretical analysis of elementary particles in an external electromagnetic field ii.—the nonrelativistic particle in a constant and uniform field*, *Il Nuovo Cimento A (1965-1970)* **70** (1970), no. 3 289–312.

[380] S. Villalba-Chávez and A. E. Shabad, *Qed with external field: Hamiltonian treatment for anisotropic medium formed by the lorentz-non-invariant vacuum*, *arXiv preprint arXiv:1206.4491* (2012).

[381] J. Richard, *Group-theoretical analysis of elementary particles in an external electromagnetic field*, *Il Nuovo Cimento A (1965-1970)* **8** (1972), no. 3 485–500.

[382] D. V. Vinnik, R. Alkofer, S. M. Schmidt, S. A. Smolyansky, V. V. Skokov, and A. V. Prozorkevich, *Coupled Fermion and Boson Production in a Strong Background Mean Field*, *Few-Body Systems* **32** (2002) 23–39, [nucl-th/0202034].

[383] F. Hebenstreit, R. Alkofer, and H. Gies, *Pair Production Beyond the Schwinger Formula in Time-Dependent Electric Fields*, *Phys. Rev.* **D78** (2008) 061701, [arXiv:0807.2785].

[384] G. R. Mocken, M. Ruf, C. Müller, and C. H. Keitel, *Nonperturbative multiphoton electron-positron-pair creation in laser fields*, *Physical Review A* **81** (Feb., 2010) 022122.

[385] V. S. Popov, *Resonant pair production in a strong electric field*, *Soviet Journal of Experimental and Theoretical Physics Letters* **18** (Oct., 1973) 255.

[386] N. B. Narozhnyǐ and A. I. Nikishov, *Pair production by a periodic electric field*, *Soviet Journal of Experimental and Theoretical Physics* **38** (Mar., 1974) 427.

[387] D. B. Blaschke, B. Kämpfer, A. D. Panferov, A. V. Prozorkevich, and S. A. Smolyansky, *Influence of Laser Pulse Parameters on the Properties of e-e+Plasmas Created from Vacuum*, *Contributions to Plasma Physics* **53** (Feb., 2013) 165–172, [`arXiv:1205.3154`].

[388] H. Gies and K. Klingmüller, *Pair production in inhomogeneous fields*, *Phys. Rev.* **D72** (2005) 065001, [`hep-ph/0505099`].

[389] L. Keldysh, *Concerning the theory of impact ionization in semiconductors*, *Sov. Phys. JETP* **21** (1965), no. 6 1135–1144.

[390] C. Schneider and R. Schützhold, *Prefactor in the dynamically assisted Sauter-Schwinger effect*, *Phys. Rev.* **D94** (2016), no. 8 085015, [`arXiv:1603.00864`].

[391] E. Akkermans and G. V. Dunne, *Ramsey Fringes and Time-domain Multiple-Slit Interference from Vacuum*, *Phys. Rev. Lett.* **108** (2012) 030401, [`arXiv:1109.3489`].

[392] Z. L. Li, D. Lu, B. S. Xie, L. B. Fu, J. Liu, and B. F. Shen, *Enhanced pair production in strong fields by multiple-slit interference effect with dynamically assisted Schwinger mechanism*, *Phys. Rev.* **D89** (2014), no. 9 093011.

[393] G. Torgrimsson, C. Schneider, J. Oertel, and R. Schützhold, *Dynamically assisted Sauter-Schwinger effect — non-perturbative versus perturbative aspects*, *JHEP* **06** (2017) 043, [`arXiv:1703.09203`].

[394] C. K. Dumlu and G. V. Dunne, *The Stokes Phenomenon and Schwinger Vacuum Pair Production in Time-Dependent Laser Pulses*, *Phys. Rev. Lett.* **104** (2010) 250402, [`arXiv:1004.2509`].

[395] M. Holthaus, *Pulse-shape-controlled tunneling in a laser field*, *Physical review letters* **69** (1992), no. 10 1596.

[396] S. L. Adler, J. Bahcall, C. Callan, and M. Rosenbluth, *Photon splitting in a strong magnetic field*, *Physical Review Letters* **25** (1970), no. 15 1061.

[397] S. L. Adler, *Photon splitting and photon dispersion in a strong magnetic field*, *Annals of Physics* **67** (1971), no. 2 599–647.

[398] S. L. Adler and C. Schubert, *Photon splitting in a strong magnetic field: Recalculation and comparison with previous calculations*, *Physical review letters* **77** (1996), no. 9 1695.

[399] T. N. Tomaras, N. C. Tsamis, and R. P. Woodard, *Pair creation and axial anomaly in light cone QED(2)*, *JHEP* **11** (2001) 008, [`hep-th/0108090`].

[400] G. V. Dunne and Q.-h. Wang, *Multidimensional Worldline Instantons*, *Phys. Rev.* **D74** (2006) 065015, [`hep-th/0608020`].

[401] F. Hebenstreit, R. Alkofer, and H. Gies, *Schwinger pair production in space and time-dependent electric fields: Relating the Wigner formalism to quantum kinetic theory*, *Phys. Rev.* **D82** (2010) 105026, [`arXiv:1007.1099`].

[402] A. A. Grib, V. M. Mostepanenko, and V. M. Frolov, *Particle creation from vacuum by a homogeneous electric field in the canonical formalism*, *Theoretical and Mathematical Physics* **13** (1972), no. 3 1207–1217.

[403] V. G. Bagrov, D. M. Gitman, and S. M. Shvartsman, *Concerning the production of electron-positron pairs from vacuum*, *Soviet Journal of Experimental and Theoretical Physics* **41** (Feb., 1975) 191.

[404] D. M. Gitman, *Processes of arbitrary order in quantum electrodynamics with a pair-creating external field*, *Journal of Physics A Mathematical General* **10** (Nov., 1977) 2007–2020.

[405] Y. I. Salamin, S. Hu, K. Z. Hatsagortsyan, and C. H. Keitel, *Relativistic high-power laser–matter interactions*, *Physics Reports* **427** (2006), no. 2-3 41–155.

[406] S. Schmidt, D. Blaschke, G. Röpke, A. V. Prozorkevich, S. A. Smolyansky, and V. D. Toneev, *Non-Markovian effects in strong-field pair creation*, *Physical Review D* **59** (May, 1999) 094005, [`hep-ph/9810452`].

[407] R. Alkofer, M. B. Hecht, C. D. Roberts, S. M. Schmidt, and D. V. Vinnik, *Pair Creation and an X-Ray Free Electron Laser*, *Physical Review Letters* **87** (Nov., 2001) 193902, [`nucl-th/0108046`].

[408] T. Kaluza, *Zum unitätsproblem der physik, Sitzungsberichte der Königlich Preußischen Akademie der Wissenschaften (Berlin), Seite p. 966-972* (1921) 966–972.

[409] O. Klein, *Quantum theory and five-dimensional theory of relativity.(in german and english)*, *Surveys High Energ. Phys.* **5** (1926) 895–906.

[410] S. P. Kim and D. N. Page, *Schwinger pair production via instantons in a strong electric field*, *Phys. Rev.* **D65** (2002) 105002, [hep-th/0005078].

[411] A. K. Geim, *Graphene: status and prospects*, *science* **324** (2009), no. 5934 1530–1534.

[412] V. Mostepanenko and V. Frolov, *Particle production from vacuum by homogeneous electric field with periodical time dependence*, *Yadernaya Fizika* **19** (1974), no. 4 885–896.

[413] H. K. Avetissian, A. K. Avetissian, G. F. Mkrtchian, and K. V. Sedrakian, *Electron-positron pair production in the field of superstrong oppositely directed laser beams*, *Physical Review E* **66** (July, 2002) 016502.

[414] D. J. Cook and R. M. Hochstrasser, *Intense terahertz pulses by four-wave rectification in air*, *Optics Letters* **25** (Aug., 2000) 1210–1212.

[415] T. Bartel, P. Gaal, K. Reimann, M. Woerner, and T. Elsaesser, *Generation of single-cycle THz transients with high electric-field amplitudes*, *Optics Letters* **30** (Oct., 2005) 2805–2807.

[416] J.-P. Blaizot and G. Ripka, *Quantum theory of finite systems*, vol. 3. MIT press Cambridge, 1986.

Acknowledgements

Declaration

Eidesstattliche Versicherung / Declaration on oath

Hiermit versichere ich an Eides statt, die vorliegende Dissertationsschrift selbst verfasst und keine anderen als die angegebenen Hilfsmittel und Quellen benutzt zu haben.

Die eingereichte schriftliche Fassung entspricht der auf dem elektronischen Speichermedium.

Die Dissertation wurde in der vorgelegten oder einer ähnlichen Form nicht schon einmal in einem früheren Promotionsverfahren angenommen oder als ungenügend beurteilt.

Hamburg, den 7. Juni 2018

_____

Ibrahim Akal